

CENTRE FOR FORENSIC SCIENCE, DEPARTMENT OF PURE AND APPLIED CHEMISTRY

UNIVERSITY OF STRATHCLYDE

High Resolution Fourier Transform Infrared Spectroscopy for the Qualitative Analysis of Explosive Precursors in the Vapour Phase

PhD Thesis

Felicity Carlisle

2014



CENTRE FOR FORENSIC SCIENCE, DEPARTMENT OF PURE AND APPLIED CHEMISTRY

High Resolution Fourier Transform Infrared Spectroscopy for the Qualitative Analysis of Explosive Precursors in the Vapour Phase

PhD Thesis

Felicity Carlisle

2014

This thesis is the result of the author's original research. It has been composed by the author and has not been previously submitted for examination which has led to the award of a degree.

The copyright of this thesis belongs to the author under the terms of the United Kingdom Copyright Acts as qualified by the University of Strathclyde Regulation 3.50. Due acknowledgement must always be made of the use of any material contained in, or derived from, this thesis.

Signed:

Date:

Acknowledgements

Thanks to my supervisor Prof. Niamh Nic Daeid for her support and advice, and putting up with my general dislike of anything mathematical. Thanks also to all the staff at the Centre for Forensic Science, especially the one and only Pat-Man Jim Christie, and thanks to the University of Strathclyde for part-funding my project.

I am most grateful to the staff at Cascade Technologies for providing me with the funding and facilities to carry out my research. Special thanks to Erwan for his advice and Kenneth for his constant help in fixing the FTS and making sure I was always supplied with liquid nitrogen.

Thanks to my fellow FFBs for helping keep me sane, making sure that I laughed lots, and reminding me that I was not alone. A special mention to my partner in crime Nicola who shared the epic Swiss adventure with me and was always prepared to share her Irn Bru, and to Tina who may be a smelly undergrad but never failed to cheer me up when I was feeling down. Thanks also to the members of PGRS, being President may have been more stressful than actually doing my PhD but it meant I made some fantastic friends and had some amazing new experiences.

Thanks to my family for their unending love and support. To Mum, my ever patient proof-reader, sorry for all the split infinitives, and Dad my unfailing IT support, thanks for reading the help guides so I didn't have to and helping out with the proofreading.

Thanks to Steven, you have put up with the moaning, tears and self-doubt while providing an unlimited supply of hugs and humour. Writing this thesis would not have been possible without you and my life is so much better with you in it.

Finally thanks to the people of the great city of Glasgow, I have been made to feel so welcome I cannot imagine having been able to carry out my studies anywhere else.

Abstract

Fourier transform infrared spectroscopy (FTIR) has applications in many areas of forensic science. The ability to produce information rich spectra is of particular use for the characterisation and discrimination of materials. High resolution FTIR can produce even more detailed spectra and therefore improved characterisation and discrimination. However, the production of information rich spectra requires suitable statistical tools for analysis, with multivariate analysis often used.

The mid infrared region contains the 'fingerprint region' which is used for the detection and identification of many different materials, and is therefore an area of investigation in the field of explosives detection.

This research aimed to utilise high resolution mid infrared FTIR for the characterisation of explosive precursors in the vapour phase. Detailed examination of the spectra produced would provide information on spectral regions that could be applied as targets for detection systems, for example those based upon Quantum Cascade Lasers (QCLs). By building up detailed knowledge of the spectra produced by different materials this research aimed to determine the most suitable spectral regions for the identification of explosive precursors.

In addition, this research aimed to investigate whether it was possible to use high resolution FTIR to discriminate between laboratory grade materials and their shop bought counterparts containing additives and impurities. Acetone, alcohols and hydrogen peroxide were analysed in this work.

The research also aimed to determine whether brand discrimination was still viable following concentration of two hydrogen peroxide containing brands. The ability to identify that a material had been concentrated but tie it back to its brand would be of great significance for intelligence gathering.

The findings of this research demonstrate that high resolution FTIR can successfully be applied to the characterisation of explosive precursors and, in combination with chemometric techniques, discriminate between different precursor brands even following concentration of the precursor material.

Conference Attendance, Presentations and Publications

SSFR Symposium 2014

High Resolution Fourier Transform Spectroscopy for the discrimination of branded explosive precursors. (Presentation)

Chemometric analysis of spectral data from explosives precursors. (Poster)

AAFS 2013

High Resolution Fourier Transform Spectroscopy for the discrimination of lab grade explosive precursors and their shop bought equivalents. (Presentation)

Statistical discrimination of explosive precursors using data gathered from high resolution Fourier Transform spectroscopy. (Poster)

SPIE Security and Defence 2012

Exploiting High Resolution Fourier Transform spectroscopy to inform the development of a quantum cascade laser based explosives detection system (Poster and conference proceedings)

EAFS 2012

Using High Resolution Fourier Transform Spectroscopy for the Development of Explosives Detection in Improvised and Homemade Explosive Devices. (Poster)

High Resolution Fourier Transform Spectroscopy as a Tool for the Characterisation and Differentiation of Explosive Precursor Chemicals. (Poster)

Forensic Science and Criminology PhD Summer School 2012 (University of Lausanne)

Contents

Acknowledgements	<i>pi</i>
Abstract	<i>p ii</i>
Conference Attendance, Presentations and Publications	<i>p iv</i>
Contents	<i>p v</i>
Table of Figures	<i>p x</i>
Table of Tables	<i>p xix</i>
Table of Equations	<i>p xxi</i>
Glossary	<i>p xxii</i>
1 Introduction	p 1
1.1 Introduction to explosive materials	p 3
1.1.1 A brief history of explosive materials	p 3
1.1.2 Chemistry of explosives	p 8
1.1.3 ‘Homemade explosives’	p 10
1.1.3.1 Peroxide based materials	p 11
1.1.3.2 Fertiliser based materials	p 12
1.1.3.3 Inorganic salt based materials	p 13
1.1.4 Classification of explosives	p 13
1.1.5 Explosive devices and improvised explosive devices (IEDs)	p 15
1.1.6 The use of explosives in terrorism	p 17
1.2 Analysis of explosive materials	p 20
1.2.1 Intelligence gathering	p 22
1.2.2 Post blast investigation	p 23
1.3 Explosives detection	p 23

1.3.1	Bulk detection of explosives	p25
1.3.2	Trace detection of explosives	p25
1.3.3	Stand-off detection of explosives	p25
1.3.4	Current detection systems	p26
	1.3.4.1 Imaging techniques	p26
	1.3.4.2 Particulate detection	p28
	1.3.4.3 Vapour detection	p29
	1.3.4.3.1 Personnel portals	p31
1.3.5	Future detection systems	p33
1.4	References	p35
2	Techniques and Instrumentation	p43
2.1	Spectroscopy	p43
2.1.1	Infrared spectroscopy	p44
	2.1.1.1 Spectral interpretation	p50
2.1.2	Fourier transform infrared spectroscopy (FTIR)	p51
	2.1.2.1 FTIR in explosives detection and analysis	p54
2.2	Infrared spectrometers	p55
2.2.1	High resolution FTIR spectrometers	p57
2.3	Lasers	p59
2.3.1	Quantum cascade lasers (QCLs)	p60
	2.3.1.1 QCLs for explosives detection	p61
2.4	Chemometrics	p61
2.4.1	Standard deviation and relative standard deviation (RSD)	p62
2.4.2	Hierarchical cluster analysis (HCA)	p62
2.4.3	Self organising feature maps (SOFM)	p64
2.5	Conclusions	p69
2.6	References	p69
3	Protocol Development and Analysis of Compounds of Interest	p73
3.1	Introduction	p73

3.2 Materials	p75
3.2.1 Protocol development	p75
3.2.2 Analysis of compounds of interest	p75
3.3 Method	p76
3.3.1 Protocol development	p77
3.3.2 Compounds of interest	p79
3.4 Results and discussion	p79
3.4.1 Diesel	p79
3.4.2 Acetone	p84
3.4.3 Ammonia	p88
3.4.4 Ethylene glycol	p91
3.4.5 Hydrazine and hydrazine hydrate	p93
3.4.6 Hydrogen peroxide	p99
3.4.7 Nitric acid	p102
3.4.8 Nitromethane	p104
3.4.9 Methanol	p106
3.4.10 Ethanol	p108
3.5 Conclusions	p112
3.6 References	p113
4 Brand Discrimination – Acetone	p115
4.1 Introduction	p115
4.2 Materials	p117
4.3 Experimental protocol	p118
4.3.1 Visual comparison	p118
4.3.2 Statistical analysis	p118
4.4 Results and discussion	p119
4.4.1 Visual comparison	p119
4.4.2 Statistical analysis	p125
4.4.2.1 Hierarchical cluster analysis	p128
4.4.2.2 Self organising feature maps	p130

4.5 Conclusions	p139
4.6 References	p140
5 Brand Discrimination – Alcohols	p142
5.1 Introduction	p142
5.2 Materials	p144
5.3 Experimental protocol	p144
5.3.1 Visual analysis	p144
5.3.2 Statistical analysis	p145
5.4 Results and discussion	p146
5.4.1 Visual analysis	p146
5.4.2 Statistical analysis	p149
5.4.2.1 Hierarchical cluster analysis	p149
5.4.2.2 Self organising feature maps	p157
5.5 Conclusions	p166
5.6 References	p167
6 Brand Discrimination – Hydrogen Peroxide	p169
6.1 Introduction	p169
6.2 Materials	p171
6.3 Experimental protocol	p172
6.3.1 Visual and statistical analysis of un-concentrated samples	p172
6.3.2 Concentrated samples	p172
6.3.2.1 Concentration of samples	p172
6.3.2.2 Titration of samples	p173
6.3.2.3 FTS and statistical analysis	p174
6.4 Results and discussion	p174
6.4.1 Un-concentrated hydrogen peroxide samples	p174
6.4.1.1 Visual analysis	p174
6.4.1.2 Statistical analysis	p179
6.4.1.2.1 Hierarchical cluster analysis	p181

6.4.1.2.2	Self organising feature maps	p184
6.4.2	Concentrated samples	p189
6.4.2.1	Sunin	p189
6.4.2.1.1	Hierarchical cluster analysis	p192
6.4.2.1.2	Self organising feature maps	p195
6.4.2.2	Health Leads	p196
6.4.2.2.1	Hierarchical cluster analysis	p199
6.4.2.2.2	Self organising feature maps	p200
6.4.2.3	Sunin and Health Leads comparison	p202
6.4.2.3.1	Hierarchical cluster analysis	p202
6.4.2.3.2	Self organising feature maps	p203
6.5	Conclusions	p206
6.6	References	p207
7	Conclusions and Future Work	p210
7.1	Summary	p210
7.2	Future work	p213
7.2.1	Compounds of interest	p213
7.2.1.1	Solid samples	p214
7.2.2	Brand discrimination	p214
7.2.3	Mixtures	p215
7.2.4	Alcohols	p216
7.2.5	Statistical analysis	p216
7.3	Conclusions	p217
Appendix 1		p218
Appendix 2		p223
Appendix 3		p225
Appendix 4		p227
Appendix 5		p228

Table of Figures

1.1	The chemical structures of A: TATP (in trimer form) and B: HMTD	p10
1.2	A block diagram representing the explosive train	p15
1.3	The Portal detection system on trial at Glasgow Airport	p32
1.4	A basic diagram of the Portal system	p33
2.1	The Electromagnetic spectrum	p43
2.2	The characteristic spectra bands of carbon dioxide, demonstrating the line-like peaks seen with rotational vibrations of vapour samples	p45
2.3	Energy level diagram for a single electronic state showing the vibrational energy levels (purple; $v=0$ to $v=3$) and the rotational energy levels (red lines)	p47
2.4	Diagram of the potential wells for two electronic states showing the electronic, vibrational and rotational energy levels with green arrows showing some of the possible transitions (dependent upon quantum numbers) between rotational and vibrational energy levels, and the blue arrow showing an electronic transition (which is not detectable by IR spectroscopy, but could be detectable with UV/vis spectroscopy)	p48
2.5	An example of a correlation chart used to identify spectral features seen in an IR spectrum	p50
2.6	An interpreted infrared spectrum for toluene	p51
2.7	Diagram representing the internal compartment structure of the FTS used in this work	p57
2.8	The sample cell removed from the FTS showing one of the circular windows that allow the infrared beam to pass through the cell	p59
2.9	Diagram representing the internal structure of the FTS with red arrows showing the path taken by the infrared beam through the instrument from source to detector	p59
2.10	Staircase diagram depicting the movement of electrons within a QCL	p60

2.11	Dendrogram produced using Minitab 16 for the farmyard animal data in table 2.2	p64
2.12	Simplified diagram demonstrating the steps of each iteration of the SOFM process	p65
2.13	Cluster map produced using Viscovery SOMine 4.0.2 for the farmyard animal data set with the clustering set to five	p67
2.14	Cluster map produced using Viscovery SOMine 4.0.2 for the farmyard animal data set with the clustering set by the matching algorithms	p67
2.15	Component maps for the farmyard animal data using Viscovery SOMine 4.0.2	p68
3.1	Diagram of the sample cell demonstrating how liquid samples were analysed in the vapour phase	p73
3.2	Diesel spectra produced at 27°C (blue), 75°C (green), 150°C (pink) showing the differences in absorption seen across the temperature range	p80
3.3	Close up of the absorption seen at 2900 cm ⁻¹ with diesel at 27°C (blue), 75°C (green) and 150°C (pink)	p82
3.4	Spectra produced with diesel at 75°C with sample volumes of 0.5 mL (green), 1 mL (pink) and 3 mL (blue)	p84
3.5	Average spectrum produced with 100 µL acetone at 27°C with the structure of acetone also shown	p85
3.6	Close up of the broad absorption band at 1220 cm ⁻¹ in the average spectrum of 100 µL acetone at 27°C that might be suitable for detection with a broadband QCL	p86
3.7	Close up of the potential detection target at 886.5 cm ⁻¹ which is part of a broader absorption peak of the average spectrum of 100 µL acetone at 27°C	p87
3.8	Excel plot showing the potential detection target at 1290 cm ⁻¹ created with the data from the average spectrum of 100 µL acetone	

	at 27°C	p87
3.9	Average spectrum produced with 100 µL ammonia in propanol at 27°C	p88
3.10	Average spectrum of 100 µL ammonia at 27°C with propanol subtracted with the structure of ammonia inset	p89
3.11	Plotted data for ammonia in propanol (green), propanol (purple) and ammonia with propanol subtracted (red) for the spectra region of the 867 cm ⁻¹ detection site	p90
3.12	Plotted data for ammonia in propanol (green), propanol (purple) and ammonia with propanol subtracted (red) for the spectral region of the 993 cm ⁻¹ detection site	p90
3.13	Average spectrum produced with 1 mL ethylene glycol at 75°C showing the structure of ethylene glycol inset	p91
3.14	Plotted values for ethylene glycol in the spectral region of the 1075 cm ⁻¹ detection site	p92
3.15	Plotted values for ethylene glycol in the spectral region of the 1160 cm ⁻¹ detection site	p93
3.16	Average spectrum produced for 100 µL hydrazine in THF at 27°C	p94
3.17	Hydrazine spectrum with THF subtracted with the structure of hydrazine inset	p94
3.18	Close up of the hydrazine spectrum with THF subtracted showing the absorption in the 918 cm ⁻¹ detection site and small peaks at approximately 1050 cm ⁻¹ and 1175 cm ⁻¹	p95
3.19	Average spectrum for 100 µL hydrazine hydrate at 27°C with the structure inset	p96
3.20	Plotted data for hydrazine hydrate in the spectral region of the 867 cm ⁻¹ detection site for ammonia	p97
3.21	Plotted data for hydrazine hydrate in the spectral region of the 918 cm ⁻¹ detection site for hydrazine	p97
3.22	Plotted data for hydrazine hydrate in the spectral region of the 993	

	cm ⁻¹ detection site for ammonia	p98
3.23	Average spectrum produced with 100 μL hydrogen peroxide at 75°C also showing the structure of hydrogen peroxide	p100
3.24	Close up of the average spectrum for hydrogen peroxide showing the two regions of interest	p100
3.25	Data plotted for hydrogen peroxide in the spectral region of the 1274 cm ⁻¹ detection site	p101
3.26	Data plotted for hydrogen peroxide in the spectral region of the 1285 cm ⁻¹ detection site	p101
3.27	Average spectrum produced with 100 μL nitric acid at 27°C also showing the structure of nitric acid	p102
3.28	Plotted data for the spectral region of the 867 cm ⁻¹ target site for nitric acid	p103
3.29	Close up of the three relatively large absorption peaks seen between 874 and 899 cm ⁻¹ in the nitric acid spectrum	p104
3.30	Average spectrum produced with 100 μL nitromethane at 27°C also showing the structure of nitromethane	p105
3.31	Close up of the 918 cm ⁻¹ target region for nitromethane	p105
3.32	Average spectrum produced with 100 μL methanol at 27°C also showing the structure of methanol	p106
3.33	Plotted data for methanol in the spectral region of a 918 cm ⁻¹ QCL	p107
3.34	Plotted data for methanol in the spectral region of a 1075 cm ⁻¹ QCL	p107
3.35	Average spectrum produced with 100 μL ethanol at 27°C also showing the structure of ethanol	p108
3.36	Close up of three absorption peaks seen with ethanol	p109
3.37	Overlaid spectra of ethanol (red), tequila (teal) and nitric acid (purple)	p109
3.38	Ethanol reference spectrum	p110
3.39	Plotted data for ethanol in the spectral region covered by an 885 cm ⁻¹ QCL	p111

3.40	Plotted data for the spectra region around 1160 cm^{-1} for ethanol	p111
4.1	Overlaid spectra of the six analyses of acetone	p120
4.2	Overlaid average spectra for acetone (green) and five nail polish removers; Sally Hansen (blue), Mavala (purple), Cutex (dark green), Allura (teal) and Boots (olive) produced with 100 μL samples at 27°C	p123
4.3	Close up of the fingerprint region of the overlaid spectra of acetone (green) and five nail polish removers; Sally Hansen (blue), Mavala (purple), Cutex (dark green), Allura (teal) and Boots (olive)	p124
4.4	Profile of variables for the 31 regions of variation across the nail polish removers and acetone spectra	p126
4.5	Dendrogram produced using the individual repeat total transmittance values for the 32 regions of variation for the five nail polish removers and acetone	p129
4.6	Dendrogram produced using the average total transmittance values for the 31 regions of variation for the five nail polish removers and acetone	p130
4.7	Cluster map for the individual repeats of acetone and acetone based nail polish removers with the clustering set to six	p131
4.8	Cluster map for acetone and acetone based nail polish removers created using the average spectral data with the clustering set to six	p132
4.9	Component maps for regions of variation between 810 and 1330 cm^{-1}	p133
4.10	Component maps for regions of variation between 1360 and 2452 cm^{-1}	p134
4.11	Component maps for regions of variation between 2565 and 3850 cm^{-1}	p135
4.12	Overlaid spectra for the six brands in the region 1300-1500 cm^{-1}	p136
4.13	Total transmittance values for the region of variation 1300 - 1500 cm^{-1}	p137
4.14	Component map for the region of variation 1300 - 1500 cm^{-1}	p137

4.15	Overlaid spectra for the six brands in the region 1640-1800 cm ⁻¹	p138
4.16	Total transmittance values for the region of variation 1640 - 1800 cm ⁻¹	p138
4.17	Component map for the region of variation 1640 - 1800 cm ⁻¹	p139
5.1	Six ethanol repeats overlaid, demonstrating the presence of variation between the spectra	p146
5.2	Average spectra for 100 µL ethanol (blue), methanol (pink), propanol (grey), Melocoton (navy blue), Gordon's gin (brown), Beefeater gin (khaki), Smirnoff (purple), Absolut vodka (red), Bacardi breezer (orange), Bacardi rum (pink), methylated spirit (aqua), surgical spirit (purple), Jose Cuervo tequila (black), Listerine (dark green), Tesco mouthwash (bright green) at 27°C	p148
5.3	Profile of variables for the 22 regions of variation	p150
5.4	Dendrogram produced using the average total transmittance values for the alcohols analysed	p152
5.5	Comparison of drinkable spirits with an alcohol concentration of 37.5% or 38%	p153
5.6	Comparison of drinkable spirits with an alcohol concentration of 40%	p154
5.7	Comparison of Beefeater and Gordon's gin showing the individual repeats	p155
5.8	Comparison of Smirnoff and Absolut vodka showing the individual repeats	p155
5.9	Comparison of Bacardi rum and Bacardi breezer showing the individual repeats	p156
5.10	Comparison of Listerine, Tesco and Colgate mouthwashes	p157
5.11	Cluster map for the six individual repeats for each of the 16 alcohols analysed	p157
5.12	Cluster map for the average values of the alcohols analysed	p159
5.13	Component maps for regions 810-1440 cm ⁻¹	p160

5.14	Component maps for regions 1450-3775 cm ⁻¹	p161
5.15	Overlaid spectra of the alcohols analysed in the region 2915-2950 cm ⁻¹	p163
5.16	Profile of variables for the region 2915-2950 cm ⁻¹	p163
5.17	Component map for the region 2915-2950 cm ⁻¹	p164
5.18	Overlaid spectra of the alcohols analysed in the region 1340-1360 cm ⁻¹	p165
5.19	Profile of variables for the region 1340-1360 cm ⁻¹	p165
5.20	Component map for the region 1340-1360 cm ⁻¹	p166
6.1	Six overlaid spectra of the six repeat analyses of hydrogen peroxide	p175
6.2	Comparison of average spectra for 100 µL hydrogen peroxide (aqua), Health Leads (green), Jerome Russell (grey), Colgate mouthwash (black), Sunin (khaki) and Botanics (orange) at 75°C	p178
6.3	Close up of the spectral region covering the two hydrogen peroxide detection targets for hydrogen peroxide (aqua), Health Leads (green), Jerome Russell (grey), Colgate mouthwash (black), Sunin (khaki) and Botanics (orange)	p179
6.4	Profile of variables for the laboratory hydrogen peroxide and hydrogen peroxide containing materials	p180
6.5	Dendrogram produced using the data from individual repeats of each material analysed	p182
6.6	Dendrogram produced using the average values for the hydrogen peroxide containing materials	p183
6.7	Cluster map for the individual repeats for each hydrogen peroxide containing material	p185
6.8	Cluster map for the average values for the six hydrogen peroxide based materials analysed	p185
6.9	Component maps covering the regions of variation between 800-2670 cm ⁻¹	p186
6.10	Component maps for the regions of variation between 2675-3790	

	cm ⁻¹	p187
6.11	Overlaid spectra for the six hydrogen peroxide brands in the region 1250-1265 cm ⁻¹	p188
6.12	Profile of variables for the region 1250-1265 cm ⁻¹	p188
6.13	Component map for the region 1250-1265 cm ⁻¹	p189
6.14	Graph showing the calculated concentration of hydrogen peroxide in Sunin at each time interval	p190
6.15	Overlaid average spectra for 50% laboratory grade hydrogen peroxide (red) and Sunin T=0 (black), T=1 (khaki), T=2 (blue), T=3 (grey), T=4 (purple), T=5 (navy)	p191
6.16	Close up of the spectral region containing two hydrogen peroxide detection features with 50% laboratory grade hydrogen peroxide (red) and Sunin T=0 (black), T=1 (khaki), T=2 (blue), T=3 (grey), T=4 (purple), T=5 (navy) overlaid	p191
6.17	Dendrogram produced using the total transmittance data from the individual repeats of the analysis of each concentration time interval for Sunin	p193
6.18	Dendrogram produced using the average total transmittance data from each of the concentration time intervals for Sunin	p194
6.19	Cluster map for the individual repeats for each time interval (T=0 to T=5) for Sunin	p195
6.20	Cluster map for the average values of the six time intervals (T=0 to T=5) for Sunin	p196
6.21	Graph showing the calculated concentrations of hydrogen peroxide in Health Leads at each time interval and the corresponding adjusted concentration values	p197
6.22	Overlaid average spectra of 50% laboratory grade hydrogen peroxide (red) and Health Leads T=0 (pink), T=1 (brown), T=2 (khaki), T=3 (purple), T=4 (navy), T=5 (green)	p198
6.23	Close up of the spectral region containing the two detection targets	

	for hydrogen peroxide with 50% laboratory grade hydrogen peroxide (red) and Health Leads T= 0 (pink), T=1 (brown), T=2 (khaki), T=3 (purple), T=4 (navy), T=5 (green) overlaid	p198
6.24	Dendrogram produced using the total transmittance data from the individual repeats from each concentration time interval	p199
6.25	Dendrogram produced using the average total transmittance data for the Health Leads concentration time intervals	p200
6.26	Cluster map for the individual repeats for the six time intervals (T=0 to T=6) for Health Leads	p201
6.27	Cluster map for the average values for the six time intervals (T=0 to T=5) for Health Leads	p201
6.28	Dendrogram produced from a comparison of the total transmittance data for Health Leads (HL) and Sunin (S)	p203
6.29	Cluster map comparing the average data for the six time intervals (T=0 to T=5) for Sunin (S) and Health Leads (HL) showing the two clusters, and contour lines separating the time intervals	p204
6.30	Component maps for regions of variation between 800-1330 cm^{-1}	p204
6.31	Component maps for regions of variation between 1230-3790 cm^{-1}	p205

Table of Tables

1.1	The short name, IUPAC name and formula of explosive materials covered in section 1.1.1	p6
1.2	The short name, IUPAC name and structure of explosive materials covered in section 1.1.1.	p7
1.3	A comparison of canine and instrumental vapour detection methods	p30
2.1	The six different vibrational modes shown in diagram form	p45
2.2	Data on farmyard animals for use in chemometric analysis	p63
3.1	Summary of the compounds of interest selected and their relevance to explosives detection	p74
3.2	The currently available and future planned wavelengths of QCLs at Cascade Technologies	p75
3.3	Source information for the 10 compounds of interest analysed	p75
3.4	FTS instrument settings used during this research	p77
3.5	The volume and temperature levels for the initial analysis of diesel	p78
3.6	The experimental procedure for the initial analysis of diesel	p78
3.7	The stepwise process for the analysis of compounds of interest	p79
3.8	Standard deviation values calculated for the whole spectrum and within the regions of absorption based on a mean where $n=4$	p81
3.9	Relative standard deviation values calculated for the different variables for the whole spectrum and within the regions of absorption	p81
4.1	Five selected nail polish removers, where they were purchased and their ingredients	p117
4.2	Regions of variation identified through visual examination of average spectra of laboratory acetone and five acetone based nail polish removers and the data for acetone in these regions (rows with red text indicate data with an RSD value above 5%)	p121
4.3	RSD values for the six materials analysed with RSD values (and their regions) above 5% shown in red	p127

5.1	Alcoholic compounds selected for analysis including alcohol content and source information	p144
5.2	Data for the six ethanol repeats across the 22 regions of variation identified	p147
5.3	RSD values for the 16 materials analysed with RSD values (and their regions) above 5% shown in red	p151
6.1	Peroxide concentration and source information for the hydrogen peroxide containing materials	p171
6.2	Protocol for the concentration of hydrogen peroxide containing materials	p173
6.3	Titration protocol for the Sunin samples	p173
6.4	Titration protocol for the Health Leads samples	p174
6.5	Breakdown of the data from six repeats of laboratory grade hydrogen peroxide	p176
6.6	Regions of variation identified from visual examination of the average overlaid spectra of hydrogen peroxide containing materials	p177
6.7	RSD values for the six materials analysed with those RSD values above 5% shown in red	p181
6.8	Summary of time intervals	p190
6.9	Summary of time intervals and adjusted concentrations	p197

Table of Equations

2.1	Infinite-range Fourier transform	p52
2.2	Discrete Fourier transform	p52
2.3	Euclidean distance for objects k and l with m variables	p63

Glossary

ANFO – Ammonium nitrate fuel oil

BCE – Before common era

CE – Common era

DIAL – Differential absorption LIDAR

Dstl – Defence Science and Technology Laboratory

FEL – Forensic Explosives Laboratory

FTS – Fourier transform spectrometer

KBr – Potassium bromide

FTIR – Fourier transform infrared spectroscopy

HME – Homemade explosive

HMTD – Hexamethylene triperoxide diamine

HMX - Octogen

HQI – Hit quality index

IMS – Ion mobility spectrometry

IR - Infrared

PETN – Pentaerythritol tetranitrate

QCL – Quantum cascade laser

RDX – Research Department explosive

RSD – Relative standard deviation

St dev – Standard deviation

TATP – Triacetone triperoxide

TNT - Trinitrotoluene

Chapter 1. Introduction

The research detailed in this thesis is focused upon the detection and characterisation of explosive precursors and explosive materials. The research aimed to inform the development of a qualitative detection system (based on the application of Quantum Cascade Lasers) for use in airports and other civilian checkpoints[1] through the characterisation of specific compounds of interest and the monitoring of modifications made to one of these compounds.

Chapter 1 focuses on a brief introduction to explosive materials and their detection and includes a short history of the development and chemistry of explosive materials, their use in terrorism and the systems for the detection of such materials. The chapter aims to give a broad overview of the topic and the many different aspects that must be considered for the characterisation and detection of explosive materials. For example, while this work did not directly deal with the structure of improvised explosive devices, the construction of an explosive device can affect the ability of a detection system to reveal a target material. Similarly while the research focus was primarily on the detection of explosive materials pre-blast, and the characterisation of explosive materials and precursors for intelligence gathering purposes, post-blast detection is also covered in this chapter as the techniques detailed in this report have the potential, with further work, also to be used in this setting.

Chapter 2 provides an overview of spectroscopy and spectroscopic techniques, focusing on infrared spectroscopy. This chapter discusses the specific spectroscopic instrumentation used in this research project. As the initial focus of this project was the development of a quantum cascade laser based explosives detection system, this technology is addressed along with a review of the literature on infrared spectroscopy and quantum cascade laser based explosives detection systems. This chapter also provides a brief introduction to the chemometric techniques that can be employed for the analysis of spectral data.

Chapter 3 details the initial development of an experimental protocol for high resolution Fourier Transform spectroscopy (FTS) using diesel as the target material. The purpose was to develop and validate a robust analytical methodology for the FTS equipment. The chapter presents the application of the developed experimental protocol to a range of compounds of interest and the interpretation of the data obtained, including the classification of spectral features and the identification of those spectral features potentially suitable for detection with Quantum Cascade Lasers (QCLs).

Chapters 4 and 5 detail the analysis of acetone and acetone based nail polish removers and the analysis of alcohols respectively, using the experimental methodology developed in Chapter 3. The purpose was to determine whether the spectral data could discriminate between laboratory grade material and shop bought materials.

Chapter 6 provides details of the analysis of hydrogen peroxide and hydrogen peroxide based materials to determine whether it was possible to discriminate between laboratory grade material and shop bought variants. This chapter also covers the analysis of shop bought hydrogen peroxide samples that had been modified through concentration under controlled circumstances in the laboratory. The purpose was to determine whether brand specificity of the concentrated material was still viable while also determining that the material had been concentrated.

Chapter 7 provides a summary of the research and some conclusions. It also presents suggestions for future work.

1.1 Introduction to explosive materials

Explosive materials surround us in our everyday lives, with many legal uses, both in a military and industrial context. Explosive compounds are also used for medical applications, for example some nitrate esters are used to treat heart disease[2]. However, despite all the positive uses, explosives can also be used in terrorist activities[2, 3].

An explosion can be defined as the fast expansion of gases as a result of a chemical or physical action that results in the formation of a pressure wave[4]. There are four basic types of explosion; mechanical, chemical, nuclear and electrical[4]. An example of a mechanical explosion would be a boiler explosion, where pressure has built up to a point that results in the failure of the boiler container[4]. A nuclear explosion involves the splitting or fusing of atoms producing very large amounts of energy in a variety of forms such as x-rays and [4]. Electrical explosions are less well understood with several theories as to the action of the explosion, however all normally involve the action of high-energy electrical arcs[4]. Chemical explosions are those which are most commonly encountered and are the main focus of this chapter.

1.1.1 A brief history of explosive materials

The first documented explosive compound was black powder (a mixture of charcoal, sulphur and potassium nitrate[5]), sometimes referred to as gun power[5], with the discovery being made in China around 220 BCE[6]. It was not introduced into Europe until around 700 CE where it was used in a military setting in the form of primitive rockets and stun grenades[7]. By the end of the 13th century, black powder was being used for breaching castle walls and city defences[7].

As with most discoveries, after the initial success, work was carried out to improve the product and search for new uses[5]. One of the ways black powder was improved was the development of the Corning Process. This improved the mixing process that brought the fuel (charcoal and sulfur) and oxidiser (potassium nitrate)

into much closer proximity, resulting in a more effective explosive mixture[6]. The mixture itself was also adjusted with the ratio of charcoal, sulfur and potassium nitrate undergoing many variations[5]. The most common ratio of charcoal, sulphur and potassium nitrate now used is 15:10:17 by weight respectively[5].

Nitroglycerine was the next documented explosive to be discovered, with Professor Ascanio Sobrero credited with the initial discovery[6, 8]. However, after he discovered the material's explosive properties, he halted his experiments and it wasn't until Immanuel Nobel developed a manufacturing process, almost twenty years later, that nitroglycerine began to be used as an alternative to black powder in the mining industry[6]. Immanuel Nobel's son, Alfred, was also involved in the manufacture of nitroglycerine and in 1864 invented the blasting cap detonator[6]. This used shock sensitive mercury fulminate to create a shock wave through its detonation which could initiate a bulk charge, such as nitroglycerine[8]. The invention of the blasting cap detonator was shortly followed by the development of ghur dynamite[6, 8], also by Alfred Nobel, which involved mixing an absorbent clay (Kieselguhr) with nitroglycerine to produce a material with reduced sensitivity and increased stability but that could be readily detonated using the blasting cap detonator. However, due to the presence of inert material, the overall explosive power was lower than that of nitroglycerine[8].

In parallel to the development of nitroglycerine another explosive compound, nitrocellulose was being developed[6]. The nitration of different materials, such as starch, paper and cotton, appears to have been carried out by several individuals, however the first official announcement of the process of nitrating cellulose was made in 1846 by Christian Schönbein[9]. Nitrocellulose, like nitroglycerine, suffered from instability problems, and it wasn't until the work of Sir Frederick Abel and E.A. Brown in the late 1860s that nitrocellulose was produced, via a pulping process, in a stable enough state for (relatively) safe use[6].

1875 saw Alfred Nobel's next discovery, gel dynamite[6]. He found that by mixing nitrocellulose and nitroglycerine a waterproof gel was formed, and this was

developed into blasting gelatine and gelatine dynamite[8]. By combining two explosive materials rather than one explosive and one inert material, Nobel was able to solve the one failing of his gher dynamite, the loss of power.[8] This discovery also led to the development of smokeless powder, or ballistite[8].

The late 19th and early 20th century saw a period of significant development in military explosives[5]. Picric acid was already known as a material dye but in the late 19th century its explosive properties began to be explored and in 1888 it formally replaced black powder in British munitions, with other nations following suit[6]. The early 20th century saw the development of tetryl, which came to be used in blasting caps[6]. Two explosives extensively used in the First World War were also developed during this period, trinitrotoluene (TNT) and nitroguanidine[6].

The inter-war years saw a period of sustained research into the development of new explosives[5]. Some came from rather unusual sources, the most obvious example being cyclotrimethylene trinitramine, better known as RDX (Research Department eXplosive[10]), which was originally developed as a medicine[11]. The chemically related HMX (or octogen) was also developed at this time, as was pentaerythritol nitrate or PETN[6]. Many of these new explosives had been documented several years earlier, but until this point suitable manufacturing processes had not been developed for these compounds. All of these explosives were used, on their own and as mixtures, during the Second World War[6, 11].

Ammonium nitrate had first been prepared in 1654, with its explosive properties also being noted at several points in the 19th century[6]. However it was only used in an explosives context in mixtures such as dynamite and Amatol (where it is mixed with TNT)[12]. It took three disastrous explosions in 1947 to convince the world of its dangerous nature[13, 14]. These explosions occurred as a result of fires in ammonium nitrate stores resulting in burning to detonation. A better knowledge of the explosive powers of ammonium nitrate came about following these explosions[13] and led to better storage and transport of fertilizer grade material in addition to the investigation of its use as an explosive compound in its own right[6].

1950 saw the development of waterproof explosives for mining, the most prominent of which was Ammonium Nitrate Fuel Oil or ANFO. This is still used in some mining operations today, although it has in part been replaced by emulsion explosives which also use ammonium nitrate but within a layer of oil[6].

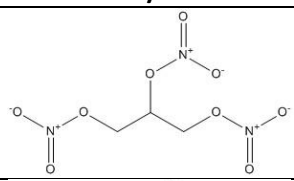
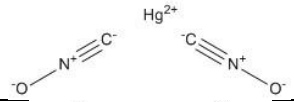
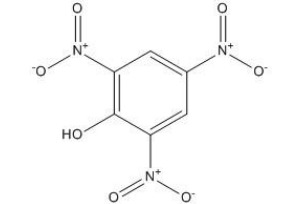
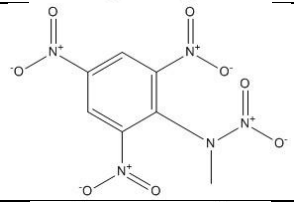
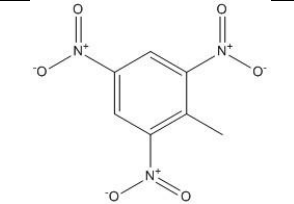
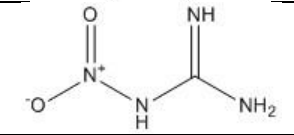
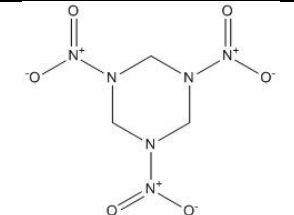
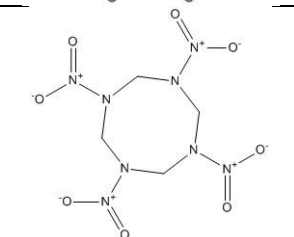
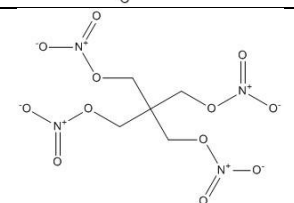
The early post war period saw the major development of plastic, or polymer bound, explosives[6, 11]. These are generally mixtures of RDX, PETN and HMX combined with a plasticiser. The plasticiser serves as a stabilising matrix surrounding the explosive crystals allowing safer handling while the mixture of explosive materials can produce a more powerful reaction[6, 11]. The most well-known plastic explosives are probably semtex (a RDX/PETN mixture) and C4 (RDX)[6].

The end of the 20th and early 21st centuries have seen few discoveries of completely new explosives within the military or mining industry, with most work focusing on improving existing explosives mixtures, both in terms of explosive power but also stability and safety of handling[6, 11]. Some work however has resulted in the development of nitrocubanes (C₈H₇NO₂) which have a very high predicted detonation velocity[11, 15, 16]. Tables 1.1 and 1.2 provide additional information on the explosive materials that have been described in this section.

Table 1.1 The short name, IUPAC name and formula of explosive materials covered in section 1.1.1

Short Name	IUPAC Name	Formula
Black powder	n/a	S, C & KNO ₃
Nitrocellulose	n/a	C ₆ H ₉ (NO ₂)O ₅
Guhr dynamite	n/a	C ₃ H ₅ N ₃ O ₉ & diatomaceous earth
Ballistite/ Smokeless powder	n/a	Picrate mixtures with an oxidiser (nitrate, chlorate or dichromate)
ANFO	n/a	NH ₄ NO ₃ and fuel oil
Semtex	n/a	PETN, RDX, with binder, plasticiser, antioxidant and dye
C4	n/a	RDX with binder and plasticiser
Heptanitrocubane	Heptanitrocubane	C ₈ H ₇ N ₇ O ₁₄
Octanitrocubane	Octanitrocubane	C ₈ H ₈ N ₈ O ₁₆

Table 1.2 The short name, IUPAC name and structure of explosive materials covered in section 1.1.1

Short Name	IUPAC Name	Structure/ Formula
Nitroglycerine	1,2,3-Trinitroxypropane	
Mercury Fulminate	Mercury (II) Fulminate	
Picric acid	2,4,6-Trinitrophenol	
Tetryl	N-methyl-N,2,4,6-tetranitroaniline	
TNT	2-Methyl-1,3,5-trinitrobenzene	
Nitroguanidine	1-Nitroguanidine	
RDX	1,3,5-Trinitroperhydro-1,3,5-triazine	
HMX	Octahydro-1,3,5,7-tetranitro-1,3,5,7-tetrazocine	
PETN	[3-Nitrooxy-2,2-bis(nitrooxymethyl)propyl] nitrate	

1.1.2 Chemistry of explosives

Chemical explosives are defined as compounds which experience violent decomposition producing heat, gas, and rapid expansion of matter[17] and can essentially be considered as a combustion reaction[4]. An explosive material will contain both a fuel and an oxidiser[6]. In some cases the fuel and oxidiser are brought together in the form of a mixture such as gunpowder, where charcoal and sulphur form the fuel component with potassium nitrate as the oxidiser[5], or the fuel and oxidiser may be contained within the same molecule, such as trinitrotoluene[6, 18]. As a general rule those compounds containing the fuel and oxidiser within the same molecule are more powerful as the two are in such close proximity[6, 18]. However, the performance of an explosive mixture can be increased by improving the mixing process[6, 7] and therefore bring the fuel and oxidiser into closer proximity with each other.

The explosive reaction can result in either a deflagration or detonation depending upon the speed of the reaction and the resulting shock (or pressure) wave. Deflagration occurs if the reaction results in an expansion of gas, known as a shock or pressure wave, that travels at a subsonic speed[4, 19]. Detonation occurs when the speed of reaction results in a supersonic shockwave[4, 19]. The effects of a detonation can be far more significant than that of a deflagration as the shock wave produced will have a greater force and therefore be more destructive, typically with a shattering and/or shearing effect[19]. However, location, and size of an explosion can also effect the destructive power[4].

As has already been stated, the reaction process undergone by an explosive is a combustion reaction. However, in the case of a deflagrating explosive the material will burn at a quicker rate and more fiercely than combustible material that is not explosive[6]. A deflagrating explosive can be initiated, or ignited in a number of ways such as shock, sparks, flame, high temperatures and friction[6].

Following initiation of a deflagrating explosive, plastic flow of the material, voids or bubbles in liquid being compressed, or friction between solid particles results in the

development of local, finite 'hotspots'. This results in the production of volatile gaseous intermediates and heat which react exothermically producing sufficient heat and energy to initiate the surrounding surfaces of the material in a process that is self-propagating[6].

The speed of reaction of a deflagration can be increased through confinement[6, 18, 19]. The process of confinement affects the speed of reaction by causing a build-up of gases produced during the reaction, and therefore an increase in internal pressure and temperature[6]. An example of the effect of confinement would be the comparison between black powder poured out and set alight and black powder within a pipe bomb. When black powder is unconfined it will burn, but when contained within a pipe bomb it will explode[19].

A detonating explosive will, following initiation, decompose through the passing of a shockwave through the material. The velocity of a shockwave in a detonation of solid and liquid explosives is typically between 1500-9000 ms^{-1} . The speed of the decomposition is dependent upon the speed of the transmission of the shockwave. There are two ways to achieve detonation, an initial shock or through burning to detonation[6].

Burning to detonation simply involves the ignition of an explosive material that is confined resulting in an increase in the burning rate. Therefore it can also apply to deflagrating explosives[6]. The other method of initiating a detonation is via a shockwave. Any shockwave used for this purpose must be of high velocity[6]. The shockwave initiates detonation by causing adiabatic heating, through the compression of particles in the explosive. This results in an increase in the temperature of the material to above the decomposition temperature. The shockwave is accelerated by the exothermic decomposition of crystals in the explosive material and when the velocity of the shockwave in the material is faster than the speed of sound the material will detonate. The time from initiation to detonation may be measured in microseconds[6].

1.1.3 'Homemade explosives'

'Homemade explosives' or HMEs are explosives that can be manufactured outside of a traditional laboratory, and with materials that are readily available to the general public[20]. Improvised explosives form a major focus in the forensic investigation of explosive-related events[21]. The internet has allowed information on how to produce HMEs, previously confined to anarchist literature, to become much more freely available[22]. Prominent examples of homemade explosives are the hydrogen peroxide based triacetone triperoxide (TATP) and hexamethylene triperoxide diamine (HMTD) whose structures are given in figure 1.1. HMTD (along with concentrated hydrogen peroxide) was the explosive used in the attacks on the London transport system on 7th July 2005[20, 21, 23]. TATP can be made using hydrogen peroxide and acetone[24, 25], both of which can be purchased easily in the form of hair bleach and nail polish remover (as well as other forms).

HMEs are typically more sensitive to stimuli than their legally manufactured counterparts[17, 26] resulting in a risk of accidental initiation[21]. This explains why although such materials have explosive properties, they have not been adopted as military or commercial explosives as they are considered too unsafe[25, 27, 28].

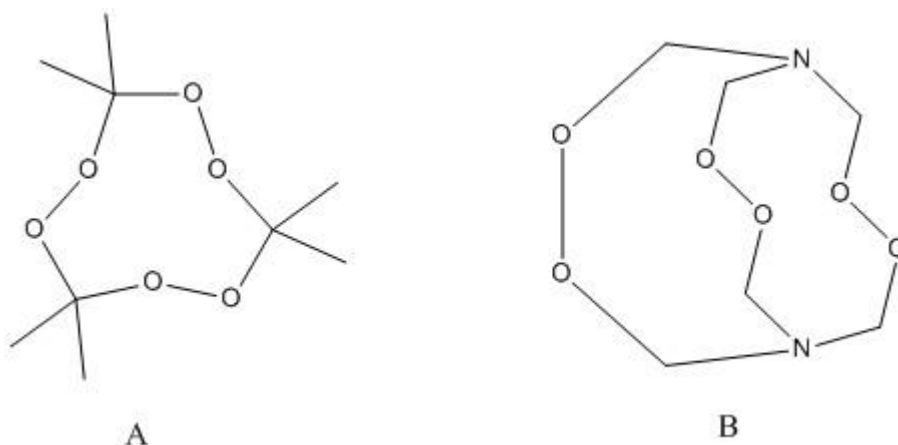


Figure 1.1 The chemical structures of A: TATP (in trimer form) and B: HMTD

1.1.3.1 Peroxide based materials

The classification of peroxide based materials covers three main explosives; TATP, HMTD and concentrated hydrogen peroxide mixed with organic materials (HPOM)[21]. TATP has been known as an explosive material since the late 19th century[2, 21, 28], however since the 1980s it has been used by terrorists with the first documented cases appearing in Israel[21, 28, 29]. As stated previously TATP can be produced using materials purchased from the High Street however, these materials are not pure and can result in the production of an impure explosive material. This is significant because the purity of the peroxide explosive will have an effect on its stability[22]. The instability and therefore risk of accidental initiation has resulted in bomb makers naming TATP "the Mother of Satan[22]". As a result of its use in terrorist attacks much research has been carried out to understand the chemistry and properties of TATP[17, 29-36]. TATP is a solid at room temperature, generally in the form of a crystalline material that is white in colour[21, 35]. In pure form, the melting point of TATP is 91-98.5°C with any impurities serving to lower this value[21, 35] and in addition to this at temperatures of around 60°C TATP has been found to sublime[21, 33]. This combined with a vapour pressure at room temperature of 6-7 Pa[21] means that it is extremely volatile which in turn means that it is very suitable for detection via a vapour detection system[21, 35]. TATP is an unusual explosive in that the mechanism by which it explodes is entropic[21, 31, 35]. This means that instead of an oxidation reaction the molecule decomposes in an entropy burst, producing acetone and carbon dioxide although thermal decomposition has also been observed in the gas phase. The detonation of TATP does not produce heat or any flames, these occur later as a result of the ignition of the acetone molecules released in the entropy burst through friction with the air[21].

HMTD emerged as an explosive used in terrorism at a similar time to TATP[28, 29, 37]. HMTD can be produced from hydrogen peroxide, hexamine and citric acid[38, 39]. While HMTD is more sensitive to stimuli such as friction than TATP, the molecule itself is more stable[21, 35, 40]. Unlike TATP where thermal

decomposition occurs in the gas phase, for HMTD this occurs in the condensed phase[21, 35, 41].

While TATP and HMTD are not the only 'homemade' organic peroxide materials that are capable of detonation, they are the only ones that have thus far been encountered by the forensic community[21].

Hydrogen peroxide vapour in a highly concentrated form can be explosive in its own right[21, 42] with hydrogen peroxide/water concentrations of around 60% capable of thermal decomposition[42]. More commonly the hydrogen peroxide is mixed with a fuel to create an explosive mixture[21]. The concentration of the hydrogen peroxide has been shown to be crucial for reliable detonation, for example the hydrogen peroxide present in the HMEs of the failed attack on the London transport system on 21st July 2005 was found not to be at a sufficiently high concentration to ensure detonation and as a result the devices failed to initiate[21].

1.1.3.2 Fertiliser based materials

In addition to illicit HME use ammonium nitrate also has several legitimate uses, as a fertilizer and in mining as the oxidiser in slurry explosives[21]. The availability of access to ammonium nitrate in the form of fertilizer has contributed to it being a common component of HMEs[21]. The fertilizer, which is generally in prill or powdered form, is mixed with a fuel such as fuel oil or sugar to create an explosive material commonly referred to as ANFO[21]. However, while ammonium nitrate explosive mixtures are common HMEs, such mixtures can suffer from large critical diameters[21]. This means that during detonation the release of energy is not fast enough to keep up with the shockwave which results in a loss of energy that is greater than the rate of energy being produced and as a consequence it is not possible to maintain a self-sustaining reaction.[21] This means that there is a risk that the explosive material will not detonate[21]. To combat this, high weights are often used for the charge, and the mixtures are confined to produce a significant increase in velocity of detonation[21].

Urea nitrate is another explosive that can be produced using fertilizer. Urea based fertilizer is reacted with nitric acid[21, 43]. Unlike ammonium nitrate mixtures where the fertilizer component is the oxidiser, in urea nitrate the fertilizer is the fuel to the nitric acid oxidiser[21]. Detonation of urea nitrate in the presence of a booster is more reliable than ammonium nitrate[21].

1.1.3.3 Inorganic salt based materials

Inorganic salt based materials tend to be physical mixtures of oxidising salts and a wide variety of fuels[22]. Inorganic salts include nitrates and nitrites, permanganates, chlorates and perchlorates[22] and as such the fertiliser based explosives described previously could also be classified as inorganic salt based explosives. Chlorate and perchlorate salts are commonly found in pyrotechnics, this is because, in general, these mixtures will deflagrate rather than detonate[21]. As a result perchlorate mixtures are only rarely used as high explosive materials; however chlorate mixtures have been used particularly in large improvised explosive devices such as the vehicle-borne devices seen in Northern Ireland during the IRA campaign of the 1980s and 1990s[22]. It is also believed that the vehicle-borne explosive device in the 2002 Bali Bombing was a mixture which included potassium chlorate[22].

Permanganate salts came to prominence in 2009 with the 'underpants bomber' Umar Farouk Abdulmutallab[22]. The initiation system for his failed explosive device was a mixture of ethylene glycol and potassium permanganate[21, 22]. The combination of an alcohol and potassium permanganate forms a hypergol[21] which is a material that can spontaneously combust[21]. Any future occurrences of permanganate salts in improvised explosive devices are most likely to be as part of initiation systems as, while sensitive to stimuli, they don't detonate[21].

1.1.4 Classification of explosives

There are two main classification systems for explosives. Neither has a significant advantage over the other and there are also other less frequently used systems in

existence. The system in use generally depends upon the nation responsible for the classification[44].

Explosive materials can be separated into two groups, primary and secondary explosives[17]. Primary explosives are generally used in detonators to initiate secondary explosives. This is because they are extremely sensitive, being initiated by friction, heat or sparks[17]. Initiation is reliable, but due to the ease of initiation it is only safe to handle such materials in small quantities. Secondary explosives are more stable than primary explosives, requiring a shockwave to initiate detonation[17, 18]. A detonator containing a primary explosive or a small amount of sensitised secondary explosive[17] is required to produce the shockwave that will detonate the bulk charge of secondary explosive.

The second classification separates explosive materials into two groups, high and low explosives[45]. While primary and secondary explosives are classified according to sensitivity, high and low explosives are classified according to their power. Low explosives are generally explosive mixtures used as propellants[46], while high explosives encompass a wider range of explosive compounds used for a variety of purposes.

An alternative to these classifications is to measure explosive compounds in terms of brisance, defined as “the destructive fragmentation effect of a charge on its immediate vicinity”[47] and could be described as a measure of the shattering that occurs to the area around the site of an explosion[4]. While it is impossible to quantify the performance of an explosive within a single parameter[47], brisance is often used as a relative measurement of performance.

Explosives can also be classified depending upon whether they deflagrate or detonate. However, this classification is somewhat fluid as a deflagrating explosive can sometimes detonate if confined. Secondary explosives and high explosives will generally detonate without confinement, however the strength of any explosion can be increased to a degree via confinement[18]. Similarly when classifying high and low explosives the separation can be carried out depending upon the speed of

the expansion of gases produced. Once again this is fluid as confinement can affect this[19].

Explosives can also be classified based on their chemical structure. This can take the form of four main categories; organic compounds with a nitro group, organic peroxides, inorganic salts and oxidiser/reducing agent mixtures[2]. Compounds containing nitro groups can be further subdivided into; nitroamines, nitrate esters and compounds where the nitro group bonds straight to a carbon atom[2].

Another alternative classification system would be to divide explosive materials by use. This has three categories; military, industrial/commercial and illicit improvised materials[2]. However, this classification does not provide a great amount of information about the explosive itself, although it is generally safe to assume that improvised materials will be more unpredictable in terms of sensitivity, stability and power[22]. To clarify, any explosive material could be deemed illicitly improvised if it was not produced under controlled, regulated conditions[21]. However, the focus of most investigation regarding improvised materials refers to 'homemade explosives' that have no commercial or military purpose[21], and are used in illegal activities[2].

1.1.5 Explosive devices and improvised explosive devices (IEDs)

The 'explosive train' is the name given to the components that make up an explosive device which result in a progressive increase of power culminating in the detonation of the main (or bulk) charge. Figure 1.2 provides a representation of the explosive train.

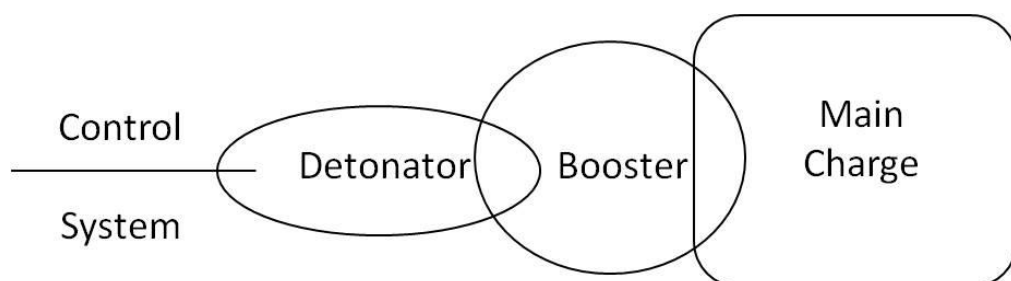


Figure 1.2 A block diagram representing the explosive train

The control system could be something as simple as a cord fuse, but generally is mechanical or electrical[17]. It is likely to contain a timing device to ensure that the operator is a safe distance away before the main charge explodes, the exceptions to this would be a device carried by a suicide bomber or a victim-initiated explosive device[17, 21, 22, 48]. The control system provides the stimulus to initiate the primary explosive within the detonator. The shockwave generated from this is sufficient to initiate a booster, normally composed of a small amount of sensitised secondary explosive which in turn produces a shockwave sufficient to initiate an explosion within the main charge that contains a bulk amount of secondary explosive. In some cases the booster is not required and the power of the detonator is sufficient to initiate the main charge. This will often depend upon the nature of the bulk explosive, and the amount of material within the main charge, generally large amounts will require a booster[17].

Improvised explosive devices (IEDs) will often contain all the parts of the 'explosive train' however, they can be differentiated from military and commercial explosive devices by the fact that at least one of the components will be improvised or 'homemade'[21, 22]. According to Beveridge[22] there are two basic elements of an IED and three additional components. The basic elements are the explosive and the initiation system[22], these can be seen as the 'explosive train'. The additional components are a container, binding material and shrapnel or other hazardous material[22] where "the nature of each device is determined by the nature of target, the ingenuity and skill of the bomb maker, and access to the components.[22]"

The control (initiation) system used in an IED will depend upon the type of explosive material within the IED and the method of initiation wanted (delay, victim or command)[22]. As stated previously, delay initiators ensure that the operator of the device is a safe distance away from the device when it detonates. In the case of an IED used in an attack this allows the perpetrator to be away from the location at the time of the explosion, and therefore potentially harder to trace after the

incident[22, 49]. A victim-initiated device is often colloquially described as a “booby trap[22]”. The initiation system will be designed to initiate the explosive without a delay, effectively like an on-off switch[22]. A command initiator will also act like an on-off switch but one that can be activated at a distance[22]. While not activated at a distance the on-off switch used in an IED carried by a suicide bomber could also be described as a command initiator[22]. Knowledge of the types of materials that may be incorporated within an IED is important for developing detection systems as the structure and makeup of an IED may mask the explosive material, potentially preventing its detection.

1.1.6 The use of explosives in terrorism

The UK threat level, at time of writing, from international terrorism is severe (on a scale of low, moderate, substantial, severe, critical[50]) , meaning that a terrorist attack is a strong possibility[51]. While terrorist attacks can take several forms, often the most common attack involves explosive materials. Terrorism, both international and domestic, is not a new problem, neither is the use of explosives as a terrorist weapon. What has changed is the scale and frequency of these attacks, and the development of the global media so that the public is more informed of attacks that occur[3].

One of the earliest, and certainly one of the best documented[21] terrorist use of explosives was the failed Gunpowder Plot in 1605[49], where a group of men led by Robert Catesby (including the now infamous Guy Fawkes) tried to assassinate King James I and the leaders of the ruling Parliament using gunpowder hidden in the cellars beneath the Houses of Parliament[21, 52]. Tensions between Irish nationalists and the British mainland led to several bombing campaigns, the first of which was as early as the 1880s[21, 51]. The targets of these attacks were mainly the police and government, and this led to the formation of the Police Special Branch as an arm of the Metropolitan Police Force (later spreading to all UK police forces) dedicated to the monitoring and prevention of threats to the State including terrorism[49]. Russia also saw a sustained bombing campaign with the Bolsheviks

carrying out attacks using explosive devices in the years that preceded them taking power[49].

While the majority of bombings are carried out by terrorist groups, there is also a threat from disaffected individuals[49]. In some ways these attackers are more dangerous as they are often harder to detect beforehand as, while the agendas of terrorist groups are often well known[49], the complaints of a particular individual may not become apparent until after the attack. Notable examples of such individuals are Ted Kaczynski, the Unabomber, who carried out a letter bomb campaign in the United States over a period of 18 years[49], Timothy McVeigh who was responsible for the Oklahoma City bombing[21, 49] and in 2011 Anders Behring Breivik who detonated a fertiliser bomb in Oslo, Norway[53, 54].

The use of explosives in terrorist attacks has changed over time[21, 49]. While the first targets were generally governments, the police or military, civilians are now also targeted[49]. Suicide attacks are also far more common and widespread, as is the idea of co-ordinated attacks where several bombs are detonated at the same time, or close together so as to cause the maximum damage and injury. Examples of this would be the Bali bombings in 2002[55] and the Boston Marathon bombing in 2013[56, 57]. The combination of explosives and other weapons has also become a method of attack, with the explosives often used to create a diversion, or panic. Two examples of this would be the terrorist attack in Mumbai in 2008[58] and the actions of Anders Behring Breivik in Norway in 2011, where a bomb detonated by government buildings in Oslo was used as a distraction to occupy police and security services while the perpetrator went on to carry out a shooting spree on the island of Utøya[54, 59, 60].

Public transport has become an increasing target for terrorist attacks[61]. Two of the most high profile attacks in the past decade were in Madrid in 2004[62] and London in 2005[63], both of which were also co-ordinated attacks. On 11 March 2004 four commuter trains in Madrid were attacked with ten explosive devices which detonated within the space of three minutes killing almost 200 people[62].

On the 7th July 2005 four explosive devices were detonated in London as people were travelling to work, three of the suicide bombers were on tube trains and the fourth was on a double-decker bus[63-65]. The four bombers and 52 civilians were killed[63-65].

The expansion of air travel has also resulted in aircraft being targeted[3]. While the first attack on a commercial aircraft using explosives actually dates back to 1949, as the number of passengers and the size of aircraft have increased so have the attacks against them with over 58 attacks on aircraft using explosives between 1970 and 2000[3]. As commercial aircraft have developed they have become targets carrying a higher number of passengers and therefore a higher number of casualties. For example, the attack on Pan Am Flight 103 involved a Boeing 747 aircraft which had 259 people on board, all of whom were killed, along with 11 people from the town of Lockerbie where the plane fell[3]. The size of IED used in this attack was relatively small[66] and demonstrates why aircraft make attractive targets to terrorists since a large number of people can be targeted with a relatively small explosive[3]. In the past 20 years there has been an increase on the number of attempted suicide attacks on commercial aircraft; in 2001 Richard Reid attempted to blow himself up on board American Airlines Flight 63 with an IED hidden in his shoe[21]. In 2006 a plan to use liquid explosives in a coordinated attack of transatlantic flights was stopped by security services[22] and in 2009 Umar Farouk Abdulmutallab attempted to blow himself up on Delta Flight 253 with a device concealed inside his underwear[22].

The materials used have also evolved[22], this can be observed by comparing the attacks on aircraft mentioned above. The explosive used in the attack on Pan Am Flight 103 was Semtex H[21], a commercially available explosive. However, in all of the attempted suicide attacks, all or at least part of the improvised explosive material was 'homemade' with TATP featuring in the initiation systems of both Reid and Abdulmutallab[21]. This shift towards HMEs is in part due to a tightening of controls on the purchase of commercial explosives, and increased security for

military explosives making such materials harder to acquire without detection[22]. Indeed an attack carried out with military or commercial explosives would suggest an act of state-sponsored terrorism[49] such as the attack on Pan Am Flight 103 for which responsibility has been taken by the Libyan government[67]. Another part of the shift towards HMEs is to evade detection, for example using an explosive material that contains no heavy metals to avoid x-ray, or metal detection[3] (although of course this can also require the construction of an IED without any metallic components to be truly effective). The use of non-nitrated explosives such as the peroxide based materials can evade detection when using older detection systems aimed at identifying the nitrogen groups present in many military and commercial explosives[22].

As security services take steps to counter the threats from IEDs, terrorists continue to innovate and develop new ways to evade detection[22]. Therefore there is a continuing need for security services to combat the threat of terrorist attacks using explosives.

1.2 Analysis of explosive materials

While there is a threat from explosives attacks there is a need for the security services and forensic science community to combat this threat[3, 19, 68]. The nature of this threat is varied and constantly evolving, meaning that new ways to prevent these attacks must continually be developed. It must also be acknowledged that due to the varied nature of the threat, a single approach is unlikely to be the best solution[3, 68, 69].

The defence against terrorist attacks can be divided into two areas; explosives detection and post blast investigation[25, 46, 69], with intelligence gathering playing a role in both areas[2, 20, 22]. These areas require different approaches, however there may be some techniques which are applicable to all aspects[68] and therefore wider knowledge of the different areas will benefit the development of a specific aspect.

With the emergences of HMEs a common part of forensic investigation of explosive crimes is linking explosive materials to their precursors[70]. Therefore the development of techniques that can assist in linking precursor materials to the explosive used in an improvised device, such as the one developed in this research project, is an area of significant development[70-73]. The ability to link an explosive material to its precursors is of substantial importance as it could help to identify the manufacturer of an HME and other parties involved in the supply of materials for its manufacture. Work currently being undertaken in Sweden, as part of the EMPHASIS project, is an example of how information on explosive precursors and waste products created during the formation of explosive materials can be utilised to identify potential bomb factories and thereby locate explosive materials. The detection system under development uses spectroscopy sensors in the sewer system to detect precursor materials, working on the theory that without proper waste disposal facilities, such materials would end up in the sewer system having been poured down sinks and toilets[74-76].

This linking technology can be applied to several forensic areas outwith the field of explosives detection and characterisation, such as drugs, document analysis and ignitable liquids[77-81] as well as other forms of illicit manufacture[82, 83]. An example of this use is demonstrated in research carried out at the University of Strathclyde that demonstrates that it is possible to determine the synthetic route used to produce methylamphetamine through the identification of route specific markers. Furthermore this research suggested that different starting products, in this case different cold medications, could also be identified from the final product[77-79]. Since HMEs are often produced in a similar way to illicit drugs such as methylamphetamine, it is likely that similar markers could be identified for explosive materials.

A common technique for this type of linking analysis is isotope ratio mass spectrometry (IRMS)[70, 79]. however FTIR and other spectroscopic techniques could prove to be a faster and cheaper alternative to elemental analysis.

1.2.1 Intelligence gathering

Intelligence gathering plays a role in both the detection of explosives and post blast investigation. Where possible intelligence gathering aims to prevent attacks from occurring by apprehending those planning an attack before they can carry it out[84-87]. However, where this hasn't been possible intelligence can be gathered from the forensic information collected at the scene of an explosion and at possible illicit explosives manufacturing sites in order to help bring the culprits to justice[20, 69, 88].

Intelligence gathering is primarily carried out by the police and security services[20, 87]. However, forensic scientists may be called upon to increase the scope of the intelligence gathered[20, 88]. For example, using forensic science to identify explosive materials in waste water in order potentially to indicate the location of an illicit bomb factory[25]. The analysis of precursor materials could also be utilised to aid the detection of bomb making factories. Intelligence gathering has prevented several major plots, for example in the UK the plot to use liquid explosives in a co-ordinated attack on commercial aircraft in 2006[22].

1.2.2 Post blast investigation

In a situation where an explosive device has fully or partially detonated, forensic scientists and the security services will investigate to determine the cause of the explosion and attempt to identify the person or persons responsible. In the United Kingdom the Forensic Explosives Laboratory (FEL), part of the Defence Science and Technology Laboratories (Dstl), undertakes much of the investigation of incidents involving explosives[89]. Work by FEL and other research laboratories around the world has led to the capability to detect even minute amounts of explosive which, after a successful detonation, may be all that remains[17].

Post blast investigation can also involve the investigation of secondary crime scenes such as a clandestine explosive laboratory[20, 22]. This can be very important if the primary scene has yielded little or no information about the type of explosive used,

as a clandestine laboratory is likely to contain precursor materials that can be used to determine the explosive material and there may also be unexploded material that had not been included in the IED[20, 88]. Even in a situation where the explosive material, or other components of the IED, have been identified at the primary scene, investigation of a clandestine laboratory can help to identify those responsible by linking the laboratory to the IED[20].

1.3 Explosives detection

Forensic science has a significant role to play in the area of detection of explosives and explosive devices. The detection of explosive devices is critical in the prevention of terrorist attacks, and therefore it is unsurprising that this is an area of substantial research[3, 68, 90-92]. Due to the wide ranging nature of the threat, the detection methods are also wide ranging[17, 68]. A method that might be suitable for scanning plane cargo is unlikely to be suitable without modification for use on the battlefield. Therefore the detection method should be tailored to the specific situation in which it is going to be utilised.

While security concerns are the primary reason for developing detection techniques and systems, there are several other circumstances where explosives detection is required. Environmental monitoring needs the capacity to detect trace amounts of explosives which may be causing contamination of water supplies[25, 27]. It is also necessary to monitor the environment within explosives manufacturing plants to ensure that workers are not exposed to dangerous levels of potentially dangerous chemicals[25, 27]. Similarly biomedical tests are required particular for those working in munitions factories, to monitor levels of explosives within the body as many explosive can have toxic effects[25, 27]. Also, analysis of explosives in industry is necessary; with the need to monitor the manufacturing process to ensure product quality through the capability to detect variation in the explosives[25, 27, 45]. Similarly, there is a need to be able to detect the degeneration of explosives in storage as changes in composition can have serious safety and performance implications[46].

The detection of illicit explosives is beset by several problems. The variety of possible explosive compounds that can be used, in particular HMEs, provide a constantly evolving collection of explosive mixtures. There is also significant variety amongst potential targets which means that a single detection technique is unlikely to be suitable for all situations. A further hindrance to explosives detection is the efforts of the bomb makers to overcome the detection methods. A prime example of this is the development of metal-free improvised explosive devices to evade detection with metal detectors[53, 93].

A successful detection system should have several key features. It needs to be sensitive and specific, but not to a level that means that it has a high false alarm rate[68]. The analysis needs to be rapid and be able to handle a high throughput[93]. The detection method shouldn't disturb the explosive material, otherwise there is a risk of initiating the explosive device through the use of the detection technique[68]. In a civilian setting, a detection system should be relatively noticeable, as in this manner it can act as a deterrent as well as detecting possible threats. In a military setting the focus is more upon portability and robustness in a harsh environment[68].

The wide variety of potential HMEs and HME precursors present a significant challenge for detection, not only through sheer weight of numbers but also because many of them do not contain the 'characteristic groups' exploited by many existing detection techniques[35]. For example many military grade explosives such as TNT contain nitro groups and these are a common detection target, however TATP does not contain nitrogen and therefore could not be detected using equipment aimed at that target[35, 68]. Therefore there is a need for innovative development of detection systems for materials such as hydrogen peroxide. Techniques such as electrochemical and chemiluminiscent detection can be applied to the detection of hydrogen peroxide[91, 94, 95].

Detection can be divided into three main areas; bulk, trace and stand-off. Each detection area is approached in a different way, although there are some aspects that can be applied to all three.

1.3.1 Bulk detection of explosives

Bulk detection of explosives is concerned with the detection of large amounts of explosive material[3], where bulk explosives can be defined as explosives and their components that are visible with the naked eye or using a low powered microscope (up to x20) [20]. Bulk detection will normally look for a specific feature associated with explosive compounds[68], for example to detect many commercial explosives such as TNT a system could aim to detect nitrogen groups. This allows a single detection system to be capable of detecting any explosive material containing a nitrogen group. However, this also means that bulk explosive detection can be prone to false alarms as these features are also present in various non-explosive compounds.

1.3.2 Trace detection of explosives

Trace detection is concerned with the detection of much smaller amounts of explosive material[3]. Trace explosives can be defined as explosives and their components that are not visible without the use of a high powered microscope (above x20)[20]. Trace detection will normally look for a specific chemical (often through comparison with a library)[68]. This can still produce false positives, but also can result in false negatives if the specific chemical has been masked[68] and therefore doesn't match with the library. The use of library comparison can also slow down the analysis which is not ideal for high throughput use[96-98].

1.3.3 Stand-off detection of explosives

Stand-off detection can be aimed at bulk or trace explosives, however the key feature of a stand-off detection system is that no contact is made with the explosive material[68]. Therefore there is a reduced risk of accidental initiation of the explosive device, and if an accidental initiation did occur the operator of the

detection system is a safe distance away from the device[99]. However, because no physical contact is made with the suspected explosive device this does pose problems as to how to carry out the analysis[68]. The majority of stand-off techniques are spectroscopy based as it is possible to direct a beam (of something such as infrared light) across a large distance to the suspect material, however there are still problems in how to return the beam to the detection device which has limited this technology[100]. Despite the potential problems the ability to analyse a suspected device at a distance is sufficiently significant that there is considerable research on this topic[90, 99, 101-108]. It has also been suggested that stand-off detection (providing suitable detectors were available) would be the most effective way to combat pedestrian suicide bombers, however, research by Kaplan and Kress [85] suggests that in fact improving intelligence gathering to identify potential suicide bombers would be more effective.

1.3.4 Current detection systems

As already discussed there are multiple different approaches to the detection of explosives and IEDs. Therefore there are several different ways that the various different detection techniques can be separated[91, 92]. One method is to use three categories; imaging techniques, vapour detection systems and particle detection systems.

1.3.4.1 Imaging techniques

Imaging techniques can be described as any techniques which produce a visual image of whatever is being scanned. These form the basis of the majority of older detection systems[3, 92].

X-ray equipment is commonplace at airports and left luggage storage areas[3]. X-ray scanning was first introduced into airport security systems to prevent hijackings, therefore focusing on hand, or carry-on, luggage and the detection of weapons[3]. However, more recently X-ray detection has also been routinely used for the

detection of explosive devices, in particular in hold, or checked, baggage[3]. Initially this proved to be less successful, with a prominent example being the bombing of Pan Am Flight 103 where the luggage had undergone X-ray scanning but the explosive device had not been detected[3]. This according to Connelly *et al.*[3] was due to two factors. Firstly the X-ray attenuation of explosive materials can be similar to that of other items found in luggage[3] and secondly checked baggage is larger and more densely packed than the luggage that the system had been previously applied to[3]. Therefore the existing basic X-ray system was not suitable for detecting explosive devices in checked baggage[3]. This was combated by the development of dual energy systems. This involves scanning an object at two different X-ray energy levels and observing the ratio between the two of them. This allows the discrimination of objects that were previously undistinguishable with basic X-rays[3]. Further improvements have been made by introducing computed tomography (CT) to X-ray systems. This involves the collection of X-ray transmission data from several angles around the object within a particular plane, which can then be used to produce a 'slice plane' image allowing a increased amount of detail to be seen[3]. There has also been progress in the development of automated systems for X-ray scanning, with the majority of hold luggage scanning being automated, although a degree of human interaction is still required[3].

Another technique used for examining luggage is neutron analysis, which works through the detection of gamma rays produced when certain elements present within explosive compounds are exposed to neutrons[27]. Due to the nature of the radiation involved in both these techniques they are only used on luggage rather than individuals, which means that on their own they cannot cover all the possible risks as the explosive device may be attached to the bomber.

Several variations of an imaging detection system that is capable of scanning members of the public have been developed and have begun to appear in airports and other national entry points. This is the full body scanner which uses electromagnetic radiation, millimetre wave, or x-ray backscattering[109] effectively

to 'see' through a person's clothing to determine if they are concealing anything. In the UK these systems began to be used from 2010, firstly at Manchester and Heathrow airports, and gradually being deployed across the other UK airports as part of an ongoing process[109-111]. However, there has been a significant amount of negative public feeling towards this process as most of the systems produce an image of the individual in which they are effectively naked. There were concerns about the control of these images and which individuals are allowed to view them[112], as well as unnecessary concerns over the safety of the electromagnetic radiation used[109-112]. Concerns were also raised about racial profiling and the methods used to determine who would need to be subject to scanning as currently not all passengers pass through these scanners[113-115]. While not technically an imaging technique as no image is produced, metal detector arches are also used as a method of scanning individuals, however with the development of metal-free explosive devices[21, 22] this is no longer the best method for identifying a potential bomb carrier.

1.3.4.2 Particulate detection

Ion mobility spectrometry (IMS) is a prominent technique used in the detection of explosive materials[91, 116]. IMS is capable of sampling both vapours and particulate samples, which has led to two avenues of detection; bench-top systems which test particulates taken by swabbing a surface, and personnel portals which sample vapours from an individual. It has also been possible to produce rugged, portable systems[116], which makes the technology suitable for use in theatre. IMS exploits the differences in drift time of different ions within a drift gas. This allows the separation of ions based upon mass, with heavier ions moving more slowly than lighter ones[117]. Most airports now have a bench-top system in place where swabs can be taken of items such as laptops, shoes and wheelchairs. The swab is then inserted into the machine where any particulates are desorbed and then analysed. The instruments have a rapid analysis time and are reasonable sensitive. However, the individuals who operate the instruments may receive only limited training and as such the performance of the system can be reduced, for example it is not

uncommon to observe the same swab being used for several different objects. With the personnel portals an individual stands in a relatively enclosed space to force any explosive vapour into the spectrometer. Once the vapour is within the instrument the analysis occurs in the same manner as with the bench-top instrument.

Thus far the majority of IMS systems have been designed to detect legally manufactured explosives, and therefore have focussed upon the detection of nitrogen containing groups, thus meaning alterations are necessary for the detection of HMEs. These improvements to increase the range of compounds detected by the equipment have, as yet, not been completely successful[91].

1.3.4.3 Vapour detection

The 'gold standard' of explosives detection is often considered to be the sniffer dog[118-120]. Canine detection is widely used, not just in the field of explosives detection but also in drug searches, fire scene investigation, and specialised cadaver dogs may be used in the search for human remains. However, despite their successes, it is an expensive process to train and care for these dogs; the dogs can only work for a certain length of time, and environmental conditions such as heat can affect performance[118] . A great deal of time must also be invested in training the dog handlers, with one of the early research reports on the training of dogs for explosives detection stating that "handler selection is a critical factor in the ultimate success or failure of the explosives detector dog concept"[121]. Despite using sniffer dogs for many years, the understanding of how the dogs work is still not complete. Therefore, research into instrumental methods that could provide an effective alternative to sniffer dogs is viewed as a priority. Table 1.3 shows a comparison of canine detection and existing instrumental methods as compiled by Connelly *et al.*[3].

As Table 1.3 shows both canine and instrumental systems have advantages and disadvantages. However, there is scope to improve instrumental techniques, but the development of vapour detection techniques has been relatively slow[91, 122-124]. This is in part due to the varying vapour pressures of explosive compounds

meaning that not all materials would be suitable for vapour detection. In particular, plastic explosives have relatively low vapour pressures due to the binding effect of the plasticisers[6, 124]. Wrapping of the explosive materials can also reduce the vapour released into the atmosphere[25]. However, the increased use of HMEs instead of commercial grade explosives means that the significant explosive threat is posed by compounds with a higher vapour pressure, making vapour pressure detection more likely and making the continued development of vapour detection techniques a priority.

Table 1.3 A comparison of canine and instrumental vapour detection methods[3]

Factor	Canines	Instruments
Sensitivity	Unknown	Characterised
Training	Specialized	Basic
Transportable	Self portable	Some portable, some not
Selectivity	Classes of compounds	Chemical selected for analysis
Processing time	Instantaneous (ms)	1s to 2 min: typical 10s
Sampling	Particle or vapour Extremely efficient	Usually one or the other Inefficient
Calibration	No field methods	Well established kits
Duty cycle	Short: one or two hour shifts	24h shift
Search	Dogs can go to source	Most acquire remote sample
Maintainability	High maintenance	Low maintenance

In addition to the varying vapour pressures of different explosive materials, another area that has posed problems with many vapour detection systems is the collection of the vapour in order to introduce it into the instrument[93]. A vapour detection system must also be capable of identifying threat materials amongst the many contaminants also present in the atmosphere such as cigarette smoke and perfumes[99, 124, 125]. Despite these problems there are some vapour based techniques in use and further systems are being developed[99, 124]. Current techniques include gas chromatography with a selection of detectors including; thermal energy analysers, ion mobility spectrometers and mass spectrometers[27]. These are used both in theatre and also for scanning luggage. However, these chromatographic methods are restricted by their reliance upon a high vapour pressure of the explosive material and the need to be in close proximity to the material.

1.3.4.2.1 Personnel portals

Personnel portals are an area of significant development. While there are already some systems in use, these can cause delays in the flow of people through a security point as for most portals an individual is required to stand for a period of time within the portal[93]. The number of explosive compounds that the current portals are able to detect is also limited.

A newly developed personnel portal system designed by Cascade Technologies and Morpho uses Quantum cascade lasers (QCLs) for detection rather than the IMS systems used by the majority of existing personnel portals. By using a mirrored multipass cell, a long path length is produced to allow for maximum interaction between any potential explosive vapours and the laser beam. Figure 1.3 shows an image of the portal on trial at Glasgow airport, while figure 1.4 provides a basic diagram of the internal structure of the portal. It is an archway design, with fans built into one side of the arch to direct the airflow across to the absorption cells; label A shows the three multipass cells where any vapour can interact with the three laser beams, label B shows three QCLs and detectors aligned with the three

multipass cells (there is space for one additional QCL and multipass cell within the housing). Also contained within the area of A and B is the computing and processing equipment to analyse and notify any detection that occurs. Label C shows where an individual passes through the arch and label D identifies the bank of fans which blow air across the individual as they pass through, directing any vapour to the multipass cells (A) The system allows for real-time monitoring of any absorption that occurs. Currently the lasers used are capable of detecting hydrogen peroxide and ammonia, both of which are seen as potential explosive precursors[91], and also as degradation products of explosive compounds. Hydrogen peroxide in high enough concentrations is also explosive in its own right.



Figure 1.3 The Portal detection system on trial at Glasgow Airport[9]

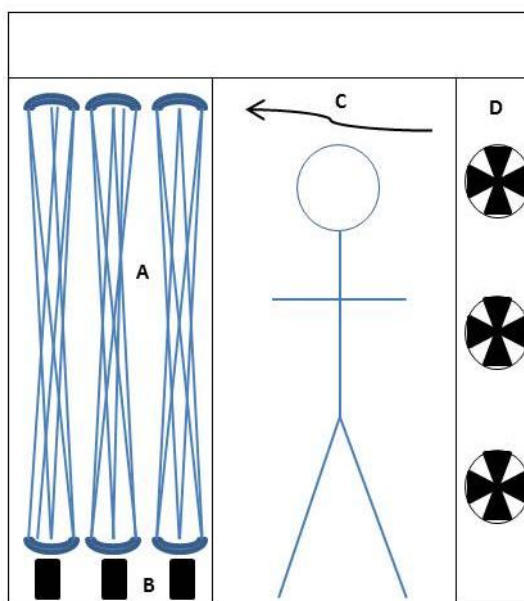


Figure 1.4 A basic diagram of the Portal system.

Further work is needed to refine the algorithms used to determine whether a compound has been detected and to develop the necessary systems for dealing with a flow of people through the detector. There is also a need to expand the number of compounds that the portal can detect, with the ultimate aim to produce a system that can easily be adapted to any new explosive threats that emerge. This research project aimed to assist the development of this system through the characterisation of materials to discover identifying spectral features that could be targeted by a QCL for detection.

1.3.5 Future detection systems

The ongoing threat of terrorist attacks and the evolution of the IEDs used means that new, or adapted, detection systems need to be developed[17, 21, 22, 68, 120].

There are several potential detection systems under development. The majority of these are spectroscopic techniques[100, 126, 127] and many are aimed at producing a detector which would allow liquids to be taken through airport security and so remove current restrictions.

While colorimetric tests have generally been replaced by instrumental techniques[46], a hydrogen peroxide vapour indicator has been developed which uses the bleaching effect of hydrogen peroxide to cause a visible colour change[128]. However, while this could prove useful as a monitor, it would only indicate the presence of hydrogen peroxide based explosives and therefore could not be used as the sole detection system.

There are some techniques used for environmental explosives detection, such as immunosensors[25, 27], which could be adapted for use in a security setting. Their use in an environmental setting has demonstrated that these techniques are suitably sensitive for detecting trace amounts of explosive compounds, and the use of antibodies make the technique very specific. However, as yet, the potential for the use of immunochemical detection devices in a security capacity has not been explored.

In addition to adapting techniques from an environmental setting, or other analytical areas, there is also significant scope to improve existing detection systems, and those currently still in the developmental and trial stages. One example would be the adaptation of the existing Portal system to detect multiple compounds.

Work is also required to improve the way a positive result is dealt with in, for example, airport security areas to offset the build-up of queues. Research has shown that Raman spectroscopy has a lot of potential for use as a detection system[91, 101, 102, 104, 129, 130]. However, there is still a need to overcome the problems of fluorescence and low signals in order for it to be truly effective. Any spectroscopic stand-off techniques need to develop a reliable way of reflecting the signal back to the detector. This is a particular issue in theatre where there may not be many naturally occurring reflective surfaces[124, 125].

To conclude, there is still much work to be done to develop effective detection systems for the prevention of explosive-based terrorist attacks. There are many considerations that must be taken into account when developing a detection

system, and due to the wide ranging nature of the threat it is unlikely that a single detection system will be appropriate for all situations.

1.4 References

1. Carlysle, F., Nic Daeid, N., Normand, E. and McCulloch, M., *Exploiting High Resolution Fourier Transform spectroscopy to inform the development of a quantum cascade laser based explosives detection system*. in *Optics and Photonics for Counterterrorism, Crime Fighting, and Defence VIII*. 2012. Edinburgh: SPIE.
2. Tamiri, T. and Zitrin, S., *Explosives: Analysis*, in *Encyclopedia of Forensic Sciences*, P.J. Saukko and J.A., Siegel, Editors. 2013, Elsevier.
3. Connelly, J.M., Curby, W.A., Fox, F.T. and Hallowell, S.F., *Detection of Hidden Explosives*, in *Forensic Investigation of Explosions*, A.D. Beveridge, Editor. 1998, Taylor and Francis.
4. Crippin, J.B., *Explosions*, in *Encyclopedia of Forensic Sciences*, P.J. Saukko and J.A. Siegel, Editors. 2013, Elsevier.
5. Hopler, R.B., *The History, Development, and Characteristics of Explosives and Propellants*, in *Forensic Investigation of Explosions*, A.D. Beveridge, Editor. 1998, Taylor and Francis.
6. Akhavan, J., *The Chemistry of Explosives*. RSC paperbacks. 2008: RSC.
7. Jeacocke, J., *The Gunpowder Era*, in *Explosives in the Service of Man: The Nobel Heritage*, J.E. Dolan and S.S. Langer, Editors. 1997, RSC.
8. Dolan, J.E., *The Nobel Era*, in *Explosives in the Service of Man: The Nobel Era*, J.E. Dolan and S.S. Langer, Editors. 1997, RSC.
9. Weisstein, E.W. *Eric Weisstein's World of Biography*. 2007 [cited 2011 06/09/2011]; Available from: <http://scienceworld.wolfram.com/biography/Schonbein.html>.
10. *Encyclopedia Britannica*. [cited 2014 14/02/2014]; Available from: <http://www.britannica.com/EBchecked/topic/492672/RDX>.
11. Sun, Y., *Field Detection Technologies for Explosives*. 2010: ILM Publications.
12. Baptista, R.J. *Amatol Explosives Factory Aintree, United Kingdom*. 2009 [cited 2011 07/09/2011]; Available from: <http://www.colorantshistory.org/AintreeExplosives.html>.
13. Braidech, M.M., Keepers, H.V., and Davis, H.H., *Texas City, Texas, Disaster*, Fire Prevention and Engineering Bureau of Texas, Dallas, Texas. The National Board of Fire Underwriters: Texas City.
14. CEDRE. *Ocean Liberty*. 2009 [cited 2011 07/09/2011]; Available from: http://www.cedre.fr/en/spill/ocean_liberty/ocean_liberty.php.
15. Qasim, M.M., Moore, B., Taylor, L., Honea, P., Gorb, L. and Leszczynski, J., *Structural characteristics and reactivity relationships of nitroaromatic and nitramine explosives - A review of our computational chemistry and spectroscopic research*. International Journal of Molecular Sciences, 2007. **8**(12): p. 1234-1264.
16. Richard, R.M. and Ball, D.W., *Density functional calculations on the thermodynamic properties of a series of nitrosocubanes having the formula C₈H_{8-x}(NO)_x (x=1-8)*. Journal of Hazardous Materials, 2009. **164**(2-3): p. 1552-1555.
17. Marshall, M. and Oxley, J.C., *Explosives: The Threats and The Materials*, in *Aspects of Explosives Detection*, M. Marshall and J.C. Oxley, Editors. 2009, Elsevier B.V. p. 11-26.

18. Akhavan, J., *Explosives and Propellants*, in *Kirk-Othmer Encyclopedia of Chemical Technology*, A. Seidal, Editor. 2004, Wiley.
19. Tilstone, W.J., Savage, K.A., and Clark, L.A., *Forensic Science: An Encyclopedia of History, Methods, and Techniques*. 2006: ABC-CLIO.
20. Speers, N., Otieno-Alego, V. and Ritchie, K., *Clandestine Explosive Laboratories*, in *Encyclopedia of Forensic Sciences*, P.J. Saukko and J.A. Siegel, Editors. 2013, Elsevier.
21. Doyle, S., *Improvised Explosives*, in *Encyclopedia of Forensic Sciences*, J.A. Siegel, Editor. 2013, Elsevier.
22. Beveridge, A.D., *Improvised Explosive Devices*, in *Encyclopedia of Forensic Sciences*, J.A. Siegel, Editor. 2013, Elsevier.
23. Lubczyk, D., Siering, C., Lorgen, J., Shifrina, Z.B., Mullen, M. and Waldvogel, S.R., *Simple and sensitive online detection of triacetone triperoxide explosive*. *Sensors and Actuators B-Chemical*, 2010. **143**(2): p. 561-566.
24. *Anarchist's Cookbook*. [cited 2013 08/11/2013]; Available from: [http://www.anarchistcookbook.com/showthread.php/8511-tricycloacetone-peroxide-\(TATP\)](http://www.anarchistcookbook.com/showthread.php/8511-tricycloacetone-peroxide-(TATP)).
25. Yinon, J., *Forensic and Environmental Detection of Explosives*. 1999: Wiley.
26. Schubert, H., *Disposal of Improvised Explosives and -Devices*, in *Detection and Disposal of Improvised Explosives*, H. Schubert and A. Kuznetsov, Editors. 2006, Springer. p. 1-6.
27. Yinon, J., *Field detection and monitoring of explosives*. *TrAC Trends in Analytical Chemistry*, 2002. **21**(4): p. 292-301.
28. Zitrin, S., *Analysis of Explosives by Infrared Spectrometry and Mass Spectrometry*, in *Forensic Investigation of Explosions*, A.D. Beveridge, Editor. 1998, Taylor and Francis.
29. Zitrin, S., S. Kraus, and Glattstein. B., *Identification of two rare explosives*. in *1st International Symposium on Analysis and Detection of Explosives* 1983. Washington D.C.: US Government Printing Office.
30. Capua, E., Cao, R., Sukenik, C.N. and Naamana, R., *Detection of triacetone triperoxide (TATP) with an array of sensors based on non-specific interactions*. *Sensors and Actuators B-Chemical*, 2009. **140**(1): p. 122-127.
31. Dubnikova, F., Kosloff, R., Almog, J., Zeiri, Y., Boese, R., Itzhaky, H., Alt, A. and Keinan, E., *Decomposition of Triacetone Triperoxide is an Entropic Explosion*. *Journal of the American Chemical Society*, 2005. **127**(4): p. 1146-1159.
32. Dubnikova, F., Kosloff, R. and Zeiri, Y., *Rational Detection Schemes for TATP NATO Advanced Research Workshop*, in *Detection and Disposal of Improvised Explosives*, H. Schubert and A. Kuznetsov, Editors. 2006, Springer.
33. Evans, H.K., Tulleners, F.A.J., Sanchez, B.L. and Rasmussen, C.A., *An Unusual Explosive, Triacetone triperoxide (TATP)*. *Journal of Forensic Sciences*, 1986. **31**(3): p. 1119-1125.
34. Matyas, R., Pachman, J., *Study of TATP: Influence of Reaction Conditions on Product Composition*. *Propellants, Explosives, Pyrotechnics*, 2010. **35**: p. 31-37.
35. Oxley, J. and Smith, J., *Peroxide Explosives*, in *Detection and Disposal of Improvised Explosives*, H. Schubert and A. Kuznetsov, Editors. 2006, Springer. p. 113-121.
36. Oxley, J., Smith, J., Brady, J., Dubnikova, F., Kosloff, R., Zeiri, L. and Zeiri, Y., *Raman and Infrared Fingerprint Spectroscopy of Peroxide-Based Explosives*. *Applied Spectroscopy*, 2008. **62**(8): p. 906-915.
37. Reutter, D.J., Bender, E.C. and Rudolph. T.L., *Analysis of an unusual explosive: methods used and conclusion drawn from two cases*. in *1st International*

- Symposium of Analysis and Detection of Explosives*. 1983. Washington D.C.: US Government Printing Office.
38. *Anarchist's Cookbook*. [cited 2014 18/02/2014]; Available from: <http://www.anarchistcookbook.com/showthread.php/22625-HMTD-Question/page6>.
 39. Aerodynamic Inventions. 1999 [cited 2014 18/02/2014]; Available from: <http://www.geocities.ws/johnwiltbank/hmtd.html>.
 40. Oxley, J.C., Smith, J., Chen, H. and Cioffi, E., *Decomposition of multi-peroxidic compounds: Part II. Hexamethylene triperoxide diamine (HMTD)*. *Thermochimica Acta*, 2002. **388**(1-2): p. 215-225.
 41. Schulte-Ladbeck, R., Vogel, M. and Karst, U., *Recent methods for the determination of peroxide-based explosives*. *Analytical and Bioanalytical Chemistry*, 2006. **386**(3): p. 559-565.
 42. Monger, J.M., Baumgartner, H.J., Hood, G. and Sanborn, C.E., *Explosive Limits of Hydrogen Peroxide Vapor*. *Journal of Chemical and Engineering Data*, 1964. **9**(1): p. 119-124.
 43. Rose, L. *What is Urea Fertilizer?* [cited 2014 19/02/2014]; Available from: <http://homeguides.sfgate.com/urea-fertilizer-48588.html>.
 44. Rudin, I., *Discussion - Principles for a new Swedish System to Codify Explosives*. *Annals of the New York Academy of Sciences*, 1968. **152**(A1).
 45. *Manufacture and storage of explosives: Manufacture and Storage of Explosives Regulations 2005*. Approved Code of Practice and Guidance. 2005: HSE Books.
 46. Yinon, J. and Zitrin, S., *The Analysis of Explosives*. Pergamon Series in Analytical Chemistry. 1981: Pergamon Press.
 47. Meyer, R., Kohler, J. and Homburg, A., *Explosives*. 5th completely revised edition ed. 2002: Wiley-VCH.
 48. Kuznetsov, A.V. and Osetrov, O.I., *Detection of Improvised Explosives (IE) and Explosive Devices (IED)*, in *Detection and Disposal of Improvised Explosives*, H. Schubert and A. Kuznetsov, Editors. 2006, Springer.
 49. Williams, C., *Terrorism Explained: The Facts about Terrorism and Terrorist Groups*. 1st ed. 2004: New Holland Publishers.
 50. [cited 2011 09/09/2011]; Available from: <http://www.homeoffice.gov.uk/counter-terrorism/current-threat-level/>.
 51. Home Office. [cited 2012 01/11/12]; Available from: <http://www.homeoffice.gov.uk/counter-terrorism/current-threat-level/>.
 52. Malam, J., *The Gunpowder Plot 5th November 1605*. *Dates with History*. 2008: Cherrytree Books.
 53. Hendrickx, J.M.H., Molina, A., Diaz, D., Grasmueck, M., Moreno, H.A. and Hernandez, R.D., *Humanitarian IED clearance in Colombia*, in *Detection and Sensing of Mines, Explosive Objects, and Obscured Targets Xiii*, R.S. Harmon, J.H. Holloway, and J.T. Broach, Editors. 2008, Spie-Int Soc Optical Engineering: Bellingham.
 54. Fekete, L., *The Muslim conspiracy theory and the Oslo massacre*. *Race and Class*, 2012. **53**(3): p. 30-47.
 55. Royds, D., Lewis, S.W. and Taylor, A.M., *A case study in forensic chemistry: The Bali Bombings*. *Talanta*, 2005. **67**(2): p. 262-268.
 56. *The Boston Marathon bombings: a post-event review of the robust emergency response*. *ED management : the monthly update on emergency department management*, 2013. **25**(7): p. 73-8.

57. Qian, L.J., Fuller, J. and Simpson, C., *A Community Sensing Framework for Threat Detection in Metropolitan Area*. 2013 IEEE International Conference on Technologies for Homeland Security. 2013, New York: IEEE. 259-264.
58. Bhandarwar, A.H., Bakhshi, G.D., Tayade, M.B., Chavan, G.S., Shenoy, S.S. and Nair, A.S., *Mortality pattern of the 26/11 Mumbai terror attacks*. Journal of Trauma and Acute Care Surgery, 2012. **72**(5): p. 1329-1334.
59. [cited 2011 01/09/2011]; Available from: <http://blogs.voanews.com/breaking-news/2011/07/23/norway-shooting-bombing-suspect-recently-bought-six-tons-of-fertilizer/>
60. Gardell, M., *Crusader Dreams: Oslo 22/7, Islamophobia, and the Quest for a Monocultural Europe*. Terrorism and Political Violence, 2014. **26**(1): p. 129-155.
61. Golan, R., Soffer, D., Givon, A. and Peleg, K., *The ins and outs of terrorist bus explosions: Injury profiles of on-board explosions versus explosions occurring adjacent to a bus*. Injury-International Journal of the Care of the Injured, 2014. **45**(1): p. 39-43.
62. Alonso, R., *The Madrid Bombings and Negotiations With ETA: A Case Study of the Impact of Terrorism on Spanish Politics*. Terrorism and Political Violence, 2013. **25**(1): p. 113-136.
63. [cited 2011 29/09/2011]; Available from: <http://edition.cnn.com/2009/WORLD/europe/05/19/london.bombings/index.html>.
64. Bruyelle, J.L., O'Neill, C., El-Koursi, E.M., Hamelin, F., Sartori, N. and Khoudour, L., *Improving the resilience of metro vehicle and passengers for an effective emergency response to terrorist attacks*. Safety Science, 2014. **62**: p. 37-45.
65. Patel, H.D.L., Dryden, S., Gupta, A. and Ang, S.C., *Pattern and mechanism of traumatic limb amputations after explosive blast: Experience from the 07/07/05 London terrorist bombings (vol 73, pg 276, 2012)*. Journal of Trauma and Acute Care Surgery, 2012. **73**(3): p. 784-784.
66. Schwartz, A.R. and Bayer, M.J., *Pan Am Flight 103 and the Aviation Security Improvement Act of 1990*. Logistics and Transportation Review, 1992. **28**(1): p. 61.
67. Murphy, S.D., *Libyan payment to families of Pan Am Flight 103 victims*. American Journal of International Law, 2003. **97**(4): p. 987-991.
68. Marshall, M. and Oxley, J.C., *The Detection Problem*, in *Aspects of Explosives Detection*, M. Marshall and J.C. Oxley, Editors. 2009, Elsevier B.V. p. 1-10.
69. Marshall, M., *Post-Blast Detection Issues*, in *Aspects of Explosives Detection*, M. Marshall and J.C. Oxley, Editors. 2009, Elsevier. p. 223-243.
70. Lock, C.M. and Meier-Augenstein, W., *Investigation of isotopic linkage between precursor and product in the synthesis of a high explosive*. Forensic Science International, 2008. **179**(2): p. 157-162.
71. [cited 2014 04/10/2014]; Available from: https://www.innovateuk.org/competition-display-page/-/asset_publisher/RqEt2AKmEBhi/content/substitutes-and-additives-to-prevent-chemicals-being-used-in-the-illicit-manufacture-of-explosives-or-to-cause-harm#search=searchandquery_string=andstart=0andfi%5Bperiod%5D=all_timeandfi%5Bsort%5D=score.
72. *Innovative Research Call - IRC 2013 - Detection of Explosives and Weapons*. [cited 2014 04/10/14]; Available from: <https://www.innovateuk.org/-/innovative-research-call-irc-2013-detection-of-explosives-and-weapons>.
73. Nazarian, A. and Presser, C., *Forensic analysis methodology for thermal and chemical characterization of homemade explosives*. Thermochimica Acta, 2014. **576**(0): p. 60-70.

74. [cited 2014 09/10/14]; Available from: <http://www.foi.se/en/Customer--Partners/Projects/EMPHASIS/EMPHASIS/>.
75. Carlisle, F. [cited 2014 09/10/2014]; Available from: https://connect.innovateuk.org/web/forensics/article-view/-/blogs/explosives-detection-sensing-in-the-sewers?p_p_auth=IPYDZFf5.
76. Morelle, R. [cited 2014 09/10/14]; Available from: <http://www.bbc.co.uk/news/science-environment-29354579>.
77. Buchanan, H.A.S., *An evaluation of isotope ratio mass spectrometry for the profiling of 3,4-methylenedioxymethamphetamine* in *Pure and Applied Chemistry*. 2009, University of Strathclyde: Glasgow. p. 313.
78. Jayaram, S., *A comprehensive chemical examination of methylamphetamine produced from pseudoephedrine extracted from cold medication*, in *Dept. of Pure and Applied Chemistry*. 2012, University of Strathclyde.
79. NicDaeid, N., Jayaram, S. and Kerr, W.J., *Elemental profiling using ICPMS of methylamphetamine hydrochloride prepared from proprietary medication using the Moscow and hypophosphorous synthesis*. *Science and Justice*, 2013. **53**(3): p. 278-285.
80. Desa, W.N.S.M., *The Discrimination of Ignitable Liquids and Ignitable Liquid Residues using Chemometric Analysis*, in *Pure and Applied Chemistry*. 2012, University of Strathclyde: Glasgow.
81. Reed, G., *Multivariate profiling of gel inks : a novel tool for the discrimination of within and between brand variation*, in *Dept. of Pure and Applied Chemistry*. 2013, University of Strathclyde.
82. Garcia, J.S., Vaz, B.G., Corilo, Y.E., Ramires, C.F., Saraiva, S.A., Schmidt, E.M., Maia, D.R.J., Cosso, R.G., Zacca, J.J. and Eberlin, M.N., *Whisky analysis by electrospray ionization-Fourier transform mass spectrometry*. *Food Research International*, 2013. **51**(1): p. 98-106.
83. Meier-Augenstein, W., Kemp, H.F. and Hardie, S.M.L., *Detection of counterfeit scotch whisky by H-2 and O-18 stable isotope analysis*. *Food Chemistry*, 2012. **133**(3): p. 1070-1074.
84. Corera, G. *Have US anti-terror tactics strayed into entrapment?* 2011 [cited 2011 29/09/2011]; Available from: <http://news.bbc.co.uk/1/hi/programmes/newsnight/9584637.stm>.
85. Kaplan, E.H. and Kress, M., *Operational effectiveness of suicide-bomber-detector schemes: A best-case analysis*. *Proceedings of the National Academy of Sciences of the United States of America*, 2005. **102**(29): p. 10399-10404.
86. Miller, S.M. and Wenzlick, D.L., *Sensitive site exploitation and forensic collection training system for armed forces relating to intelligence gathering, e.g., combat support agencies, has training facility with reconfigurable training area for conducting training scenario*, WASHINGTON SECURITY GROUP INC (WASH-Non-standard). p. 40.
87. Schoemaker, R., Sandbrink, R. and van Voorthuijsen, G., *Unattended Monitoring of Suspicious Behaviour for Route Surveillance*, in *Unattended Ground, Sea, and Air Sensor Technologies and Applications Xii*, E.M. Carapezza, Editor. 2010, Spie-Int Soc Optical Engineering: Bellingham.
88. Christian, D.R., *Field Guide to Clandestine Laboratory Identification and Investigation*. 2004: CRC Press.
89. [cited 2014 04/02/2014]; Available from: <https://www.dstl.gov.uk/security>.
90. Bochkarev, O.V., Gavryuchenkov, A.V., Polishchuck, A.M. and Udaltsov, A.Y., *Concealed Explosives Detector Based On Portable Neutron Generator*, in *Detection*

- and Disposal of Improvised Explosives*, H. Schubert and A. Kuznetsov, Editors. 2006, Springer. p. 205-216.
91. Burks, R.M. and Hage, D.S., *Current trends in the detection of peroxide based explosives*. Analytical and Bioanalytical Chemistry, 2009. **395**: p. 301-313.
 92. Caygill, J.S., Davis, F. and Higson, S.P.J., *Current trends in explosive detection techniques*. Talanta, 2012. **88**: p. 14-29.
 93. Linker, K.L., *Explosives Detection Personnel Portals*, in *counterterrorist Detection Techniques of Explosive*, J. Yinon, Editor. 2007, Elsevier B.V. p. 367-393.
 94. Bui, M.P.N., Pham, X.H., Nan, K.N., Li, C.A., Kim, Y.S. and Seong, G.H., *Electrocatalytic reduction of hydrogen peroxide by silver particles patterned on single-walled carbon nanotubes*. Sensors and Actuators B-Chemical, 2010. **150**(1): p. 436-441.
 95. Hanaoka, S., Lin, J.M. and Yamada, M., *Chemiluminescent flow sensor for H₂O₂ based on the decomposition of H₂O₂ catalyzed by cobalt(II)-ethanolamine complex immobilized on resin*. Analytica Chimica Acta, 2001. **426**(1): p. 57-64.
 96. Melange, W., Bruneel, H., Steyaert, B., Claeys, D. and Walraevens, J., *A Continuous-time Queuing Model With Class Clustering And Global FCFS Service Discipline*. Journal of Industrial and Management Optimization, 2014. **10**(1): p. 193-206.
 97. de Lange, R., Samoilovich, I. and van der Rhee, B., *Virtual queuing at airport security lanes*. European Journal of Operational Research, 2013. **225**(1): p. 153-165.
 98. Lee, A.J. and Jacobson, S.H., *The impact of aviation checkpoint queues on optimizing security screening effectiveness*. Reliability Engineering and System Safety, 2011. **96**(8): p. 900-911.
 99. Committee on the Review of Existing and Potential Standoff Explosives Detection Techniques, *Existing and Potential Standoff Explosives Detection Techniques*, ed. N.R.C.o.t.N. Academies. 2004, Washington D.C.: The National Academies Press.
 100. Bauer, C., Sharma, A.K., Willer, U., Burgmeier, J., Braunschweig, B., Schade, W., Blaser, S., Hvozدارa, L., Muller, A. and Holl, G., *Potentials and limits of mid-infrared laser spectroscopy for the detection of explosives*. Applied Physics B-Lasers and Optics, 2008. **92**(3): p. 327-333.
 101. Carter, J.C., Angel, S.M., Lawrence-Snyder, M., Scaffidi, J. Whipple, R.E. and Reynolds, J.G., *Standoff Detection of High Explosive Materials at 50 Meters in Ambient Light Conditions Using a small Raman Instrument*. Applied Spectroscopy, 2005. **59**(6): p. 769-775.
 102. Chirico, R., Almagiva, S., Botti, S., Cantarini, L., Colao, F., Fiorani, L., Nuvoli, M. and Palucci, A., *Stand-off detection of traces of explosives and precursors on fabrics by UV raman spectroscopy*. in *Optics and Photonics for Counterterrorism, Crime Fighting and Defence VIII*. 2012. Edinburgh: SPIE.
 103. Fischer, C., Pohl, T., Weber, K., Vogel, A., van Haren, G. and Schweikert, W., *TATP Stand-off Detection with Open Path - FTIR Techniques*. in *Optics and Photonics for Counterterrorism, Crime Fighting and Defence VIII*. 2012. Edinburgh: SPIE.
 104. Gaft, M. and Nagli, L., *UV gated Raman spectroscopy for standoff detection of explosives*. Optical Materials, 2008. **30**(11): p. 1739-1746.
 105. Izake, E.L., *Forensic and homeland security applications of modern portable Raman spectroscopy*. Forensic Science International, 2010. **202**(1-3): p. 1-8.
 106. Moros, J., Lorenzo, J.A., Lucena, P., Miguel Tobarria, L. and Laserna, J.J., *Simultaneous Raman Spectroscopy-Laser-Induced Breakdown Spectroscopy for Instant Standoff Analysis of Explosives Using a Mobile Integrated Sensor Platform*. Analytical Chemistry, 2010. **82**(4): p. 1389-1400.

107. Pacheco-Londono, L.C., Ortiz-Rivera, W., Primera-Pedrozo, O.M. and Hernandez-Rivera, S.P., *Vibrational spectroscopy standoff detection of explosives*. Analytical and Bioanalytical Chemistry, 2009. **395**: p. 323-335.
108. Pettersson, A., Johansson, I., Wallin, S., Nordbery, M and Ostmark, H., *Near Real-time Standoff Detection of Explosives in a Realistic Outdoor Environment at 55m Distance*. Propellants Explosives and Pyrotechnics, 2009. **34**: p. 297-306.
109. [cited 2014 01/04/2014]; Available from: <https://www.gov.uk/government/publications/information-on-the-implementation-of-security-scanners>.
110. Edinburgh Airport. [cited 2014 01/04/2014]; Available from: <http://www.edinburghairport.com/prepare/airport-security/body-scanners>.
111. Gatwick Airport. [cited 2014 04/04/2014]; Available from: http://www.gatwickairport.com/Documents/passengers/security/50317_A5_SecurityScanningLeaflet_Jan2014.pdf.
112. Mullins, J. *Full-body scanners: we reveal all*. 2010 [cited 2011 14/09/2011]; Available from: <http://www.newscientist.com/article/dn19746-fullbody-scanners-we-reveal-all.html>.
113. Sawyer, P. [cited 2014 01/04/2014]; Available from: <http://www.telegraph.co.uk/news/uknews/terrorism-in-the-uk/6924417/Muslim-MP-security-profiling-at-airports-is-price-we-have-to-pay.html>.
114. Schmidt, M.S. and Lichtblau. E. [cited 2014 01/04/2014]; Available from: http://www.nytimes.com/2012/08/12/us/racial-profiling-at-boston-airport-officials-say.html?pagewanted=all&_r=0.
115. Schneier, B. [cited 2014 01/04/2014]; Available from: <http://www.forbes.com/sites/bruce-schneier/2012/05/09/the-trouble-with-airport-profiling/>.
116. Wilson, R. and Brittain, A., *Explosives Detection by Ion Mobility Spectrometry*, in *Explosives in the service of man: The Nobel Heritage*, J.E. Dolan and S.S. Langer, Editors. 1997, Royal Society of Chemistry.
117. Wilson, P.F., Prince, B.J. and McEwan, M.J., *Application of Selected-Ion Flow Tube Mass Spectrometry to the Real-Time Detection of Triacetone Triperoxide*. Analytical Chemistry, 2006. **78**(2): p. 575-579.
118. Oxley, J.C. and Waggoner, L.P., *Detection of Explosives by Dogs*, in *Aspects of Explosives Detection*, M. Marshall and J.C. Oxley, Editors. 2009, Elsevier B.V. p. 27-40.
119. Osborn, T., Burns, W.A., Green, J. and Reeve, S.W., *An Optical Nose Approach to Explosive Detection: One Strategy for Optically Based Sensing*. Spectroscopy, 2011. **26**(1): p. 34-45.
120. Mostak, P. and Stancl, M., *IEDS Detection by Existing Detection Techniques*, in *Detection and Disposal of Improvised Explosives*, H. Schubert and A. Kuznetsov, Editors. 2006, Springer. p. 33-41.
121. Krauss, M., *Explosives Detecting Dogs*. 1971, Mississippi University.
122. Bobrovnikov, S., *Development of Methods and Equipment for Detection of Explosives' Vapours in the Atmosphere with Laser*, in *Detection and Disposal of Improvised Explosives*, H. Schubert and A. Kuznetsov, Editors. 2006, Springer. p. 51-68.
123. Oxley, J.C., *What's Special About Liquid Explosives?*, in *Detection of Liquid Explosives and Flammable Agents in Connection with Terrorism*, H. Schubert and A. Kuznetsov, Editors. 2008, Springer. p. 27-38.

124. Wallin, S., Pettersson, A., Ostmark, H. and Hobro, A., *Laser-based standoff detection of explosives: a critical review*. Analytical and Bioanalytical Chemistry, 2009. **395**(2): p. 259-274.
125. Desilets, S., Ho, N., Mathieu, P., Simard, J.R., Puckrin, E., Theriault, J.M., Lavoie, H., Theberge, F., Babin, F., Gay, D., Forest, R., Maheux, J., Roy, G. and Chateauneuf, M., *Standoff detection of explosives, a challenging approach for optical technologies*, in *Micro- and Nanotechnology Sensors, Systems, and Applications Iii*, T. George, M.S. Islam, and A.K. Dutta, Editors. 2011, Spie-Int Soc Optical Engineering: Bellingham.
126. Willer, U. and Schade, W. *Photonic sensor devices for explosive detection*. Analytical and Bioanalytical Chemistry, 2009. **395**: p. 275-282.
127. Fountain, A.W., Christesen, S.D., Moon, R.P., Guicheteau, J.A. and Emmons, E.D., *Recent Advances and Remaining Challenges for the Spectroscopic Detection of Explosive Threats*. Applied Spectroscopy, 2014. **68**(8): p. 795-811.
128. Mills, A., Grosshansa, P. and Snaddena, E., *Hydrogen peroxide vapour indicator*. Sensors and Actuators B: Chemical, 2008. **136**(2): p. 458-463.
129. Chalmers, J.M., Edwards, H.G.M. and Hargreaves, M.D., *Infrared and Raman Spectroscopy in Forensic Science*. 1st ed. 2012: Wiley.
130. Izake, E.L., *Forensic and homeland security applications of modern portable Raman spectroscopy*. Forensic Science International, 2010. **202**: p. 1-8.

Chapter 2. Techniques and Instrumentation

2.1 Spectroscopy

Spectroscopy involves the study of the interaction of electromagnetic radiation with matter using an instrument known as a spectrometer[1]. This interaction falls broadly into three categories; absorption, emission and scattering. Emission spectroscopy detects the release of excess energy as a molecule moves from a higher to a lower energy state, while absorption spectroscopy detects the net absorption of energy by a molecule[2]. Scattering occurs when energy passes through a molecule causing the photons to be dispersed as they leave the molecule[3].

Different spectroscopic techniques are used to characterise compounds as a result of the exposure to energy from across the electromagnetic spectrum (figure 2.1). Infrared spectroscopy is a significant area of research as it can provide a large amount of information about the structure of a molecule through monitoring the characteristic vibrations which the bonds within the molecule experience. Raman spectroscopy is often considered to be a complementary technique to infrared spectroscopy[4].

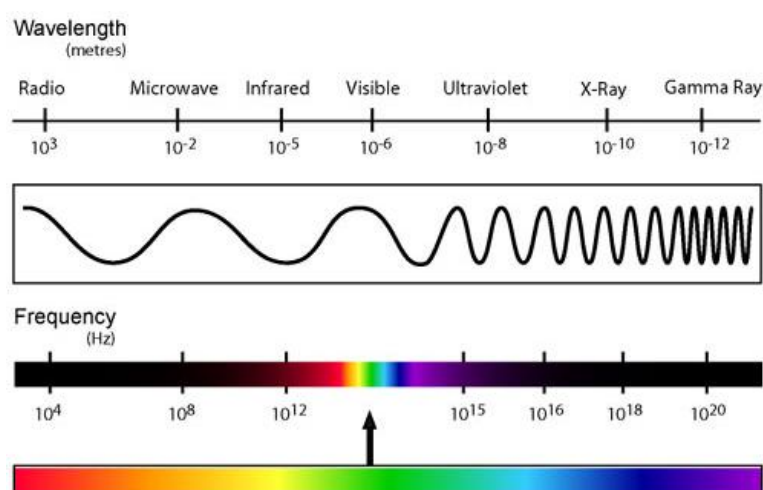


Figure 2.1 The Electromagnetic spectrum[5]

Spectroscopy has an important role to play in forensic science, and spectroscopic techniques are frequently used in forensic laboratories for both quantitative and qualitative analysis[6].

2.1.1 Infrared spectroscopy

Infrared (IR) spectroscopy is an important analytical technique, it is regularly used by organic chemists to determine the structure of molecules[7] and IR spectroscopy is a universal technique used to identify the class of compounds present within a molecule[6]. If spectroscopy involves the interaction of light with matter, infrared spectroscopy involves the interaction of infrared light with matter[8]. Infrared spectroscopy can be divided into three areas depending on the wavenumbers involved. Wavenumbers below 650 cm^{-1} are classed as the far infrared region, wavenumbers between 650 and 4000 cm^{-1} are classed as the mid-infrared region and wavenumbers above 4000 cm^{-1} the near infrared[9]. The majority of infrared spectroscopy work is focused on the mid-infrared[9]. Both wavenumber units (cm^{-1}) and wavelength units (μm) are used, with the choice of unit used often down to the user[9, 10].

Infrared spectroscopy involves the interaction of infrared energy with molecular bonds, where two chemically bonded atoms vibrating is analogous to two balls bound by a spring vibrating[9]. There are six main modes of vibration, which are shown in Table 2.1, in addition to this, the analysis of vapour samples can yield rotational vibrations which produces characteristic line-like peaks on the spectrum, the example of carbon dioxide peaks is given in Figure 2.2.

Table 2.1. The six different vibrational modes shown in diagram form

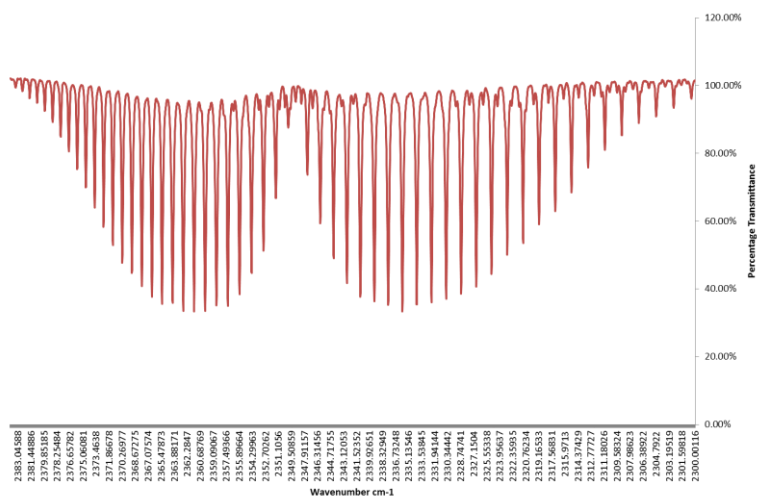
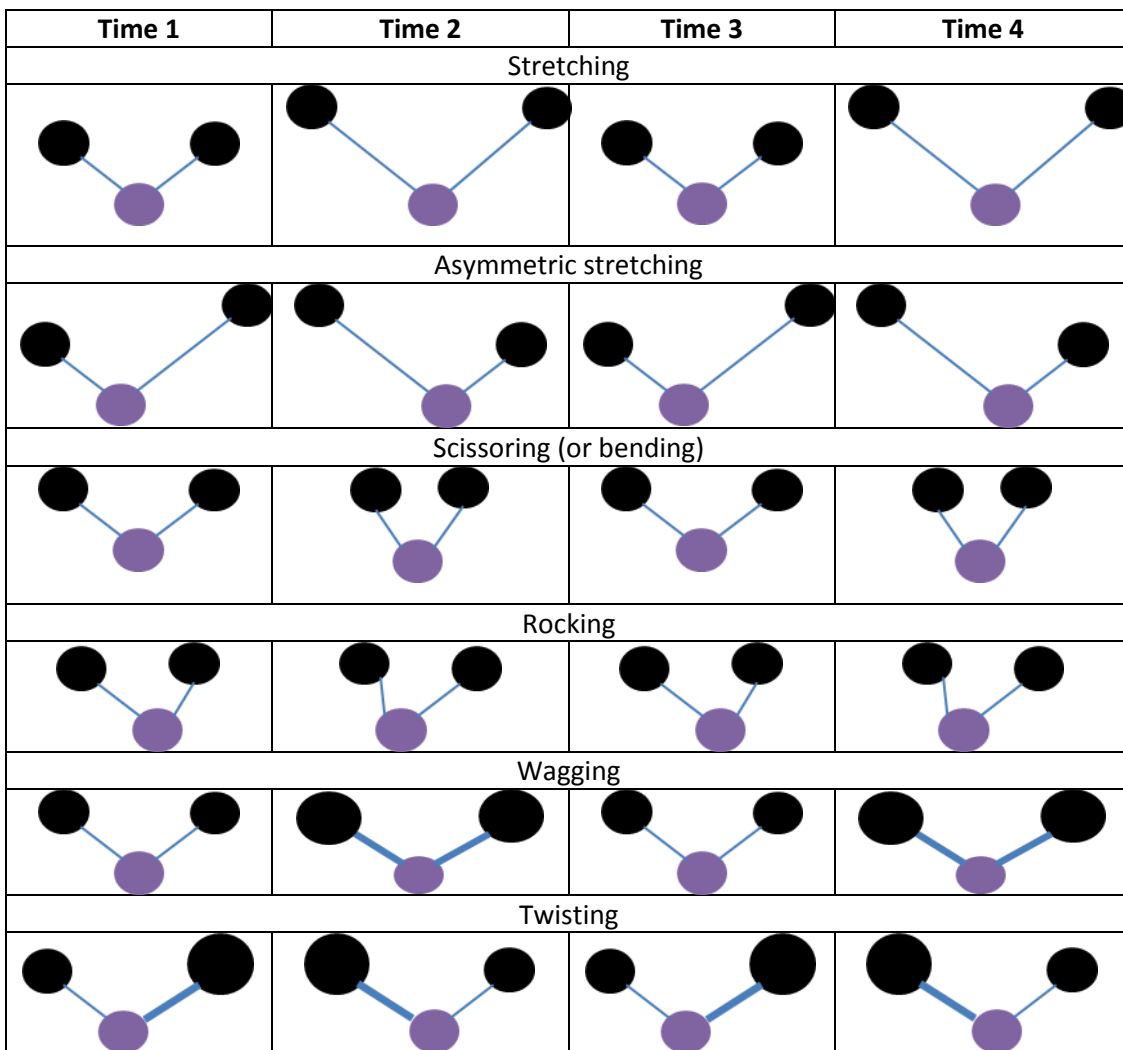


Figure 2.2 The characteristic spectral bands of carbon dioxide, demonstrating the line-like peaks seen with rotational vibrations of vapour samples

The type of vibration occurring when the molecule is exposed to infrared light, and its detection using infrared spectroscopy, depends upon the chemical bonds within that molecule. Single atoms do not contain any molecular bonds and therefore have no vibrations and will not be detected using infrared spectroscopy, and for the same reason neither will monatomic ions[8]. Homonuclear diatomic molecules such as N_2 and O_2 vibrate when exposed to infrared radiation, but only in the form of a symmetrical stretch[8] which has zero peak intensity, because in order for an IR active vibration to occur there needs to be a change in dipole moment[11]. A dipole moment occurs in covalent bonds where the electrons are not shared equally, resulting in a difference in charge for each molecule. Such a bond is termed polar, and a change in the dipole within this molecule refers to a movement of the electrons within this bond[2]. The need for a dipole moment is what is termed a gross selection rule, this is the overarching rule that must be obeyed when determining whether a vibration will be infrared active[11]. However, the specific vibrational and rotational transitions that occur within a molecule are determined by selection rules relating to quantum numbers[12]. Quantum numbers relate to the orbitals in an atom and the movement of electrons between different orbitals. For vibrational spectroscopy the specific selection rule for a diatomic molecule is $\Delta v = \pm 1$, where v is a vibrational energy level[2]. The selection rules are different for different types of spectroscopy, as such a vibration that is not infrared active may be Raman active[11]. This can be seen with homonuclear diatomic molecules which do not produce an infrared spectrum but will be visible with Raman, while water is not visible with Raman but can be observed using infrared spectroscopy[11].

For a diatomic molecule when a vibrational transition occurs the rotational quantum number will change by plus or minus 1, giving a simultaneous vibrational and rotational change[2]. The type of vibration of a bond will have an effect upon the rotational transitions possible. There are several types of rotation that can occur; spherical, symmetric top, asymmetric top and linear[2]. The selection rules for a change in rotational energy are dependent upon the associated vibration. An example of this is seen with the CO_2 spectrum shown in figure 2.2. This

demonstrates the spectrum produced with linear rotation and a parallel vibration. The presence of parallel vibration results in a selection rule of $\Delta J = \pm 1$ (where J is a rotational energy level) for a transition between the lowest and first vibrational energy levels ($v=0$ and $v=1$). This creates the two sets of line like peaks observed in figure 2.2. These are known as P and R branches[2] where P is a result of transitions where $\Delta J = -1$ and R where $\Delta J = +1$. If there was an angular momentum about the axis of the molecule being analysed $\Delta J = 0$ becomes an allowed transition. This would result in a peak as the result of the vibrational transition between $v = 0$ and $v = 1$ with zero change in the rotational energy level, this is known as the Q branch, and would be located between the P and R branches[2].

The vibrations that occur when the molecules are exposed to infrared radiation are a result of a change in the energy level of the molecule. The transitions that are observed in the infrared are rotational and vibrational[12]. Figure 2.3 shows a diagram of the vibrational and rotational levels within a single electronic state. It can be seen from this diagram that a large number of rotational transitions can occur within a single vibrational transition.

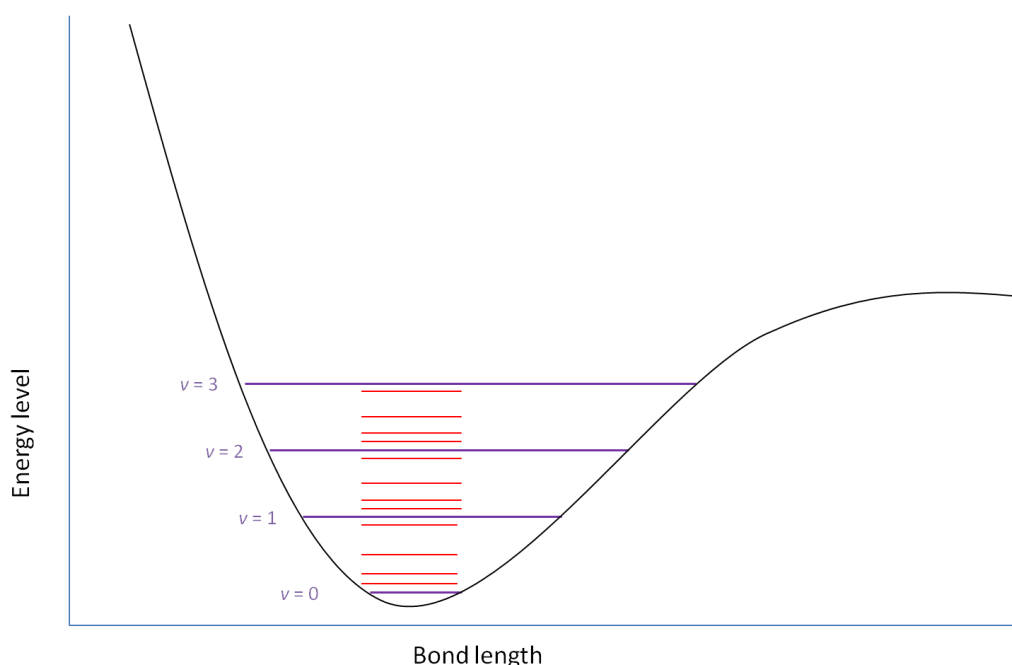


Figure 2.3 Energy level diagram for a single electronic state showing the vibrational energy levels (purple; $v=0$ to $v=3$) and the rotational energy levels (red lines) (adapted from[12])

A diatomic molecule will have two electronic states (this is shown in figure 2.4 which also shows some of the different possible transitions). A larger molecule with more bonds will have more vibrational and rotational energy levels (as each bond will have its own)[12]. This means that the complexity of an infrared spectrum is increased, and the combination of features on the spectrum become individual to a specific molecule[12]. The different functional groups within a molecule will absorb energy with the vibrations within specific regions of the spectrum, allowing them to be identified[13]. The structure of the rest of the molecule should not have a significant effect on the position of the absorption within the spectrum for each functional group[13], however there can be a degree of shift seen, as well as the effects of the state of the molecule[11]. Therefore spectra produced for solids, liquids and gases will all be different even for the same molecule being analysed[11] and as such it is important when interpreting a spectrum to know the state of the compound being analysed.

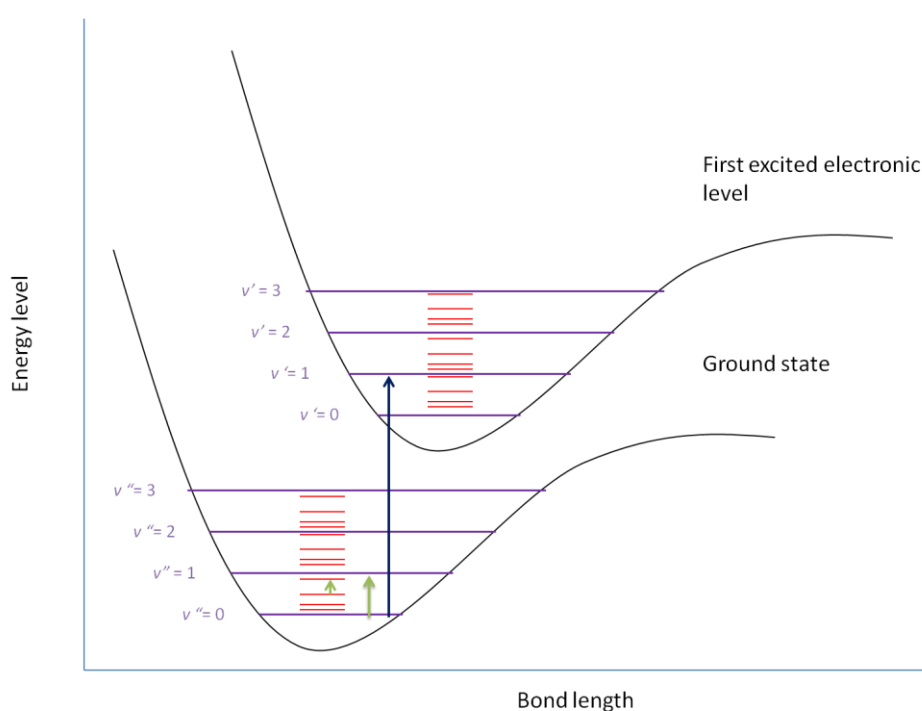


Figure 2.4 Diagram of the potential wells for two electronic states showing the electronic, vibrational and rotational energy levels with green arrows showing some of the possible transitions (dependent upon quantum numbers) between rotational and vibrational energy levels, and the blue arrow showing an electronic transition (which is not detectable by IR spectroscopy, but could be detectable with UV/vis spectroscopy) (adapted from [12])

Infrared spectroscopy has several advantages. Firstly it can detect a wide range of molecules, particularly when looking at the mid-infrared region[8]. Secondly, the spectra produced contain a lot of information, with the positions of peaks providing insight into the molecular structures within a sample, while peak intensities are indicative of the concentration of molecules present within a sample. Further insight can be gained through examination of peak widths, which will alter as a result of the chemical matrix of a sample[8]. Depending upon the instrumentation and information required from the analysis it is quick and simple to obtain results, and basic infrared spectroscopy equipment is relatively cheap[8].

However, despite these advantages, there are some disadvantages to the use of infrared spectroscopy. Firstly, although the technique can detect a large proportion of molecules there are some, such as the noble gases, which are not able to be detected[8]. Secondly, infrared spectroscopy can be more challenging to interpret when analysing mixtures, this is because it can be difficult to separate which spectral features belong to the different molecules in a mixture[8]. The interference of water is also a problem, with absorption in several areas of the spectrum[8]. While water present in the atmosphere should be removed through subtraction of a background spectrum, when the sample is contained within an unsealed chamber there can be changes in the water concentration between the background and sample analyses that will then appear on the spectrum. A sample that contains water, i.e. a sample in an aqueous solution, will also have water absorption in the spectrum, generating peaks which can have high intensities and be very broad[8] and this can potentially mask the peaks of interest from the compound in the solution. With an unsealed sample chamber both carbon dioxide and water vapour can produce inverse peaks, which occur when there is a reduction in the concentration of these molecules between taking the background spectrum and the analysis of the sample[8].

2.1.1.1 Spectral interpretation

In order to interpret an IR spectrum, correlation charts are used[13]. These provide information on the most commonly occurring vibrations for functional groups and where they are likely to occur on the spectrum. Figure 2.5 shows an example of a correlation chart, and this highlights one of the difficulties associated with IR spectral interpretation, that there is overlap between different groups across the spectrum. This is not a significant issue when identifying spectral features for a known material, but makes the identification of an unknown material more challenging if a database of known spectra is not also available for comparison. Figure 2.6 shows an infrared spectrum of toluene with the spectral features identified, however it must be remembered that different instruments may produce slightly different spectra, especially if there are differences in resolution, and it is important to note the physical state of the material being analysed as this can also affect the spectrum.

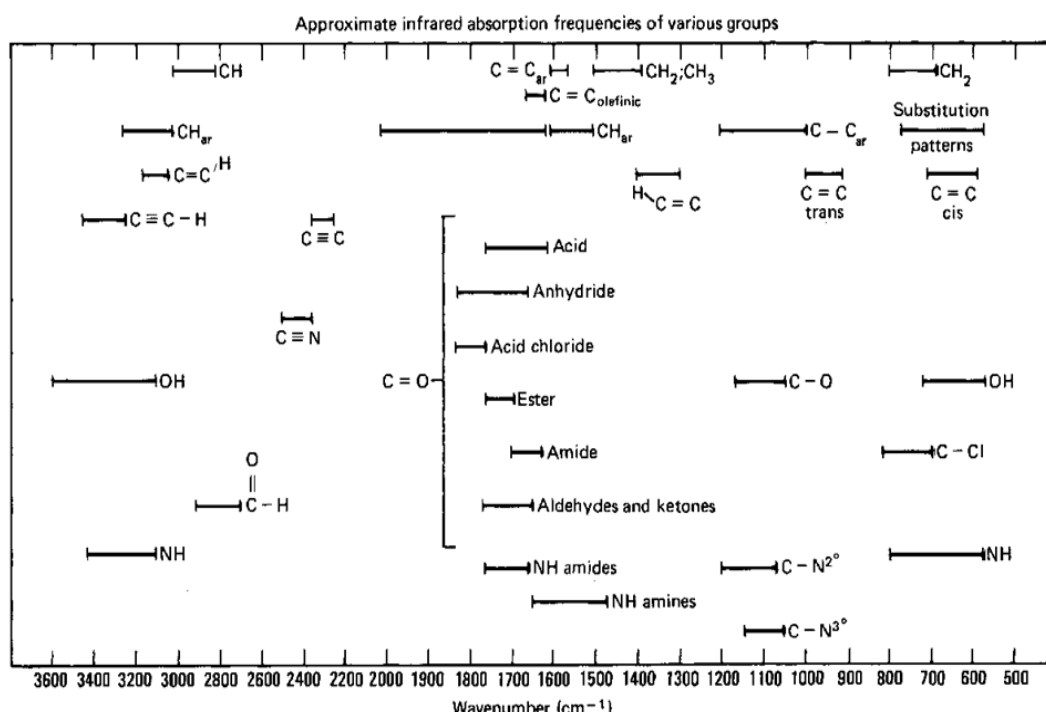


Figure 2.5 An example of a correlation chart used to identify spectral features seen in an IR spectrum[14]

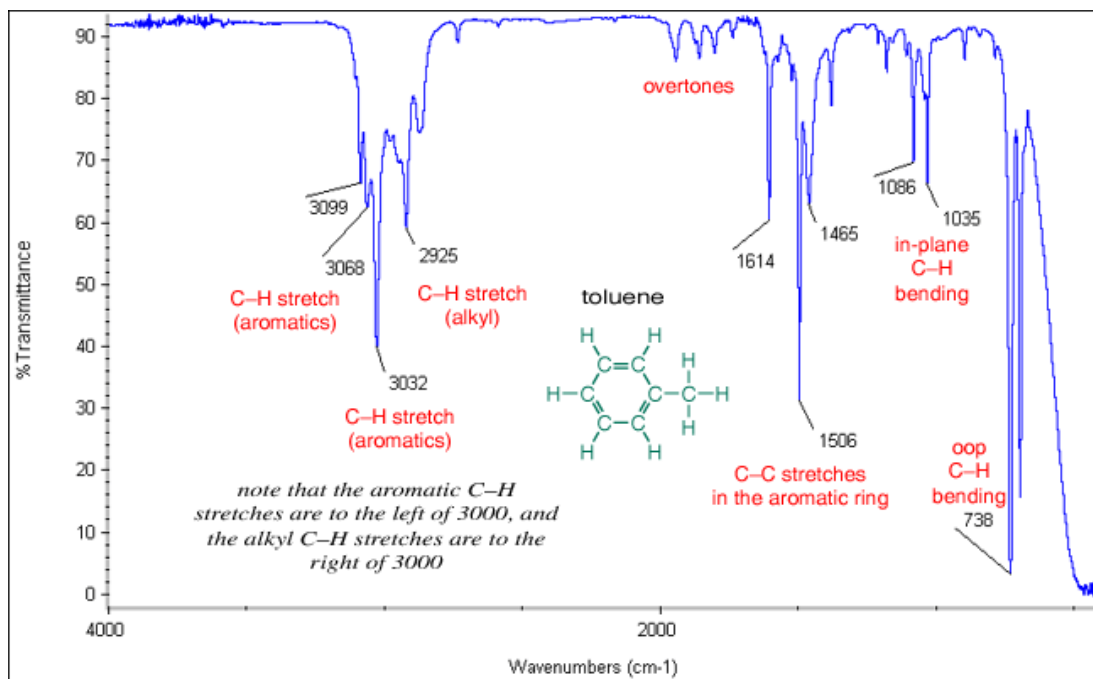


Figure 2.6 An interpreted infrared spectrum for toluene[15]

2.1.2 Fourier transform infrared spectroscopy (FTIR)

FTIR is a form of absorption spectroscopy where samples are exposed to radiation in the infrared region of the electromagnetic spectrum [1]. A molecule will absorb different amounts of this radiation depending upon its structure, as it is the chemical bonds within the molecule which absorb the infrared radiation[13]. Different functional groups will absorb radiation within different wavenumber ranges making it possible to deduce from the spectrum the presence or absence of specific functional groups (figures 2.5 and 2.6 demonstrate this). FTIR, while being a form of IR spectroscopy, has several advantages over conventional IR spectroscopy[7]. In an FTIR instrument the whole spectral bandwidth is used simultaneously, this has a significant time saving effect, and as a knock-on effect of this multiple scans can easily be taken producing an overall spectrum with an improved signal-to-noise ratio. FTIR is also more sensitive than older IR techniques[7]. FTIR instruments are able to utilise the whole spectrum as a result of the use of a Michelson interferometer and the Fourier transform equation. The Michelson interferometer creates an interference pattern called an interferogram,

which can be converted into a spectrum through the use of the Fourier transform. Equation 2.1 shows an infinite-range Fourier transform of a spectrum of a sample, where $I(x)$ is an interferogram and x and ν are continuous variables. Equation 2.2 shows a discrete Fourier transform as rather than an infinite amount of data there are instead a fixed number of datapoints, where x and ν become $n\Delta x$ and $k\Delta \nu$ respectively[16].

$$S(\nu) = \int_{-\infty}^{\infty} I(x) e^{-i2\pi\nu x} dx$$

Equation 2.1 Infinite-range Fourier transform[16]

$$S_{k\Delta\nu} = \sum_{n=0}^{N-1} I_{n\Delta x} e^{-i(2\pi/N)kn}$$

Equation 2.2 Discrete Fourier transform[16]

Two types of spectra can be produced, transmittance and absorbance. A transmittance spectrum has peaks pointing downwards with the scale in terms of percentage transmittance. The large peaks indicate wavenumbers where the sample transmitted only a small percentage of the radiation, with the rest being absorbed by the sample. Where the line is close to 100% the sample was transmitting the majority of the radiation. An absorbance spectrum will have peaks pointing upwards and will be almost a mirror image of a transmittance spectrum for the same sample. A high peak indicates that, at that wavenumber, the sample was absorbing the majority of the radiation (with only a small amount being transmitted), while where the line of the spectrum is close to zero the sample was absorbing very little of the radiation with the majority being transmitted.

The main weakness of FTIR as an analytical technique, as with other IR technologies, is that spectral interpretation becomes more challenging when analysing mixtures; the more complex the mixture, the more complex the resulting spectrum[17]. While different functional groups will absorb at different wavenumber regions there is a degree of overlap between some of these regions and this can make it extremely difficult to determine the functional groups present in a sample. However, this is

less of a problem when the technique is used to identify an unknown mixture using a library of spectra as, rather than trying to identify the specific spectral features within the spectrum, the spectrum is compared to a library of known mixtures and compounds. The similarity between spectra is described by the Hit Quality Index (HQI)[17] and the top matches will be shown to the analyst. However, care must be taken when using a library comparison as the algorithms used can sometimes generate false matches. A degree of human interaction is required to ensure that the correct match is made. The complexity of the spectra of mixtures can be exploited to demonstrate individualisation, this would be of particular interest in a forensic examination when trying to identify whether materials come from a common source.

FTIR also suffers from interference from water, with $-OH$ bonds giving multiple peaks across the spectrum. This is a particular issue when trying to analyse an aqueous sample, as in some situations the peaks due to water can obscure peaks caused by the sample. Atmospheric water interference can be reduced to a degree through subtracting a background spectrum from the sample spectrum, however there can still be interference if there are any atmospheric changes between the background and sample analyses. FTIR is also not suitable for analysing homonuclear molecules as they lack a dipole. Raman spectroscopy does not suffer from water interference and can analyse homonuclear molecules, however it suffers from weak signal strength and interference from Rayleigh scattering and fluorescence[6, 11, 12]. Therefore the two techniques can be considered complementary[4].

High resolution Fourier transform spectroscopy has the advantage, over general FTIR, of increased resolution. Resolution in this context is the ability to distinguish between two features on a spectrum. The closer together two features may be while still being distinguishable dictates the resolution [1, 7]. Therefore a high resolution FTIR instrument can distinguish between features much closer together than a general FTIR instrument. This allows for the identification of smaller potential

identifying features that would otherwise be missed. However, increased resolution can also increase the amount of time it takes for analysis, and a balance has to be struck between the duration of analysis and resolution.

2.1.2.1 FTIR in explosives detection and analysis

FTIR and the wider field of IR spectroscopy have an important role to play in the field of explosives detection and analysis, with substantial pre-existing and on-going research in this area[18-23]. IR spectroscopy is advantageous in a detection setting as it has the potential to be used for stand-off detection[20, 24, 25]. However, IR spectroscopy can also be applied to post blast analysis[19, 26] and the identification of unknown samples[18, 19, 27-29].

While research is ongoing into the use of spectroscopic techniques for stand-off detection, instrumentation is not yet commercially available to detect explosives from stand-off distances[30]. This is because the stand-off detection of explosives presents a complex problem[31]. Due to the varying vapour pressures of different explosive materials a stand-off system needs to be extremely sensitive as there may be only trace amounts of vapour to be detected, similarly if the explosive material has been well packaged there is likely to be limited vapour present in the environment for detection[31, 32]. While some research has been carried out into the stand-off analysis of packaged materials instead of vapour[22, 33, 34] this has predominantly been carried out on opaque packaging such as bottles[22, 34] and other plastics[33] and therefore wouldn't be suitable for all situations. There are some explosive materials, such as HMX (0.38 ng/L at 25°C[35]), that have such low vapour pressures that vapour detection is likely to be near impossible[31]. In these cases the stand-off detection of explosive particles would be required[31]. The molecular size of many explosive materials can also make the identification of explosive materials more complex as the size of the molecule can affect the definition of spectral features[31]. However, this could be overcome to a degree by detecting a single feature that appears in multiple explosive materials rather than attempting to identify a single specific explosive material. Stand-off detection is also

made challenging by the nature of the environments it would be used in, with the atmosphere presenting many interfering materials that could prevent detection of explosives, or cause false positives[31]. The environment also presents problems in the loss of signal to the environment, especially over long distances, significantly reducing the signal reaching a detector[31].

While there are some examples of FTIR being used for stand-off detection[21, 25, 36], it is not that commonly used, especially when compared to Raman spectroscopy[33]. This is in part due to the fact that there is a belief among the scientific community that the technologies with the greatest potential for being able to detect and identify many substances whilst also being fast and upgradeable to detect new materials are laser-based spectroscopic methods for trace detection[31]. FTIR uses the whole spectrum and is therefore not laser based[8]. However, as IR and Raman spectroscopy are complementary techniques[4], there are several pieces of research looking at combining the two techniques for detection[4, 20, 23, 33].

FTIR is more commonly used for detection in a contact situation[37] or for the analysis of post blast traces or unknown samples[33, 38-40]. In this way the difficulties encountered with loss of signal and interferences in the environment can be avoided. As FTIR can analyse solid, liquid and gaseous samples[8], low vapour pressure of some explosive materials is also no longer a problem. However, there is still scope for further investigation and improvement of FTIR techniques for use in the field of explosives detection and characterisation[19, 20, 23, 33].

2.2. Infrared spectrometers

A spectrometer can be divided into four main sections; the source, sample compartment, dispersing element or Michelson interferometer, and detector. The source provides the electromagnetic radiation, and can either span a wide range of frequencies, or be focused on a narrow band. There are several types of source, but probably the two most common are thermal emission sources, such as a globar, and laser sources. Thermal emission sources use heat to excite an element causing a

release of radiation. The element used will depend upon the frequency of the radiation required, for example tungsten is commonly used for infrared radiation. The sample compartment is where the sample is exposed to the radiation. Ideally the path length should be as long as possible through the sample compartment to allow for the maximum interaction between the sample and the radiation, but this is not always possible due to space constraints. One way to increase the path length without increasing the compartment size is to create a multipass sample cell. This uses two astigmatic mirrors which effectively 'bounce' the radiation back and forth within the cell several times before it exits through a hole in one of the mirrors[41] creating a longer path length and so increasing the possible interaction between the radiation and sample. Spectroscopy can be carried out on solid, liquid and gaseous samples, although some techniques are more suitable for certain samples than others, therefore the sample compartment must be able to hold a variety of sample types.

The dispersing element varies according to the instrument, however it generally consists of a single slit (monochromators) or diffraction grating. The purpose of the dispersing element is to separate the wavelengths prior to detection. This results in a portion of the radiation being discarded, particularly if a monochromator is used where a single slit allows only a small wavelength range to reach the detector. In Fourier transform instruments a Michelson interferometer is used instead. This consists of three main elements; a moveable mirror, beam splitter and compensator. The beam of radiation leaves the sample compartment (the incident beam) and passes through the beam splitter which will divide the beam into two, with the path difference between the two beams dependent upon the position of the moveable mirror, which is constantly moving back and forth. This creates an oscillating signal and it is the varying intensity of signal that is ultimately detected. The two beams then pass through a compensator to ensure that both beams are passed through the same thickness of material thus ensuring any effects occur to both beams[2]. This process enables all the incident radiation to reach the detector, thus increasing the sensitivity compared to other spectrometers.

The detector is responsible for converting the incident beam into a voltage or electric current which can then be processed by a computing element. A Fourier transform instrument must apply the Fourier transformation in order to convert the results of the differences between the two beams into an integrated signal (equations 2.1 and 2.2).

2.2.1. High resolution FTIR spectrometers

The Bruker Fourier Transform Spectrometer (FTS) used in this study is a high resolution FTIR instrument which is capable of resolving linewidths of less than 0.0009cm^{-1} [42]. The instrument forms an uneven T shape, which is shown in Figure 2.7. This arrangement, and the arrangement of mirrors and flaps within the instrument, provides an extremely flexible path length from source to detector [43]. However, the sample cell has a fixed path length.

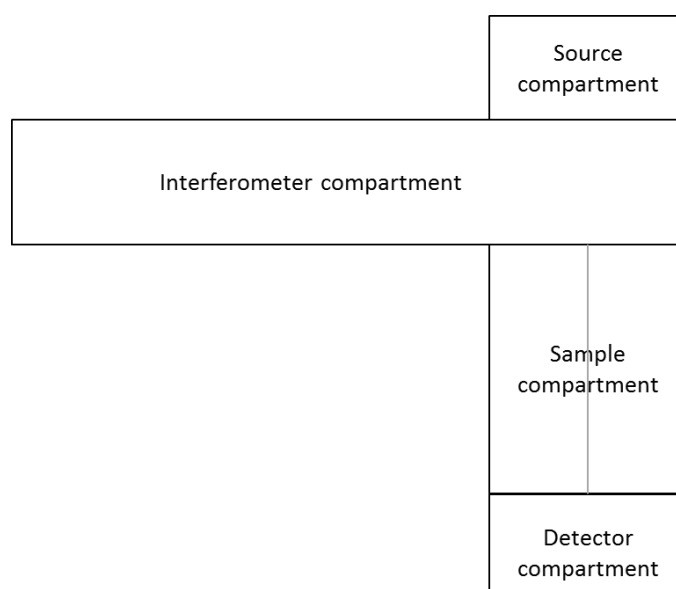


Figure 2.7 Diagram representing the internal compartment structure of the FTS used in this work

The source compartment houses the infrared source which provides the infrared radiation that interacts with the samples. The source utilised during this work was a Mid-infrared globar (thermal) source. Unlike most FTIR systems, rather than the source beam passing through the sample prior to entering the Michelson interferometer, the radiation from the source immediately passes through a

potassium bromide (KBr) beamsplitter. From the beamsplitter, the beams are focused directly onto the interferometer mirrors.

The interferometer compartment is very large in order to house the moveable mirror, which sits on two tracks within the long arm of the compartment. It is this moveable distance that gives the FTS such high resolution as it can produce a significant path difference[42]. Due to the path of the beams, and the positioning of the mirrors within the interferometer, it is generally described as a modified Michelson interferometer[43, 44].

From the interferometer compartment the radiation is directed into the sample compartment, which is itself split into two compartments to increase the possible analyses. Only one compartment was used during this work, and the sample cell was situated within this sample compartment. This self-contained unit (shown in Figure 2.8) allows for compounds which could cause damage to the internal workings of the instrument to be tested, and safer handling of samples. It also allows for the controlled heating of samples as it has the capacity to be heated to at least 200°C, using a digital control box. In order for the radiation to reach the sample, the sample cell has two salt windows which sit in line with the path of the radiation. This results in some loss of signal, but this can be improved by ensuring that the windows are as efficient as possible resulting in only the minimum loss of signal. The efficiency of the windows can be increased by ensuring that they are clean, and that they are thin so that the infrared beam doesn't have to pass through a large amount of material when entering and exiting the sample cell. Once the radiation has passed through the sample compartment it reaches the detector compartment which contains a detector cooled with liquid nitrogen. The data collected is then processed by the software system OPUS, to produce a spectrum. Figure 2.9 graphically shows the path taken by the infrared radiation through the instrument from source to detector.



Figure 2.8 The sample cell removed from the FTS showing one of the circular windows that allow the infrared beam to pass through the cell

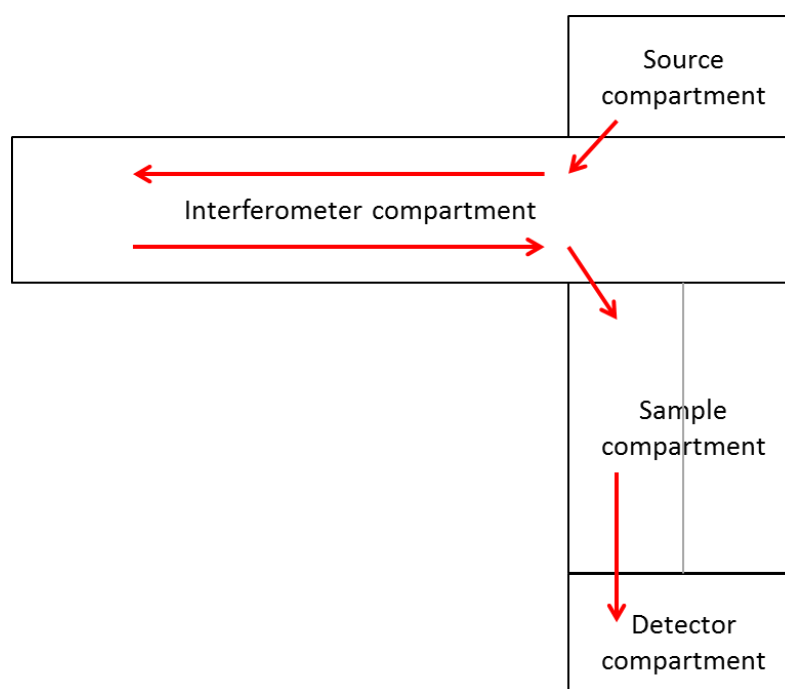


Figure 2.9 Diagram representing the internal structure of the FTS with red arrows showing the path taken by the infrared beam through the instrument from source to detector

It is possible to vary several parameters within the instrument; these include pre-amplification gain, aperture size, resolution and number of scans, allowing the optimisation of the spectra produced. The software also has functions to aid with the manipulation of the data produced. Full instrument settings can be found in table 3.3 (Ch.3).

2.3 Lasers

Lasers are now commonplace in spectroscopic techniques, in particular in raman spectroscopy and laser induced breakdown spectroscopy (LIBS)[31]. The word laser

is in fact an acronym of light amplification by stimulated emission of radiation[2, 45]. A photon is emitted through stimulation of a material in an excited state. That photon is at the same frequency as the excited state, and as such it is possible to vary the frequency of the radiation. The presence of photons at the same frequency will stimulate further production of photons from the material in a positive feedback loop[2]. This means that a laser will operate at a single, or narrow band wavelength[45], and therefore a laser would not be a suitable source for an FTIR instrument as FTIR covers a wider spectrum[8].

2.3.1 Quantum cascade lasers (QCLs)

Quantum cascade lasers are relatively new, with the first QCL laser produced in 1994[46]. A QCL is composed of extremely thin layers of semiconductor materials. These layers create quantum wells down which electrons ‘cascade’ almost like an object falling down a staircase. At each ‘stair’ a photon is released as the energy level decreases[47, 48] (figure 2.10). This allows QCLs to emit more power than a conventional laser. While the lasing wavelength for a conventional laser is determined by the semiconductor material used, with a QCL the wavelength is determined by the thickness of the material layers. This provides far greater coverage across the spectrum[48].

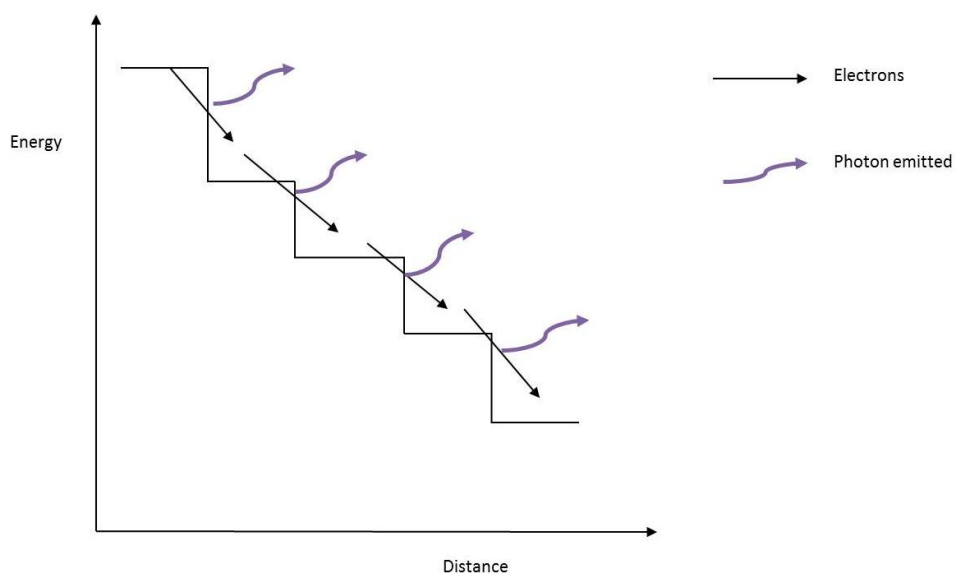


Figure 2.10 Staircase diagram depicting the movement of electrons within a QCL (adapted from[47])

There are currently only a limited number of companies manufacturing this type of laser and associated systems. However, one such company is Cascade Technologies who have developed gas sensors for industrial chimney stacks and other trace gas detection systems. By using mirrored multipass cells the QCLs (which are themselves approximately the size of a pin head[48]) and other hardware can be contained within a relatively small housing without reducing the sensitivity.

One area of development within this is the production of a multi-wavelength laser. Currently QCLs are tuned to a single wavelength (although this will actually cover approximately a 6 cm^{-1} range 'spectral window') for detection; therefore, for each compound requiring detection a separate laser is needed. However, the industry is very close to producing a multi-wavelength laser which could vastly increase the detection capability of the technology already developed.

2.3.1.1 QCLs for explosives detection

The potential for the use of QCLs in the detection of explosive vapour has been already identified. The suitability for such lasers in stand-off detection has been demonstrated by work carried out at Oak Ridge National Laboratory, where the explosive PETN was detected at a distance of 50m[49] and the use of pulsed QCLs for the stand-off detection of RDX molecules that had been adsorbed on surfaces has also been seen[50]. Similarly, the suitability for use in an airport setting has been demonstrated by the trial of the portal undergoing development at Cascade Technologies in 2011. However, while in principle these techniques have been shown to be suitable, there is still further research required before the technology is ready for commercial use. In particular research regarding the loss of signal to the environment in stand-off systems, and the restricted range of compounds that can be detected using a single wavelength system.

2.4 Chemometrics

Spectroscopy is a technique which can generate a large amount of data and the high resolution spectra produced during this work contained over 100,000 data points per spectrum. Such a large data set will often require sophisticated data

handling methods as more basic systems cannot perform calculations with a large volume of data. Similarly when comparing a number of variables, basic statistical methods are not suitable[51].

2.4.1 Standard deviation and relative standard deviation (RSD)

Both the standard deviation and relative standard deviation (RSD) of a data set provide a measure of the variability of the data. The standard deviation demonstrates the spread of the data in comparison to the average value for the data. A low standard deviation indicates that the data points are close to the average value, a high standard deviation indicates a wide spread of data points and therefore a greater degree of variability.

The RSD is a percentage value that represents the degree of variability of the data. As with standard deviations a low RSD value indicates that there is not a large amount of variation and a higher RSD value suggests that there is more variability in the data set. Whether the variability in the data set demonstrated by the RSD values is acceptable or not depends upon the experiment and the amount of variation expected, however it is common in analytical chemistry to set a threshold of 5%[52, 53].

2.4.2 Hierarchical cluster analysis (HCA)

HCA is a form of multivariate analysis, this is the analysis data derived for multiple variables. Multivariate analysis is commonly used when comparing spectral data and different spectral features measured within that data. Individual data points across a spectrum can also be taken as variables for comparison[51]. HCA compares the values for each variable for each dataset to determine how similar or dissimilar each dataset is to the others. In this way it is possible to 'cluster' together similar datasets.

There are four main ways that similarity, or dissimilarity, can be measured; Euclidean distance, the correlation coefficient, Manhattan distance and Mahalanobis distance[54]. The Euclidean distance was chosen for this research as it

is the most commonly used of the four measures[54, 55]. The Euclidean distance between two objects can be calculated using equation 2.3, where m is the number of variables and k and l are the two objects[54, 56].

$$D_{kl} = \sqrt{\sum_{j=1}^m (x_{kj} - x_{lj})^2}$$

Equation 2.3 Euclidean distance for objects k and l with m variables[54]

A common way to present the results of HCA is using a dendrogram. This is a tree-like diagram that uses distance to represent the level of similarity between different datasets. The further away two datasets are the less similar they are. Clustering occurs at the point where two datasets are joined at a 'branch' of the dendrogram.

To illustrate this, table 2.2 shows a collection of data for five farmyard animals, where a 1 indicates yes and a 0 no to the presence of that particular feature, with the exception of the number of legs feature. This data has then been processed using HCA to produce the dendrogram shown in figure 2.11.

Table 2.2 Data on farmyard animals for use in chemometric analysis

Animal	Number of legs	Wings	Cloven hoof	Chews cud	Feathers	Webbed feet
Horse	4	0	0	0	0	0
Cow	4	0	1	1	0	0
Pig	4	0	1	0	0	0
Duck	2	1	0	0	1	1
Chicken	2	1	0	0	1	0

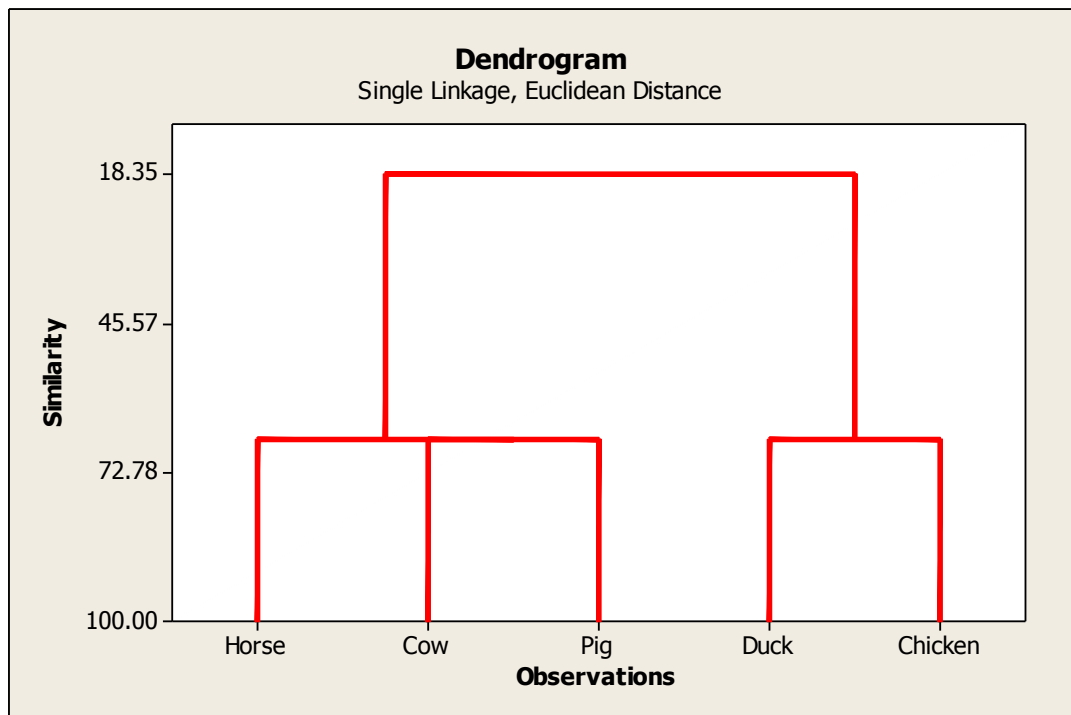


Figure 2.11 Dendrogram produced using Minitab 16 for the farmyard animal data in table 2.2

The dendrogram shows how, unsurprisingly, the birds have formed a separate cluster from the non-avians, given that for three of the variables these two animals had different values to the other animals. However, it can also be seen that while the birds cluster together it is with a similarity of approximately 70%, this is due to the difference in the webbed feet variable. The horse, cow and pig cluster together also at approximately 70% similarity. This is perhaps a little more surprising as the horse has two variables with different results compared to the cow, and one different from the pig so one might have expected the pig and horse to cluster before the cow. However, the pig only has one variable different from the cow (ruminates) and therefore this is why all three have clustered together.

This highlights the fact that while this technique is effective for separating groups with gross differences, when the differences are smaller the clustering may not show all the levels of variation.

2.4.3 Self organising feature maps (SOFM)

SOFM is a relatively new statistical technique[57], which provides an alternative to HCA and principal component analysis (PCA) for multivariate data[58]. It works

through a process of 'matching' different data entries looking for the Best Matching Unit (BMU) i.e. the most similar data, building up a network by then looking at neighbouring data[57]. This occurs in a stepwise process that is given in figure 2.12. In addition to the number of iterations T , there are two other important features of the process; the neighbourhood width (σ) and the learning rate (α)[57].

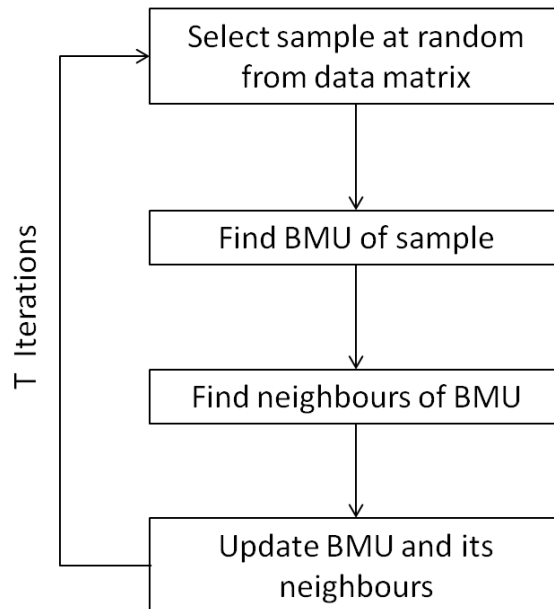


Figure 2.12 Simplified diagram demonstrating the steps of each iteration of the SOFM process (adapted from [57])

The neighbourhood width relates to the maximum distance a data unit can be from the BMU and still be updated in that iteration[57]. The updating of a data unit results in it become more similar to the BMU. The neighbourhood width starts a large value, so that in the initial iterations a substantial proportion of the data units are updated, and then decreases monotonically with each iteration, so that eventually only the BMU and its closest neighbours are updated[57].

The learning rate relates to the maximum amount a data unit can be updated (or learn) to represent a sample, i.e. how similar two units can become similar each other in terms of their weighting. The learning rate is a number between 1 and 0 and, as with the neighbourhood width, decreases monotonically with each iteration[57].

The data gained from this can be used to visualise the data in the form of a cluster map, or unified matrix. This matrix is created through the calculation for each data unit of the sum of the similarities between the weighting of that unit and the units around it. This gives a unit who is similar in weighting to its neighbours a low value, and a unit that is dissimilar to its neighbours a high value. These different values can be converted into a colour scale to visualise the different clusters[57].

What makes SOFM different from HCA is that it is also possible to separate out the different variables (or components) and look at the similarity levels seen in each variable, thereby allowing the user to perform principal component analysis and determine which variables are important for the discrimination of each dataset. SOFM also has the possibility for use with more complex statistical problems[59], such as a known set of data is entered to produce an initial cluster map and then unknown data is entered to identify the unknowns based upon where they cluster[58]. However, for the purposes of this research, as a proof of concept, it was sufficient to use SOFM in its most basic form. The cluster maps produced in this research are effectively training sets for future work. Therefore, it is possible to tune the clustering of the map to the number of clusters that you would be expecting. When taking the work further these training sets would be used as the basis for mapping unknown samples to determine if the discrimination of samples could be applied to unknown materials.

Using the data in table 2.2 an example cluster map is shown in figure 2.13. This shows that when the clustering is set to five, five clusters can be seen, one corresponding to each animal. However, when the clustering is not set, the matching algorithms only produce three clusters, albeit with shading differences showing five regions (figure 2.14). This highlights the fact that assumptions must be made when setting the clustering, in this instance five clusters were expected so the clustering was set to five, there is a risk that in some circumstances this could produce a map that suggests there is discrimination when there isn't.

This is why the colour shading is also important, as it is linked to the degree of similarity between each pixel, and so it can be seen that while there are only three defined clusters in figure 2.14, there are five regions of different shading.

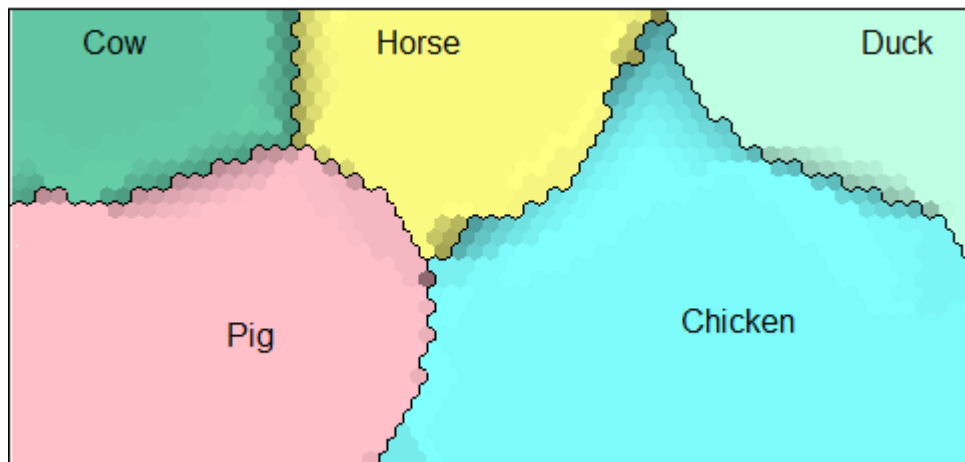


Figure 2.13 Cluster map produced using Viscovery SOMine 4.0.2 for the farmyard animal data set with the clustering set to five

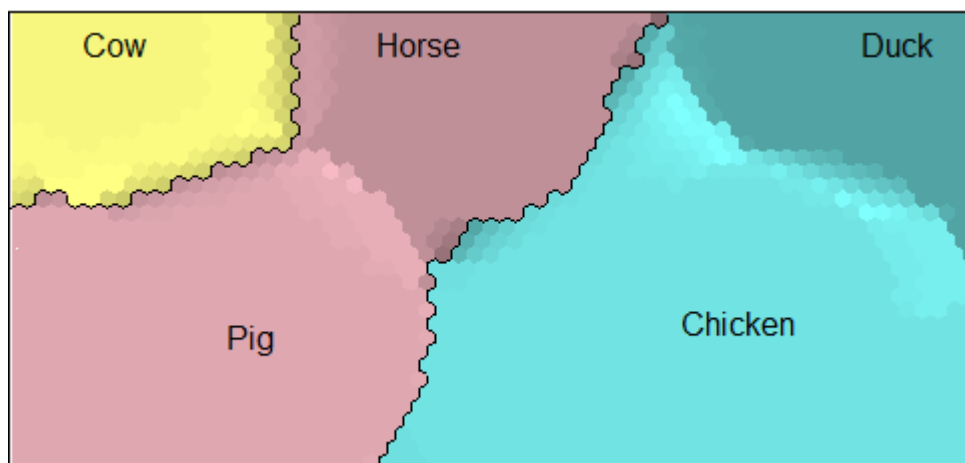


Figure 2.14 Cluster map produced using Viscovery SOMine 4.0.2 for the farmyard animal data set with the clustering set by the matching algorithms

Figure 2.15 reveals the component maps for the data, with five clusters set. The graded bar at the bottom of each component refers to the level of similarity in the cluster, ideally a component that is individual to a single dataset will have one red cluster, for example the Chew cud and Webbed feet components both have one red cluster, for cow and duck respectively. However, even where there isn't a single red cluster information can be gained from the shading as it is possible to see for each component which data sets give the same, or close to the same, result. For example

the Legs component has the duck and chicken clusters appearing blue and the horse, pig and cow appearing red, therefore it can be deduced that the duck and chicken have the same number of legs as do the horse, cow and pig, with the two groups having a different number of legs.

Despite the relative newness of the technique, it has already been applied to many areas, from the development of the technique by Kohonen in 1982, within the first 20 years around 4000 publications had appeared on the topic[59]. The ability to discriminate between similar materials, and to investigate the principal components in a visual and informative manner has made this a desirable technique for use in forensic science[55, 60-64], in particular for spectroscopic data analysis.

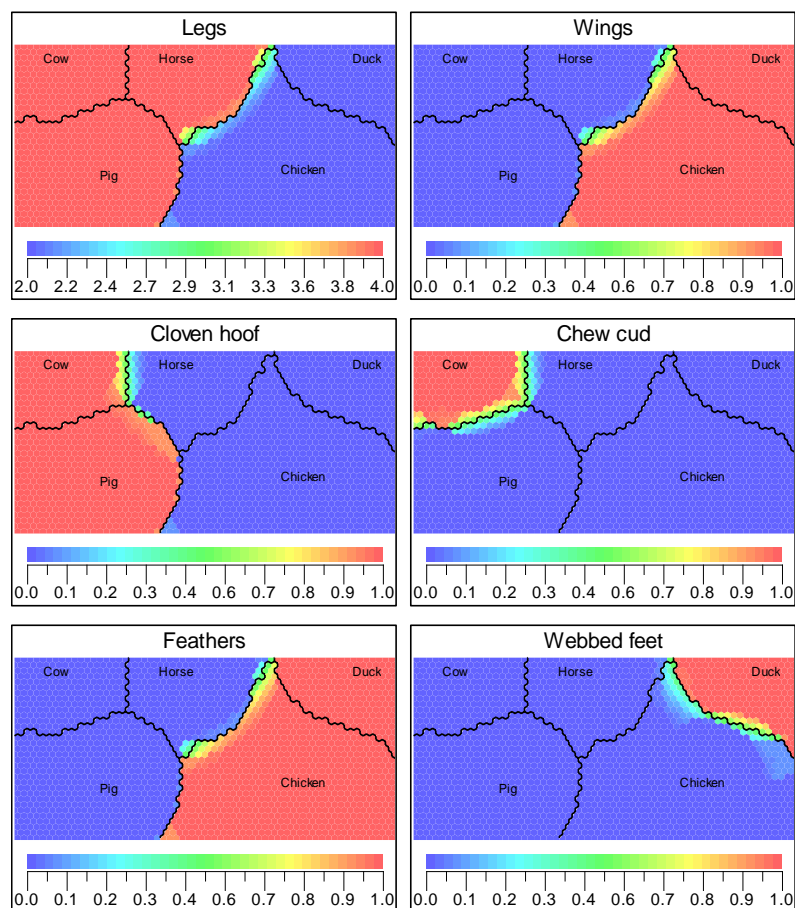


Figure 2.15 Component maps for the farmyard animal data using Viscovery SOMine 4.0.2

2.5 Conclusions

The available literature demonstrates that FTIR is a valid technique to employ for the detection and qualitative characterisation of explosive materials. However, the data generated needs to be handled correctly in order to be interpreted correctly and usefully. Therefore, there is a need to develop not only sound protocols for the gathering of data, but also sound data analysis to handle the large data sets produced.

2.6 References

1. Clugston, M.J., *Dictionary of Science*. 2nd ed. 2004: Penguin Reference.
2. Atkins, P. and De Paula, J., *Atkins' Physical Chemistry*. 2010: Oxford University Press.
3. Bernath, P.F., *Spectra of Atoms and Molecules*. 1st ed. 1995: Oxford University Press.
4. López-López, M., Ferrando, J.L. and García-Ruiz, C., *Comparative analysis of smokeless gunpowders by Fourier transform infrared and Raman spectroscopy*. *Analytica Chimica Acta*, 2012. **717**(0): p. 92-99.
5. [cited 2014 07/05/2014]; Available from: <https://effieboo.wordpress.com/2010/09/22/what-i-learned-in-chemistry/electromagnetic-spectrum/>.
6. Lim, K.F. and Lewis, S.W., *Spectroscopic Techniques*, in *Encyclopedia of Forensic Sciences*, P.J. Saukko and J.A. Siegel, Editors. 2013, Elsevier.
7. Harwood, L.M. and Claridge, T.D.W., *Introduction to Organic Spectroscopy*. Oxford University Primers. 1997: Oxford University Press.
8. Smith, B.C., *Fundamentals of Fourier Transform Infrared Spectroscopy*. 2nd ed. 2011: CRC Press.
9. Kemp, W., *Organic Spectroscopy*. 3rd ed. 1991: Macmillan.
10. *Spectroscopy*, ed. M.L. Gary. 2010: Australia ; United States : Brooks/Cole Cengage Learning.
11. Larkin, P.J., *IR and Raman Spectroscopy: Principles and Spectral Interpretation*. 2011: Elsevier.
12. Linne, M.A., *Spectroscopic Measurement: An Introduction to the Fundamentals*. 2002: Academic Press, Elsevier.
13. Smith, B.C., *Infrared Spectral Interpretation: A systematic approach*. 1999: CRC Press.
14. Zubrick, J.W. *Infrared Spectroscopy Part 1* [cited 2014 05/05/2014]; Available from: <http://what-when-how.com/organic-chemistry-laboratory-survival-manual/infrared-spectroscopy-part-1-laboratory-manual/>.
15. [cited 2014 05/05/2014]; Available from: <http://orgchem.colorado.edu/Spectroscopy/irtutor/aromaticsir.html>.
16. Hadden, J.M., *Protein Structure and Conformational Changes Studied By Fourier Transform Infrared Spectroscopy*, in *Department of Protein and Molecular Biology*. 1994, University of London: London.
17. Oxley, J. and Smith, J., *Peroxide Explosives*, in *Detection and Disposal of Improvised Explosives*, H. Schubert and A. Kuznetsov, Editors. 2006, Springer. p. 113-121.

18. Carlisle, F., Nic Daeid, N., Normand, E. and McCulloch, M., Exploiting High Resolution Fourier Transform spectroscopy to inform the development of a quantum cascade laser based explosives detection system. in *Optics and Photonics for Counterterrorism, Crime Fighting, and Defence VIII*. 2012. Edinburgh: SPIE.
19. Chalmers, J.M., Edwards, H.G.M. and Hargreaves, M.D., *Infrared and Raman Spectroscopy in Forensic Science*. 1st ed. 2012: Wiley.
20. Desilets, S., Ho, N., Mathieu, P., Simard, J.R., Puckrin, E., Theriault, J.M., Lavoie, H., Theberge, F., Babin, F., Gay, D., Forest, R., Maheux, J., Roy, G. and Chateauneuf, M., *Stand-off detection of explosives, a challenging approach for optical technologies*, in *Micro- and Nanotechnology Sensors, Systems, and Applications Iii*, T. George, M.S. Islam, and A.K. Dutta, Editors. 2011, Spie-Int Soc Optical Engineering: Bellingham.
21. Dewitt, K.M. and Dewitt, M.J., *Fourier transform infrared spectrometer for e.g. detecting hazardous air-borne for tracing chemical and explosives detection, has transceiver receiving radiation from analyte material upon irradiating by output beam*, SYSTEM PLANNING CORP (SYST-Non-standard). p. 15.
22. Itozaki, H. and Sato-Akaba, H., *Detection of bottled explosives by near infrared*, in *Optics and Photonics for Counterterrorism, Crime Fighting and Defence Ix; and Optical Materials and Biomaterials in Security and Defence Systems Technology X*, D. Burgess, et al., Editors. 2013, Spie-Int Soc Optical Engineering: Bellingham.
23. James, R.L., Hargreaves, M.D. and Brown, C.D. (2010) *Handheld FT-IR and Raman as Tools in the Analysis of Improvised Explosive Materials*. *Spectroscopy: Solutions for Materials Analysis*, 3.
24. Bauer, C., Sharma, A.K., Willer, U., Burgmeier, J., Braunschweig, B., Schade, W., Blaser, S., Hvozدارa, L., Muller, A. and Holl, G., *Potentials and limits of mid-infrared laser spectroscopy for the detection of explosives*. *Applied Physics B-Lasers and Optics*, 2008. **92**(3): p. 327-333.
25. Fischer, C., Pohl, T., Weber, K., Vogel, A., van Haren, G. and Schweikert, W., *TATP Stand-off Detection with Open Path - FTIR Techniques*. in *Optics and Photonics for Counterterrorism, Crime Fighting and Defence VIII*. 2012. Edinburgh: SPIE.
26. Marshall, M., *Post-Blast Detection Issues*, in *Aspects of Explosives Detection*, M. Marshall and J.C. Oxley, Editors. 2009, Elsevier. p. 223-243.
27. Bertino, A.J. and Bertino, P.N., *Forensic Science: Fundamentals and Investigations*. 1st ed. 2009: South-Western Cengage Learning.
28. Saukko, P.J. and Siegel, J.A., *Encyclopedia of Forensic Sciences*. 2013, London: Elsevier/Academic Press.
29. Zitrin, S., *Analysis of Explosives by Infrared Spectrometry and Mass Spectrometry*, in *Forensic Investigation of Explosions*, A.D. Beveridge, Editor. 1998, Taylor & Francis.
30. Waterbury, R., Vunck, D., Hopkins, A.J., Pohl, K., Ford, A. and Dottery, E., *Recent Improvements and Testing of a Check Point Explosives Detection System*, in *Chemical, Biological, Radiological, Nuclear, and Explosives*, A.W. Fountain, Editor. 2012, Spie-Int Soc Optical Engineering: Bellingham.
31. Wallin, S., Pettersson, A., Ostmark, H. and Hobro, A., *Laser-based stand-off detection of explosives: a critical review*. *Analytical and Bioanalytical Chemistry*, 2009. **395**(2): p. 259-274.
32. Nabiev, S.S., Stravrovskii, D.B., Palkina, L.A., Zbarskii, L.A., Yudin, N.V., Vaks, V.L., Domracheva, E.G. and Cheryaeva, M.B., *Spectrochemical properties of some explosives in the vapor state*. *Russian Journal of Physical Chemistry B*, 2013. **7**(3): p. 203-219.

33. López-López, M. and García-Ruiz, C., *Infrared and Raman spectroscopy techniques applied to identification of explosives*. TrAC Trends in Analytical Chemistry, 2014. **54**(0): p. 36-44.
34. Itozaki, H., Miyamura, R. and Sato-Akaba, H., *Detection of bottled explosives by near infrared*. in *Optics and Photonics for Counterterrorism, Crime Fighting and Defence VIII*. 2012. Edinburgh: SPIE.
35. Krausa, M. and Alekseyvitch Reznev, A., *Vapour and Trace Detection of Explosives for Anti-Terrorism Purposes*. NATO Science Series. 2004: Kluwer Academic Publishers.
36. Kumar, M., Islam, M.N., Terry, F.L., Freeman, M.J., Chan, A., Neelakandan, m. and Manzur, T., *Stand-off detection of solid targets with diffuse reflection spectroscopy using a high-power mid-infrared supercontinuum source*. Applied Optics, 2012. **51**(15): p. 2794-2807.
37. Doherty, W.J., Falvey, B., Rhodes, G.V., Krasnobaev, L. and Vachon, K., *A handheld FTIR spectrometer with swappable modules for chemical vapor identification and surface swab analysis*. Next-Generation Spectroscopic Technologies Vi, 2013. **8726**.
38. Castro, K., de Valleguelo, S.F.O., Astondoa, I., Goni, F.M. and Madariaga, J.M., *Are these liquids explosive? Forensic analysis of confiscated indoor fireworks*. Analytical and Bioanalytical Chemistry, 2011. **400**(9): p. 3065-3071.
39. Shishkov, P., Nedkova, M., Atanasova, P. and Glavchev.I., *UV-VIS and FTIR Investigations of Long-Term Aged Explosives Part 1*. Central European Journal of Energetic Materials, 2011. **8**(4): p. 293-301.
40. Shishkov, P., Nedkova, M., Atanasova, P. and Glavchev.I., *UV-VIS and FTIR Investigations of Long-Term Aged Explosives Part 2*. Central European Journal of Energetic Materials, 2011. **8**(4): p. 303-310.
41. McManus, J.B., Kebabian, P.L. and Zahniser, M.S., *Astigmatic mirror multipass absorption cells for long-path-length spectroscopy*. Applied Optics, 1995. **34**(18): p. 3336-3348.
42. Bruker, *IFS 125HR*. 2005.
43. Zachmann, G. Vacuum FT-IR Spectrometers for Synchrotron Application. in *WIRMS*. 2009. Banff Canada.
44. Krauss, M., *Explosives Detecting Dogs*. 1971, Mississippi University.
45. Hitz, C.B., *Introduction to laser technology [internet resource]*, ed. J.J. Ewing, et al. 2001: New York : IEEE Press.
46. Faist, J., Capasso, F., Sivco, D.L., Sirtori, C., Hutchinson, A.L. and Cho, A.Y., *Quantum Cascade Laser*. Science, 1994. **264**(5158): p. 553-556.
47. Hay, K., *Gas sensing using quantum cascade lasers*, in *Department of Physics*. 2010, University of Strathclyde: Glasgow. p. 198.
48. Demtroder, W., *Laser Spectroscopy: Basic Concepts and Instrumentation*. 3rd ed. 2003: Springer.
49. Capasso, F. *Quantum Cascade Lasers: Compact Widely Tailorable Light Sources from 3 to 300 μ m*. in *CLEO/IQEC*. 2009.
50. Liu, X., Van Neste, C.W., Gupta, M., Tsui, Y.Y., Kim, S. and Thundat, T., *Stand-off reflection-absorption spectra of surface adsorbed explosives measured with pulsed quantum cascade lasers*. Sensors and Actuators B: Chemical, 2014. **191**(0): p. 450-456.
51. Mendlein, A., Szkudlarek, C. and Goodpaster, J.V., *Chemometrics*. 2nd ed. Encyclopedia of Forensic Sciences, ed. J.A. Siegel. 2013: Elsevier.

52. Gonzalez, A.G. and Herrador, M.A., *A practical guide to analytical method validation, including measurement uncertainty and accuracy profiles*. Trac-Trends in Analytical Chemistry, 2007. **26**(3): p. 227-238.
53. Taverniers, I., De Loose, M. and Van Bockstaele, E., *Trends in quality in the analytical laboratory. II. Analytical method validation and quality assurance*. TrAC Trends in Analytical Chemistry, 2004. **23**(8): p. 535-552.
54. Brereton, R.G., *Chemometrics: Data Analysis for the Laboratory and Chemical Plant*. 2003: Wiley.
55. Thanasoulas, N.C., Parisis, N.A. and Evmiridis, N.P., *Multivariate chemometrics for the forensic discrimination of blue ball-point pen inks based on their Vis spectra*. Forensic Science International, 2003. **138**(1-3): p. 75-84.
56. Doble, P., Sandercock, M., Du Pasquier, E., Petocz, P., Roux, C. and Dawson, M., *Classification of premium and regular gasoline by gas chromatography/mass spectrometry, principal component analysis and artificial neural networks*. Forensic Science International, 2003. **132**(1): p. 26-39.
57. Brereton, R.G., *Chemometrics for Pattern Recognition*. 2009: Wiley.
58. Desa, W.N.S.M., *The Discrimination of Ignitable Liquids and Ignitable Liquid Residues using Chemometric Analysis*, in *Pure and Applied Chemistry*. 2012, University of Strathclyde: Glasgow.
59. Kohonen, T., *Self-Organising Maps*. 3rd ed. 2001: Springer.
60. Desa, W., Nic Daeid, N., Ismail, D. and Savage, K., *Application of Unsupervised Chemometric Analysis and Self-organizing Feature Map (SOFM) for the Classification of Lighter Fuels*. Analytical Chemistry, 2010. **82**(15): p. 6395-6400.
61. Mat-Desa, W.N.S., Ismail, D. and NicDaeid, N., *Classification and Source Determination of Medium Petroleum Distillates by Chemometric and Artificial Neural Networks: A Self Organizing Feature Approach*. Analytical Chemistry, 2011. **83**(20): p. 7745-7754.
62. Gonzalez-Rodriguez, J., Sissons, N. and Robinson, S., *Fire debris analysis by Raman spectroscopy and chemometrics*. Journal of Analytical and Applied Pyrolysis, 2011. **91**(1): p. 210-218.
63. Muehlethaler, C., Massonnet, G. and Esseiva, P., *The application of chemometrics on Infrared and Raman spectra as a tool for the forensic analysis of paints*. Forensic Science International, 2011. **209**(1-3): p. 173-182.
64. Thanasoulas, N.C., Piliouris, E.T., Kotti, M.S.E. and Evmiridis, N.P., *Application of multivariate chemometrics in forensic soil discrimination based on the UV-Vis spectrum of the acid fraction of humus*. Forensic Science International, 2002. **130**(2-3): p. 73-82.

Chapter 3. Protocol Development and Analysis of Compounds of Interest

3.1 Introduction

Prior to the analysis of materials of interest, a basic analytical protocol was required using the Fourier Transform Spectrometer (FTS). This was to determine both the optimum sample sizes and analytical temperatures for the analysis of liquid samples in the vapour phase (see figure 3.1 for the instrumental set-up). While some adaptations might have to be made to this protocol for less volatile materials it would still provide a starting point for any future analysis. The initial liquid chosen for protocol development was diesel as it presented a relatively complex mixture with some components within the liquid being sufficiently volatile to produce vapour at room temperature while others required the liquid to be heated.

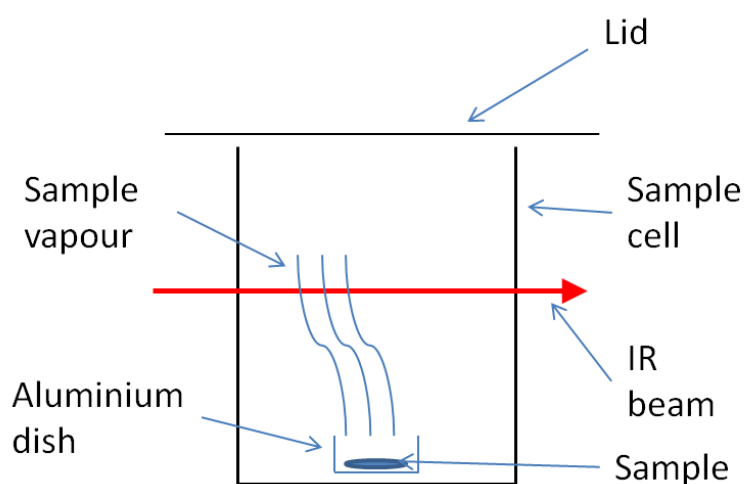


Figure 3.1 Diagram of the sample cell demonstrating how liquid samples were analysed in the vapour phase

Once the experimental protocol for liquids was developed, a range of explosive or explosive precursor materials were analysed to create a reference library to demonstrate the efficacy of the protocol. Sample choice was made to encompass a

range of compounds of interest, primarily focusing either within the spectral windows of currently available QCLs or wavelengths likely to be available in the near future. In addition, compounds of interest were selected for their roles as explosive precursors, with some materials having explosive properties in their own right. Table 3.1 lists the compounds of interest selected and their relevance to explosives detection.

Previous research into the vapour detection of these materials in an explosives detection context has mainly focused on colorimetric or electrochemical techniques[1-6]. The detection of ethylene glycol has predominantly been focused upon its detection in a toxicological context[7, 8]. However, some research has been carried out on the vapour phase detection of EGDN[9]. The materials listed have not previously been analysed with the specific aim of determining suitable spectral features for detection with a QCL based detection system. Analysis of these compounds of interest in the vapour phase could provide greater spectral information[10]. Furthermore, this will provide information suitable for stand-off detection systems, as many of these are reliant on detection of vapour[11].

Table 3.1 Summary of the compounds of interest selected and their relevance to explosives detection

Material	Formula	Relevance
Acetone	C ₃ H ₆ O	Important constituent of TATP[12-14]
Ammonia	NH ₃	Important constituent of ammonium nitrate (AN), ANFO and AN slurries[15, 16]
Ethanol	C ₂ H ₆ O	Can act as a fuel in the presence of an oxidiser, for example when mixed with nitric acid it forms a rocket fuel-like mixture[17]
Ethylene glycol	C ₂ H ₆ O ₂	Important constituent of EGDN (ethylene glycol dinitrate)[15]
Hydrazine	N ₂ H ₄	Important constituent of many rocket fuels[18, 19]
Hydrazine hydrate	N ₂ H ₄ · H ₂ O	Important constituent of many rocket fuels[18, 19]
Hydrogen peroxide	H ₂ O ₂	Important constituent of peroxide based explosives such as TATP and HMTD[12, 20-22]
Methanol	CH ₄ O	Important constituent of methyl nitrate[23, 24]
Nitric acid	HNO ₃	Important constituent of methyl nitrate[23], EDGN[15], can form a rocket fuel-like mixture with ethanol[17]
Nitromethane	CH ₃ NO ₂	Found in explosive compositions mixed with a sensitizer[25], or mixed with AN, classed as a liquid propellant when on its own[16]

Each material was characterised using high resolution FTIR focusing primarily on the regions covered by the identified QCL wavelengths given in table 3.2, but also examining across the whole spectrum for features that might be suitable for detection with a new wavelength QCL or for features that might be detectable with multiwavelength QCLs. Such multiwavelength lasers are capable of spanning approximately 100 cm^{-1} , and an array of such lasers could cover a significant portion of the mid-infrared region.

Table 3.2 The currently available and future planned wavelengths of QCLs at Cascade Technologies

Currently available (cm^{-1})	Future wavelengths (cm^{-1})
867	885
918	1024
993	1106
1274	1160
1285	1184

3.2 Materials

3.2.1 Protocol development

Diesel was sourced from stocks held within the University of Strathclyde. The samples were held within the sample cell using aluminium dishes purchased from Sigma Aldrich UK.

3.2.2 Analysis of compounds of interest

10 materials were selected for analysis; these materials are shown in table 3.3.

Table 3.3 Source information for the 10 compounds of interest analysed

Material	Source
Acetone	Sigma Aldrich UK
Ammonia (in propanol)	Sigma Aldrich UK
Ethanol	Sigma Aldrich UK
Ethylene glycol	Sigma Aldrich UK
Hydrazine (in Tetrahydrofuran)	Sigma Aldrich UK
Hydrazine hydrate	Sigma Aldrich UK
Hydrogen peroxide	Sigma Aldrich UK
Methanol	Sigma Aldrich UK
Nitric acid	Sigma Aldrich UK
Nitromethane	Sigma Aldrich UK

Two of the materials, ammonia and hydrazine, were dissolved in solvents due to their volatile nature. Both of these solvents, propanol and tetrahydrofuran (THF), were also analysed so that their effects on the spectra of ammonia and hydrazine respectively could be investigated. Both propanol and THF were sourced from Sigma Aldrich UK.

Samples were held within the sample cell in aluminium dishes purchased from Sigma Aldrich UK with the exception of nitric acid, hydrazine and hydrazine hydrate which were analysed in a dimpled ceramic tile, sourced in house, due to the risk of these materials reacting with the aluminium dishes.

3.3 Method

Samples were transferred into the sample cell using either a syringe or micropipette, depending upon the volume being analysed and any risk of the material reacting with the plastic pipette tips (nitric acid, hydrazine and hydrazine hydrate in particular). The instrument settings are given in table 3.4.

Table 3.4 FTS instrument settings used during this research

General:	Setting
Resolution	0.1 cm ⁻¹
Sample scan time	100 scans
Background scan time	100 scans
Save data from	800 - 2000 cm ⁻¹
Result spectrum	Transmittance
Datablocks to be saved	Transmittance, Single channel, Background
Optic:	
External synchronisation	Off
Source setting	MIR
Beamsplitter	KBr
Aperture setting	0.5 mm
Measurement channel	Front sample compartment
Background measurement channel	Front sample compartment
Detector setting	LN-MCT MidFOV = 30°[Internal Pos.1]
Preamp gain	B
Scanner velocity	40 kHz
Sample signal gain	x1
Background signal gain	x1
Delay after device change	0 seconds
Delay before measurement	0 seconds
Optical bench ready	Detector cooled
Acquisition:	
Wanted high frequency limit	15000 [15798.02 cm ⁻¹]
Wanted low frequency limit	0 [0.00 cm ⁻¹]
Laser wavenumber	15798.02 cm ⁻¹
Interferogram size	287918 points. FT size 1024K
High pass filter	Open
Low pass filter	40 kHz [15978 cm ⁻¹]
Acquisition mode	Single sided, forward-backward
Correlation mode	Off
FT:	
Phase resolution	8
Phase interferogram points	7109
Phase correction mode	Mertz
Apodization function	Blackman-Harris 3-term
Zerofilling factor	2
Perform interferogram non-linearity correction before FT	No
Display limits:	
X axis	5000 to 0
Y axis	-0.1 to 1.1

3.3.1 Protocol development

A two factor, three level experimental design was used. Two factors, sample volume and temperature, were identified as potentially having significant effects on the

spectra produced. Sample volume was likely to have an effect because the more sample present, the greater amount of absorption of the infrared beam possible. Temperature was likely to have an effect as the higher the temperature the more vapour likely to be produced from the sample and therefore the more vapour available for interaction with the infrared beam. Three levels; low, medium and high, were selected for each factor and these are shown in table 3.5.

Table 3.5 The volume and temperature levels for the initial analysis of diesel

	Volume (mL)	Temperature (°C)
Low level	0.5	27
Medium level	1	75
High level	3	150

Each combination of the two factors at the three levels was repeated four times (based on previous research[26]), resulting in a total of 36 analytical runs to examine the effects of the two factors on the diesel spectra produced.

The sample analysis followed an eight step experimental procedure shown in table 3.6. The order of the different factor combinations was determined by the fact that the sample cell could not actively cool itself, therefore it was necessary to start with the lowest temperature level first.

Table 3.6 The experimental procedure for the initial analysis of diesel

Step	Action
1	Background scan taken of empty sample cell at lowest temperature
2	Analysis of each sample size level at lowest temperature
3	Sample cell heated to medium temperature
4	New background scan taken of empty sample cell at medium temperature
5	Analysis of each sample size level at medium temperature
6	Sample cell heated to high temperature
7	New background scan taken of empty sample cell at high temperature
8	Analysis of each sample size level at high temperature

The resulting spectra were examined visually using the OPUS software (version 6.5) provided by Bruker with the instrument, and this software was used to calculate average spectra and standard deviations. The data was then transferred to

Microsoft Excel (2010 version) to enable further statistical analysis, and closer examination of any regions of absorption that had been identified using OPUS.

3.3.2 Compounds of interest

The analysis of the compounds of interest followed the protocol developed using diesel. The stepwise process for the analysis is given in table 3.7.

Table 3.7 The stepwise process for the analysis of compounds of interest

Step	Action
1	Background scan taken of empty sample cell at 27°C
2	100 µL sample analysed at 27°C
3	Repeat step 2 for five additional samples
4	Create an average spectrum (and standard deviation) for the six repeats
5	If there are absorption features visible (excluding water and carbon dioxide) proceed to data analysis otherwise move to step 6
6	Increase the temperature to 75°C take a background scan of the empty cell and the repeat the analysis six times
7	Create an average spectrum (and standard deviation) for the six repeats
8	If there are absorption features visible (excluding water and carbon dioxide) proceed to data analysis otherwise move to step 9
9	Increase the sample volume to 1 mL and repeat the analysis six times
10	Create an average spectrum (and standard deviation) for the six repeats and proceed to data analysis

Following the production of an average spectrum and standard deviation for a sample set using the OPUS software, the data was transferred to Microsoft Excel to enable further statistical analysis.

3.4 Results and discussion

3.4.1 Diesel

The spectra from all possible level combinations with diesel showed two regions of absorption, aside from the carbon dioxide and water absorptions, at 2900 cm⁻¹ and 1400 cm⁻¹. Based upon the chemical makeup of diesel, which contains both long chain and branched alkanes, these regions of absorption are most likely to be caused by C-H bonds, and the broad nature of these absorption features suggest that they are a result of multiple bond vibrations that have overlapped. Temperature was shown to have a significant effect on the level of absorption with

the greatest absorption seen at 150°C and the least at 27°C. These differences can be seen in Figure 3.2. While an increased temperature increased the absorption, it also resulted in an increase in variability. This can be seen in tables 3.8 and 3.9 which show the standard deviations and relative standard deviations taken from the diesel spectra.

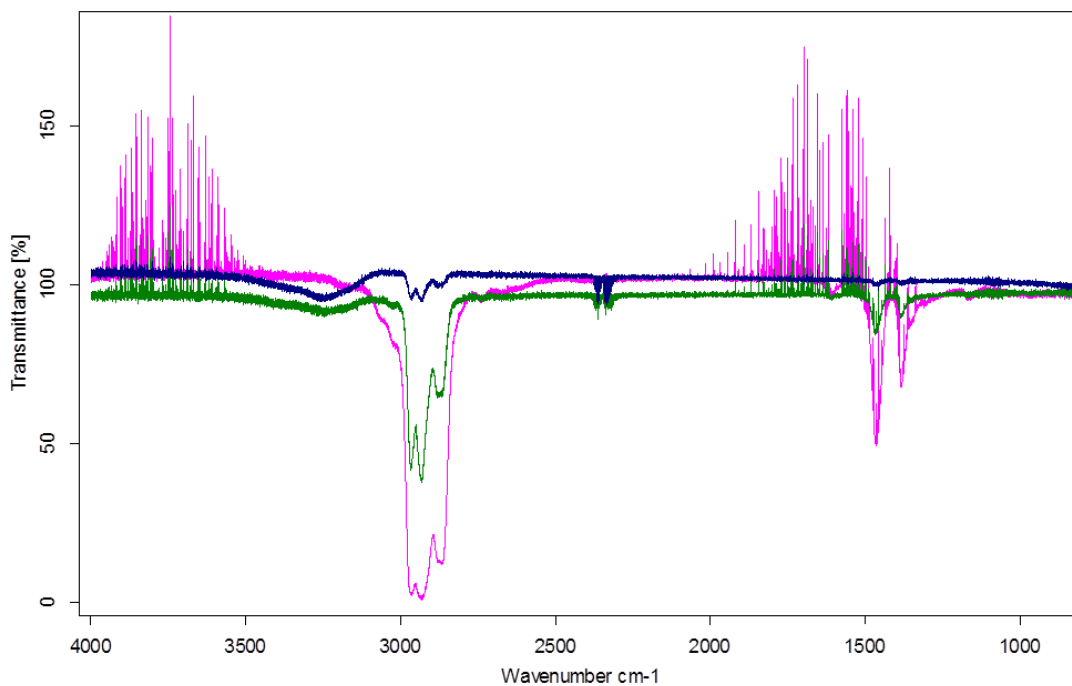


Figure 3.2 Diesel spectra produced at 27°C (blue), 75°C (green) and 150°C (pink) showing the differences in absorption seen across the temperature range

Table 3.8 Standard deviation values calculated for the whole spectrum and within the regions of absorption based on the mean where n=4

		27°C		75°C		150°C	
		Highest standard deviation	Average standard deviation	Highest standard deviation	Average standard deviation	Highest standard deviation	Average standard deviation
0.5 mL	Whole spectrum	0.08	0.03	0.13	0.01	0.03	0.02
	1400cm ⁻¹ region	0.04	0.02	0.10	0.01	0.18	0.04
	2900cm ⁻¹ region	0.04	0.04	0.02	0.02	0.08	0.04
1 mL	Whole spectrum	0.03	0.01	0.11	0.02	0.28	0.02
	1400cm ⁻¹ region	0.01	0.01	0.06	0.01	0.24	0.03
	2900cm ⁻¹ region	0.02	0.01	0.03	0.02	0.05	0.03
3 mL	Whole spectrum	0.03	0.00	0.20	0.02	0.25	0.03
	1400cm ⁻¹ region	0.01	0.00	0.04	0.01	0.16	0.05
	2900cm ⁻¹ region	0.01	0.00	0.03	0.02	0.11	0.04

Table 3.9 Relative standard deviation values calculated for the different variables for the whole spectrum and within the regions of absorption

		27°C		75°C		150°C	
		Highest RSD	Average RSD	Highest RSD	Average RSD	Highest RSD	Average RSD
0.5 mL	Whole spectrum	7.10	2.53	11.57	1.40	91.94	3.65
	1400cm ⁻¹ region	4.33	2.14	8.70	1.27	20.76	5.55
	2900cm ⁻¹ region	4.52	3.57	6.15	2.17	91.94	15.21
1 mL	Whole spectrum	2.84	0.87	9.14	1.51	195.30	3.68
	1400cm ⁻¹ region	1.34	0.68	4.92	1.22	18.84	4.39
	2900cm ⁻¹ region	1.71	1.13	2.98	1.56	195.30	12.27
3 mL	Whole spectrum	2.87	0.39	20.97	1.63	113.70	4.34
	1400cm ⁻¹ region	0.90	0.38	2.58	1.15	17.01	5.65
	2900cm ⁻¹ region	1.04	0.41	4.80	2.09	113.70	16.20

The standard deviation values were calculated using the OPUS software and give data for the whole spectrum as well as the two regions of absorption. The RSDs were calculated using the data produced by OPUS for the average and standard

deviation values. Two values are given for each level, the highest value and the average value, in order to give a broader perspective on the data.

The general trend observed was that as the temperature or volume increased, both the standard deviation and RSD values increased. When examining the two regions of absorption a trend was also seen, with the region at 2900 cm^{-1} showing higher RSD values, both in terms of the highest single RSD value and the average RSD value. This is probably because this is a larger region of absorption where the larger the absorption peak the more likely it is that there will be variation. The majority of the standard deviation and RSD values are below 5% indicating that while there is a degree of variability it is not at a high enough level to affect the overall analysis. The RSD values at 150°C indicate that at this temperature the level of variation seen could have a detrimental effect on the analysis.

It should also be noted that while a large amount of absorption is preferable, as this makes it easier to identify the absorption features, too much absorption will result in saturation and flattening of the peaks. Figure 3.3 shows the absorption bands at 2900 cm^{-1} across the three temperature levels and shows that, at 150°C , the percentage transmittance is almost zero, which suggests that at this high temperature level there is a risk of saturation.

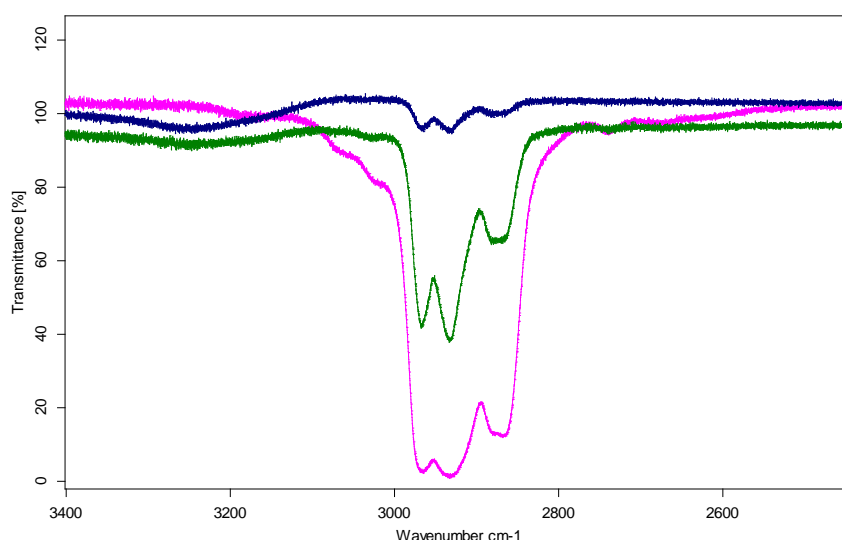


Figure 3.3 Close up of the absorption seen at 2900 cm^{-1} with diesel at 27°C (blue), 75°C (green) and 150°C (pink)

The results suggest that 27°C would be a suitable starting temperature as, while there is less absorption seen than at higher temperatures, there still are visible absorption bands. This indicates that compounds of similar or greater volatility than diesel would show visible absorption bands at this temperature. For less volatile compounds if no absorption bands were visible at 27°C the temperature could then be increased to 75°C.

Figure 3.4 shows the variation seen between the three sample volumes tested at 75°C. The variation is substantially less than that seen with the different temperature levels, with the main variation occurring in the levels of carbon dioxide and water absorption observed and a degree of offset of the baseline. This suggests that temperature is the dominant factor for determining the level of absorption. This is supported by the fact that the amount of variation between the spectra generated for different sample volumes increased as the temperature increased. This also means that at lower temperatures, such as 27°C, there is less variation and therefore the sample volume is less significant and smaller volumes can be used without any significant reduction in the amount of absorption observed. Smaller volumes are advantageous as they are easier and safer to handle. Whilst the smallest volume used in the diesel analysis was 0.5 mL, based upon the results, a starting volume of 0.1 mL would be appropriate for compounds of interest; with the ability to increase the volume to 1 mL for less volatile compounds if a temperature increase alone proved insufficient to produce visible absorption bands.

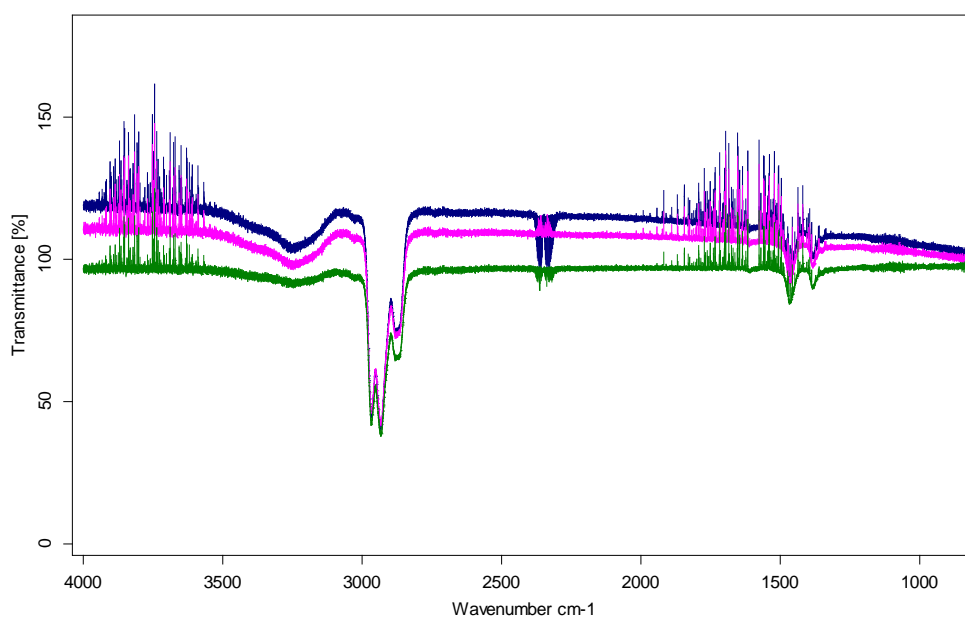


Figure 3.4 Spectra produced with diesel at 75°C with sample volumes of 0.5 mL (green), 1 mL (pink) and 3 mL (blue)

To summarise, the results of the diesel analysis have produced a basic protocol for the analysis of liquid compounds of interest. The start temperature for analysis should be 27°C and the start volume 100 μL . If these conditions do not produce suitable absorption for characterisation, the temperature should be increased to 75°C, at first with the sample volume still 100 μL , but if necessary with the volume increased to 1 mL.

3.4.2 Acetone

Information from Cascade Technologies suggested that there was a broad absorption band at 1220 cm^{-1} that would be too broad for absorption with current QCLs but would be an ideal target for detection with a broad band laser. The whole spectrum was analysed to gather an overall view with the expectation that, in addition to a band at 1220 cm^{-1} , the majority of absorption bands present would be too broad for detection with currently available QCLs. However, it was also examined in the regions of the currently available and future wavelengths to identify any regions that might be suitable for detection prior to the development of broad band QCLs. Due to the highly volatile nature of acetone, the spectra

produced were also carefully monitored to determine if there was saturation at any point of the spectrum.

Figure 3.5 shows the average spectrum produced with 100 μL acetone at 27°C. As expected there are several broad absorption bands, which appear to reach close to saturation, with a flattening of the bottom of the peaks observed. In addition to these larger peaks there are also several narrower absorption bands that might be suitable for detection with a narrow band QCL.

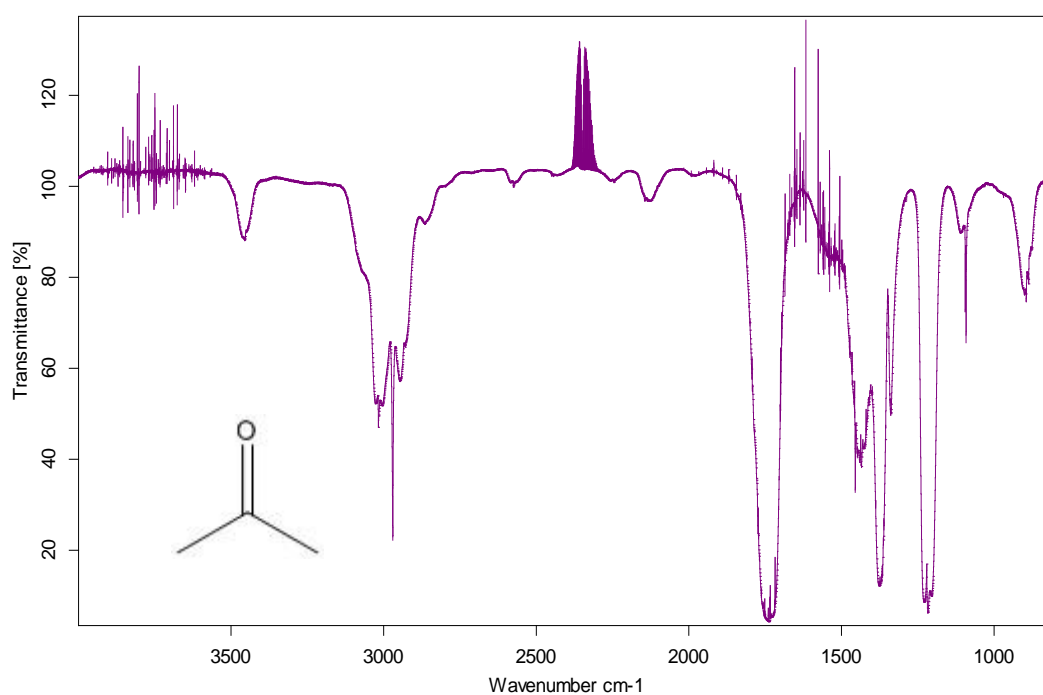


Figure 3.5 Average spectrum produced with 100 μL acetone at 27°C with the structure of acetone also shown

Figure 3.6 shows the absorption present at 1220 cm^{-1} , and indicates that the predicted broad band is present in this region.

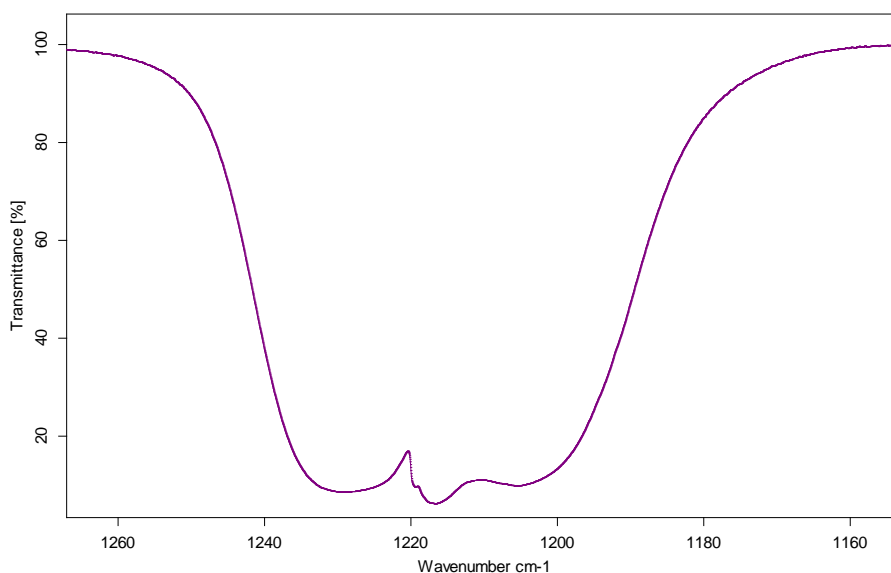


Figure 3.6 Close up of the broad absorption band at 1220 cm^{-1} in the average spectrum of $100\ \mu\text{L}$ acetone at 27°C that might be suitable for detection with a broadband QCL

This band would be suitable for detection with a broad band QCL however the band has the disadvantage of being close to saturation, and includes an inverse peak which could potentially interfere with detection. Based upon classification tables[27] the absorption at 1220 cm^{-1} was believed to be due to C-H stretching.

The examination of the regions of currently available, and future QCL wavelengths, revealed that for the majority of the wavenumbers there is either no absorption or the absorption present is part of a broader band and therefore not suitable for detection at this time. However, there were two regions that might be suitable for detection with current or planned narrow beam QCLs. There is a small peak at approximately 886.5 cm^{-1} which, although found within a larger peak, might be suitable for detection with an 885 cm^{-1} laser (see figure 3.7). This peak and the associated broader peak was believed to be due to C-H out of plane bending. The second peak is found at approximately 1290 cm^{-1} , which might be detectable with a QCL at 1285 cm^{-1} although it might fall just outside the spectral window (see figure 3.8). This absorption was believed to be due to C-H bond stretching.

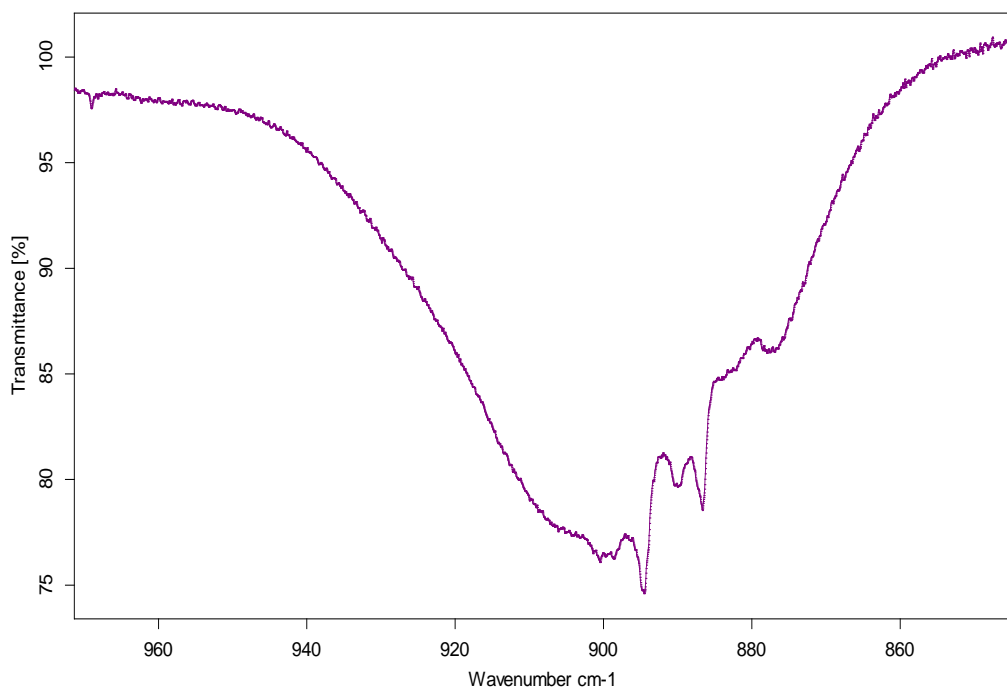


Figure 3.7 Close up of the potential detection target at 886.5 cm^{-1} which is part of a broader absorption peak of the average spectrum of $100\text{ }\mu\text{L}$ acetone at 27°C

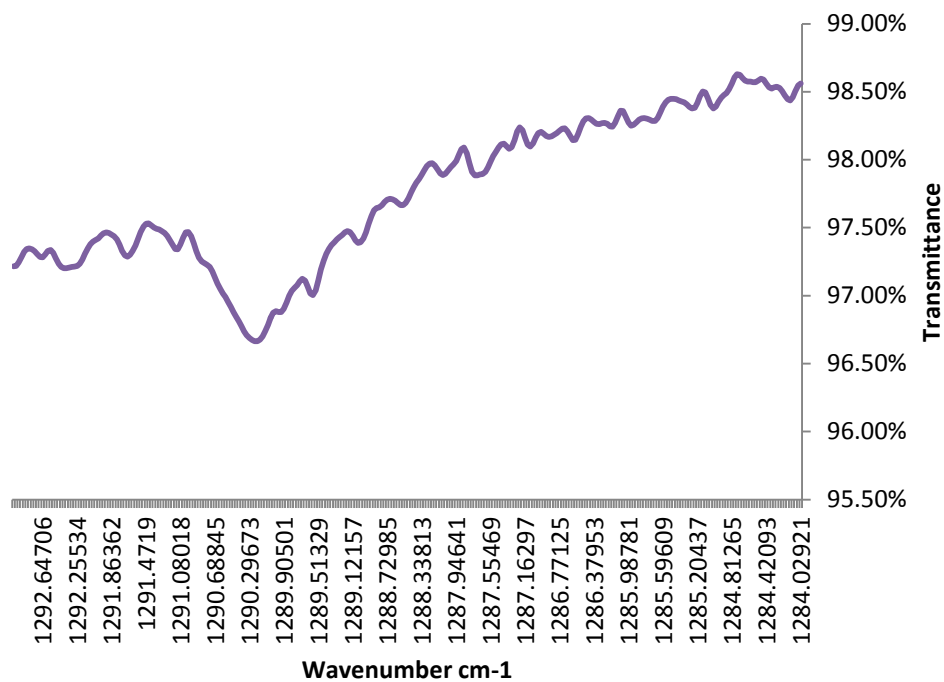


Figure 3.8 Excel plot showing the potential detection target at 1290 cm^{-1} created with the data from the average spectrum of $100\text{ }\mu\text{L}$ acetone at 27°C

To summarise, based upon the spectra obtained, acetone produces significant absorption. However the majority of the absorption bands are too broad for detection with the currently available narrow band QCLs. The development of broadband QCLs would facilitate the detection of acetone and one region at 1220 cm^{-1} has already been identified for this purpose.

3.4.3 Ammonia

The ammonia analysed was in propanol which was expected to have an effect on the spectra produced. In order to overcome this, propanol was analysed under the same conditions and the average spectrum produced was subtracted from the ammonia in propanol average spectrum. The two spectra, ammonia in propanol and the subtracted spectrum are shown in figures 3.9 and 3.10.

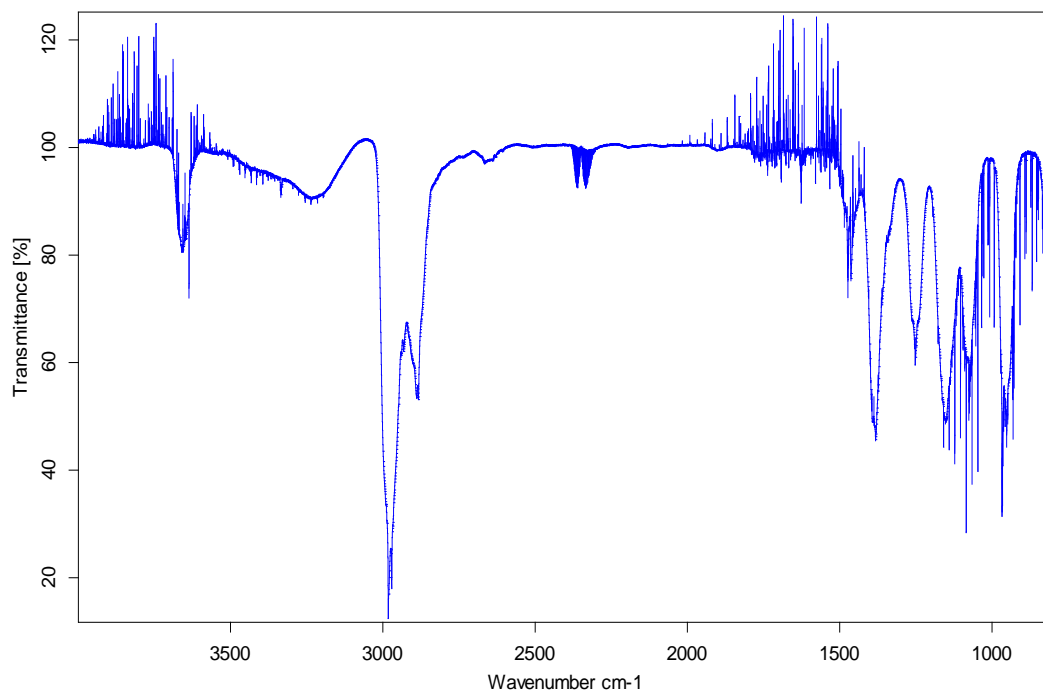


Figure 3.9 Average spectrum produced with 100 μL ammonia in propanol at 27°C

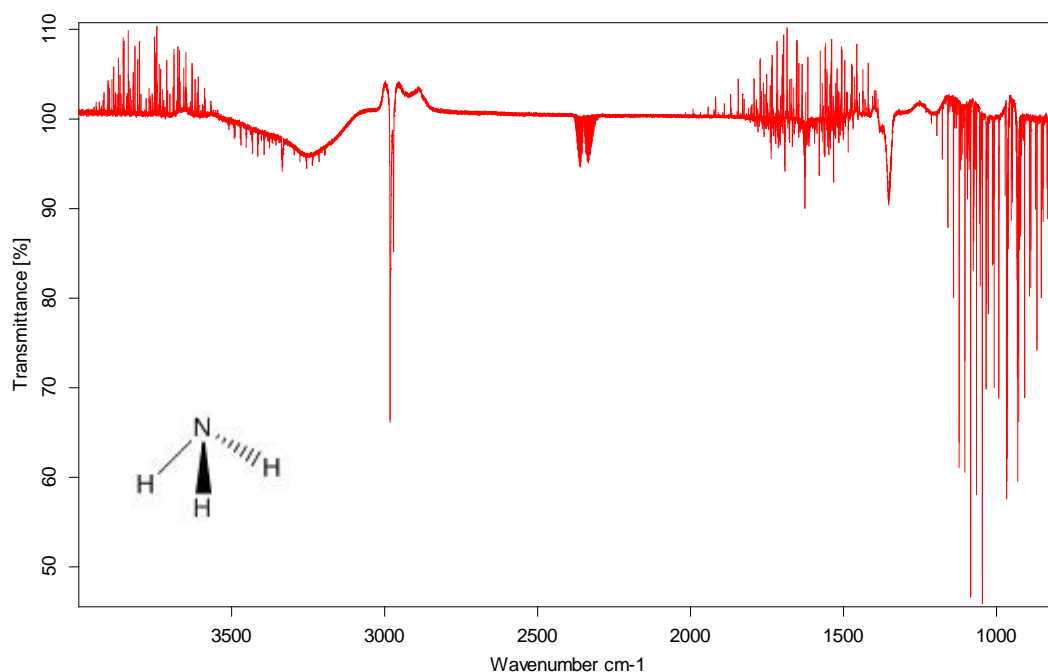


Figure 3.10 Average spectrum of 100 μL ammonia at 27°C with propanol subtracted with the structure of ammonia inset

Data from Cascade Technologies indicated that there would be absorption present at 867 and 993 cm^{-1} . A visual analysis of the spectra suggested that absorption was indeed present in these regions, however, the absorption at 993 cm^{-1} could be affected by the presence of propanol. Both the original and the subtracted spectra, along with propanol, were plotted in Microsoft Excel for the two regions of absorption, and the results indicate that the propanol did not have a significant effect on the level or shape of either of the absorption bands (see figures 3.11 and 3.12).

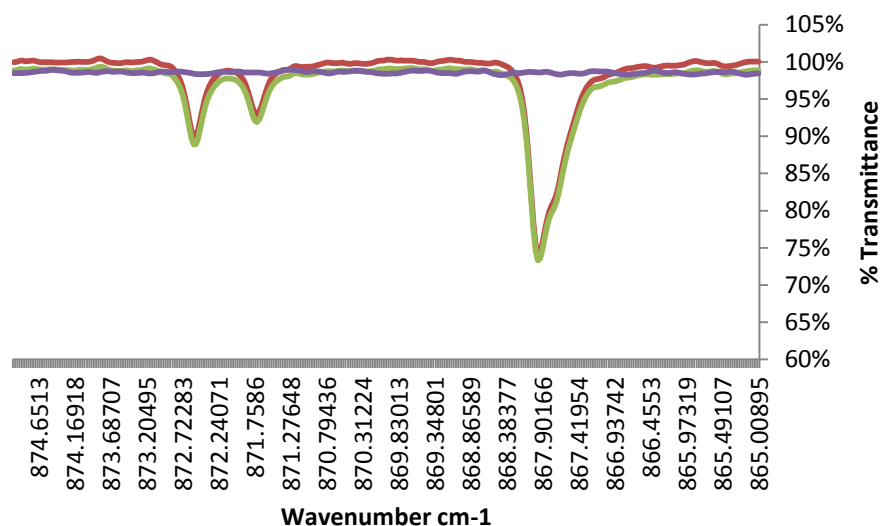


Figure 3.11 Plotted data for ammonia in propanol (green), propanol (purple) and ammonia with propanol subtracted (red) for the spectral region of the 867 cm⁻¹ detection site

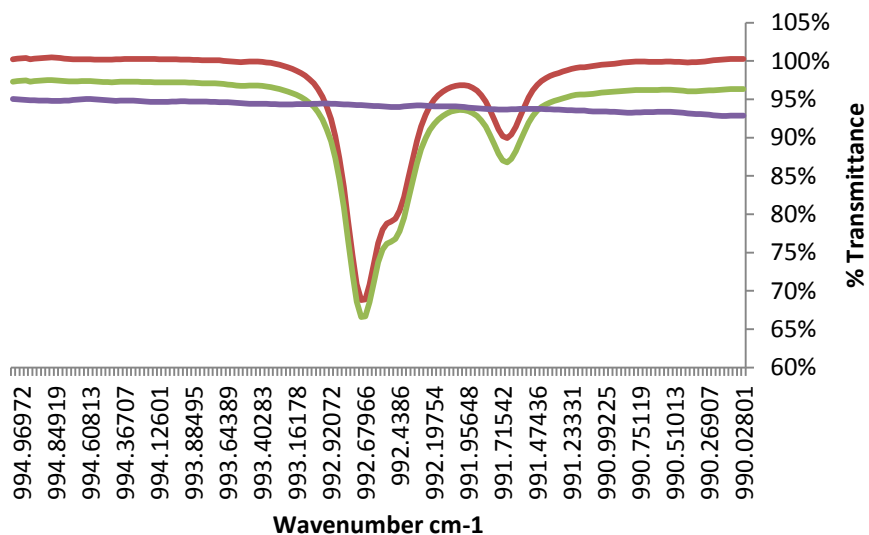


Figure 3.12 Plotted data for ammonia in propanol (green), propanol (purple) and ammonia with propanol subtracted (red) for the spectral region of the 993 cm⁻¹ detection site

The absorption bands, derived from the N-H bonding, were found to be slightly offset from the predicted wavenumbers, with the 867 cm⁻¹ band closer to 866 cm⁻¹ and the 993 cm⁻¹ band closer to 992 cm⁻¹. However, the bands still fall within the QCL spectral windows. Neither of the absorption bands of interest appear to be discrete peaks with both having a shoulder, suggesting that the absorption is

comprised of two peaks combined rather than a single peak. However, this does not prevent the use of the absorption band for detection.

To summarise, both the regions predicted to show absorption did have peaks present, but in both cases the peaks were approximately 1 cm^{-1} away from their predicted location. Propanol was shown not to have a significant effect on either of the absorption bands of interest through subtraction of a propanol spectrum from the ammonia in propanol average spectrum. Based upon these results both the absorption band at 866 cm^{-1} and 992 cm^{-1} would be suitable for QCL detection.

3.4.4 Ethylene glycol

Ethylene glycol is substantially less volatile than diesel, and therefore it was predicted that it would be necessary to increase the temperature to 75°C in order to produce spectra suitable for characterisation. This proved to be the case and figure 3.13 shows the average spectrum obtained at 75°C . In addition, to enhance the spectra, the sample volume was increased to 1 mL. Data from Cascade Technologies had indicated the potential presence of absorption bands at 1075 and 1160 cm^{-1} and therefore these were the regions focused upon for characterisation.

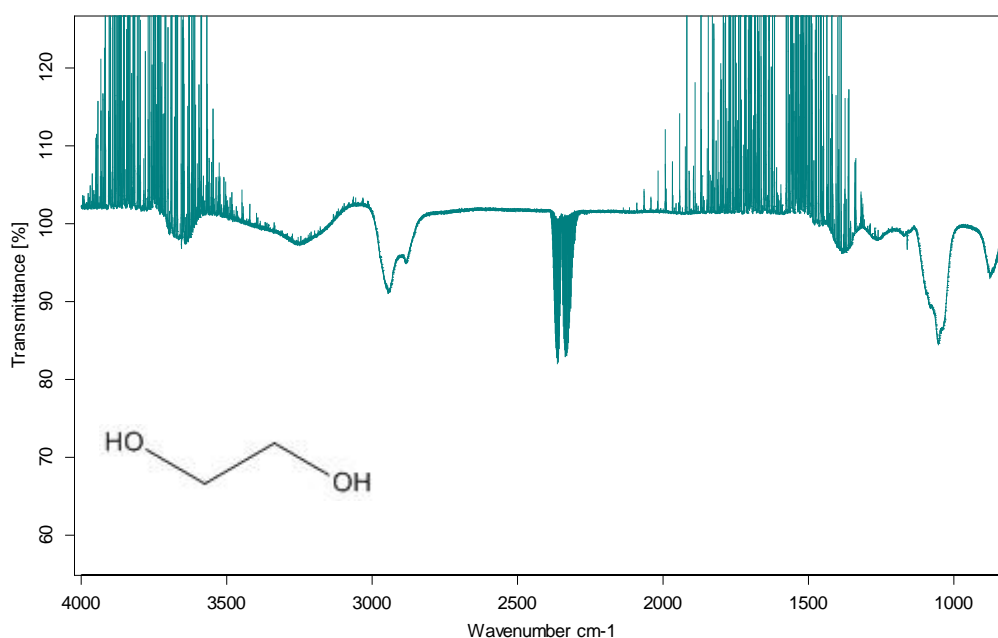


Figure 3.13 Average spectrum produced with 1 mL ethylene glycol at 75°C showing the structure of ethylene glycol inset

Initial visual analysis of the spectra suggested that absorption bands were indeed present at the predicted wavenumbers, with the band at 1075 cm^{-1} significantly larger than at 1160 cm^{-1} . When these regions were plotted using Microsoft Excel it became clear that, while there was an absorption band at 1075 cm^{-1} , it was too broad for the spectral window of a conventional QCL at this wavenumber (see figure 3.14). The smaller absorption band was found to be slightly apart from the predicted wavenumber at approximately 1160.5 cm^{-1} (see figure 3.15). This still falls within the spectral window for a QCL at 1160 cm^{-1} and the absorption band forms a discrete peak which is ideal for detection. The absorption at 1075 and 1160.5 cm^{-1} are both believed to be a result of $>\text{C-O}$ stretching.

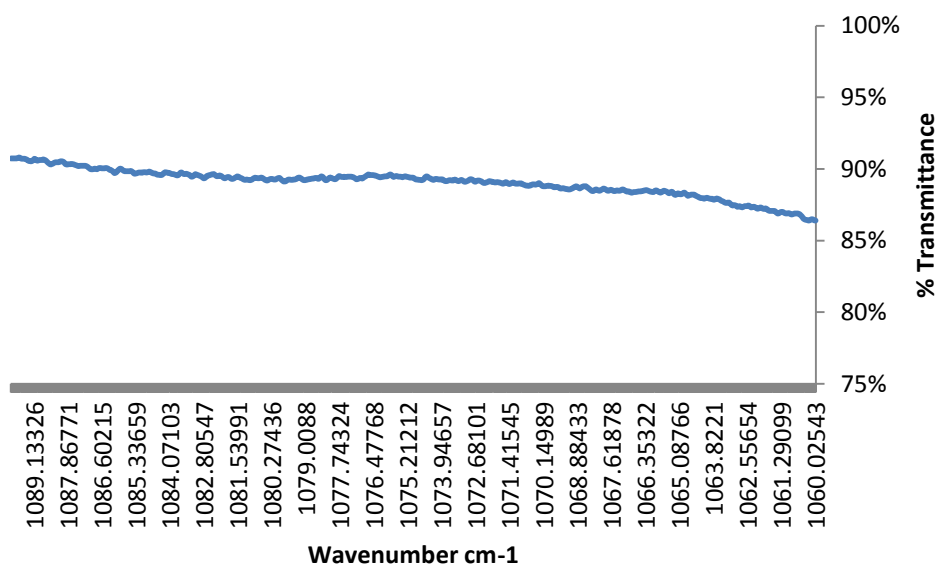


Figure 3.14 Plotted values for ethylene glycol in the spectral region of the 1075 cm^{-1} detection site

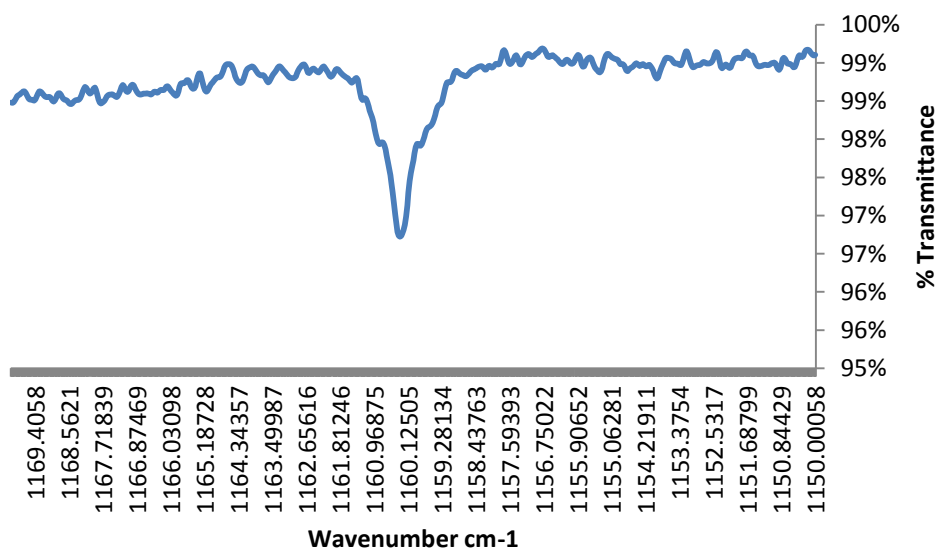


Figure 3.15 Plotted values for ethylene glycol in the spectral region of the 1160 cm^{-1} detection site

To summarise, the results of the ethylene glycol analysis indicate that there is an absorption band at 1160.5 cm^{-1} that would be suitable for QCL detection. However, the predicted absorption band at 1075 cm^{-1} , while present, was too broad for detection with current QCLs.

3.4.5 Hydrazine and hydrazine hydrate

Reference information provided by Cascade Technologies indicated the presence of a significant absorption peak at 918 cm^{-1} . However, hydrazine was only available in solvent and reference spectra suggested that hydrazine solutions could produce a significantly different spectrum to pure hydrazine. Hydrazine in THF was analysed, and, as predicted, the absorption was shifted compared to the reference information for pure hydrazine. In addition to this THF reference spectra suggested that it would produce absorption in the same region, and this was seen to be the case with a broad peak present in this region when viewing the average spectrum (see figure 3.16). Therefore a spectrum for THF was produced and subtracted from the spectrum of hydrazine in THF (see figure 3.17).

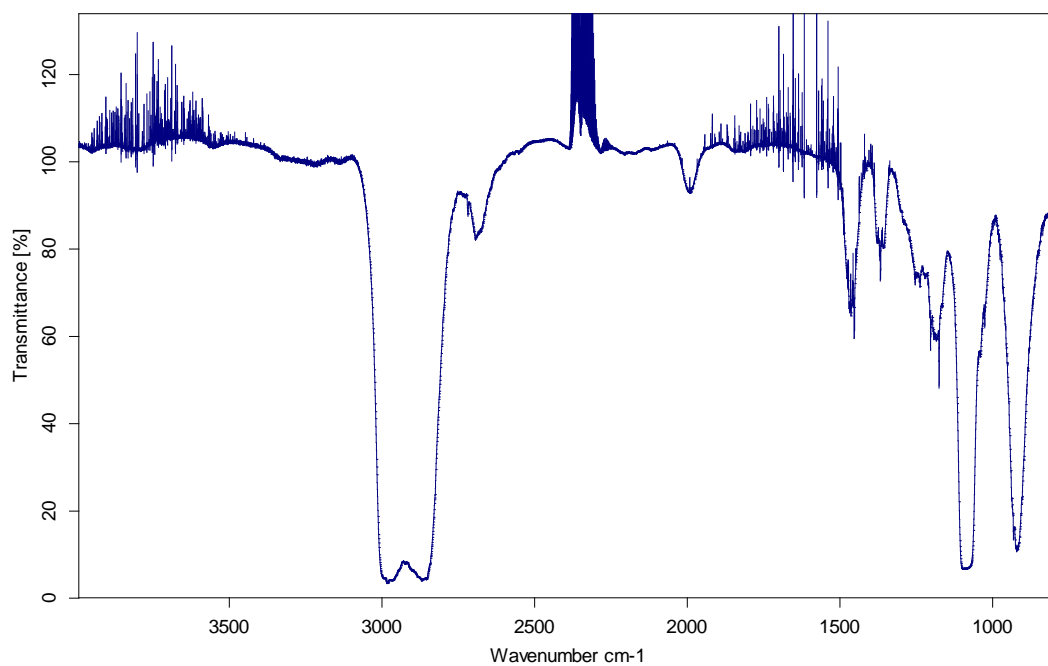


Figure 3.16 Average spectrum produced for 100 μL hydrazine in THF at 27°C

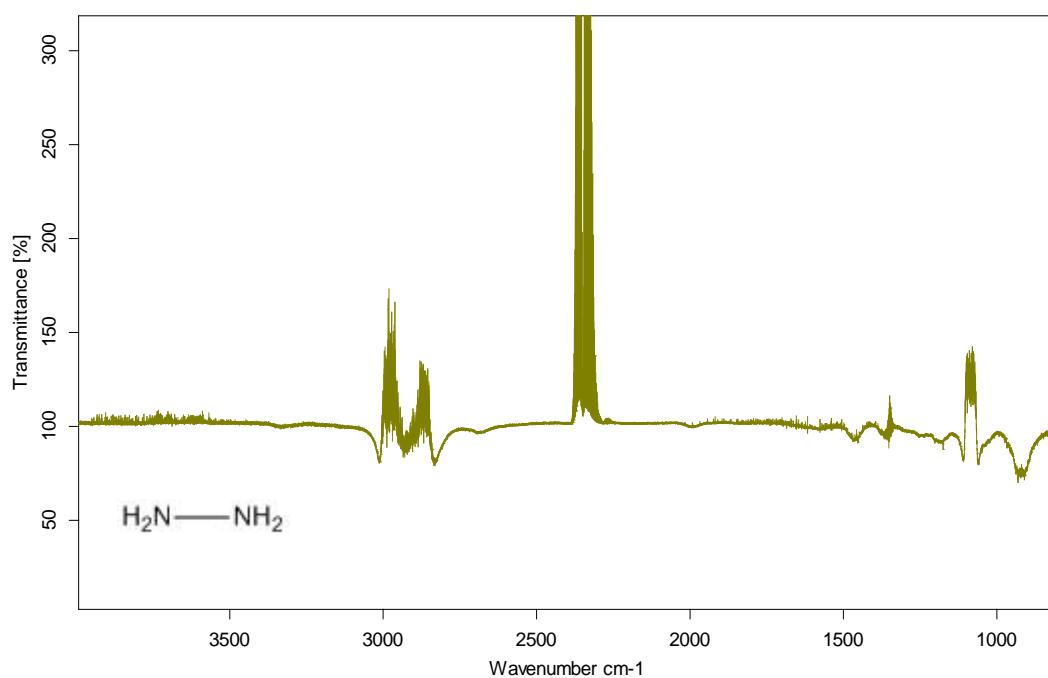


Figure 3.17 Hydrazine spectrum with THF subtracted with the structure of hydrazine inset

The subtracted spectrum shows multiple inverse peaks. These indicate regions where the THF spectrum had greater absorption than the spectrum of hydrazine in THF. This was not expected, however it is possible that THF is more volatile than the hydrazine THF solution and this would result in greater absorption. A close up of the

region around the 918 cm^{-1} detection site showed that there was absorption seen in the subtracted spectrum (see figure 3.18) which is part of a broader peak and therefore is unlikely to be suitable with currently available QCLs. Nonetheless, the region of the spectrum shown in figure 3.18 does show smaller peaks at approximately 1050 cm^{-1} and 1175 cm^{-1} which could be suitable for narrow QCL detection, although this would require the development of new laser wavelengths. The absorption peak at 918 cm^{-1} is believed to be caused by an N-H wag.

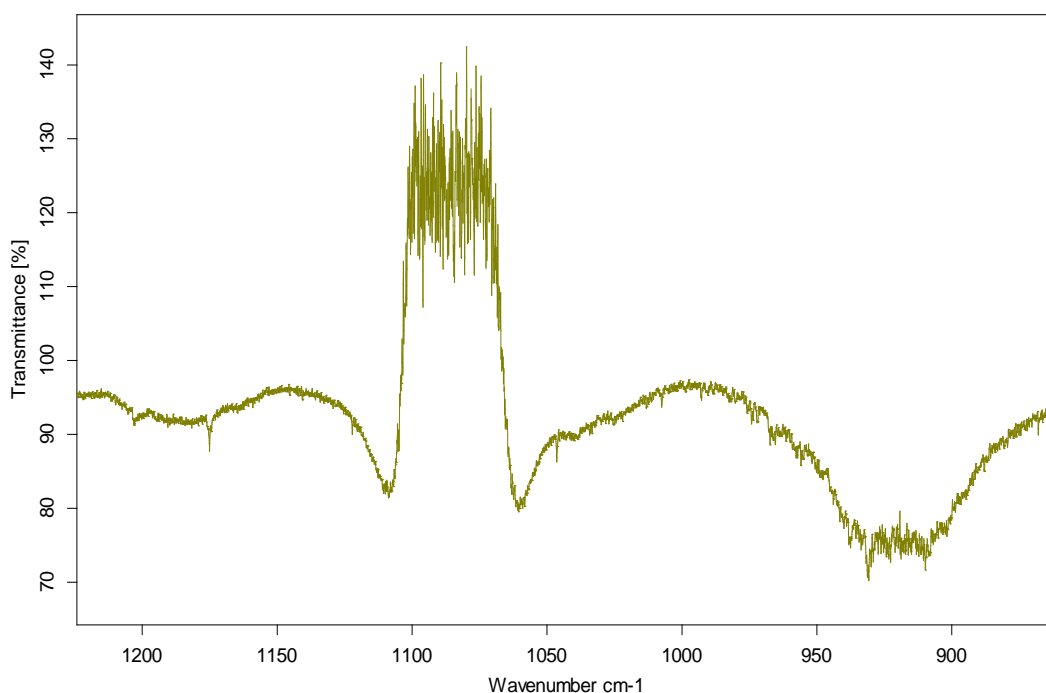


Figure 3.18 Close up of the hydrazine spectrum with THF subtracted showing the absorption in the 918 cm^{-1} detection site and small peaks at approximately 1050 cm^{-1} and 1175 cm^{-1}

Despite the relative success of the subtraction, the spectrum produced will vary depending upon the nature of the solution containing the hydrazine, and this will have a significant effect upon detection in a real world situation where the material is unlikely to be in a pure form.

Hydrazine hydrate was selected as an alternative to hydrazine in THF. It was predicted that, while the spectrum produced would share some characteristics with hydrazine, there would also be similarities with the ammonia spectrum due to the presence of NH_3 groups. If features matching those seen with hydrazine hydrate

and ammonia were found, then the two features could be combined for an added layer of detection and identification since the presence of both would indicate hydrazine hydrate whereas the presence of only one of the features would suggest either hydrazine hydrate or ammonia. Figure 3.19 shows the average spectrum produced for hydrazine hydrate, while figures 3.20-3.22 show the hydrazine hydrate data plotted in the regions identified for ammonia and hydrazine.

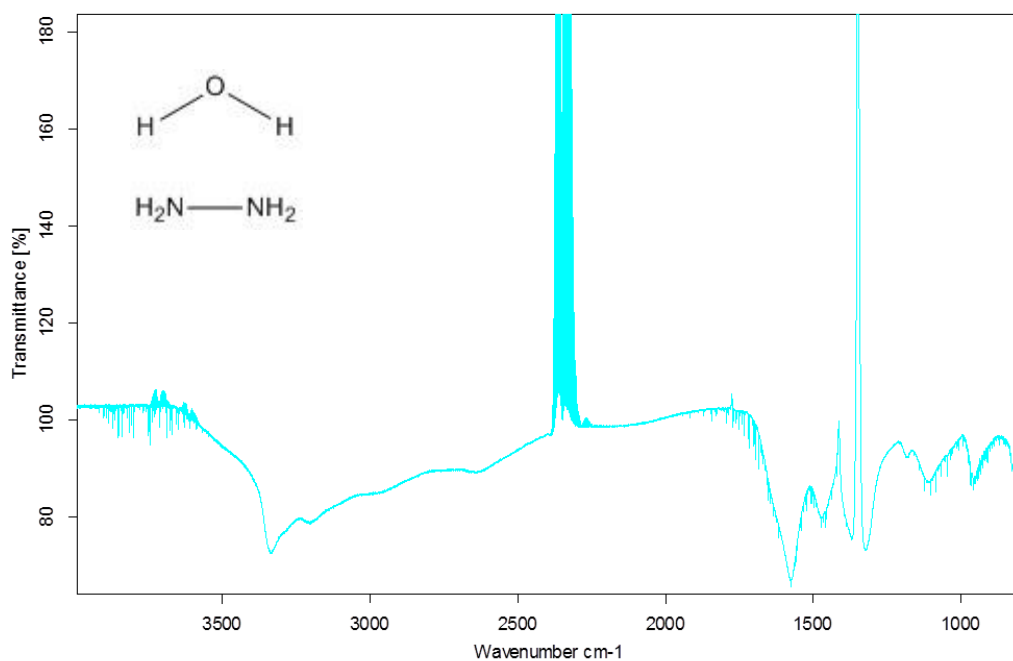


Figure 3.19 Average spectrum for 100 μ L hydrazine hydrate at 27^oC with the structure inset

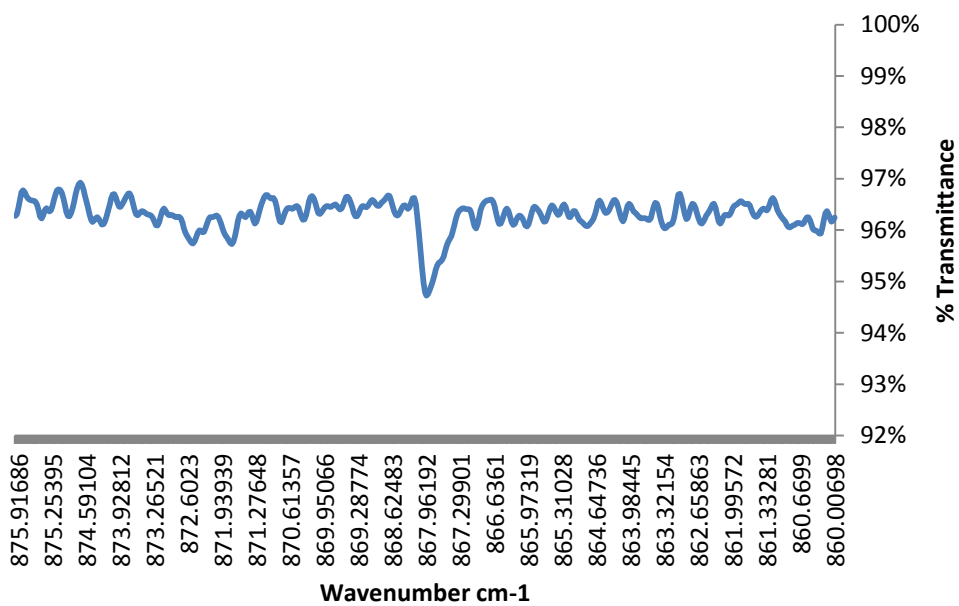


Figure 3.20 Plotted data for hydrazine hydrate in the spectral region of the 867 cm⁻¹ detection site for ammonia

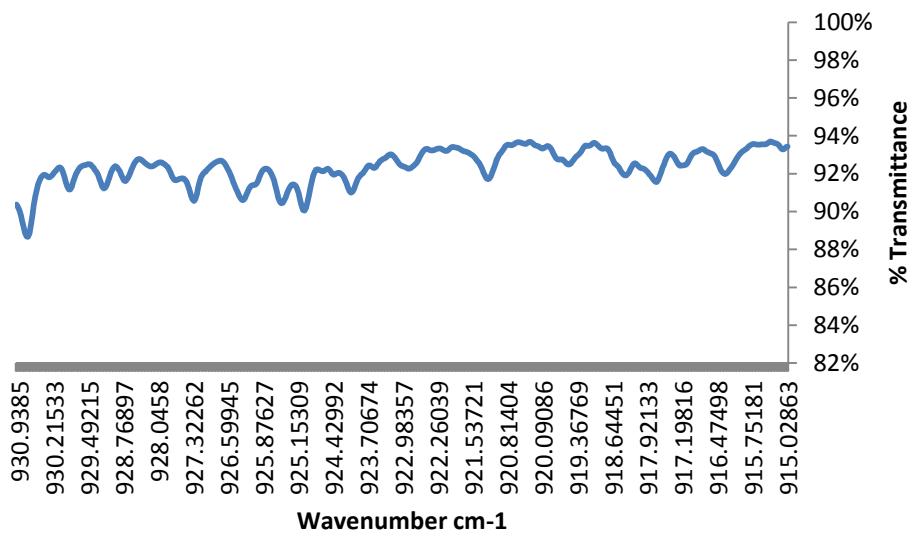


Figure 3.21 Plotted data for hydrazine hydrate in the spectral region of the 918 cm⁻¹ detection site for hydrazine

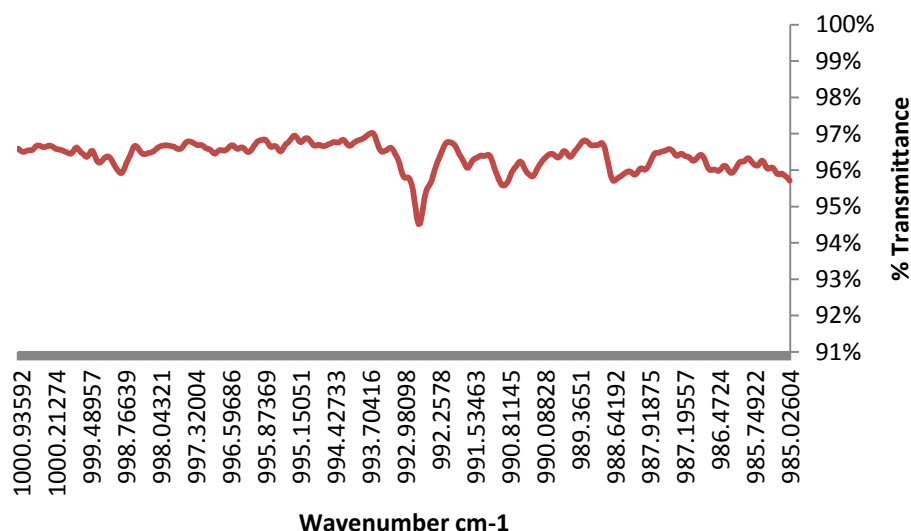


Figure 3.22 Plotted data for hydrazine hydrate in the spectral region of the 993 cm^{-1} detection site for ammonia

The plotted data demonstrates that there is absorption present for hydrazine hydrate in the same regions as for ammonia, and possibly absorption in the same region as for hydrazine but it is small and slightly offset from the expected wavenumber. These results would suggest that it is possible to detect hydrazine hydrate using a combination of ammonia and hydrazine detection targets based on absorption caused by N-H bonding.

The hydrazine hydrate spectrum had a large inverse peak observed at approximately 1350 cm^{-1} . This is due to the hygroscopic nature of hydrazine hydrate absorbing water from the atmosphere of the sample cell, causing a reduction in the water present compared to the background spectrum.

In addition to the absorption features shared with ammonia and hydrazine, hydrazine hydrate also has absorption features elsewhere in the spectrum that could be suitable for detection with a QCL. As with the majority of the other compounds analysed, there are also several peaks which are too broad for detection with conventional QCLs but that might be suitable for detection with a broadband QCL.

To summarize, both hydrazine and hydrazine hydrate showed features that could be detected using a QCL. THF was analysed and subtracted from the spectrum of hydrazine in THF, and this demonstrated that there was absorption present due to hydrazine rather than being due to the presence of THF. Hydrazine hydrate had absorption features also seen with ammonia and hydrazine. This could aid its detection as it would not require a specific QCL of its own. Detection algorithms could be designed to detect when both the ammonia and hydrazine absorptions were detected and determine that this meant the compound was in fact hydrazine hydrate.

3.4.6 Hydrogen peroxide

Information provided by Cascade Technologies indicated the presence of absorption features, at 1274 and 1285 cm^{-1} , that would be suitable for QCL detection. Due to the structure of hydrogen peroxide, and the fact that the sample was in the form of a 50% solution in water, the hydrogen peroxide spectra suffered from considerable interference resulting in a noisy spectrum. At 27°C the absorption within the expected regions was very small, therefore following the protocol the temperature was increased to 75°C. Figure 3.23 shows the average spectrum produced at 75°C and figure 3.24 shows a close up of the spectrum covering both of the regions of interest.

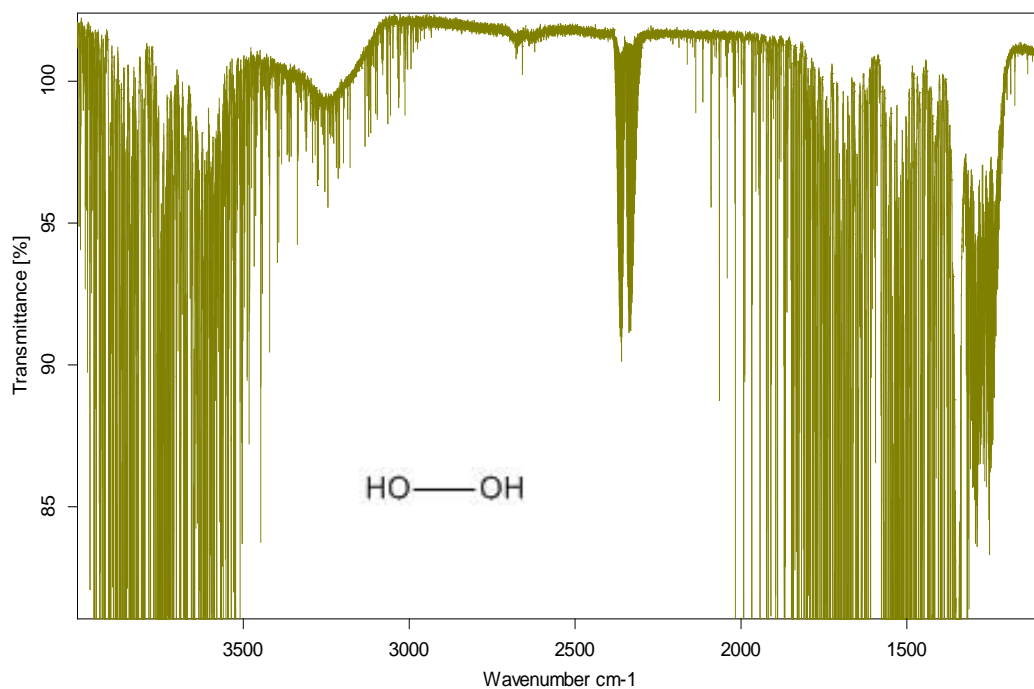


Figure 3.23 Average spectrum produced with 100 μ L hydrogen peroxide at 75°C also showing the structure of hydrogen peroxide

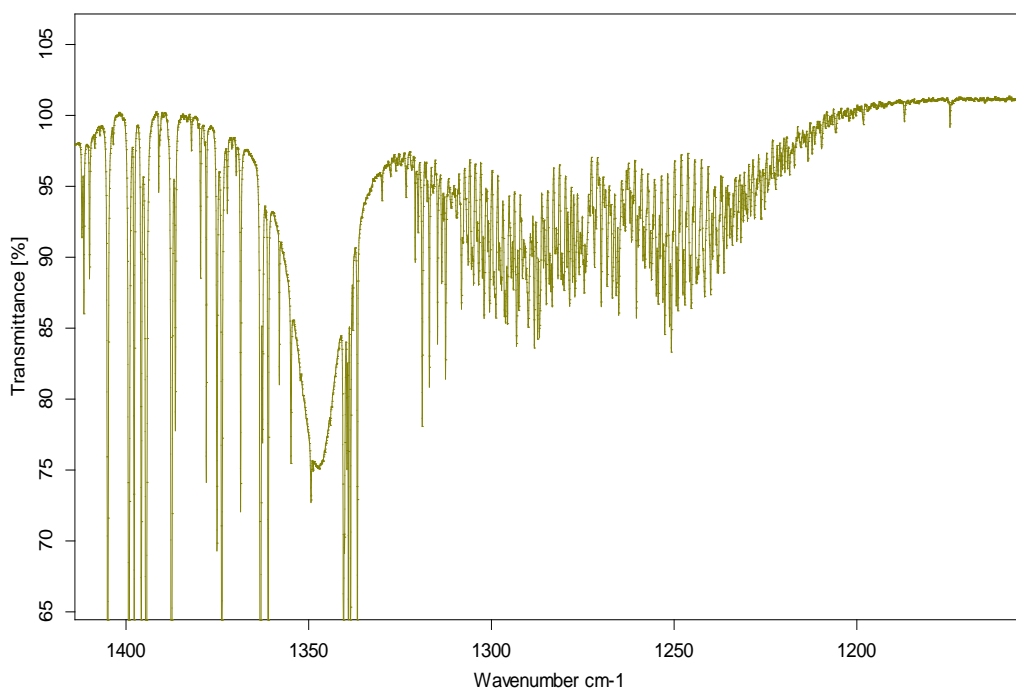


Figure 3.24 Close up of the average spectrum for hydrogen peroxide showing the two regions of interest

There is absorption present in both the predicted regions. These absorption features are relatively close together and with a broadband laser could almost be

taken as a single feature. Rather than forming a discrete peak the absorption bands present in these regions of interest form an oscillating pattern. Plotting the two regions in Microsoft Excel (figures 3.25 and 3.26) showed that, while there is an oscillating pattern it is not regular in appearance. However, this may be beneficial as it is likely to make it more individual and therefore more specific as a region for detection. The oscillating patterns were classified as absorption caused by O-H rotation. The presence of rotational absorption in the spectrum is due to the sample being analysed in vapour form.

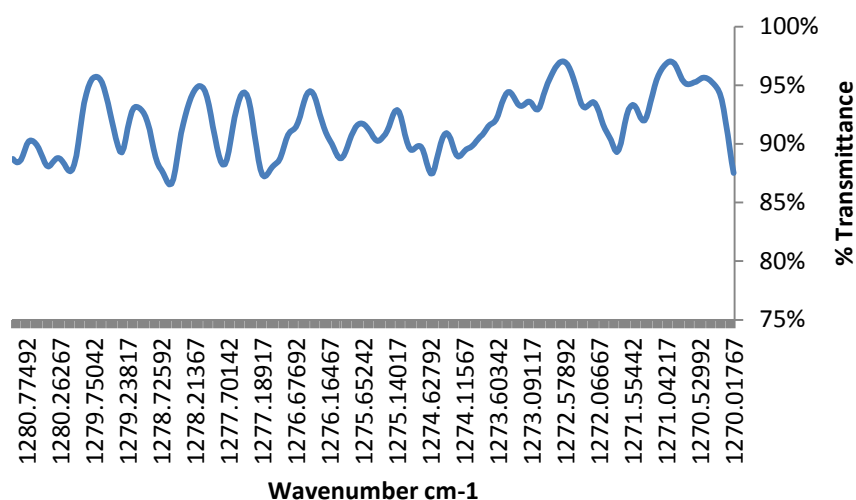


Figure 3.25 Data plotted for hydrogen peroxide in the spectral region of the 1274 cm^{-1} detection site

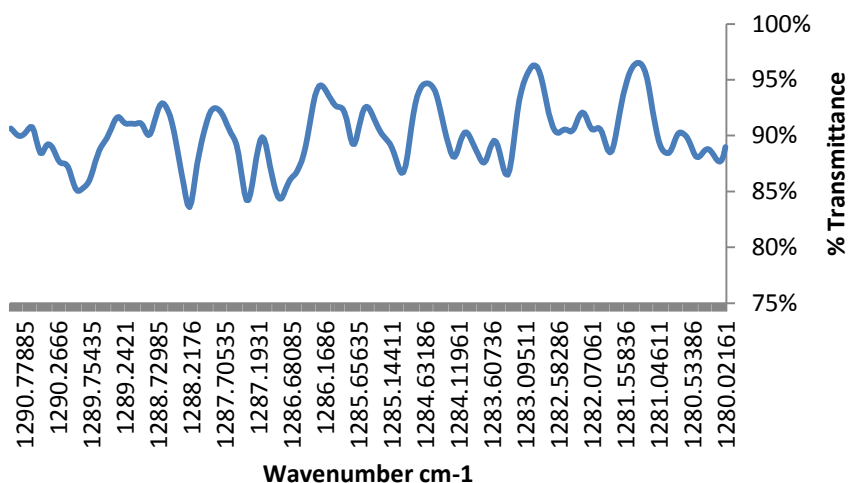


Figure 3.26 Data plotted for hydrogen peroxide in the spectral region of the 1285 cm^{-1} detection site

Figure 3.24 also suggests that, in addition to the oscillating regions at 1274 and 1285 cm^{-1} , there is a peak at approximately 1350 cm^{-1} which might be suitable for QCL detection.

To summarise, the hydrogen peroxide spectra showed absorption in the areas expected. This absorption at 1274 and 1285 cm^{-1} took the form of an oscillating pattern rather than discrete peaks, however this form of absorption band is still suitable for QCL detection.

3.4.7 Nitric acid

Information provided by Cascade Technologies suggested that there would be two absorption bands at 867 and 885 cm^{-1} . The average spectrum produced (figure 3.27) suggested that not only was absorption present in these regions, there were other absorption bands across the spectrum that might be suitable for detection when other QCLs become available.

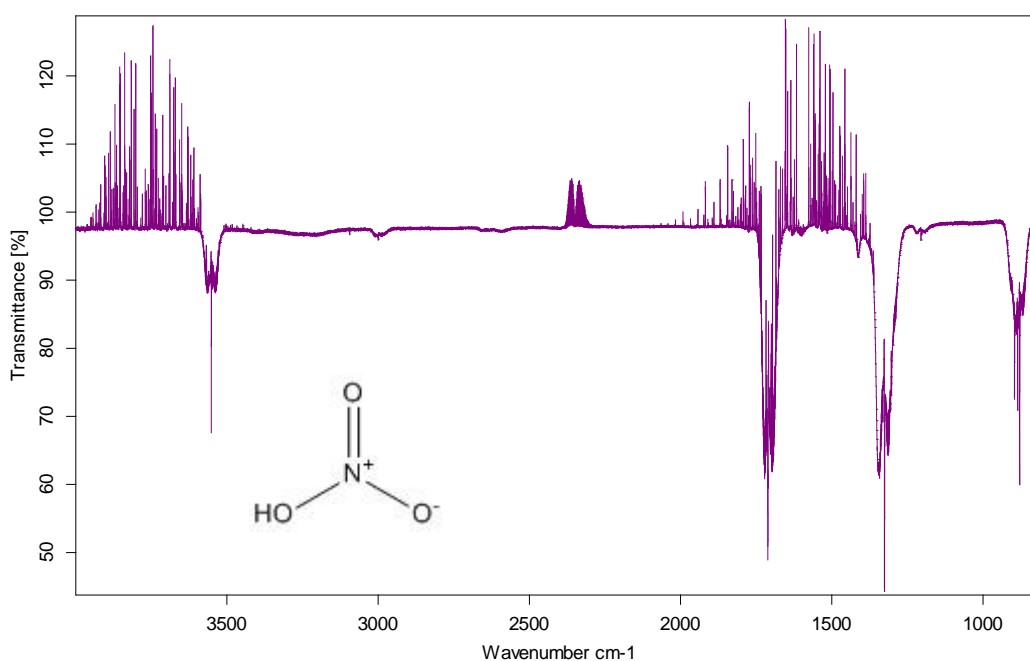


Figure 3.27 Average spectrum produced with 100 μL nitric acid at 27°C also showing the structure of nitric acid

The absorption at 867 cm^{-1} is not a discrete peak, instead an oscillating pattern is seen (figure 3.28). Despite not being a discrete peak, as with the hydrogen peroxide

absorption features, this oscillating pattern is detectable with a QCL and as a result the 867 cm^{-1} region is a suitable region for detection. This absorption is believed to be caused primarily by $>\text{N-O}$ stretching and N-O stretching, with possible rotational overtones.

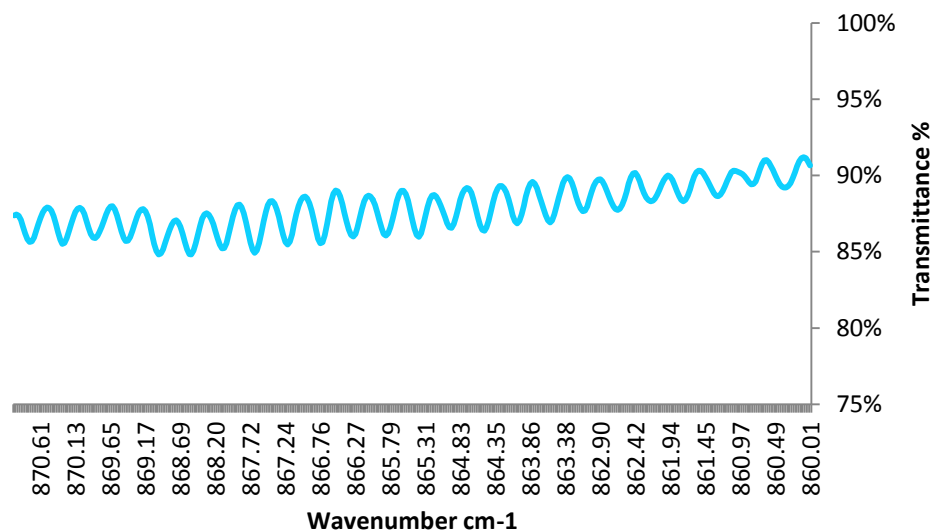


Figure 3.28 Plotted data for the spectral region of the 867 cm^{-1} target site for nitric acid

There are three relatively large absorption peaks in close proximity between 899 and 874 cm^{-1} (figure 3.29). These peaks could prove to be a useful detection feature when broadband QCLs become available however, in order for this to be possible, further investigation of the relative intensities and precise determination of the peak positions would be needed. These absorption peaks are also believed to be a result of $>\text{N-O}$ and N-O stretching with possible rotational overtones.

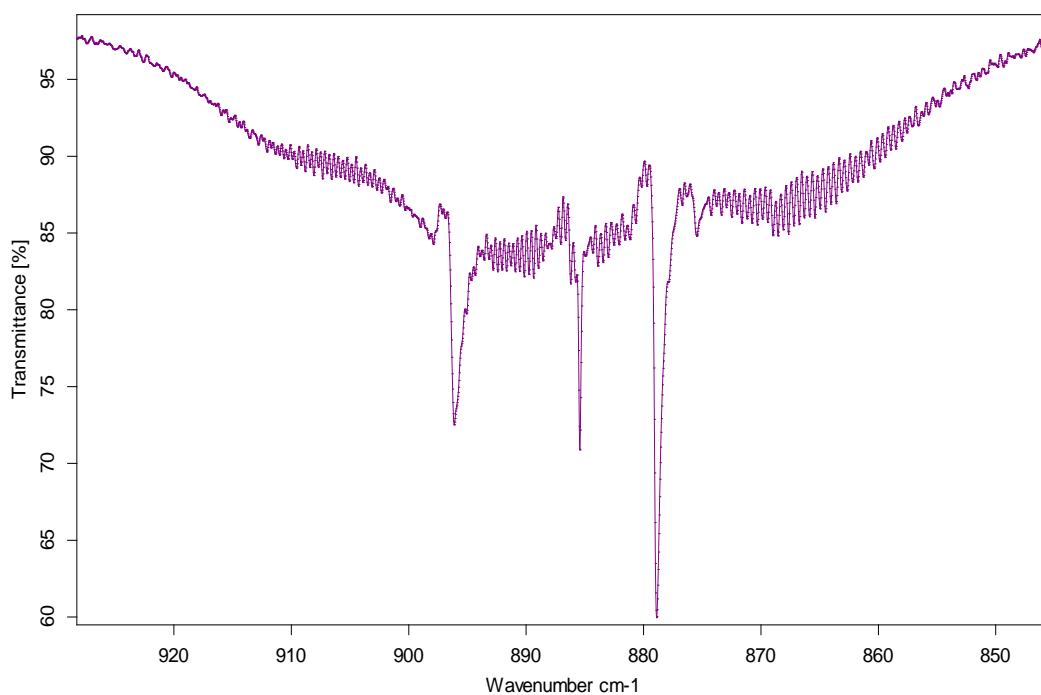


Figure 3.29 Close up of the three relatively large absorption peaks seen between 874 and 899 cm^{-1} in the nitric acid spectrum

To summarise, the two regions predicted to show absorption, 867 and 885 cm^{-1} , both showed suitable absorption features for QCL detection. However, while the absorption feature at 885 cm^{-1} was a discrete peak, at 867 cm^{-1} an oscillating pattern is present. In addition to these features several additional regions have been identified that would be suitable for detection with a broadband QCL.

3.4.8 Nitromethane

Information provided by Cascade Technologies indicated that there would be an absorption band at 918 cm^{-1} that would be suitable for QCL detection. The average spectrum produced (figure 3.30) suggested that absorption was present in this region. A close up of this region (figure 3.31) showed that two peaks were present with 4 cm^{-1} of each other. The larger peak is slightly away from 918 cm^{-1} at approximately 917.7 cm^{-1} , however both peaks are within the 6 cm^{-1} spectral window of a QCL. The presence of the second smaller peak at 914 cm^{-1} suggests that this region could be used for more sophisticated detection through identifying the presence of both peaks together and their relative intensities to each other.

Both of these absorption peaks would be suitable for QCL detection and are believed to be a result of >C-N and C-N stretching.

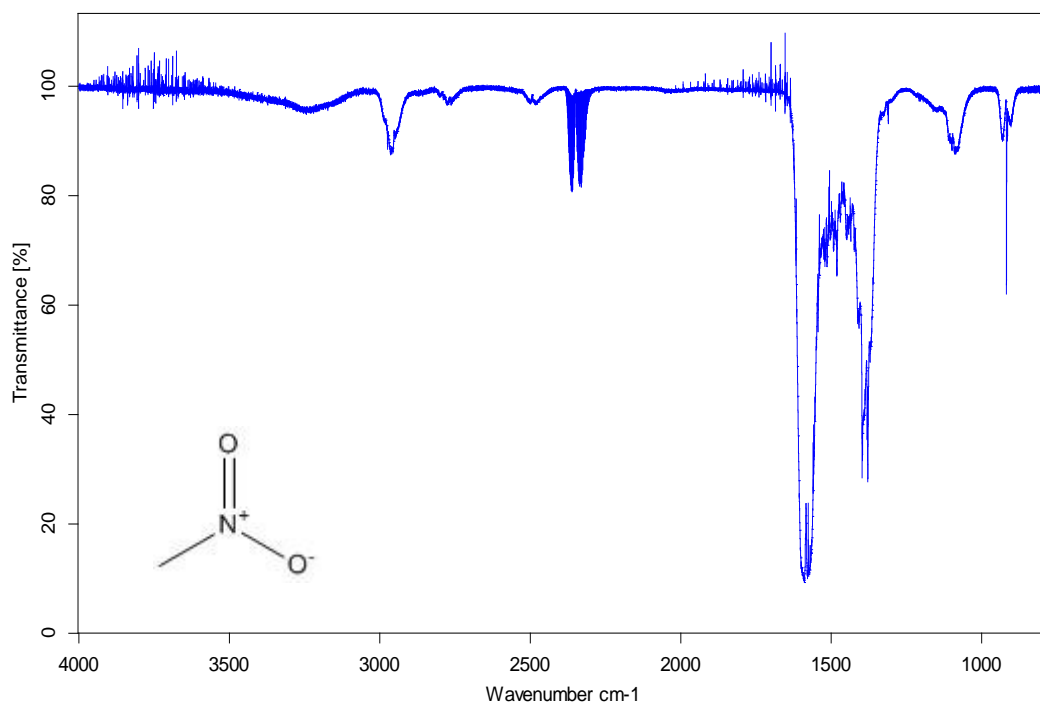


Figure 3.30 Average spectrum produced with 100 μ L nitromethane at 27°C also showing the structure of nitromethane

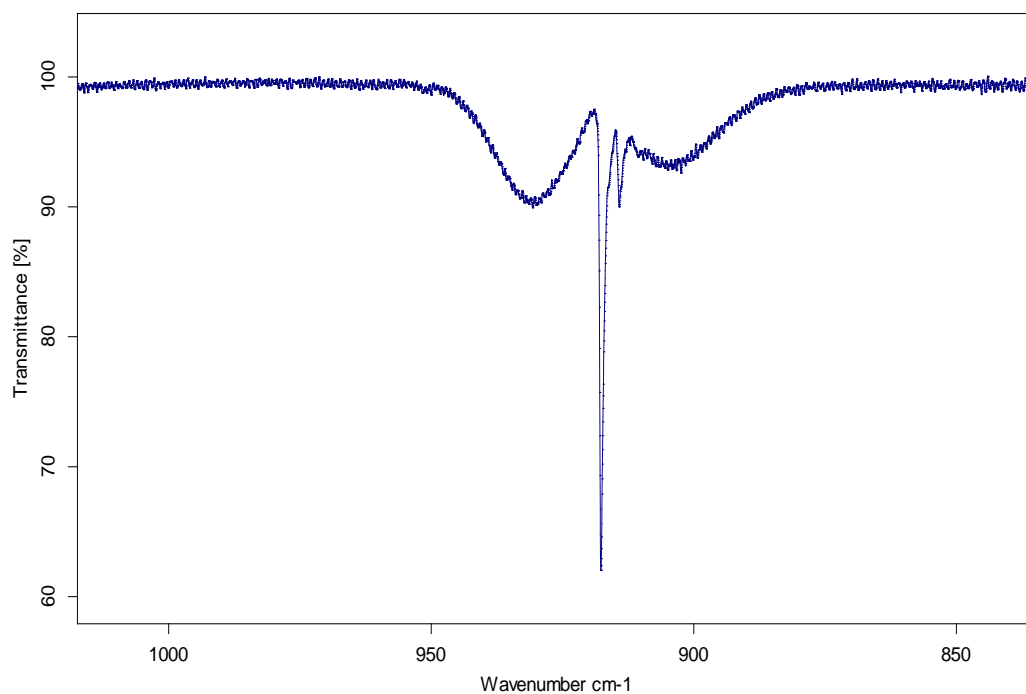


Figure 3.31 Close up of the 918 cm⁻¹ target region for nitromethane

To summarise, the region predicted to show absorption at 918 cm^{-1} in fact had two peaks within the spectral window of a QCL at 917.7 cm^{-1} and 914 cm^{-1} . Both of these absorption peaks would be suitable for QCL detection.

3.4.9 Methanol

Methanol was analysed with the view to identify detection sites for future broadband QCLs as the spectrum was expected to contain absorption bands too broad for detection with currently available QCLs. Figure 3.32 shows the average spectrum obtained with $100\text{ }\mu\text{L}$ methanol at 27°C .

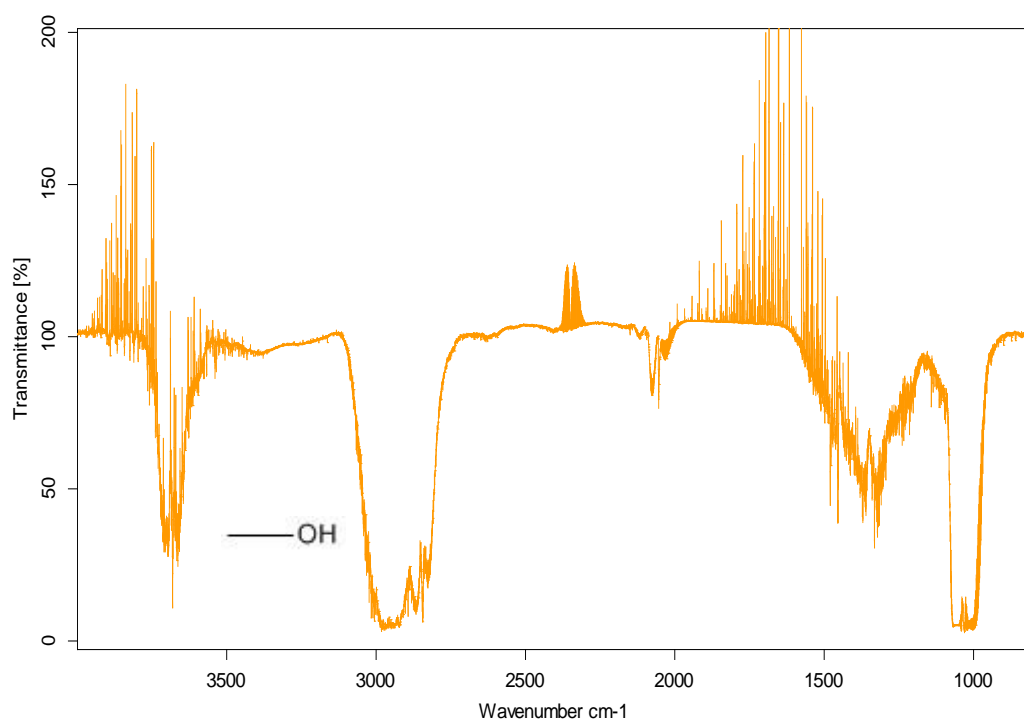


Figure 3.32 Average spectrum produced with $100\text{ }\mu\text{L}$ methanol at 27°C also showing the structure of methanol

As predicted the majority of the absorption bands are broad and therefore currently unsuitable for detection. Within the regions identified for other compounds of interest there were two regions with absorption bands that could potentially be detected with current QCLs. A small peak can be seen at approximately 916 cm^{-1} (figure 3.33) which could be suitable for detection with a 918 cm^{-1} QCL, and an oscillating pattern is present in the spectral window of a 1075 cm^{-1} QCL (figure 3.34). The small peak at 916 cm^{-1} is believed to be a result of C-H bending or C-O

stretching and the oscillating pattern at 1075 cm^{-1} a result of C-O stretching and possibly rotational overtones.

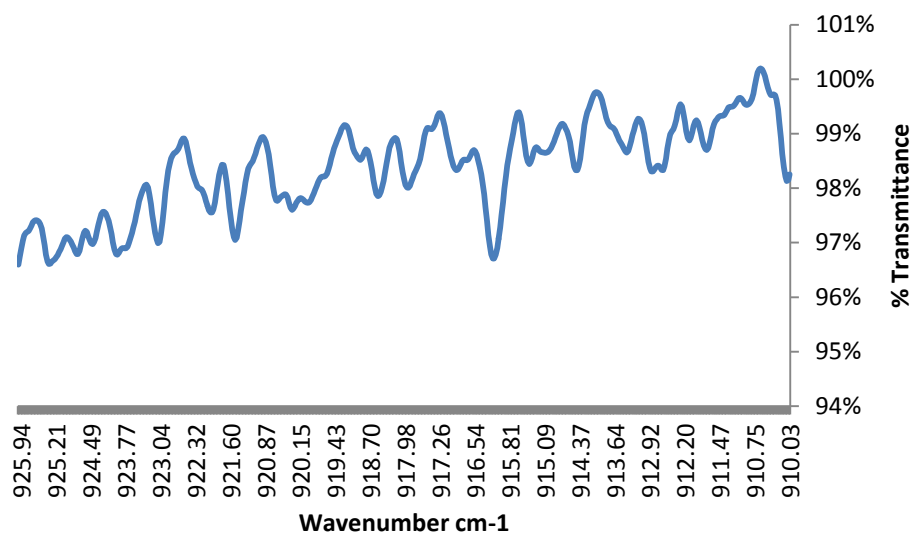


Figure 3.33 Plotted data for methanol in the spectral region of a 918 cm^{-1} QCL

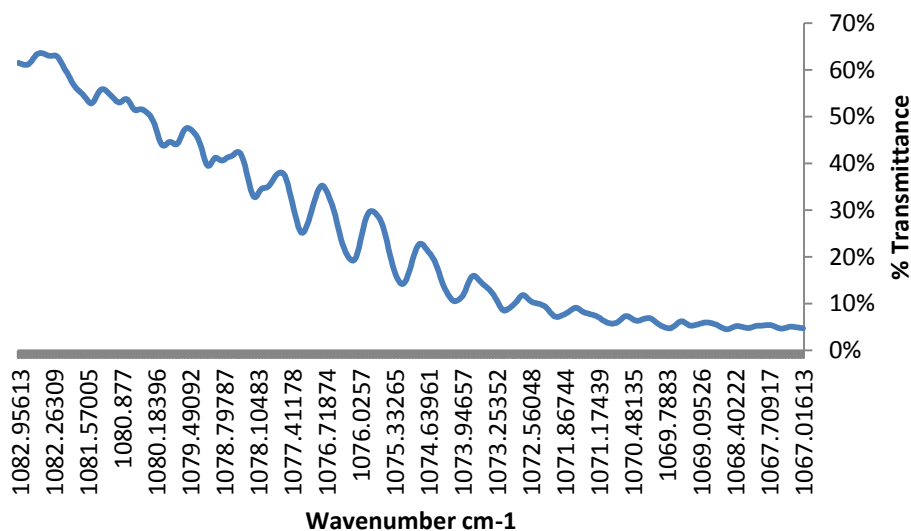


Figure 3.34 Plotted data for methanol in the spectral region of a 1075 cm^{-1} QCL

To summarise, the majority of the absorption seen within the methanol spectrum was too broad for detection with current QCLs, however there were two regions that could be suitable for detection with lasers at 918 cm^{-1} and 1075 cm^{-1} . Furthermore the absorption seen in other regions of the spectrum could be suitable for the detection in the future using broadband QCLs.

3.4.10 Ethanol

Following the successful analysis of methanol, ethanol was also analysed. The average spectrum for ethanol is shown in figure 3.35. As with methanol, the majority of the absorption bands seen were too broad for detection using currently available narrow band QCLs.

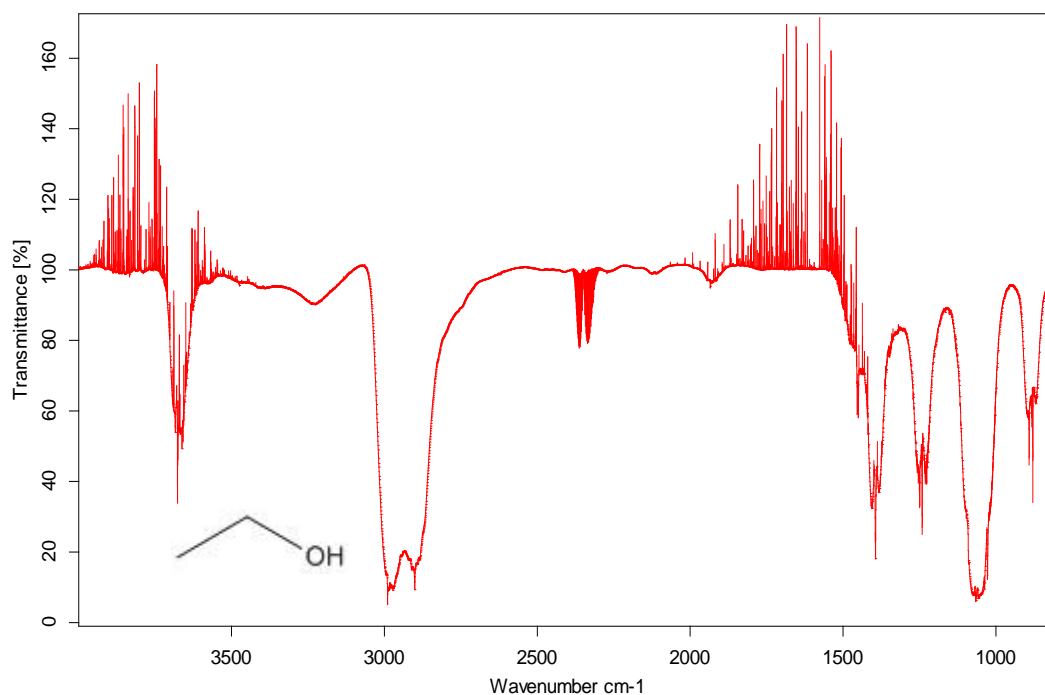


Figure 3.35 Average spectrum produced with 100 μL ethanol at 27°C also showing the structure of ethanol

In addition to this there were three absorption peaks (figure 3.36) which initially appeared to be the same as those seen between 899-874 cm^{-1} within the nitric acid spectrum. However, when the nitric acid and ethanol spectra were overlaid it could be seen that the peaks were slightly offset and the relative proportions between the peaks were different and therefore not caused by any potential nitric acid contamination in the ethanol samples. It was thought that the presence of these peaks may have been as a consequence of additives in the ethanol to prevent the consumption of the laboratory grade material. However, the peaks were also observed in the spectrum of ethanol available for consumption (tequila). Figure 3.37 shows the overlaid spectral of ethanol, tequila and nitric acid.

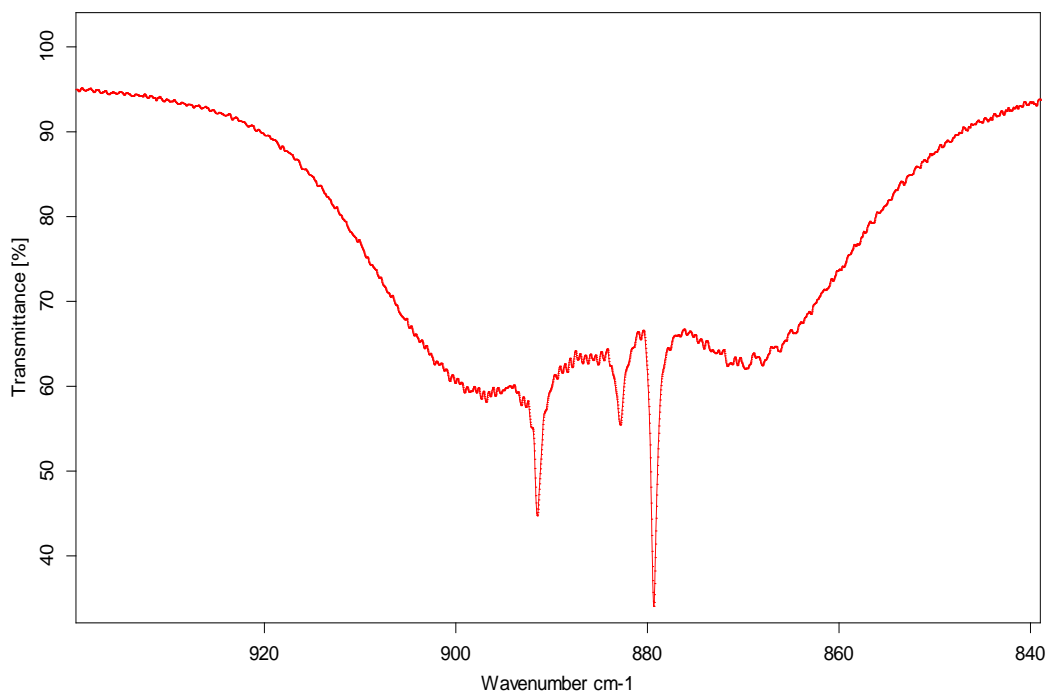


Figure 3.36 Close up of three absorption peaks seen with ethanol

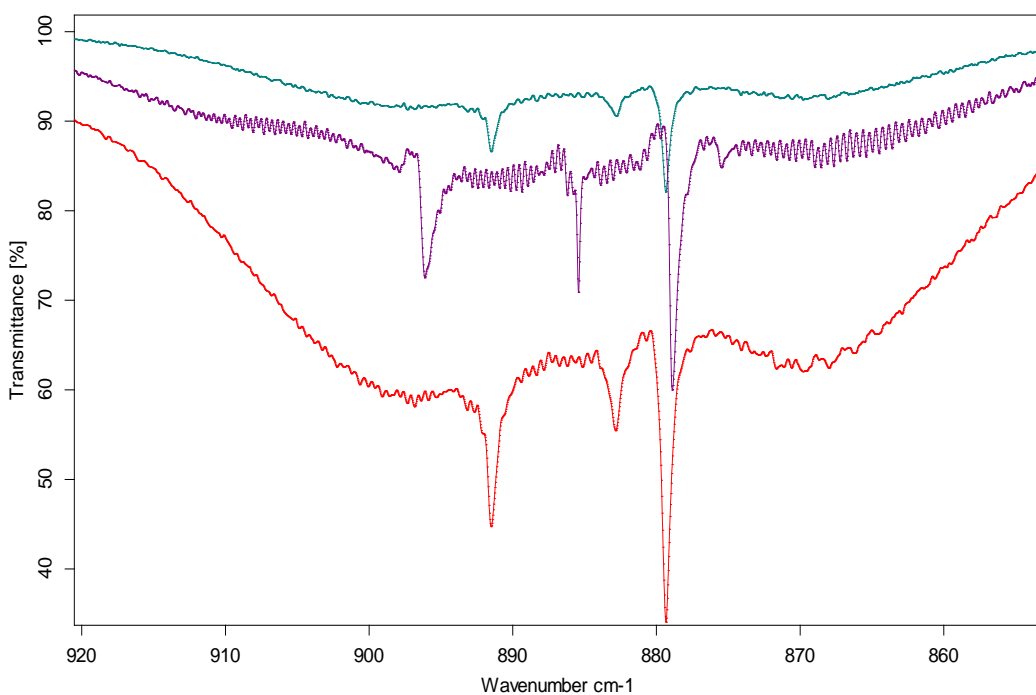


Figure 3.37 Overlaid spectra of ethanol (red), tequila (teal) and nitric acid (purple)

An infrared spectrum of ethanol in the gas phase revealed peak separation in a similar region (figure 3.38). While the appearance of the peaks is slightly different this could be a result of the use of different instrumentation. The presence of peaks

in this region of the spectrum suggests that while the peaks seen in the ethanol spectra produced in this work appear different from reference spectra this is most likely due to differences in resolution, or because the majority of reference spectra are conducted in the liquid phase. The three absorption peaks in the $870 - 900 \text{ cm}^{-1}$ region are believed to be a result of C-H out of plane bending.

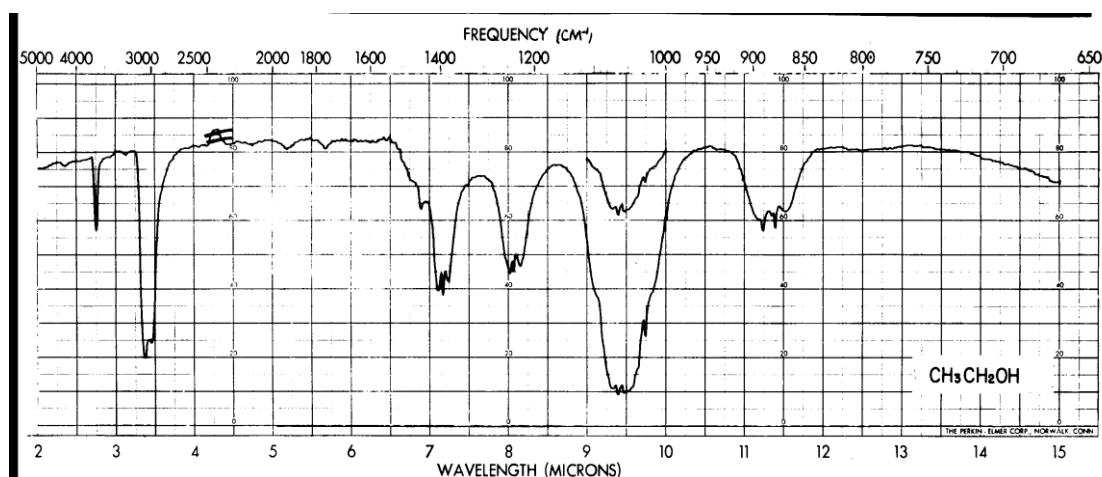


Figure 3.38 Ethanol reference spectrum[28]

The ethanol spectrum was examined with regards to the regions of interest identified for the other compounds covered by currently available QCLs. As with methanol the majority of the target regions for the other compounds of interest either contained no absorption or contained absorption that was part of a larger absorption band too broad for current QCL detection. However, there were two regions which could potentially be used for detection using available QCLs. There is a small absorption peak present at approximately 882.7 cm^{-1} which would be suitable for detection with an 885 cm^{-1} QCL; in addition to this there is a small oscillating pattern at 885 cm^{-1} which might also be suitable for detection (figure 3.39). The combination of both features within the spectral window of a single QCL could make this region a strong detection site for ethanol. These absorption features are believed to be a result of C-H out of plane bending and possibly rotational overtones.

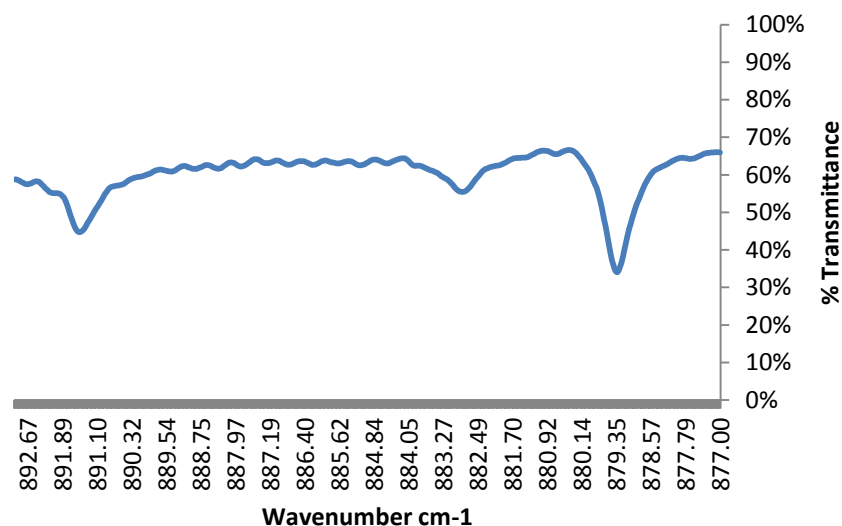


Figure 3.39 Plotted data for ethanol in the spectral region covered by an 885 cm⁻¹ QCL

A small absorption peak was also present at 1161.5 cm⁻¹, which might be detected with an 1160 cm⁻¹ QCL. There were several other absorption peaks in relatively close proximity to the peak at 1161.5 cm⁻¹, however, they fall outside the spectral window of the currently available QCL (see figure 3.40). This suggests that future detection systems could use this region for identification of ethanol when broadband QCLs become readily available. This absorption is believed to be a result of C-H wagging.

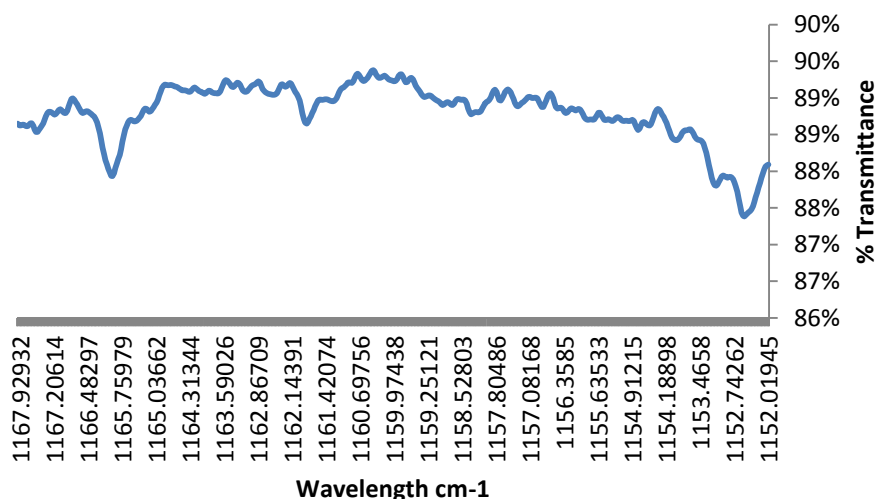


Figure 3.40 Plotted data for the spectral region around 1160 cm⁻¹ for ethanol

To summarise, the analysis of ethanol revealed two regions suitable for detection with currently available QCLs. It was also possible to see differences between the spectra of ethanol and methanol, suggesting that discrimination between chemically similar materials might be possible.

3.5 Conclusions

The results of the diesel analysis have shown that suitable starting conditions for liquid analysis are a volume of 0.1 mL and a temperature of 27°C. Where required, for less volatile compounds, both the temperature and volume can be increased to 75°C and 1 mL respectively. The temperature could be further increased, but the results of this analysis suggested that this would result in a risk of saturation of the detector and an increase in intra-sample variation and therefore is not advisable.

The analysis of compounds of interest demonstrated that the protocol developed from the diesel analysis was fit for purpose. All of the compounds analysed had detectable absorption bands, however not all of these were suitable for detection with currently available QCLs. This was either because the absorption bands were too broad or fell outside the spectral windows of the currently available lasers. These bands are likely to be suitable for detection in the future either with broadband QCLs or the development of lasers which have a spectral window covering the wavenumber region of the absorption. This highlights the importance of analysing a wide spectrum (800-4000 cm^{-1}) rather than focusing on known regions of potential absorption as this might result in information for future detection being overlooked.

The analysis of acetone in propanol and hydrazine in THF and the subsequent subtraction of propanol and THF from the respective spectra demonstrated that this was a suitable method for handling materials that are in solvent. The analysis of ethanol demonstrated that the high resolution of the instrument allowed for the detection of absorption features that otherwise might not be visible, in particular absorption present when materials are in the vapour state.

The information gathered through this analysis of the compounds of interest has created a library of spectra that could be used to inform the development of explosives detection systems.

3.6 References

1. Kostesha, N.V., Alstrom, T.S., Johnsen, C., Nielsen, K.A., Jeppesen, J.O., Larsen, J., Jakobsen, M.H. and Boisen, A., *Development of the colorimetric sensor array for detection of explosives and volatile organic compounds in air*. Advanced Environmental, Chemical, and Biological Sensing Technologies VII, 2010. **7673**.
2. Lim, S.H., Feng, L., Kemling, J.W., Musto, C.J. and Suslick, K.S., *An optoelectronic nose for the detection of toxic gases*. Nature Chemistry, 2009. **1**(7): p. 562-567.
3. Janzen, M.C., Ponder, J.B., Bailey, D.P., Ingison, C.K. and Suslick, K.S., *Colorimetric sensor Arrays for volatile organic compounds*. Analytical Chemistry, 2006. **78**(11): p. 3591-3600.
4. Lin, H.W. and Suslick, K.S., *A Colorimetric Sensor Array for Detection of Triacetone Triperoxide Vapor*. Journal of the American Chemical Society, 2010. **132**(44): p. 15519-15521.
5. Amisar, S., *Detecting explosive substances comprises providing sample on collection medium, contacting sample with nitro aromatic compound, and comparing color change to color chart to ascertain the presence of nitro aliphatic explosive*, MISTRAL DETECTION LTD (MIST-Non-standard) MISTRAL DETECTION LTD (MIST-Non-standard). p. 28.
6. Schnorr, J.M., van der Zwaag, D., Walsh, J.J., Weizmann, Y. and Swager, T.M., *Sensory Arrays of Covalently Functionalized Single-Walled Carbon Nanotubes for Explosive Detection*. Advanced Functional Materials, 2013. **23**(42): p. 5285-5291.
7. [cited 2014 28/09/2014]; Available from: <http://www.atsdr.cdc.gov/toxprofiles/tp96-c7.pdf>.
8. Hlozek, T., Bursova, M. and Cabala, R., *Fast determination of ethylene glycol, 1,2-propylene glycol and glycolic acid in blood serum and urine for emergency and clinical toxicology by GC-FID*. Talanta, 2014. **130**: p. 470-4.
9. Bousquet, M., Bry, M., Eymard, S., Frenois, C., Genevray, P., Hairault, L., Maillou, T., Nony, S., Noui, J. and Pin, N. *The analysis and detection of explosive in atmosphere: development and test of sampling and concentration tools*. Actualite Chimique, 2010(342-43): p. 70-74.
10. Smith, B.C., *Fundamentals of Fourier Transform Infrared Spectroscopy*. 2nd ed. 2011: CRC Press.
11. Committee on the Review of Existing and Potential Standoff Explosives Detection Techniques, *Existing and Potential Standoff Explosives Detection Techniques*, ed. N.R.C.o.t.N. Academies. 2004, Washington D.C.: The National Academies Press.
12. *Anarchist's Cookbook*. [cited 2013 08/11/2013]; Available from: [http://www.anarchistcookbook.com/showthread.php/8511-tricycloacetone-peroxide-\(TATP\)](http://www.anarchistcookbook.com/showthread.php/8511-tricycloacetone-peroxide-(TATP)).
13. Dunayevskiy, I., Tsekoun, A., Prasanna, M., Go, R. and Patel, C.K.N., *High-sensitivity detection of triacetone triperoxide (TATP) and its precursor acetone*. Applied Optics, 2007. **46**(25): p. 6397-6404.

14. Evans, H.K., Tulleners, F.A.J., Sanchez, B.L and Rasmussen, C.A., *An Unusual Explosive, Triacetone triperoxide (TATP)*. Journal of Forensic Sciences, 1986. **31**(3): p. 1119-1125.
15. Akhavan, J., *The Chemistry of Explosives*. RSC paperbacks. 2008: RSC.
16. Nazarian, A. and Presser, C., *Forensic analysis methodology for thermal and chemical characterization of homemade explosives*. Thermochemica Acta, 2014. **576**(0): p. 60-70.
17. Urben, P.G., Pitt, M.J. and Bretherick, L., *Bretherick's Handbook of Reactive Chemical Hazards: Vol. 1-2*. 2007: Elsevier.
18. Sabate, C.M. and Delalu, H., *Methylated Azoles, 2-Tetrazenes, and Hydrazines*. Zeitschrift Fur Anorganische Und Allgemeine Chemie, 2014. **640**(10): p. 1843-1854.
19. Pakdehi, S.G., Rezaei, S., Motamedoshariati, H. Keshavarz, M.H., *Sensitivity of dimethyl amino ethyl azide (DMAZ) as a non-carcinogenic and high performance fuel to some external stimuli*. Journal of Loss Prevention in the Process Industries, 2014. **29**: p. 277-282.
20. Zitrin, S., Kraus, S. and Glattstein, B., *Identification of two rare explosives*. in *1st International Symposium on Analysis and Detection of Explosives* 1983. Washington D.C.: US Government Printing Office.
21. [cited 2013 08/11/2013]; Available from: <http://web.mit.edu/semenko/Public/Military%20Manuals/RogueSci-Mirror/explo/HMTD.html>.
22. Oxley, J.C., Smith, J.L., Chen, H. and Cioffi, E., *Decomposition of multi-peroxidic compounds: Part II. Hexamethylene triperoxide diamine (HMTD)*. Thermochemica Acta, 2002. **388**(1-2): p. 215-225.
23. Black, A.P. and Babers, H., *Methyl Nitrate*. Organic Syntheses, 1939. **19**(64).
24. [cited 2014 27/09/2014]; Available from: <https://sites.google.com/site/msexplosives/e/methyl-nitrate>.
25. James, M.J., *Gelled nitromethane explosive containing fluid encapsulations*. 1967, Google Patents.
26. Buchanan, H.A.S., *An evaluation of isotope ratio mass spectrometry for the profiling of 3,4-methylenedioxymethamphetamine in Pure and Applied Chemistry*. 2009, University of Strathclyde: Glasgow. p. 313.
27. Bruno, T.J. and Svoronos, P.D.N., *Handbook of Basic Tables for Chemical Analysis*. 2nd ed. 2003: CRC Press.
28. Coblenz Society. *NIST Webbook*. 1963 [cited 2012 26/11/12]; Available from: <http://webbook.nist.gov/cgi/cbook.cgi?ID=C64175&Type=IR-SPEC&Index=1#IR-SPEC>.

Chapter 4. Brand Discrimination - Acetone

4.1 Introduction

Homemade and improvised explosives present both a continuing and an evolving threat and can be prepared outside of a laboratory where the precursor materials can be purchased on the high street. Acetone is one of the compounds identified as an important precursor in HED/IED manufacture[1], where, in combination with hydrogen peroxide, it can be used to produce TATP[2, 3]. Both hydrogen peroxide and acetone can be readily purchased outside of a laboratory environment.

The detection of acetone as both a precursor and decomposition product of TATP has seen substantial research as acetone has the potential to be used for not only the detection of explosive devices but also as a compound associated with bomb factories[1]. The main technique employed for detection is spectroscopy, with research into Raman [4], differential absorption lidar (or DIAL, differential absorption LIDAR)[1, 5] and photoacoustic spectroscopy (PAS) using quantum cascade lasers[6, 7]. Other systems such as thin film based sensors have also been reported[8]. Current research has focused on the development of detection systems that have been calibrated for laboratory grade acetone[1, 4-8], and while some have examined the possible effects of environmental interferences and varying concentrations of acetone[1, 5, 9] they have not examined the potential for interfering compounds present within the precursor itself to influence the resultant spectra.

Acetone is commonly available as nail polish remover which may also contain stabilisers, perfumes and conditioners all of which could have an effect on the FTIR spectrum produced when analysed. There are also likely to be differences in the concentration of the precursor material present, and this might be particularly noticeable when compared with laboratory grade materials. These differences could be exploited to allow for the detection and identification of brand types and

which could highlight any interfering effects that might occur in homemade explosives made from shop bought materials instead of laboratory grade materials.

The importance of developing mathematical algorithms and protocols for discrimination of gaseous mixtures has been highlighted by several researchers [9-14]. Several neural network based methods have been presented, with a substantial focus on combining neural networks with fuzzy systems[9-11, 13-15] for the discrimination of gaseous materials. However, while the use of self organising feature maps (SOFM) has been applied to several areas of forensic science[16, 17] thus far it has not been applied to the analysis of explosive precursors.

Therefore the basic premise for exploring the use of high resolution FTS in the analysis of acetone was to test a set of different brands as well as the corresponding laboratory grade material. This was followed by comparison of the spectra produced to determine if it was possible to discriminate between the laboratory grade material and the shop bought material, as well as the potential to discriminate between the brands themselves.

4.2 Materials

Laboratory grade acetone was purchased from Sigma Aldrich UK. Five nail polish removers were purchased from retail outlets and are presented in Table 4.1.

Table 4.1 Five selected nail polish removers, where they were purchased and their ingredients

Brand	Purchased from	Ingredients
Boots Essentials nail polish remover	Boots, Glasgow	Acetone, aqua, Ricinus communis oil, Linseed acid, Triethanolamine, Denatonium benzoate, CI 60725
Sally Hansen Regular Polish Remover	Boots, Glasgow	Acetone, aqua, Parfum, Ethoxydiglycol, PPG-12-PEG-50 lanolin, Benzophenone-3, Panthenol, Tocopheryl acetate, Propylene glycol, Prunus armeniaca (Apricot) extract, Fruit extract, Sodium benzoate, Methylparaben, Benzyl cinnamate, Benzyl salicylate, Cinnamyl alcohol, Hydroxyisohexyl 3-cyclohexane carboxaldehyde, Sorbic acid
Cutex Ultra cleansing nail polish remover	Boots, Glasgow	Acetone, Aqua, Glycerin, Propylene carbonate, Saccharum officinarum, Benzyl benzoate, Benzophenone-1, PEG-7-Glyceryl cocoate, Parfum, Methyl cluceth-20, Tocopheryl acetate, Propylene glycol, Denatured alcohol, Pyrus mallus (Apple) fruit extract, Camellia sinensis leaf extract, Linalool, Mineral Oil, Cocos nucifera (Coconut) oil, Citrus medica limonum (Lemon) fruit extract, Citrus aurantium dulcis (Orange) fruit extract, Phenoxyethanol, Denatonium benzoate, Hydroxyisohexyl 3-cyclohexene carboxaldehyde, Aloe barbadensis leaf extract, Butylparaben, CI 60730, CI 42090
Mavala nail polish remover	Boots, Glasgow	Acetone, Water (Aqua), Butyl acetate, Ricinus communis (Castor) seed oil, Green 6 (CI 61565)
Allura nail polish remover	Poundland, Glasgow	Aqua, Acetone, Ethyl acetate, Glycerine, CI 17200, Parfum

4.3 Experimental protocol

The protocol used for each sample followed that developed through the diesel analysis (Chapter 3). Each nail polish remover and the laboratory grade acetone were analysed at 27°C. In each case six separate 100 µL samples for each brand were analysed.

4.3.1 Visual comparison

Visual comparison of the resultant spectra was carried out using the OPUS software (version 6.5) provided with the FTS instrument and involved overlaying the average spectra (n=6) for each brand. The zoom feature was used to examine more closely the spectra for any differences.

4.3.2 Statistical analysis

The statistical analysis had two stages; firstly, the FTS data underwent data reduction using Excel (2010 version). Secondly Minitab (version 16) and Viscovery SOMine (version 4.0.2) were used to carry out the multivariate analysis of the reduced data set.

Reduction of the data was required due to the large number of data points within each spectrum (106,198 datapoints for a spectrum produced at 0.1 cm⁻¹ resolution). This volume of data was impractical to insert directly into the statistical software that was available, therefore a method of reducing the data size was required. This was linked to the visual comparison, as regions of variation observed when comparing the spectra were selected from the data to put into the statistical software. Excel was used to extract the data points within these regions. Further data reduction was achieved by summing the transmittance values for the data points within each region of variation ('binning') to produce a total transmittance value for each region for each sample. This method is commonly used as a means of reducing the size of large datasets such as those encountered in spectroscopic analysis[18-21]. Data binning has the advantage of being relatively fast, and allows for the exclusion of spectral features present as a result of carbon dioxide and

water. However, while it takes into account variations in transmittance, the method could potentially struggle to differentiate between a broad shallow peak and several deep sharp peaks within the same region. In addition to this where data regions are non-uniform in size, as in this case, differences in the size of the total transmittance values between regions can occur.

A possible alternative to binning might have been to set a threshold level of absorption where only the data from any peaks observed above this threshold are utilised. Such a data reduction technique is more appropriate for the examination of quantitative data where the concentration of compounds within the analyte is of importance as opposed to qualitative data where the presence or absence of differences within the data is of relevance. As a consequence a threshold approach was not pursued.

Once data reduction had been completed the resultant matrices were analysed using hierarchical cluster analysis (HCA) and self organising feature maps (SOFM). Principal component analysis was also considered as a statistical technique, however preliminary attempts at data analysis using PCA were unsuccessful.

4.4 Results and discussion

4.4.1 Visual comparison

A visual examination of the six repeats for acetone, shown in figure 4.1, demonstrated the presence of variation in terms of the peak areas observed. This had been observed in the initial validation work using diesel, and is most likely due to a combination of factors. Firstly, the sample chamber was not fully sealed, potentially allowing the escape of vapour both during the analysis and the time period between the sample being inserted into the chamber and the analysis being started. The lack of a full seal could also have resulted in variation in the levels of carbon dioxide and water vapour observed in the spectra. Secondly, because a fresh sample of each material, taken from the stock solution, was analysed for each repeat there is likely to have been very small amounts of variation in the amount of

sample analysed. Given that the focus of the analysis was qualitative rather than quantitative, these differences were not critical and emphasised that the generation of an average spectrum was more appropriate.

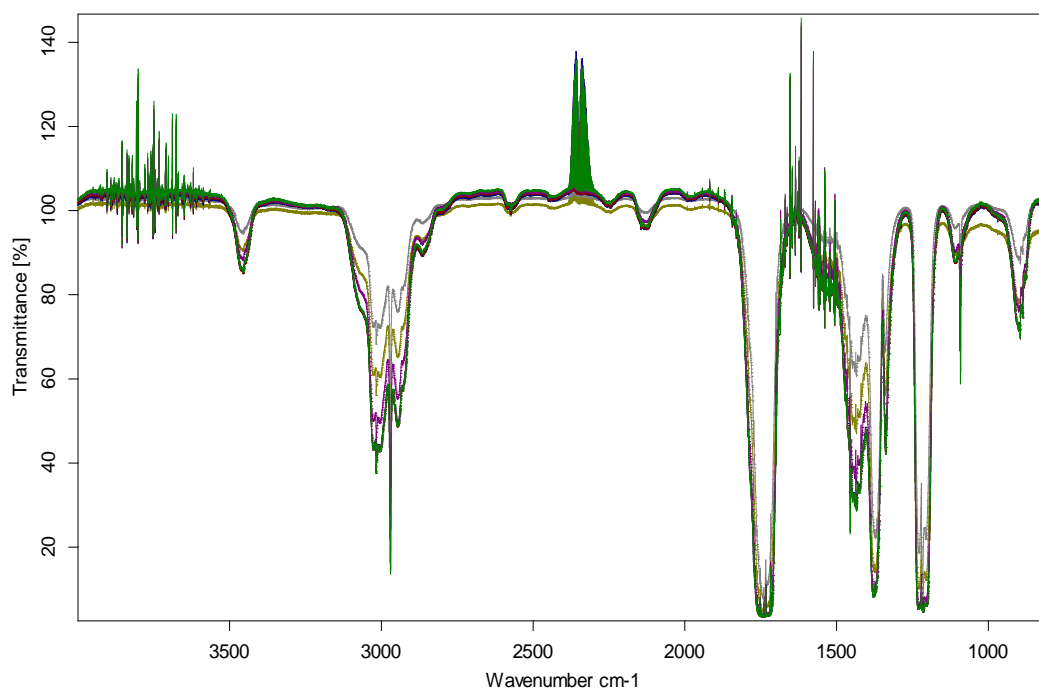


Figure 4.1 Overlaid spectra of the six analyses of acetone

The data from each repeat was examined more closely through monitoring the relative standard deviation of the binned transmission values across the identified regions of interest and this is presented in table 4.2.

The 31 regions represented in table 4.2 were those chosen as a result of visual comparison across the laboratory grade samples and the branded samples where differences in the spectra were observed. In general the data was reproducible with the RSD values of only 6 regions (19%) greater than 5%. These six regions are shown in red in table 4.2.

Table 4.2 Regions of variation identified through visual examination of average spectra of laboratory acetone and five acetone based nail polish removers and the data for acetone in these regions - the total transmittance values, mean, standard deviation and RSD (rows with red text indicate data with an RSD value above 5%)

Region (cm ⁻¹)	Acetone 1	Acetone 2	Acetone 3	Acetone 4	Acetone 5	Acetone 6	Mean	Std dev	RSD
810-825	502.14	537.74	537.18	538.15	539.33	539.67	532.37	13.55	2.54
860-950	2603.35	2854.24	2568.19	2565.47	2651.37	2572.51	2635.86	102.09	3.87
968-970	94.84	100.27	98.06	98.21	99.15	98.57	98.18	1.67	1.70
1025-1040	512.13	538.60	533.65	535.31	538.02	538.64	532.73	9.39	1.76
1050-1120	2164.37	2304.93	2166.92	2170.79	2215.49	2183.50	2201.00	49.55	2.25
1250-1295	1460.97	1524.87	1480.96	1483.61	1501.34	1490.73	1490.41	19.62	1.32
1150-1285	2885.21	3227.66	2693.95	2692.33	2792.41	2701.27	2832.14	190.00	6.71
1287-1291	158.74	165.63	160.77	161.04	162.97	161.79	161.82	2.12	1.31
1305-1330	733.52	792.34	686.44	685.32	716.11	687.41	716.86	38.21	5.33
1360-1390	223.48	325.55	139.62	138.04	160.33	137.45	187.41	68.72	36.67
1300-1500	3992.14	4646.27	3238.73	3218.93	3530.32	3220.87	3641.21	526.40	14.46
1640-1800	2666.86	3072.92	2274.92	2267.39	2424.47	2272.08	2496.44	293.94	11.77
1878-1886	298.08	304.42	304.65	305.48	306.67	307.19	304.41	3.00	0.99
1932-1934	100.90	101.72	102.57	102.89	103.07	103.49	102.44	0.88	0.86
1950-2042	3109.31	3166.96	3187.03	3196.39	3203.87	3214.66	3179.70	34.78	1.09
2040-2042	100.26	101.92	103.06	103.37	103.48	103.98	102.68	1.25	1.22
2064-2066	101.06	102.82	103.72	104.03	104.21	104.63	103.41	1.19	1.15
2088-2092	165.39	169.00	167.94	168.39	169.39	169.32	168.24	1.37	0.82
2100-2180	2637.64	2707.50	2647.39	2653.02	2682.05	2667.78	2665.90	23.46	0.88
2236-2252	563.69	575.37	571.56	573.07	576.73	576.38	572.80	4.46	0.78
2440-2452	434.03	441.61	442.14	443.47	445.34	446.20	442.13	3.97	0.90
2565-2585	693.60	708.24	699.74	701.57	707.47	705.95	702.76	5.11	0.73
2895-2910	471.78	499.79	439.49	439.96	458.57	443.15	458.79	21.68	4.73
2860-3050	4706.89	5252.30	3933.92	3920.57	4262.48	3940.08	4336.04	495.58	11.43
3050-3135	2583.31	2711.39	2436.32	2436.42	2523.74	2448.70	2523.31	99.71	3.95
3305-3315	364.75	368.91	370.55	371.26	371.71	372.52	369.95	2.58	0.70
3330-3340	365.79	369.96	372.09	372.87	373.25	374.34	371.38	2.83	0.76
3392-3398	231.85	234.89	234.95	235.46	236.23	236.50	234.98	1.52	0.65
3415-3500	2705.26	2790.71	2635.97	2638.54	2693.49	2651.25	2685.87	53.78	2.00
3500-3540	1364.32	1384.40	1381.45	1385.47	1392.83	1393.96	1383.74	9.77	0.71
3600-3850	8438.25	8540.08	8586.95	8619.02	8653.60	8681.24	8586.52	80.28	0.93

Figure 4.2 presents an overlay of the average spectra for laboratory grade acetone and the five nail polish remover brands analysed in the study (n=6 in each case).

It was possible to identify several regions where variation was present. In particular the average spectrum for the Allura nail polish remover revealed a large amount of variation from the other spectra. The variation observed was not restricted solely to the fingerprint region of the spectra (which is shown in figure 4.3).

In total 31 regions of variation were identified through visual examination of the overlaid spectra, although there was some overlap which was necessary in order to differentiate between all of the samples, rather than just two.

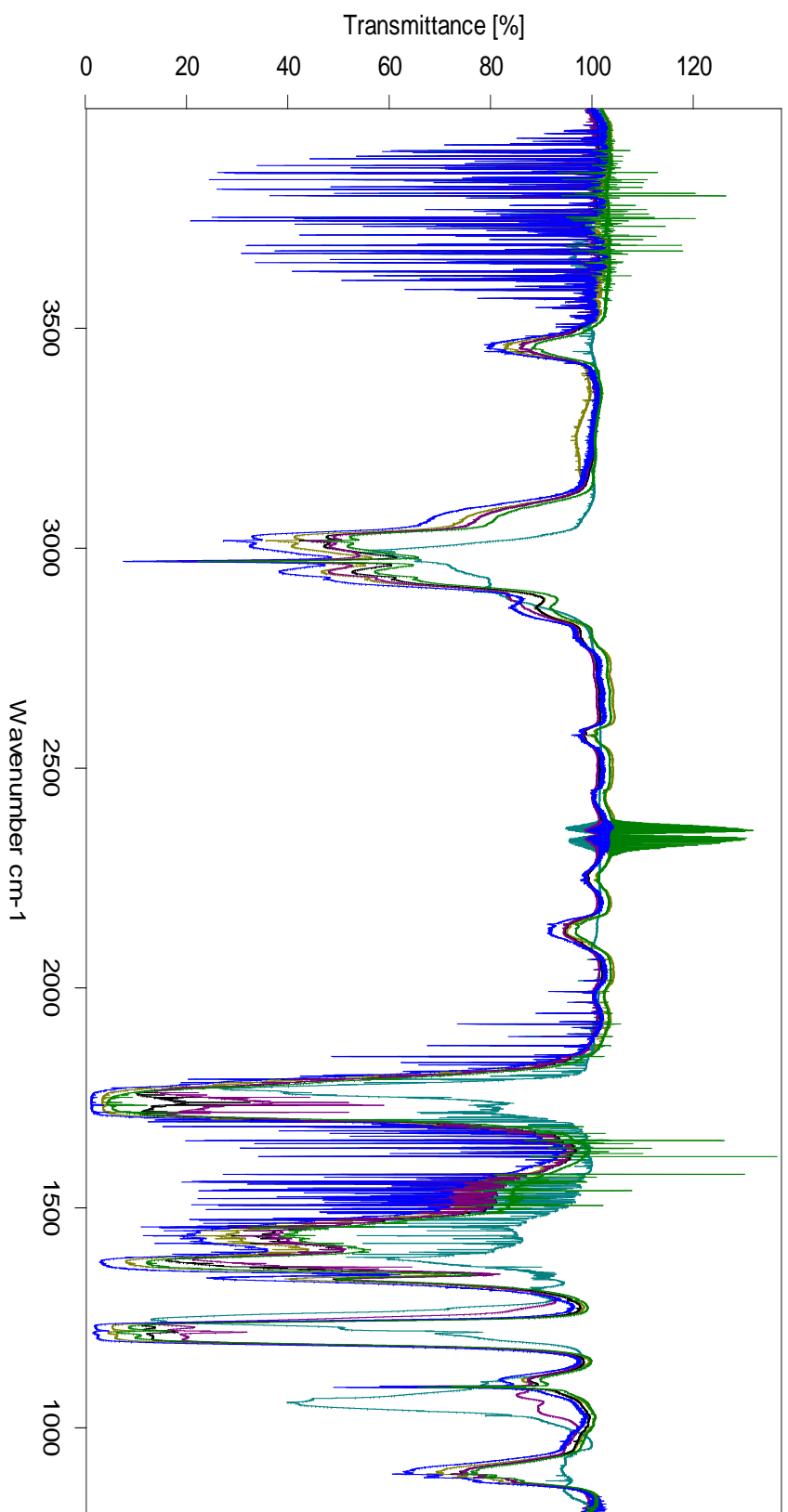


Figure 4.2 Overlaid average spectra for acetone (green) and five nail polish removers; Sally Hansen (blue), Mavala (purple), Cutex (dark green), Allura (teal) and Boots (olive) produced with 100 μ L samples at 27°C

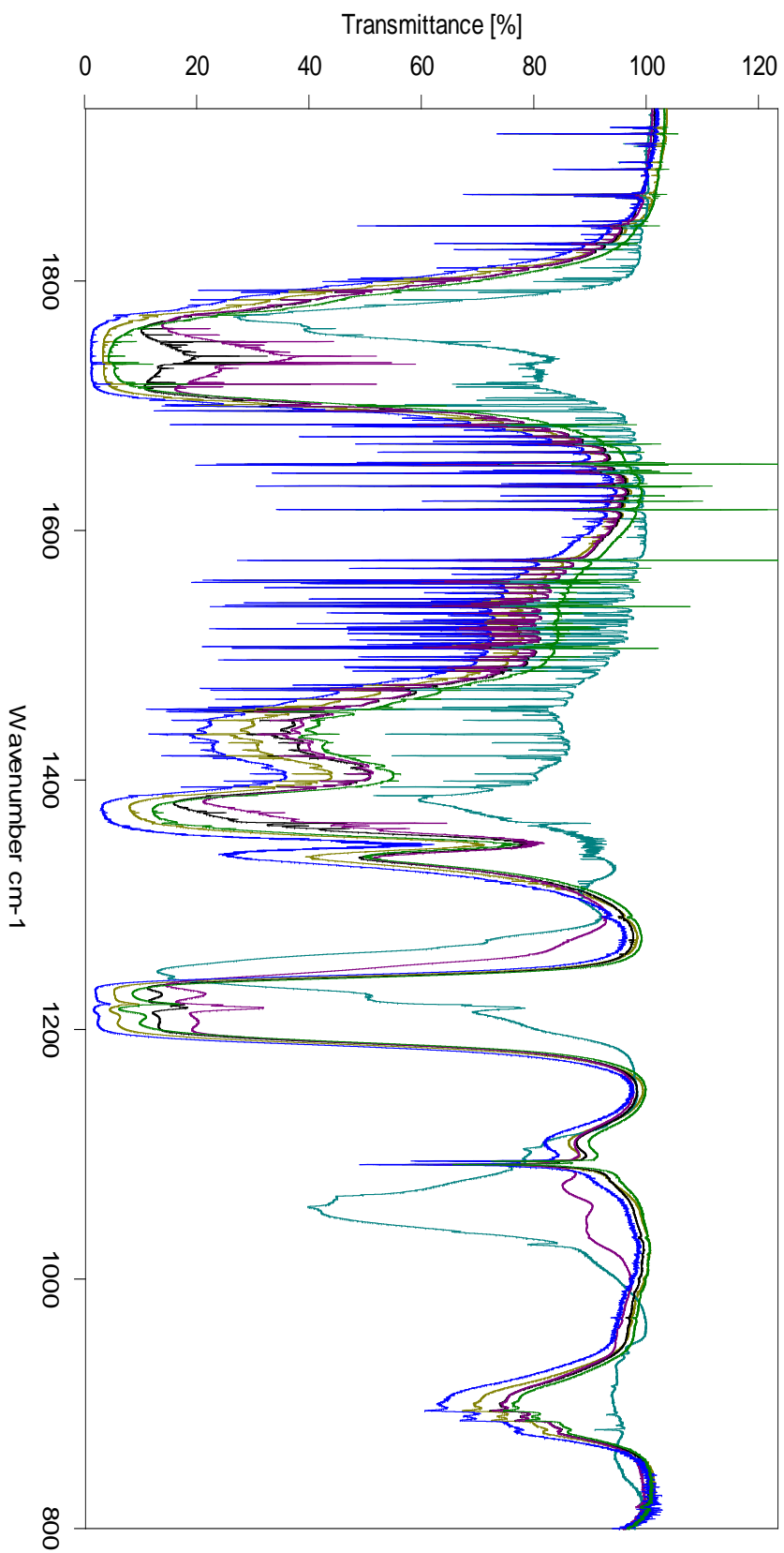


Figure 4.3 Close up of the fingerprint region of the overlaid spectra of acetone (green) and five nail polish removers; Sally Hansen (blue), Mavala (purple), Cutex (dark green), Allura (teal) and Boots (olive)

4.4.2 Statistical analysis

The 31 total transmittance values were plotted to give a profile of variables prior to inputting these values into the statistical software. Figure 4.4 shows the profile of variables for all 31 regions. This highlights the variation both within and between the different regions, however it is somewhat skewed by the larger total transmittance values. Data pre-treatment methods such as square root or fourth root could be used to moderate the overall differences between the transmittance values from region to region. However, such pre-processing could also detrimentally affect the differences within the regions of variation, and given the emphasis was on qualitative rather than quantitative analysis, the decision was taken to use the raw data rather than pre-processing the data (examples of pre-processed data are given in appendix 1). Table 4.3 shows wavelengths of the 31 regions of variation and the RSD values for the six brands taken from the average spectral data for each brand across six repetitive measurements of each brand.

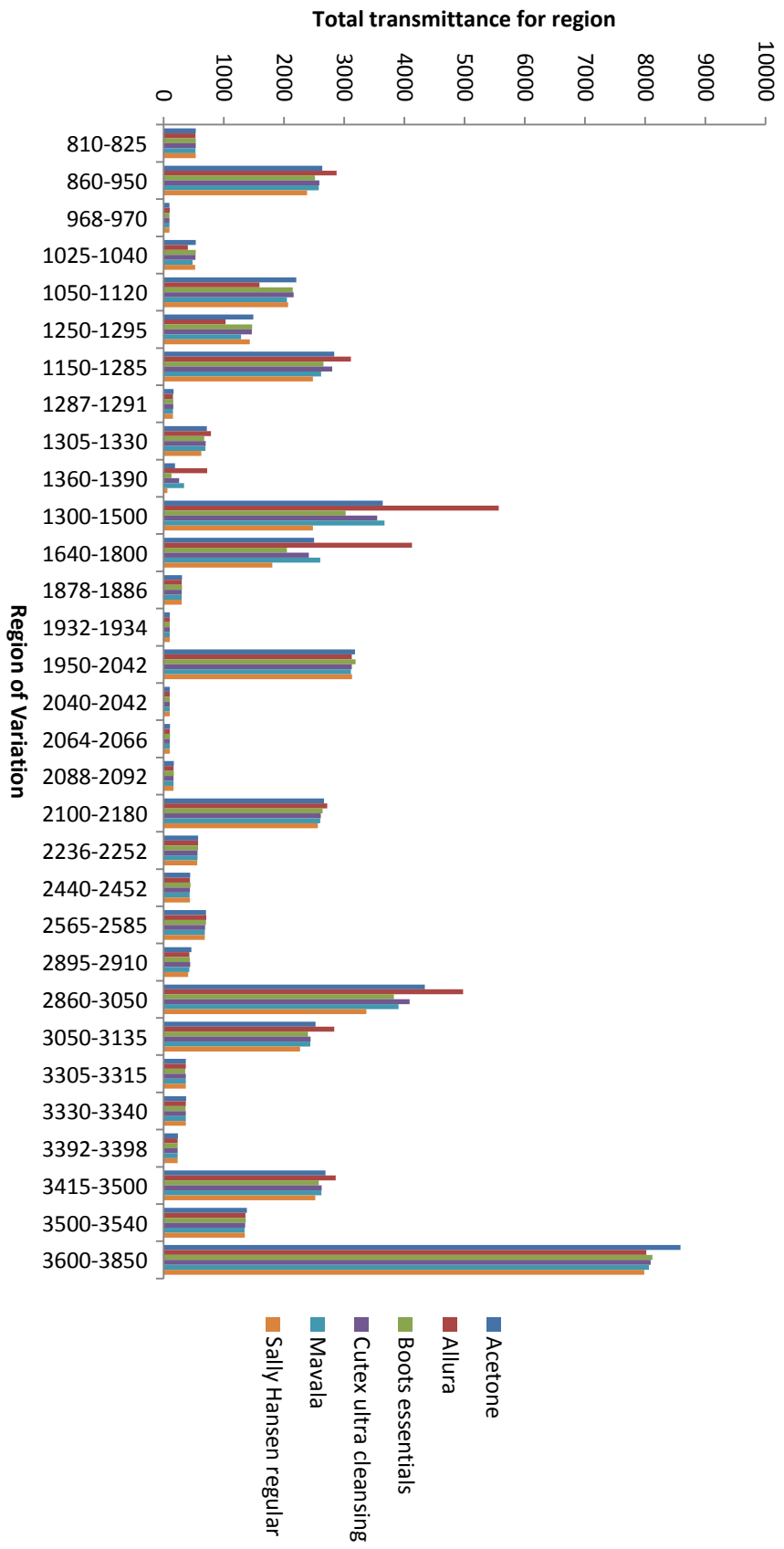


Figure 4.4 Profile of variables for the 31 regions of variation across the nail polish removers and acetone spectra

Table 4.3 RSD values for the five brands and laboratory acetone analysed with RSD values (and their regions) above 5% shown in red

Region (cm ⁻¹)	Acetone	Allura	Boots	Cutex	Mavala	Sally Hansen
810-825	2.54	0.15	0.16	0.08	0.19	0.14
860-950	3.87	1.85	3.63	1.24	4.25	3.83
968-970	1.70	0.21	0.55	0.18	1.13	0.94
1025-1040	1.76	4.81	0.24	0.07	1.94	0.37
1050-1120	2.25	7.57	1.77	0.69	3.33	2.17
1250-1295	1.32	7.13	0.68	0.24	3.43	1.12
1150-1285	6.71	11.67	4.11	1.47	7.69	3.67
1287-1291	1.31	1.84	0.70	0.24	1.76	1.14
1305-1330	5.33	3.18	4.76	1.65	5.85	5.16
1360-1390	36.67	18.91	23.12	4.89	17.76	27.02
1300-1500	14.46	8.18	11.96	4.06	13.80	12.21
1640-1800	11.77	12.66	9.05	3.48	11.35	8.60
1878-1886	0.99	0.30	0.66	0.15	0.09	0.20
1932-1934	0.86	0.48	0.94	0.32	0.26	0.30
1950-2042	1.09	0.50	0.88	0.30	0.18	0.25
2040-2042	1.22	0.57	1.03	0.35	0.32	0.38
2064-2066	1.15	0.49	0.96	0.32	0.24	0.30
2088-2092	0.82	0.26	0.52	0.17	0.32	0.34
2100-2180	0.88	0.30	0.40	0.12	0.90	0.87
2236-2252	0.78	0.46	0.52	0.17	0.30	0.36
2440-2452	0.90	0.57	0.84	0.28	0.07	0.22
2565-2585	0.73	0.50	0.53	0.15	0.49	0.52
2895-2910	4.73	4.65	3.69	1.35	5.73	4.54
2860-3050	11.43	7.10	9.44	3.29	12.57	9.91
3050-3135	3.95	1.01	3.20	1.12	4.18	3.78
3305-3315	0.70	0.09	0.35	0.13	0.08	0.13
3330-3340	0.76	0.18	0.14	0.17	0.14	0.17
3392-3398	0.65	0.20	0.11	0.13	0.09	0.19
3415-3500	2.00	0.44	1.86	0.59	2.28	2.12
3500-3540	0.71	0.24	0.45	0.12	0.34	0.35
3600-3850	0.93	0.39	0.52	0.49	0.80	0.93
Average	4.03	3.13	2.83	0.90	3.29	2.97

The RSD values for the brands confirmed the visual observations reported within the six overlaid spectra for each brand (figure 4.1). Some spectral variation was evident across the six brands, but this was minimal with the overall RSD value for all

regions less than 5% for each brand. The regions which demonstrated the greatest variation across the branded samples correspond to the regions with RSDs above 5% observed with the six acetone repeats (table 4.2) and accounted for 29% of the areas of interest; however in all but one of these regions (1360-1390 cm^{-1} ; 3% of the total regions of variation) the RSD was less than 15% and this again corroborated the laboratory acetone data.

4.4.2.1 Hierarchical cluster analysis

The spectral data was inputted into Minitab for hierarchical cluster analysis. This included both the individual repeats for each brand and the average values calculated for each brand. The dendrograms were produced using single linkage and Euclidean distance, although other combinations were also tried.

The dendrogram produced for the individual spectra are presented in figure 4.5. Unsurprisingly, the results revealed that acetone exhibited similarities with all of the nail polish removers, and that Allura, which had the most spectral differences, was the least similar to the other nail polish removers. Statistical analysis of the individual repeats demonstrated that for some of the samples there was a degree of overlap highlighted by the RSD values across some areas of the spectra.

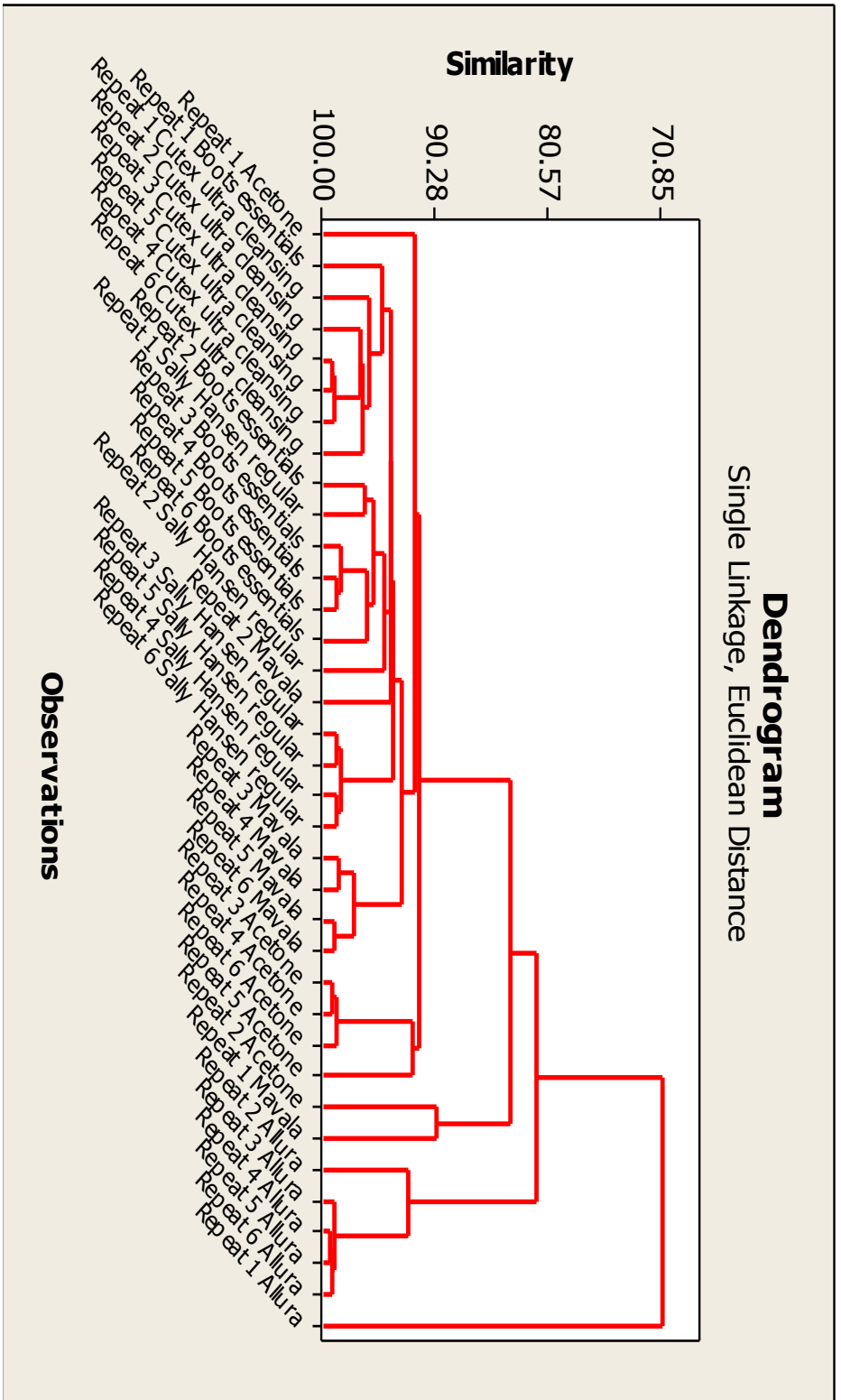


Figure 4.5: Dendrogram produced using the individual repeat total transmittance values for the 31 regions of variation for the five nail polish removers and acetone

When the average spectra across each brand of acetone nail polish remover were analysed, the samples were discriminated completely and the resultant dendrogram is presented in figure 4.6.

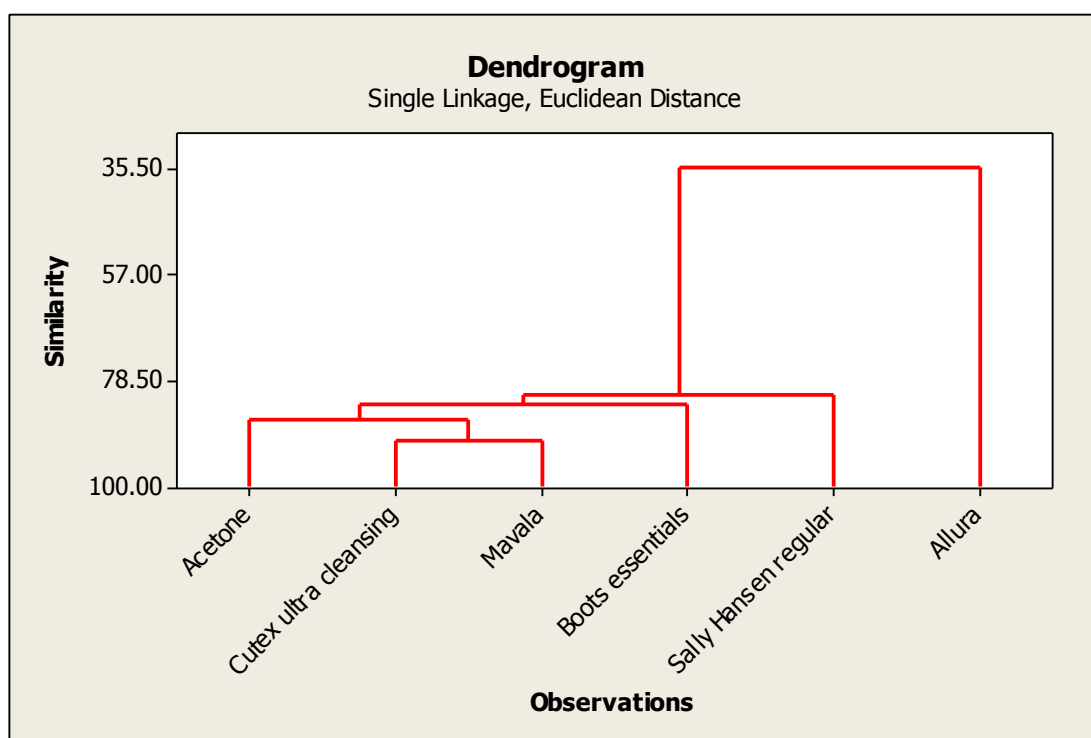


Figure 4.6 Dendrogram produced using the average total transmittance values for the 31 regions of variation for the five nail polish removers and acetone

4.4.2.2 Self organising feature maps

The data was then subjected to SOFM neural network analysis and Figure 4.7 is the cluster map for the individual repeats, with the clustering pre-set to six. This corroborates the overlap that was observed with the HCA dendrogram with the comingling of the individual samples rather than discrete separation by brand. One of the Allura samples (repeat 1) separated completely from the other samples, mirroring the result observed for this sample in the dendrogram. The rest of the Allura repeats formed a cluster, again corresponding to the clustering seen with the HCA dendrogram. Five of the acetone repeats form another cluster, with the sixth (repeat 1) forming a large cluster with repeats of Cutex ultra cleansing, Mavala and Sally Hansen. The other Sally Hansen and Mavala repeats form another cluster. Unlike the dendrogram all of the Boots Essentials repeats cluster together.

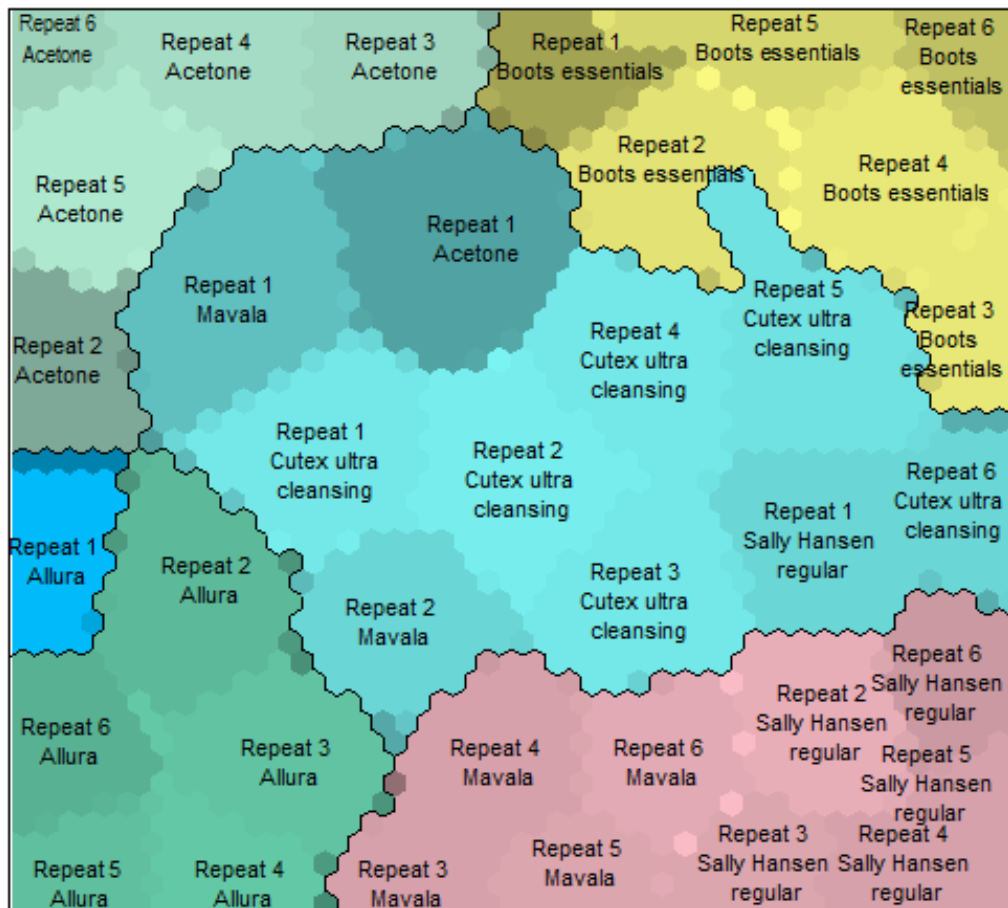


Figure 4.7 Cluster map for the individual repeats of acetone and acetone based nail polish removers with the clustering set to six

The average data produced the cluster map presented in Figure 4.8 when the clustering was set to six, and it can be seen that the samples have separated correctly by brand. This supports the findings of the HCA.

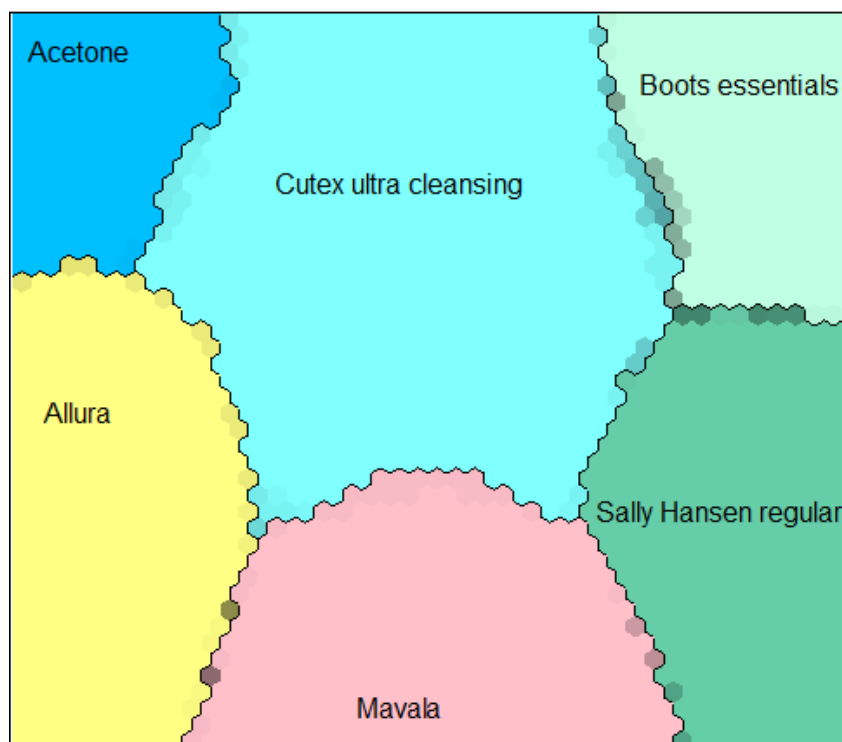


Figure 4.8 Cluster map for acetone and acetone based nail polish removers created using the average spectral data with the clustering set to six

Figures 4.9-4.11 show the component maps for the 31 regions of variation used as variables in the data. The maps show that some spectral features are discriminators for specific brands, while some show variation across all six brands. The region $3600-3850\text{ cm}^{-1}$ is an example of a discriminatory region for laboratory grade acetone, with a single red cluster representing these samples while all other samples are differentiated to lesser degrees from each other (all appearing as various shades of blue). Red shading indicates a high level of similarity while blue demonstrates the lowest level of similarity. As discussed in chapter 2, the ideal component map for a feature that acts as a discriminator for a single brand will have a single cluster with a high level of similarity for that brand and the rest of the component map will be blue. However, a component map with each cluster shaded differently indicates that this feature could discriminate between all the brands to differing degrees.

The range of shading seen within each component demonstrates that the spectral regions selected all have some variation between the clusters. This suggests that a

combination of spectral features is required for successful discrimination of all six of the brands from each other, however further work could be done to determine whether the number of spectral features required could be reduced from 31, as this would increase the potential for use in a portable detection system.

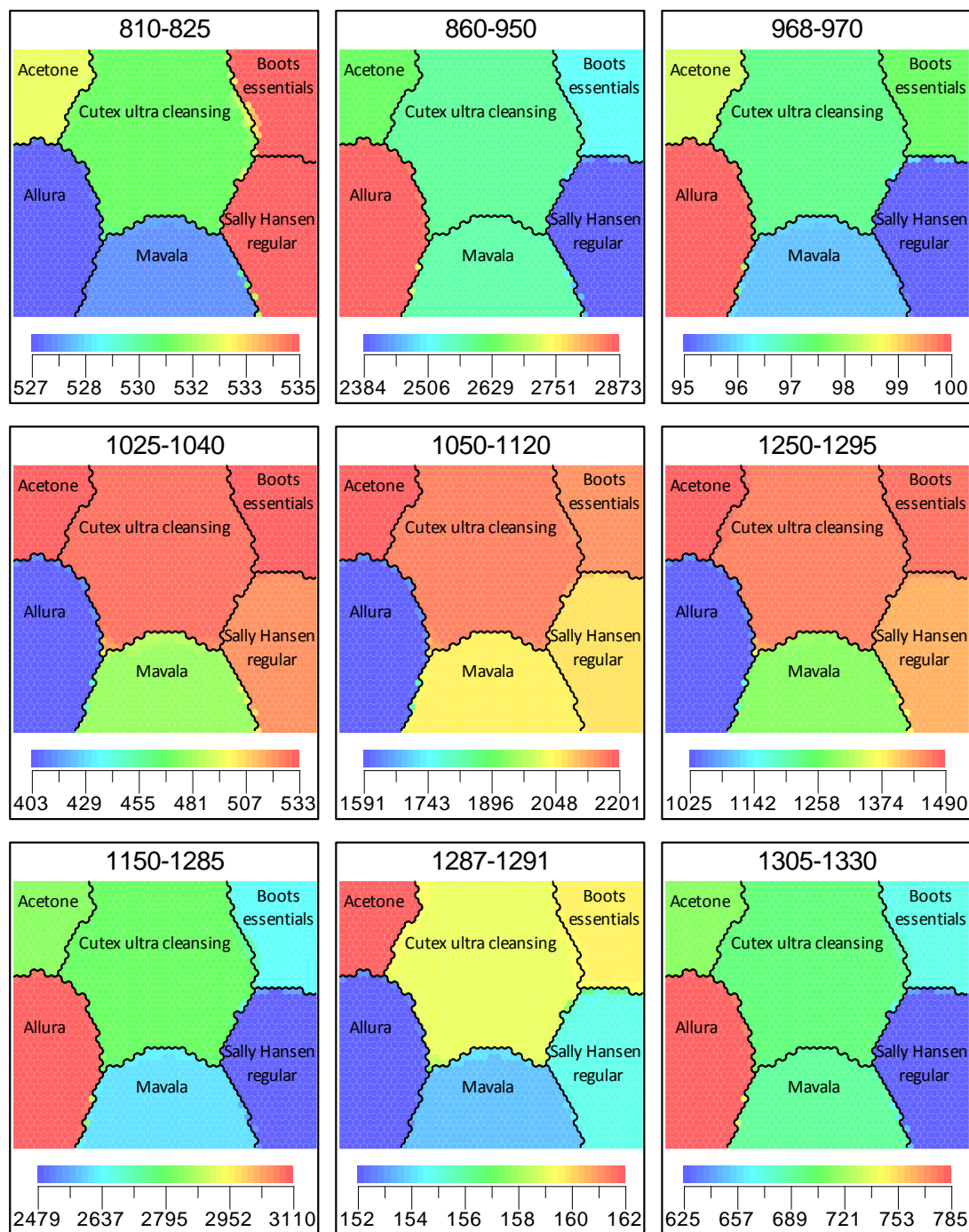


Figure 4.9 Component maps for regions of variation between 810 and 1330 cm^{-1}

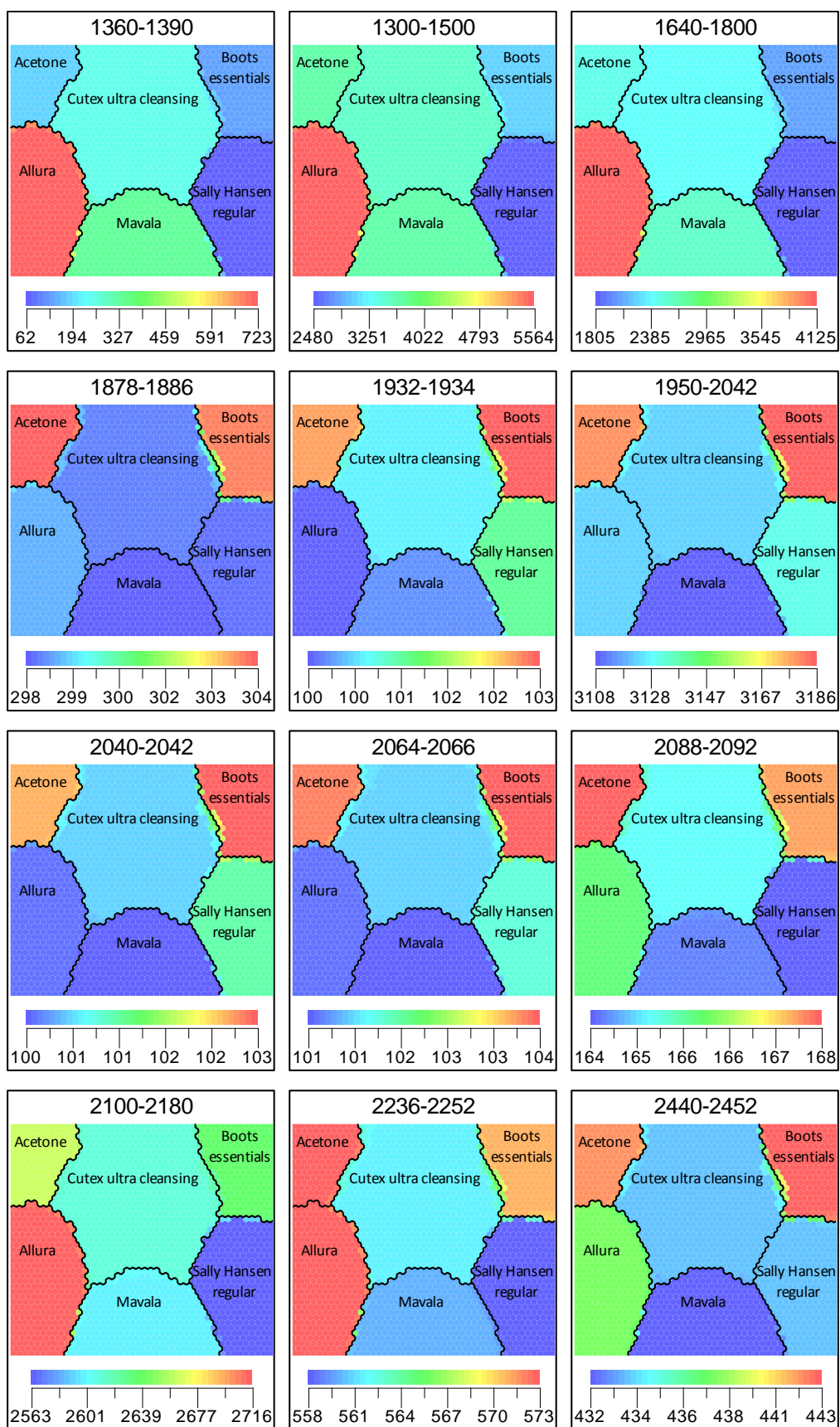


Figure 4.10 Component maps for regions of variation between 1360 and 2452 cm⁻¹

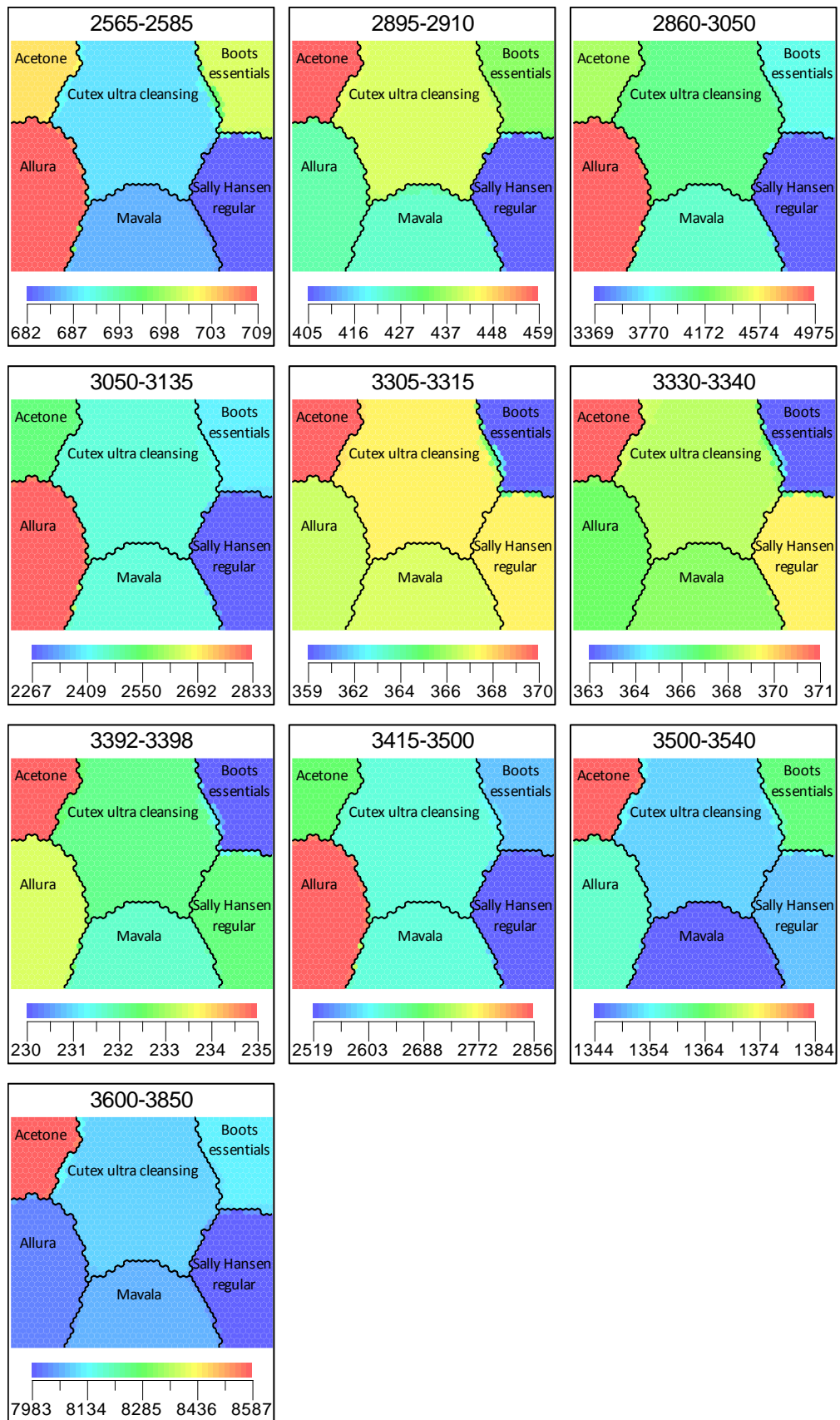


Figure 4.11 Component maps for regions of variation between 2565 and 3850 cm^{-1}

It is also possible to link the component maps back to the profile of variables and the original spectra. For example the region of variation 1300 – 1500 cm^{-1} has the six spectra shown in figure 4.12, the profile shown in figure 4.13 and the component map shown in figure 4.14. The spectrum shows all the % transmittance values that were then used for data analysis for this region. The profile of variables demonstrates that in this feature there is predominantly variation between Allura and the other brands, with a small amount of variation between all of the six brands, suggesting that this feature would be discriminatory for Allura. The component map supports this with the Allura cluster shaded red, and the other five compounds having similar shading towards the blue end of the scale. The absorption seen in this region is thought to be primarily as a result of the presence of CH_3 groups.

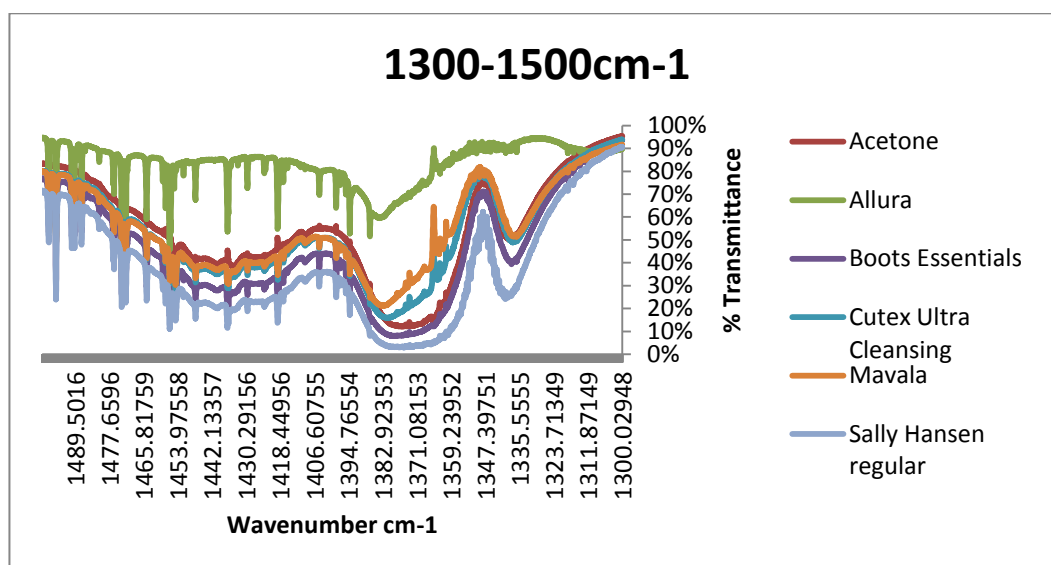


Figure 4.12 Overlaid spectra for the six brands in the region 1300-1500 cm^{-1} (plotted in Microsoft Excel)

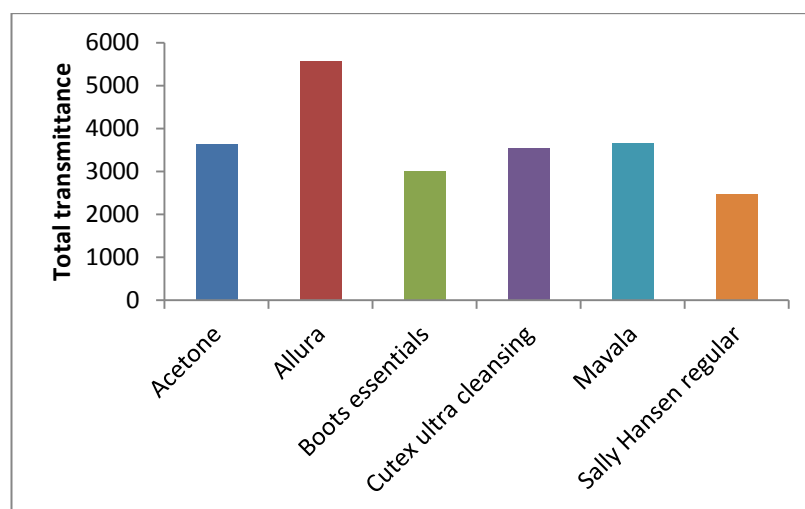


Figure 4.13 Total transmittance values for the region of variation 1300 - 1500 cm^{-1}

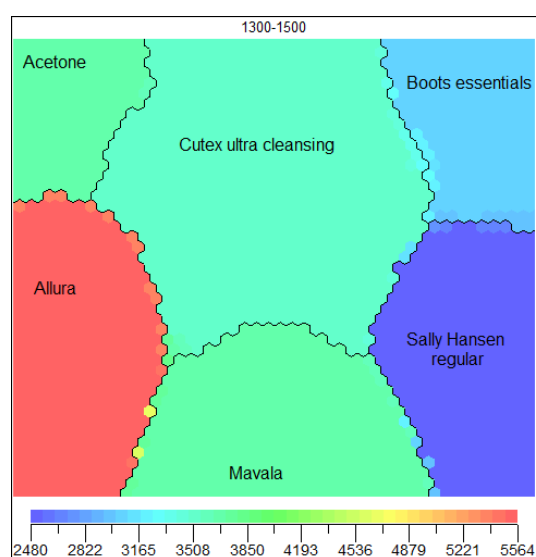


Figure 4.14 Component map for the region of variation 1300 - 1500 cm^{-1}

In comparison the region of variation 1640-1800 cm^{-1} (spectra shown in figure 4.15) shows some grouping across the six brands, with Allura once again appearing quite distinctly separate, and with Mavala and Cutex showing similarities to each other but differences to the other brands. Figure 4.16 shows the profile of variables. This then corresponds to the component map (figure 4.17) where Allura is shaded a different colour to the other brands, Mavala and Cutex shaded a similar colour to each other and the remaining three brands shaded the same colour. Therefore, while this feature is not necessarily discriminatory for a single brand it provides a

degree of discrimination across the brands. The absorption in this region is thought to be primarily as a result of the presence of C=O stretching, however as the exact chemical composition of the different nail polish removers is not known it is impossible to be completely certain.

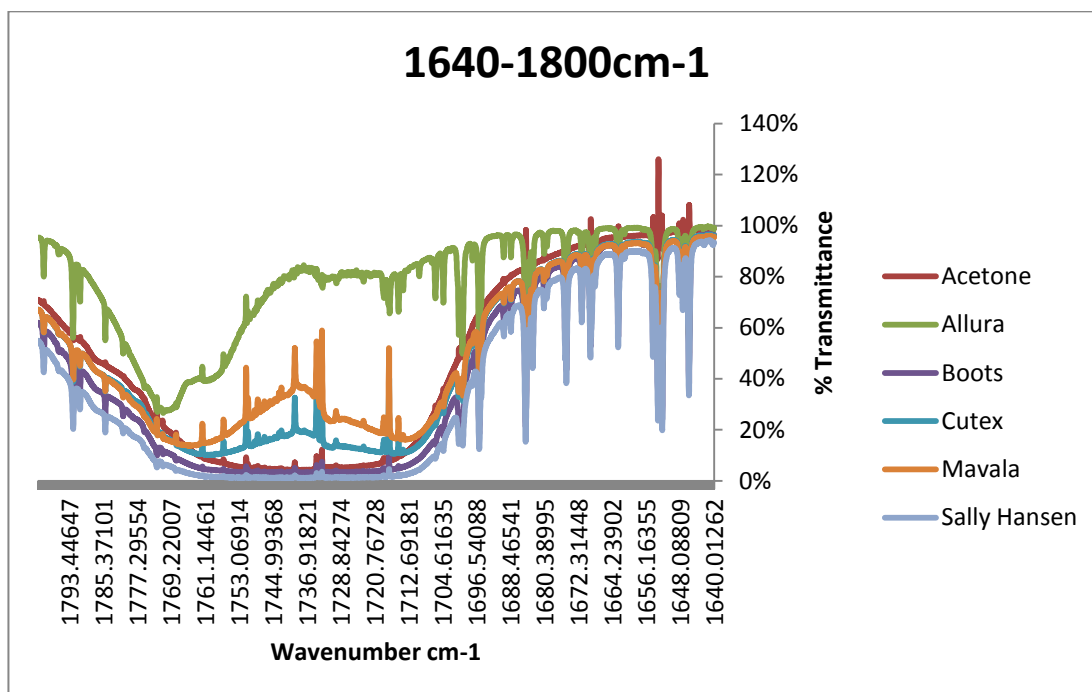


Figure 4.15 Overlaid spectra for the six brands in the region 1640-1800 cm⁻¹ (plotted in Microsoft Excel)

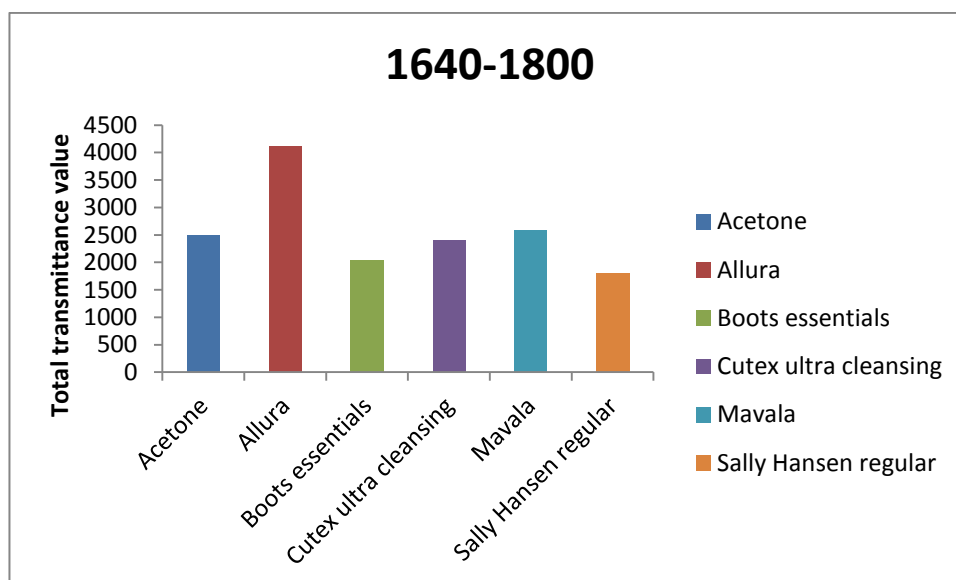


Figure 4.16 Total transmittance values for the region of variation 1640 - 1800 cm⁻¹

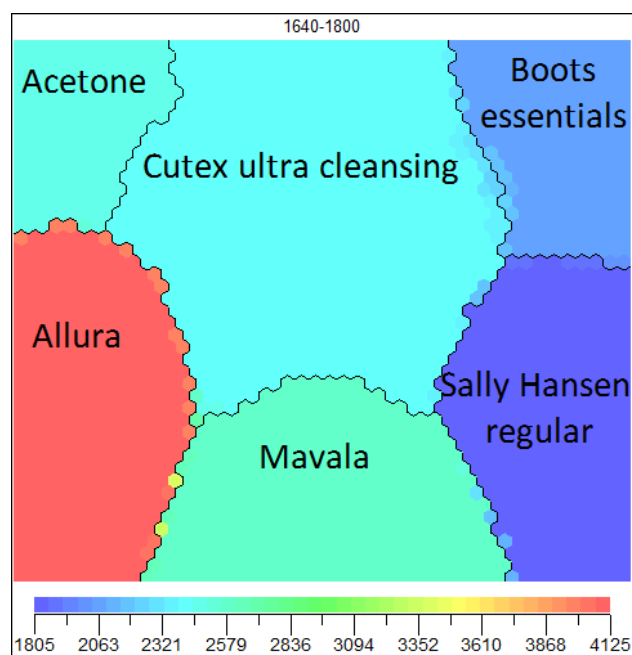


Figure 4.17 Component map for the region of variation 1640 - 1800 cm^{-1}

The ability to break the data down into the separate components and visually represent the differences between the brands through a colour scale means that SOFM is simpler to interpret and more informative than HCA.

4.5 Conclusions

The analysis of acetone and acetone based nail polish removers successfully proved the concept that a combination of high resolution Fourier Transform spectroscopy and statistical analysis can discriminate between laboratory grade material and its shop bought counterparts.

This is significant because it gives the potential for intelligence gathering, and providing an aid to security services in the identification of those trying to produce a homemade explosive device. As discussed in chapter 1, the linking of explosive materials to precursors is an area of great importance. The results of this research could further inform the development of technology for linking HMEs to their precursors.

In addition, the results raise concerns as to whether the differences seen in the spectrum of a precursor material would also have an effect on the spectrum of the final explosive produced as this could have significant implications for detection.

The results indicate that it is important to carry out a visual examination of the spectra as well as the statistical analysis, and that repeat analysis of each brand is required for accurate discrimination. Examination of the component maps suggests that the original 31 regions selected as discriminatory regions of variation might be reduced without losing the discriminating power of the analysis.

4.6 References

1. Fiorani, L., Puiu, A., Rosa, O. and Palucci, A., *Lidar/DIAL detection of bomb factories*, in *Electro-Optical Remote Sensing, Photonic Technologies, and Applications VII; and Military Applications in Hyperspectral Imaging and High Spatial Resolution Sensing*, G.W. Kamerman, et al., Editors. 2013, Spie-Int Soc Optical Engineering: Bellingham.
2. Oxley, J.C., Smith, J.L., Brady, J.E. and Steinkamp, L., *Factors Influencing Destruction of Triacetone Triperoxide (TATP)*. *Propellants Explosives Pyrotechnics*, 2014. **39**(2): p. 289-298.
3. Egorshv, V.Y., Sinditskii, V.P. and Smirnov, S.P., *A comparative study on two explosive acetone peroxides*. *Thermochimica Acta*, 2013. **574**: p. 154-161.
4. Brady, J.J. and Pellegrino, P.M., *Next Generation Hazard Detection via Ultrafast Coherent Anti-Stokes Raman Spectroscopy*. *Chemical, Biological, Radiological, Nuclear, and Explosives (Cbrne) Sensing Xiv*, 2013. **8710**.
5. Mitev, V., Babichenko, S., Bennes, J., Borelli, R., Dolfi-Bouteyre, A., Fiorani, L., Hespel, L., Huet, T., Palucci, A., Pistilli, M., Puiu, A., Rebane, O. and Sobolev, I., *Mid-IR DIAL for high-resolution mapping of explosive precursors*, in *Lidar Technologies, Techniques, and Measurements for Atmospheric Remote Sensing IX*, U.N. Singh and G. Pappalardo, Editors. 2013, Spie-Int Soc Optical Engineering: Bellingham.
6. Dunayevskiy, I., Tsekoun, A., Prasanna, M., Go, R. and Patel, C.K.N., *High-sensitivity detection of triacetone triperoxide (TATP) and its precursor acetone*. *Applied Optics*, 2007. **46**(25): p. 6397-6404.
7. Patel, C.K.N., *Laser photoacoustic spectroscopy helps fight terrorism: High sensitivity detection of chemical Warfare Agent and explosives*. *European Physical Journal-Special Topics*, 2008. **153**: p. 1-18.
8. Chowdhuri, A., Sharma, A. and Gupta, V., *Detection of TATP precursor acetone at trace levels using rf sputtered SnO₂ thin film based sensors*. *Chemical, Biological, Radiological, Nuclear, and Explosives (Cbrne) Sensing Xii*, 2011. **8018**.

9. Cho, J.W., Li, X.P., Gu, Z.Y. and Kurup, P.U., *Recognition of Explosive Precursors Using Nanowire Sensor Array and Decision Tree Learning*. *Ieee Sensors Journal*, 2012. **12**(7): p. 2384-2391.
10. Osowski, S., Linh, T.H. and Brudzewski, K., *Neuro-fuzzy TSK network for calibration of semiconductor sensor array for gas measurements*. *Ieee Transactions on Instrumentation and Measurement*, 2004. **53**(3): p. 630-637.
11. Gulbag, A. and Temurtas, F., *A study on quantitative classification of binary gas mixture using neural networks and adaptive neuro-fuzzy inference systems*. *Sensors and Actuators B-Chemical*, 2006. **115**(1): p. 252-262.
12. Hwang, J., Choi, N., Park, A., Park, J., Baek, S., Cho, S.G., Baek, S. and Choo, J., *Fast and sensitive recognition of various explosive compounds using Raman spectroscopy and principal component analysis*. *Journal of Molecular Structure*, 2013. **1039**(0): p. 130-136.
13. Wang, X.D., Ye, M.Y. and Duanmu, C.J., *Classification of data from electronic nose using relevance vector machines*. *Sensors and Actuators B-Chemical*, 2009. **140**(1): p. 143-148.
14. Cho, J.H., Kim, Y.W., Na, K.J. and Jeon, G.J., *Wireless electronic nose system for real-time quantitative analysis of gas mixtures using micro-gas sensor array and neuro-fuzzy network*. *Sensors and Actuators B-Chemical*, 2008. **134**(1): p. 104-111.
15. Xu, Z., Shi, X.J., Wang, L.Y., Luo, J., Zhong, C.J. and Lu, S.S., *Pattern recognition for sensor array signals using Fuzzy ARTMAP*. *Sensors and Actuators B-Chemical*, 2009. **141**(2): p. 458-464.
16. Desa, W., Nic Daeid, N., Ismail, D. and Savage, K., *Application of Unsupervised Chemometric Analysis and Self-organizing Feature Map (SOFM) for the Classification of Lighter Fuels*. *Analytical Chemistry*, 2010. **82**(15): p. 6395-6400.
17. Muehlethaler, C., Massonnet, G. and Esseiva, P., *The application of chemometrics on Infrared and Raman spectra as a tool for the forensic analysis of paints*. *Forensic Science International*, 2011. **209**(1-3): p. 173-182.
18. Rao, W., Scurr, D.J., Burston, J., Alexander, M.R. and Barrett, D.A., *Use of imaging multivariate analysis to improve biochemical and anatomical discrimination in desorption electrospray ionisation mass spectrometry imaging*. *Analyst*, 2012. **137**(17): p. 3946-3953.
19. Tan, B., Hardy, J.K. and Snavely, R.E., *Accelerant classification by gas chromatography/mass spectrometry and multivariate pattern recognition*. *Analytica Chimica Acta*, 2000. **422**(1): p. 37-46.
20. Bodle, E.S. and Hardy, J.K., *Multivariate pattern recognition of petroleum-based accelerants by solid-phase microextraction gas chromatography with flame ionization detection*. *Analytica Chimica Acta*, 2007. **589**(2): p. 247-254.
21. Burger, F., Dawson, M., Roux, C., Maynard, P., Doble, P. and Kirkbride, P., *Forensic analysis of condom and personal lubricants by capillary electrophoresis*. *Talanta*, 2005. **67**(2): p. 368-376.

Chapter 5. Brand Discrimination - Alcohols

5.1 Introduction

Alcohols have a role in many chemical processes including the production of homemade explosive materials. Due to the organic nature of alcohols they have the potential to be used as fuels in explosive mixtures, and due to their flammable nature alcohols could also be included in an explosive device in order to increase the damage caused by that device. Methanol and ethanol had both been identified as compounds of interest in chapter 3.

Alcohol is readily available in many forms, and these forms contain various additives that can allow for the discrimination of different alcoholic materials. For example methylated spirit is coloured purple to prevent accidental consumption, and the presence of this colouring could alter the appearance of the infrared spectrum of methylated spirit from other alcoholic materials thereby allowing for its discrimination.

The analysis of alcohols, in particular ethanol, has been the subject of substantial research, focusing primarily on two areas, law enforcement[1] and food safety[2]. A wide variety of techniques have been utilised for analysis in the past, however the two most successful techniques for analysis of alcohols are gas chromatography and infrared spectroscopy[1, 3]. Much of the research into the use of infrared spectroscopy for the discrimination of different alcohols has focused upon discriminating wines[4-7] with many projects utilising a WineScan™ spectrometer[4-6, 8, 9]. This instrument is produced by Foss and has been specifically designed for the FTIR analysis of wines (as well as being applied to other alcoholic beverages)[10]. Analysis using this instrument is fixed for liquid samples at 40°C with a resolution of 4 cm⁻¹[4, 5, 9, 10]. This results in a spectrum composed of 1056 data points[4, 8] compared to the 106,198 data points produced with the FTS at 0.1 cm⁻¹. This difference in resolution was also seen in research carried out on

more conventional FTIR instruments[2, 11] with the highest resolution described being 2 cm^{-1} .

Multivariate analysis is frequently used in the analysis of alcohols for the purpose of discriminating between different brands of the same alcohol type and identifying adulterants, however the technique most commonly employed is principle component analysis[2, 4-8]. Self organising feature maps do not appear to have thus far been applied to the analysis of alcohols, and the focus has been on discriminating between different brands of the same alcohol type, for example identification of different wines, rather than taking a broader look across different alcohol types.

There has been limited research into the detection and analysis of alcohol in the vapour phase. This research has focused upon spectroscopic techniques, with some research focusing upon the detection of alcohol in breath for the identification of toxic levels of ethanol[11]. This research was principally aimed at a quantitative measurement, and was carried out at relatively low resolution (4 cm^{-1}). Standoff detection of alcohol has also been investigated for the purpose of identifying drivers who are under the influence of alcohol through the detection of alcohol vapour inside car cabins[12, 13]. This technique utilises lidar, focused upon a single wavelength ($3.39\text{ }\mu\text{m}$) for the detection of alcohol.

The premise of this research was to apply high resolution FTIR and the chemometric techniques described in Chapter 4 to the analysis of a range of alcohol types, in the vapour phase at approximately room temperature, to determine whether discrimination of the alcohol types was possible.

5.2 Materials

A range of commercially available alcohol containing materials and laboratory standards were selected for investigation with a range of alcohol concentrations and potential additives and are given in table 5.1.

Table 5.1 Alcohol containing materials selected for analysis

Material	Concentration (% v/v)	Source
Methanol (laboratory grade)	99.9	Sigma Aldrich UK
Ethanol (laboratory grade)	99.9	Sigma Aldrich UK
Propanol (laboratory grade)	99.9	Sigma Aldrich UK
Methylated spirit	60-100 ethanol 1-5 methanol	Cotswold Outdoor
Surgical spirit	90 ethanol 5 methanol	Boots
Listerine mouthwash	Not specified	Boots
Tesco everyday value mouthwash	Not specified	Tesco
Colgate Peroxyl mouthwash	9.6	Boots
Bacardi Breezer	4	Tesco
Melocoton	20	Just a Glass
Bacardi rum	37.5	Just a Glass
Gordon's gin	37.5	Just a Glass
Beefeater gin	40	Just a Glass
Smirnoff vodka	37.5	Just a Glass
Absolut vodka	40	Just a Glass
Jose Cuervo Especial tequila	38	Sourced 'in house'

A breakdown of the different ingredients in each shop bought alcohol can be found in appendix 3. Samples were held within the FTS using aluminium dishes purchased from Sigma Aldrich UK.

5.3 Experimental protocol

The protocol used for each sample followed that developed through the diesel analysis (Chapter 3). Each alcohol was analysed at 27°C with six 100 µL samples analysed from the stock solutions.

5.3.1 Visual analysis

Visual comparison of the resultant spectra was carried out using the OPUS software (version 6.5) provided with the FTS instrument. Spectra were examined both

individually and as an overlay of the average spectra (n=6) for each alcohol. The zoom feature was used to examine the finer detail of the spectra.

5.3.2 Statistical analysis

The statistical analysis followed the same process as applied to the acetone data (Chapter 4), the transmittance values from each region of variation were 'binned' to give a total transmittance value for each region. These values were then input into Minitab (version 16) and Viscovery SOMine (version 4.0.2). Data normalisation was also employed prior to the data reduction in order to combat a drift in the starting baseline that was observed across the analyses.

The normalisation aimed to adjust the data so that all of the spectra began at 100% transmittance as a baseline. This was achieved by calculating how far from 100% the first point (at 4000 cm^{-1}) of the spectrum was and adjusting every point on the spectrum by this value. This method, while not sophisticated, ensured that all the spectra started at the same point.

The baseline drift could result from the long duration of the use of the instrument. Over time the liquid nitrogen utilised to cool the detector will have been consumed, and while this did not reach a level that prevented the detector from functioning, it potentially could have caused the baseline drift observed. While this drift was substantial enough to require baseline normalisation of the data prior to the statistical analysis, it did not affect the peak position. Therefore the variation observed was due to differences in the alcohols analysed resulting in different spectra rather than instrumental variation.

5.4 Results and discussion

5.4.1 Visual analysis

A visual examination of the six repeats for ethanol, shown in figure 5.1 demonstrated the presence of variation in terms of the peak areas observed. Similar variation had been observed in the initial validation work using diesel and in the analysis of acetone and acetone based nail polish removers.

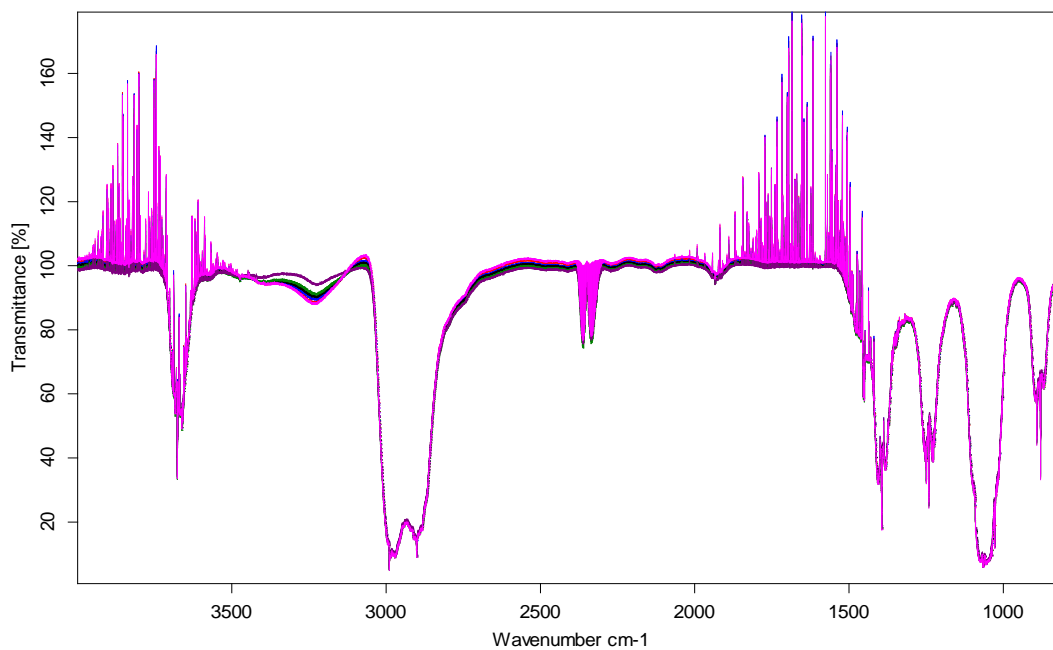


Figure 5.1 Six ethanol repeats overlaid, demonstrating the presence of variation between the spectra

As with the nail polish removers in Chapter 4 the data from each repeat was examined more closely through monitoring the RSD of the binned transmission values across the identified regions of interest. The data for each repeat, including the mean, standard deviation and RSD for each region of interest, along with the wavenumbers for each of the 22 regions identified, are presented in table 5.2. While there is some variation across the repeats the data collected is reproducible with none of the regions identified having an RSD value of above 5%.

Table 5.2 Data for the six ethanol repeats across the 22 regions of variation identified

Region (cm ⁻¹)	Ethanol 1	Ethanol 2	Ethanol 3	Ethanol 4	Ethanol 5	Ethanol 6	Average	St dev	RSD
810-840	1052.64	1057.51	1051.39	1052.41	1054.43	1054.13	1053.75	1.97	0.19
860-910	1235.74	1232.35	1230.29	1228.36	1228.67	1220.22	1229.27	4.75	0.39
920-100	2649.27	2664.93	2654.53	2657.11	2666.28	2664.55	2659.44	6.27	0.24
970-1020	1295.83	1298.45	1295.92	1296.39	1299.33	1293.49	1296.57	1.90	0.15
1020-1050	263.62	265.06	260.74	262.50	261.55	255.74	261.54	2.94	1.12
1050-1100	382.28	387.86	378.95	382.30	381.39	373.11	380.98	4.42	1.16
1140-1150	348.04	350.21	349.33	349.76	351.25	350.97	349.93	1.07	0.31
1120-1200	2482.45	2496.09	2490.81	2493.62	2503.78	2500.19	2494.49	6.84	0.27
1200-1280	1725.46	1722.83	1723.39	1723.12	1725.70	1711.56	1722.01	4.81	0.28
1300-1340	1517.80	1526.61	1523.56	1526.85	1533.63	1530.89	1526.56	5.08	0.33
1340-1360	588.52	591.09	588.49	590.79	592.66	591.04	590.43	1.49	0.25
1360-1440	1605.91	1602.17	1595.43	1602.69	1603.47	1587.83	1599.58	6.15	0.38
1440-1460	563.30	564.53	559.39	565.16	566.79	564.21	563.90	2.28	0.40
1450-1480	887.23	890.53	880.51	891.38	894.38	891.25	889.21	4.42	0.50
1900-1970	2487.95	2515.85	2507.88	2518.24	2535.90	2541.01	2517.80	17.60	0.70
2000-2100	3634.58	3679.57	3669.50	3684.01	3711.55	3721.50	3683.45	28.39	0.77
2620-2680	2126.17	2156.15	2154.47	2164.23	2183.46	2189.70	2162.36	20.84	0.96
2800-2860	1529.53	1540.98	1545.93	1550.32	1561.07	1556.48	1547.38	10.33	0.67
2850-2915	733.59	734.96	732.43	736.40	736.68	723.10	732.86	4.61	0.63
2915-2950	333.70	334.28	331.77	334.45	333.81	326.12	332.36	2.92	0.88
2950-3100	3269.03	3313.98	3308.98	3328.77	3354.77	3348.20	3320.62	28.39	0.85
3600-3775	5387.20	5437.66	5383.05	5461.36	5496.59	5495.34	5443.53	45.97	0.84

The average spectra for all of the alcohols analysed are presented in figure 5.2. The spectra showed several regions of variation, but also some absorption features characteristic of all the alcohols. This suggested that it should be possible to discriminate between the alcohols, whilst still being able to identify all the spectra as being produced by an alcohol.

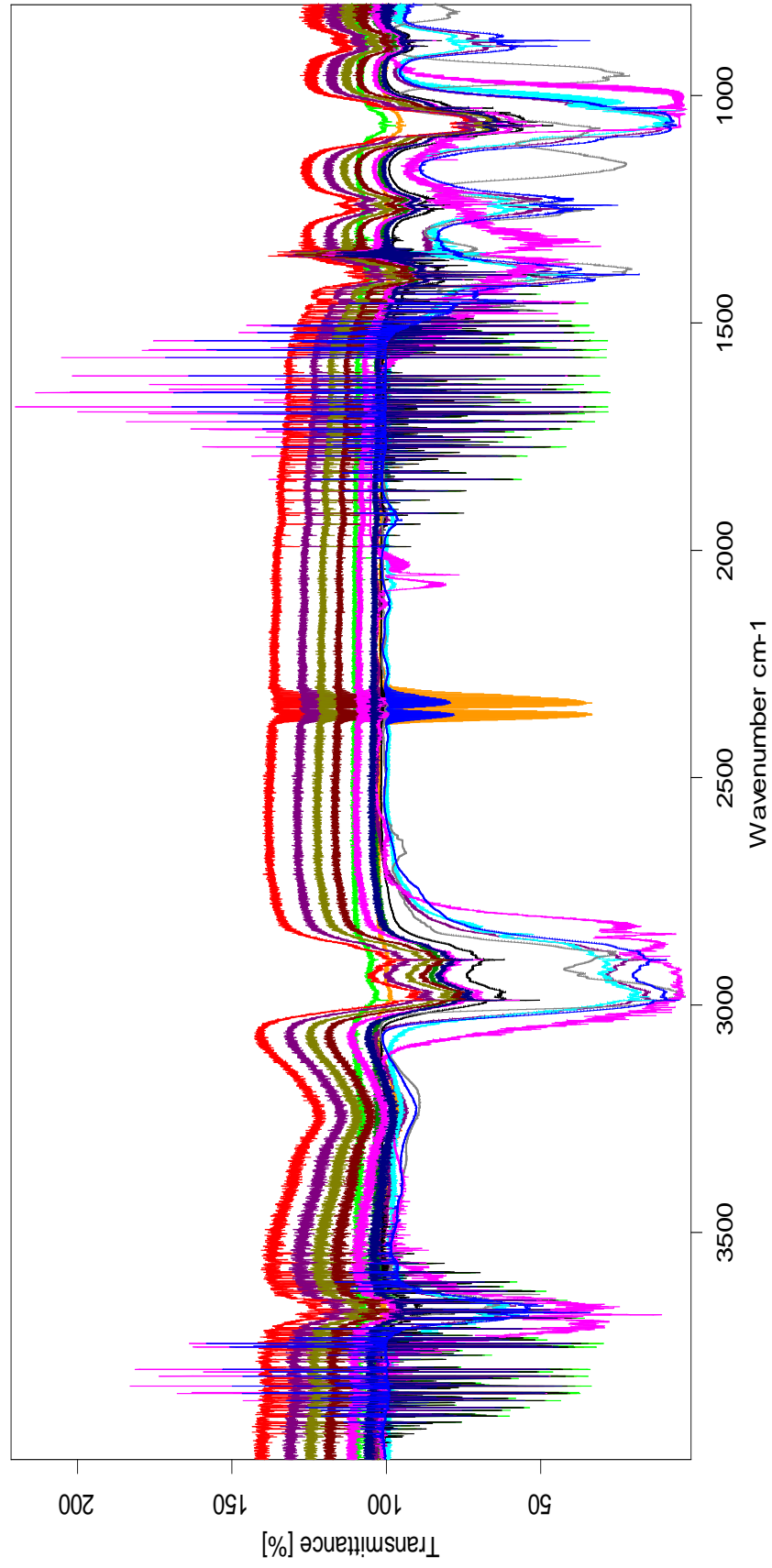


Figure 5.2 Average spectra for 100 μL ethanol (blue), methanol (pink), propanol (grey), Melocoton (navy blue), Gordon's gin (brown), Beefeater gin (khaki), Smirnoff (purple), Absolut vodka (red), Bacardi breezer (orange), Bacardi rum (pink), methylated spirit (purple), Jose Cuervo tequila (black), Listerine (dark green), Tesco mouthwash (bright green) at 27°C

5.4.2 Statistical analysis

Following normalisation, the data for the 22 regions of variation were separated out and total transmittance values calculated for each region. As with the acetone data these total transmittance values were plotted to give a profile of variables, which is shown in figure 5.3. The wavelengths of the 22 regions of variation and the RSD values across the average data (n=6) for the 16 alcohols are presented in table 5.3.

The data in table 5.3 confirmed what had been observed in the visual analysis, that there was some variation seen with the different alcohols. However, only seven of the 22 regions (32%) had alcohols with RSD values of 5% or above, which were restricted to four of the 16 alcohols; Colgate peroxy mouthwash, methanol, surgical spirit and methylated spirit. It is possible that these alcohols were more sensitive to the risk of loss of sample through evaporation before and during the analysis due to increased volatility. Table 5.3 also contains the average (n=22) RSD values for each alcohol and none of these values are above 5%.

The total transmittance values were used for multivariate analysis using HCA and SOFM.

5.4.2.1 Hierarchical cluster analysis

Figure 5.4 shows the dendrogram produced when comparing together the average spectra for all of the different alcohols tested across all 22 regions of interest. Methanol and propanol showed the lowest level of similarity to the other alcohols tested, which is understandable as the alcohol present in alcoholic drinks, and mouthwashes, is ethanol. Methylated spirit and surgical spirit group with ethanol, this is likely to be because the overall ethanol concentration is higher in these alcohols than the alcohol drinks and mouthwashes. However, it would have been expected that methylated spirit and surgical spirit might also show some similarities with methanol, but this is not readily apparent from the dendrogram.

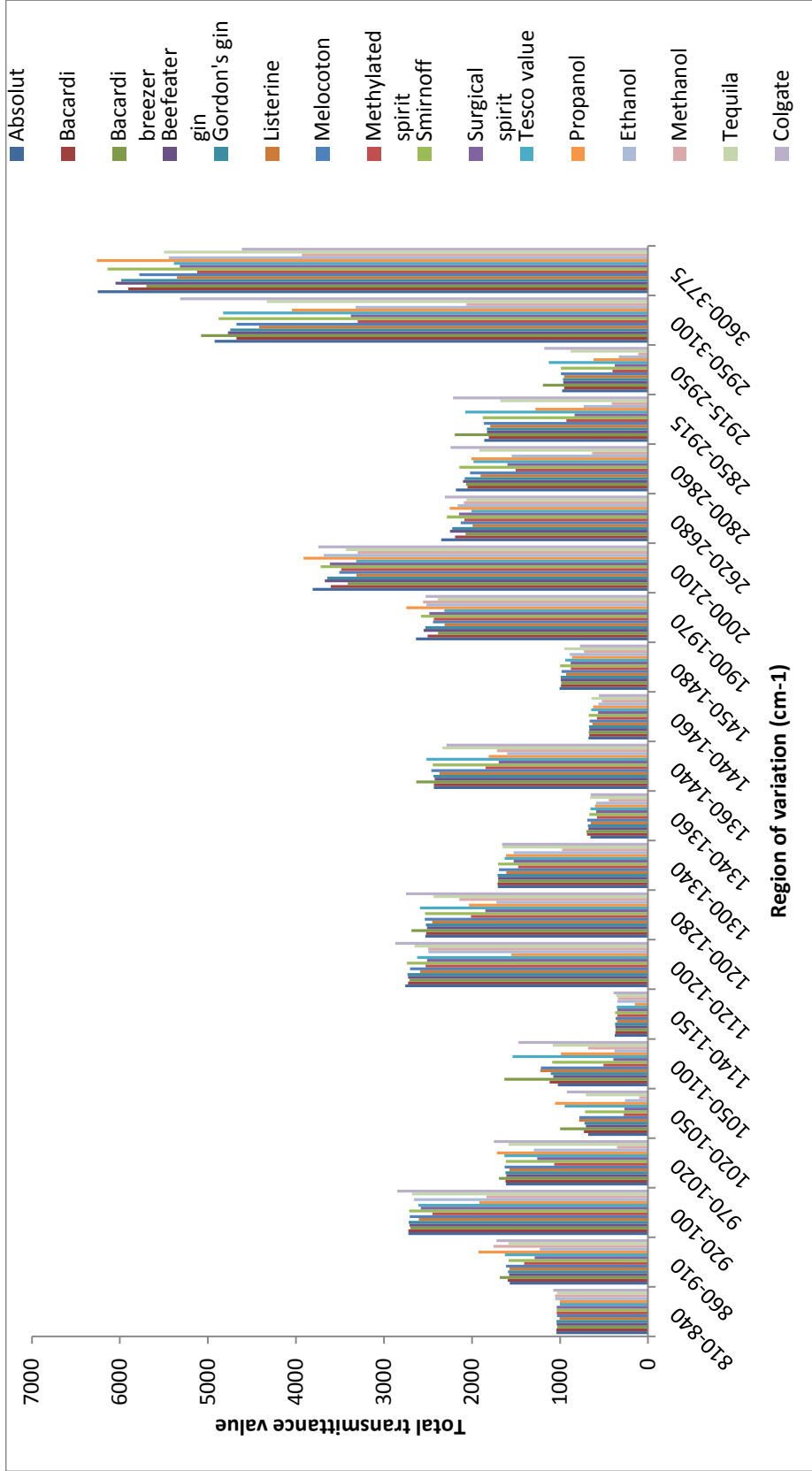


Figure 5.3 Profile of variables for the 22 regions of variation

Table 5.3 RSD values for the 16 alcohols analysed with RSD values (and their regions) above 5% shown in red

Region (cm ⁻¹)	Methanol	Ethanol	Propanol	Surgical spirit	Methylated spirit	Colgate mouthwash	Tesco mouthwash	Listerine mouthwash	Melocoton	Tequila	Bacardi breezer	Bacardi rum	Gordon's gin	Beefeater gin	Smirnoff vodka	Absolut vodka
810-840	0.18	0.19	0.27	0.44	0.87	0.83	1.07	1.12	1.12	0.22	0.91	0.43	0.79	0.71	1.43	0.84
860-910	0.18	0.39	0.50	2.76	2.24	0.91	1.10	1.12	1.19	0.28	0.92	0.47	0.68	0.94	1.72	0.85
920-100	0.99	0.24	1.25	0.70	1.16	0.84	1.06	1.11	1.02	0.23	0.84	0.45	0.75	0.75	1.47	0.83
970-1020	3.46	0.15	0.32	2.67	3.50	0.91	1.04	1.07	1.08	0.25	0.84	0.45	0.67	0.91	1.69	0.89
1020-1050	5.01	1.12	0.37	13.09	11.06	1.33	1.19	1.49	1.52	1.65	0.92	1.07	1.42	2.26	3.18	2.02
1050-1100	1.72	1.16	2.44	13.68	9.88	1.43	1.22	1.66	1.60	1.97	0.94	1.24	1.67	2.63	3.58	2.37
1140-1150	0.56	0.31	3.18	0.74	1.04	0.85	0.98	1.08	1.07	0.23	0.84	0.42	0.70	0.76	1.50	0.89
1120-1200	0.59	0.27	2.19	0.93	1.11	0.86	0.99	1.06	1.06	0.22	0.84	0.41	0.71	0.79	1.52	0.90
1200-1280	1.11	0.28	1.43	3.68	2.87	0.94	1.01	1.06	1.17	0.36	0.86	0.50	0.67	1.03	1.80	1.00
1300-1340	2.14	0.33	0.61	1.28	1.41	1.78	1.08	1.28	1.15	0.21	0.87	0.44	0.72	0.75	1.61	0.84
1340-1360	1.49	0.25	0.79	2.05	1.59	2.34	1.28	1.77	1.38	0.33	0.82	0.45	0.80	0.87	1.80	1.06
1360-1440	1.82	0.38	1.44	4.44	3.57	4.16	1.19	1.11	1.24	0.52	0.87	0.57	0.74	1.16	1.93	1.09
1440-1460	1.07	0.40	0.93	2.14	1.95	5.70	1.26	1.14	1.17	0.31	0.88	0.50	0.72	0.96	1.69	0.98
1450-1480	1.22	0.50	1.15	1.69	1.73	7.31	1.33	1.16	1.15	0.30	0.89	0.50	0.74	0.93	1.67	0.97
1900-1970	0.57	0.70	0.68	0.52	1.33	1.15	0.93	1.03	1.38	0.35	0.96	0.36	0.72	0.84	1.46	1.21
2000-2100	0.58	0.77	0.68	0.64	1.39	0.84	0.90	1.03	1.42	0.39	0.99	0.36	0.73	0.85	1.44	1.25
2620-2680	0.73	0.96	0.77	0.55	1.48	0.88	0.88	1.00	1.61	0.40	1.19	0.36	0.72	0.91	1.47	1.34
2800-2860	4.25	0.67	1.05	2.35	2.40	0.95	0.91	0.96	1.68	0.22	1.29	0.52	0.75	1.02	1.62	1.32
2850-2915	5.74	0.63	2.71	9.54	7.53	1.20	1.02	1.11	1.80	1.04	1.29	1.04	1.33	1.69	2.40	1.65
2915-2950	6.41	0.88	3.22	11.99	9.67	1.27	1.04	1.17	1.83	1.25	1.32	1.14	1.49	1.86	2.57	1.79
2950-3100	2.11	0.85	0.95	2.59	2.45	1.05	0.96	0.98	1.77	0.43	1.38	0.70	0.91	1.22	1.87	1.35
3600-3775	1.31	0.84	1.06	1.06	1.42	7.31	1.32	1.10	1.64	0.24	1.04	0.48	0.79	0.98	1.58	1.16
Average	1.97	0.56	1.27	3.62	3.26	2.04	1.08	1.16	1.37	0.52	0.99	0.58	0.87	1.13	1.86	1.21

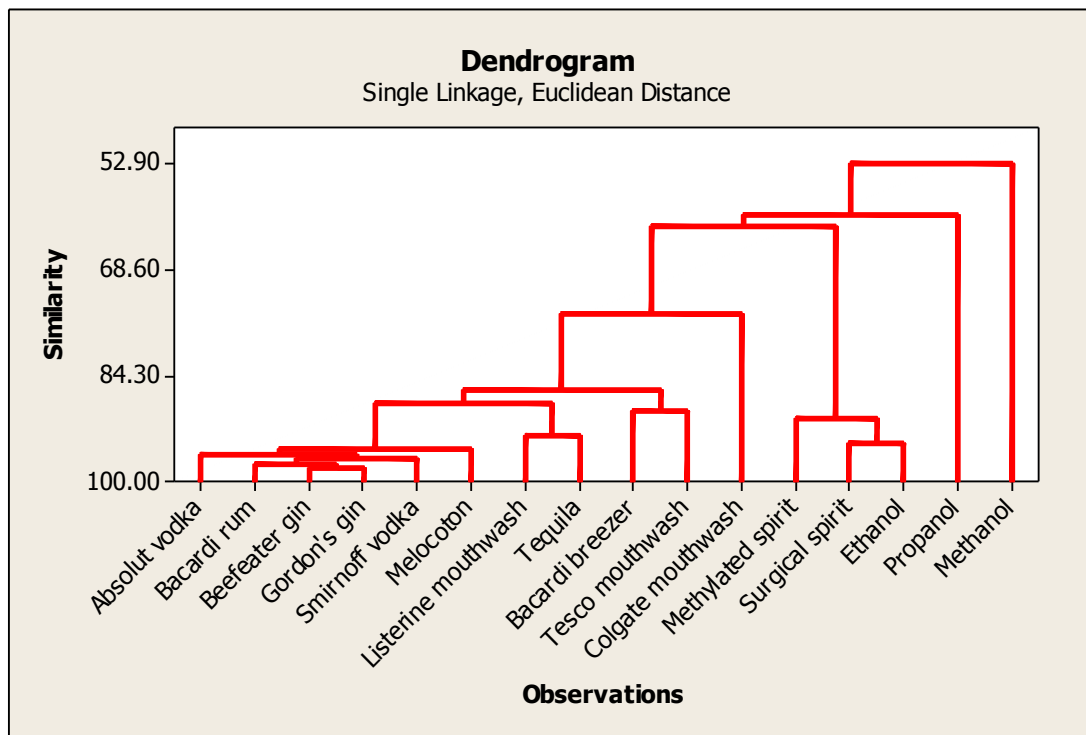


Figure 5.4 Dendrogram produced using the average total transmittance values for the alcohols analysed

Generally speaking, the pure alcohols (laboratory grade ethanol, methanol and propanol) and the samples containing mixtures of alcohol with few other components (surgical and methylated spirits) have clustered together. The other alcohol containing materials have similarly clustered together with various sub-clusters formed.

Further analysis was carried out, using the data from the individual repeats of various sub-groups, to determine whether concentration of alcohol or the composition of the matrix would have a greater effect on the discrimination observed.

Figure 5.5 shows a comparison of Bacardi rum (37.5% alcohol concentration), Gordon's gin (37.5% alcohol concentration), Smirnoff vodka (37.5% alcohol concentration) and Jose Cuervo tequila (38% alcohol concentration).

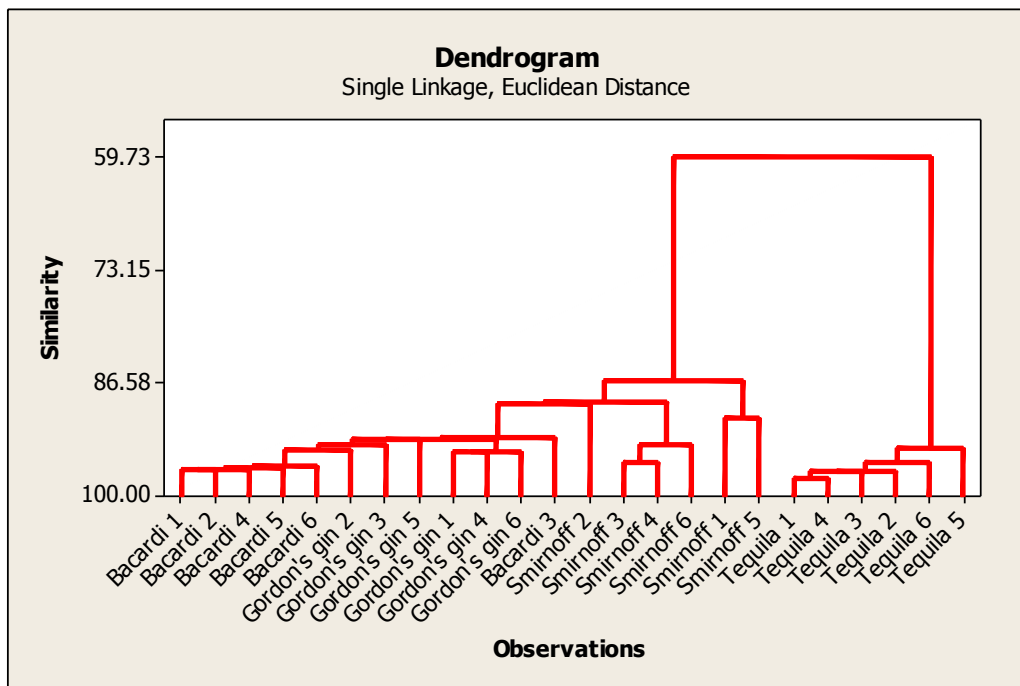


Figure 5.5 Comparison of drinkable spirits with an alcohol concentration of 37.5% or 38%

This seems to suggest that the gin, vodka and rum based drinks will cluster together, however a degree of separation between the three was apparent within the larger grouping. The tequila was clearly separated, however, it cannot be readily established whether this separation results from the slightly higher alcohol content, the different matrix composition or a combination of both.

Figure 5.6 shows a comparison of Beefeater gin (40% alcohol concentration) and Absolut vodka (40% alcohol concentration). In both cases, while there is a small degree of overlap, the six repeats of the different drinks generally cluster together separating the two samples correctly. This mirrors the results obtained between gin and vodka at 37.5% alcohol concentration (figure 5.5) and does suggest that a degree of discrimination between the type of alcoholic drink (vodka, gin etc.) may be possible.

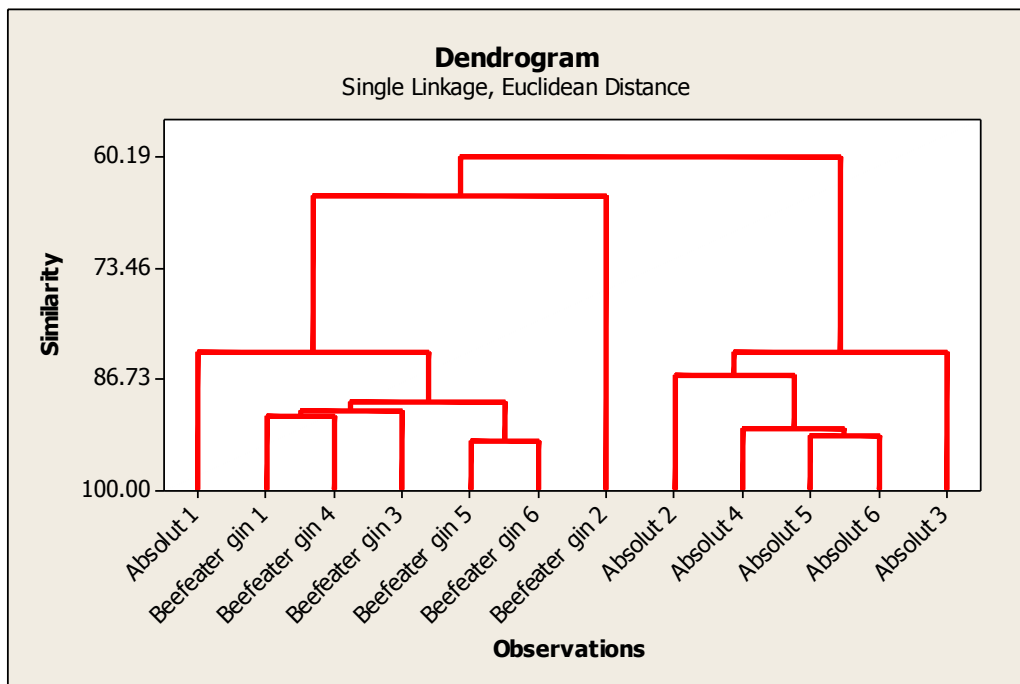


Figure 5.6 Comparison of drinkable spirits with an alcohol concentration of 40%

When comparing the samples from the same drink type (vodka or gin) differentiation is much less successful irrespective of differences in alcohol concentration. This suggests that it is the matrix of the solutions rather than the alcohol percentage that plays a critical factor in discrimination. This is confirmed when comparing Beefeater gin (40% alcohol concentration) and Gordon’s gin (37.5% alcohol concentration), shown in figure 5.7 and Absolut vodka (40% alcohol concentration) and Smirnoff vodka (37.5% alcohol concentration), shown in figure 5.8.

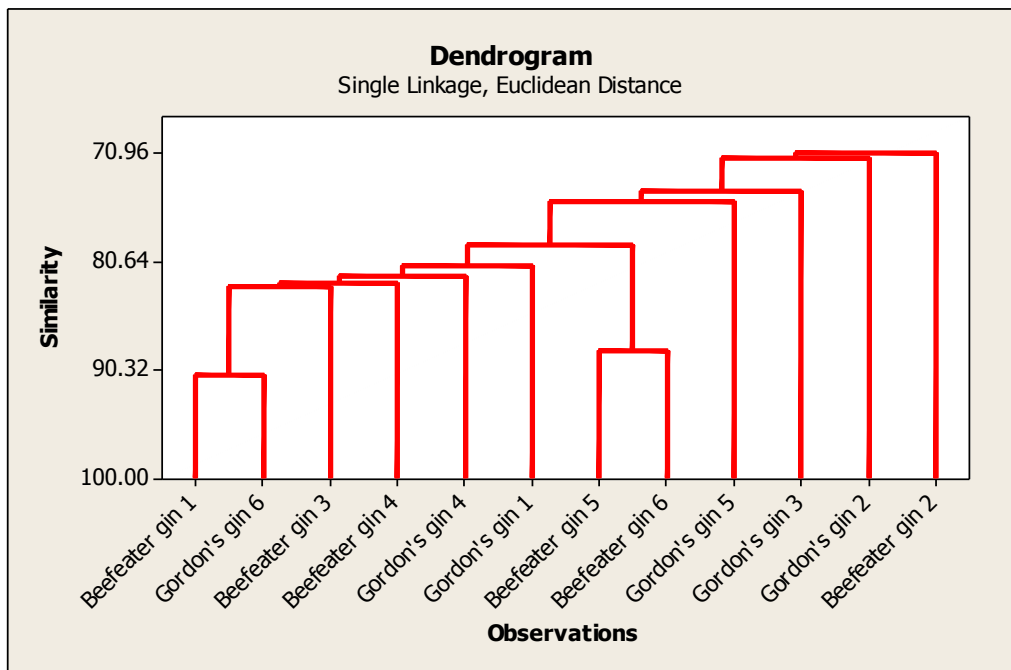


Figure 5.7 Comparison of Beefeater gin (40% alcohol) and Gordon's gin (37.55 alcohol) showing the individual repeats

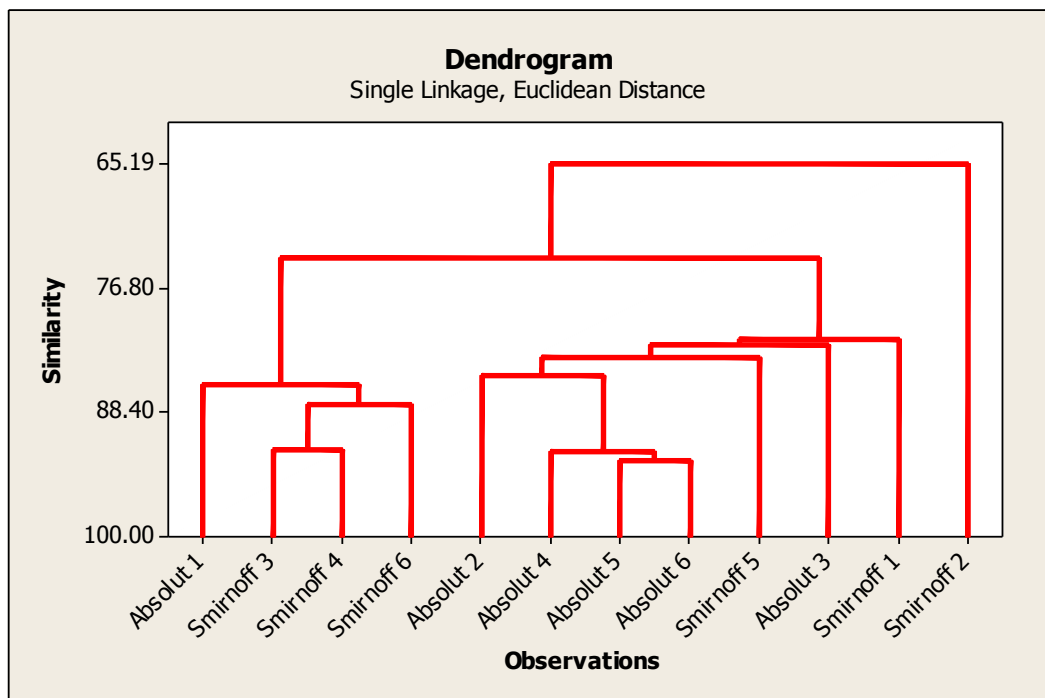


Figure 5.8 Comparison of Smirnoff vodka (37.5% alcohol) and Absolut vodka (40% alcohol) showing the individual repeats

However, it does appear that when a much larger difference in alcohol content is in evidence this does have an influence on the clustering which occurs. This is apparent through the HCA analysis of Bacardi rum (37.5% alcohol concentration)

and Bacardi breezer (4% alcohol concentration) where, despite both containing the same type of alcohol (rum), the six repeats for each drink cluster by sample type with a similarity between the two clusters of only 19.73% (figure 5.9).

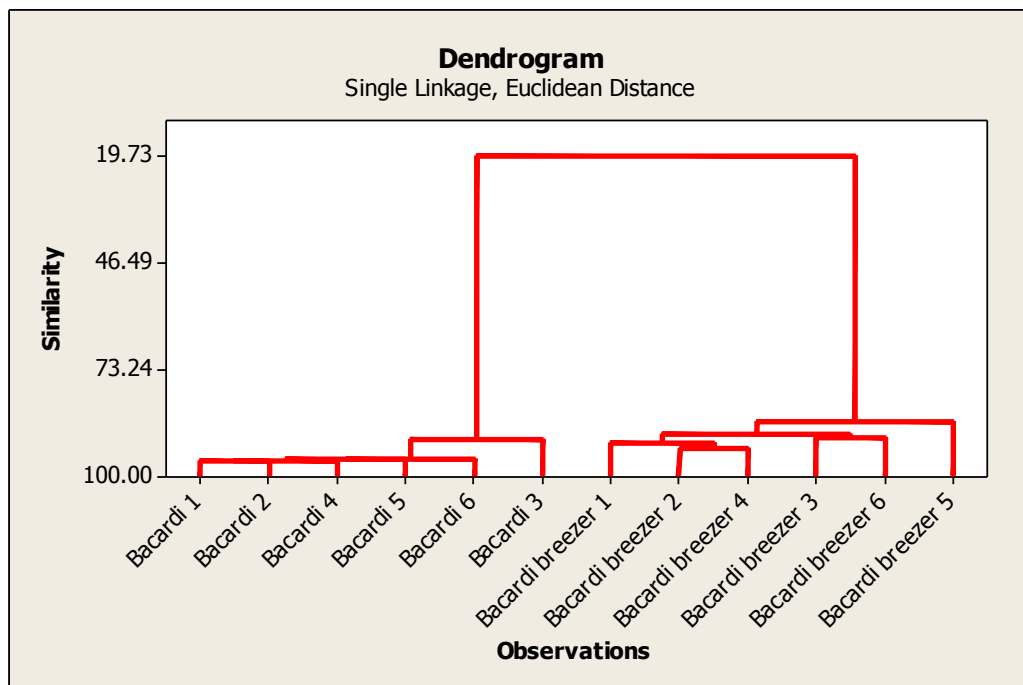


Figure 5.9 Comparison of Bacardi rum and Bacardi breezer showing the individual repeats

A comparison of the three mouthwashes further demonstrates the discrimination possible for materials of similar alcohol concentration but different compositions. All of the mouthwashes are likely to have low alcohol concentrations, however as figure 5.10 demonstrates, the individual repeats for each mouthwash cluster separately and therefore discrimination is possible.

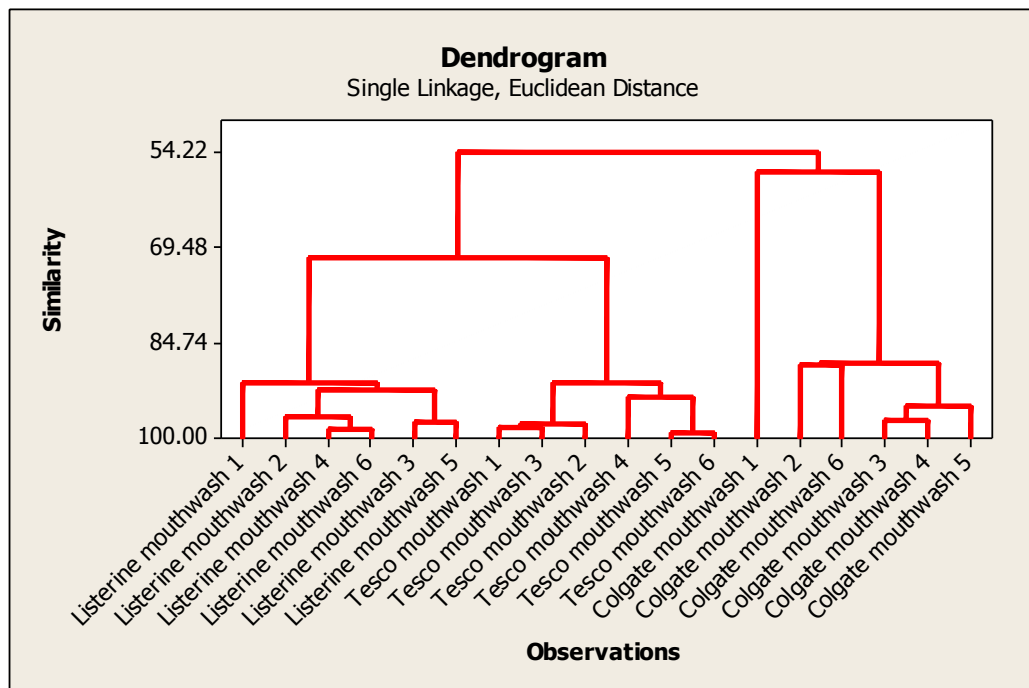


Figure 5.10 Comparison of Listerine, Tesco and Colgate mouthwashes

5.4.2.2 Self organising feature maps

The same data was analysed using SOFM. The cluster map for the individual repeats for each alcohol is shown in figure 5.11 with the clustering set to 16.

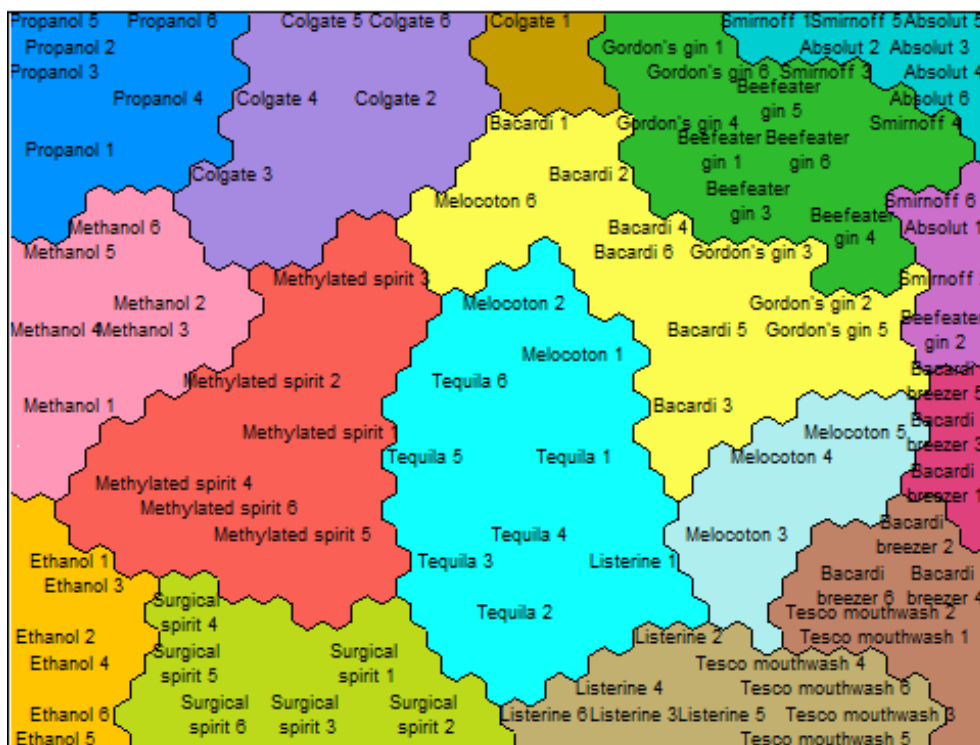


Figure 5.11 Cluster map for the six individual repeats for each of the 16 alcohols analysed

The cluster map allows for the examination of the data in a way that wasn't possible with HCA as the dendrogram of the individual repeats was too crowded to view. The SOFM of the individual repeats allows for the examination of the clustering of the individual repeats.

The cluster map reveals that propanol, methanol, ethanol, methylated spirit, and surgical spirit form separate clusters. These are the alcohols with the fewest additives and highest alcohol concentrations. It is also notable that the clusters of each of these alcohols are found next to each other. In this case the methylated spirit sits beside both methanol and ethanol reflecting its composition in a way not observed with the HCA analysis.

Five of the Colgate mouthwash repeats have also formed a cluster, with the remaining repeat (Colgate 1) forming a cluster of its own. While the alcohol concentration of the Colgate mouthwash is similar to that of the Listerine and Tesco mouthwashes it is not surprising that it has clustered separately as it also contains hydrogen peroxide which will produce absorption features that will not appear in any of the other alcohols analysed in this data set.

The Tesco and Listerine mouthwashes formed a cluster together, although one Listerine repeat (Listerine 1) has clustered with tequila and melocoton and two Tesco repeats (Tesco mouthwash 1 and Tesco mouthwash 2) have clustered with three Bacardi breezer repeats (Bacardi breezer 1, 3 and 5). The remaining three Bacardi breezer repeats form a single cluster. The six tequila repeats have clustered together, but the cluster also includes two melocoton repeats (Melocoton 1 and 2) and a Listerine repeat (Listerine 1). Three of the other melocoton repeats (Melocoton 3, 4 and 5) have formed a cluster, with the remaining repeat (Melocoton 6) forming a large cluster with Barcardi and Gordon's gin. The remaining spirits have formed several mixed clusters.

When the data from the average (n=6) spectra are used, successful clustering of the samples was achieved and figure 5.12 illustrates this. In this map, unlike with the individual repeats, it is surgical spirit rather than methylated spirit that sits between

ethanol and methanol. This reflects the composition of surgical spirit, but also suggests that methylated spirit and surgical spirit have a degree of interchangeability. This corresponds to the fact that both are primarily composed of ethanol and methanol. The cluster map demonstrates a trend across the map, from left to right, from low to high alcohol concentration with the mouthwashes and Bacardi breezer found to the left and the laboratory grade alcohols found towards the right. This gives a different perspective compared to that obtained from the HCA where the matrix composition was the main discriminator apart from in cases where there was a significant difference in the alcohol concentration.

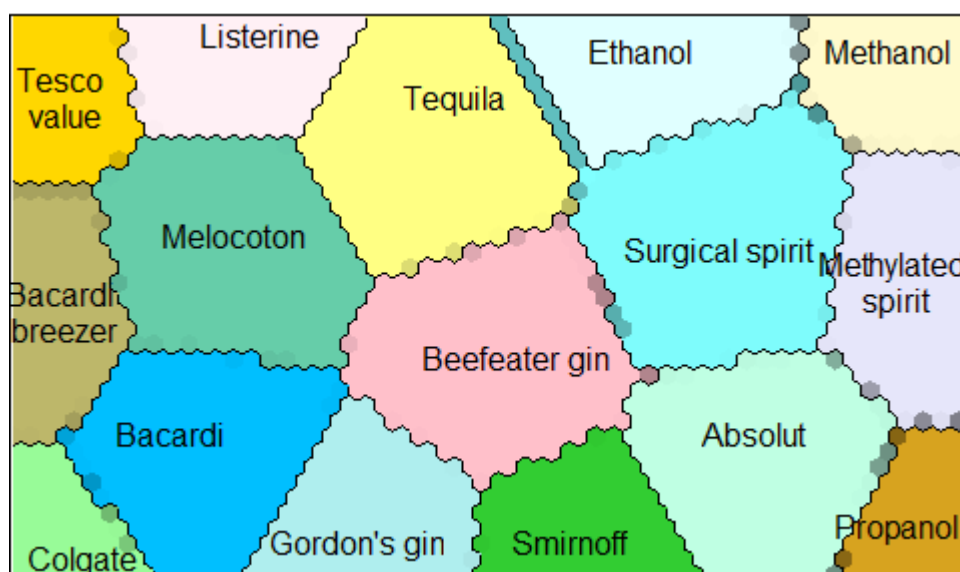


Figure 5.12 Cluster map for the average values of the alcohols analysed

As with acetone it was possible to view the component maps for the average values. These are shown in figures 5.13-5.14.

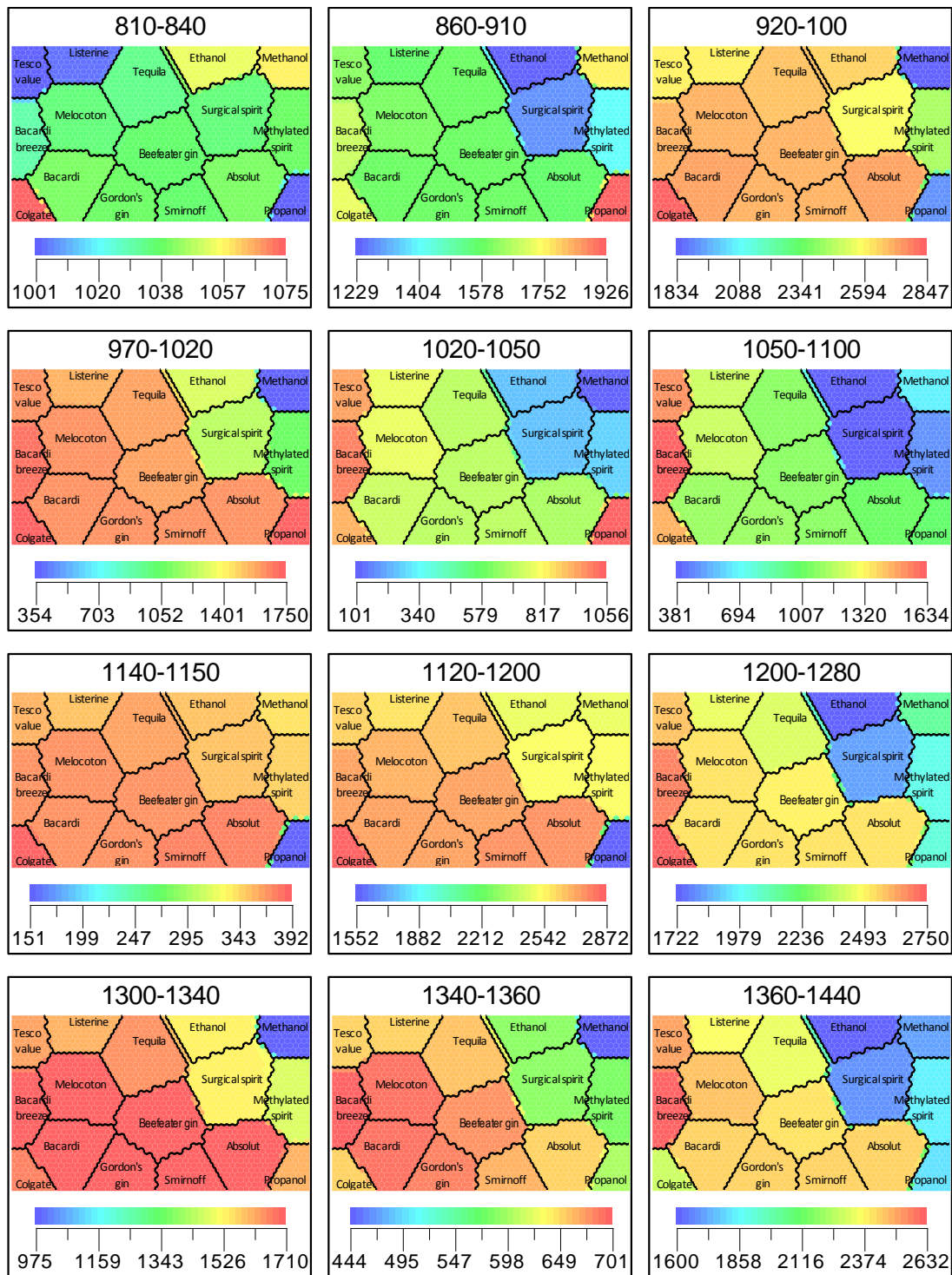


Figure 5.13 Component maps for regions 810-1440 cm⁻¹

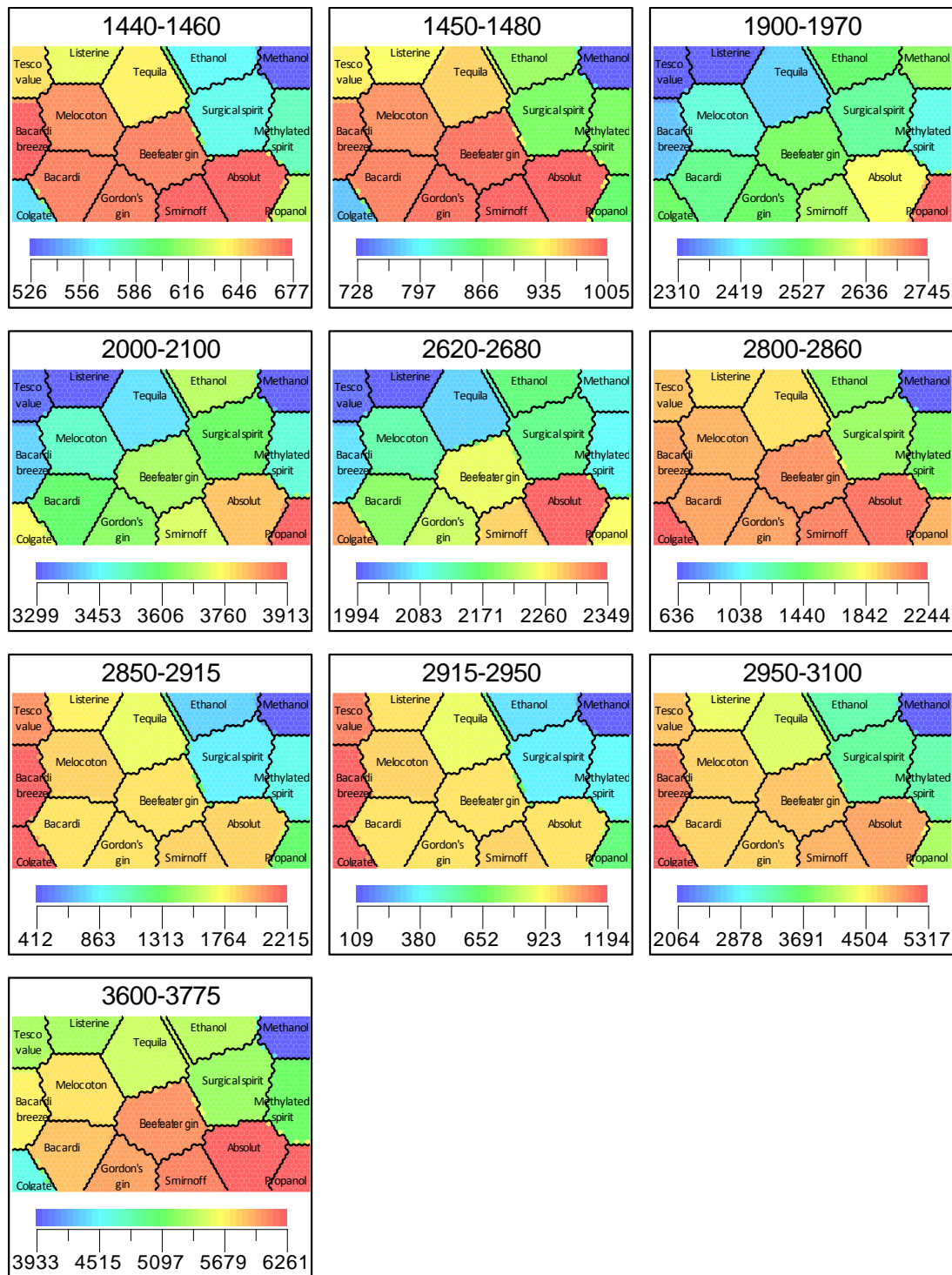


Figure 5.14 Component maps for regions 1440-3775 cm^{-1}

The component maps show how, with this larger dataset (compared to acetone), there are no instances where one region is a strong discriminator for a single alcohol (one red cluster with the rest shaded blue). However, each region shows

clusters with a range of shading, therefore demonstrating that the regions can discriminate between multiple alcohols, but that several regions would be required for strong discrimination.

The component maps correspond to the clustering seen with the individual repeats, in that for many of the regions the drinkable spirits have a similarity between them, as did the Tesco mouthwash and Listerine, while methanol and propanol in particular stand out as being dissimilar to the other alcohols.

The component maps also help to highlight the left to right, low to high concentration trend seen in the cluster map. Figure 5.15 shows the overlaid spectra for the region 2915-2950 cm^{-1} , this shows all the transmittance data that was then used for the data analysis. Figure 5.16 shows the profile of variables and figure 5.17 shows the corresponding component map. This region is an example of the trend, with the lower concentrations shaded red, the middle section with the slightly higher concentrations shaded orange and the highest concentrations appearing green and blue. It also corresponds to the findings of the dendrogram with methanol and propanol appearing the least similar in terms of colour to any of the other alcohols. It is thought that the absorption observed in this region was predominantly due to C-H stretching. However, as the full chemical composition of the alcohols analysed is not known it is not possible to conclusively identify the causes of the absorption.

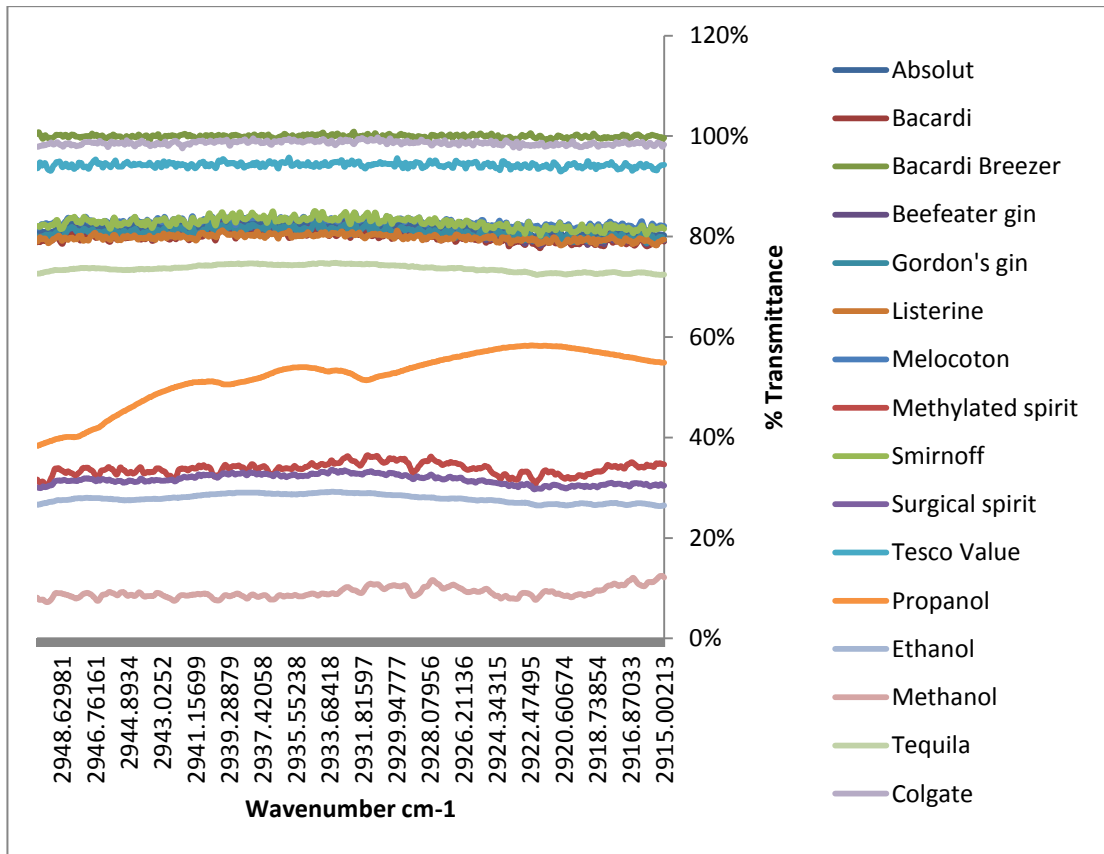


Figure 5.15 Overlaid spectra of the alcohols analysed in the region 2915-2950 cm^{-1} (plotted in Microsoft Excel)

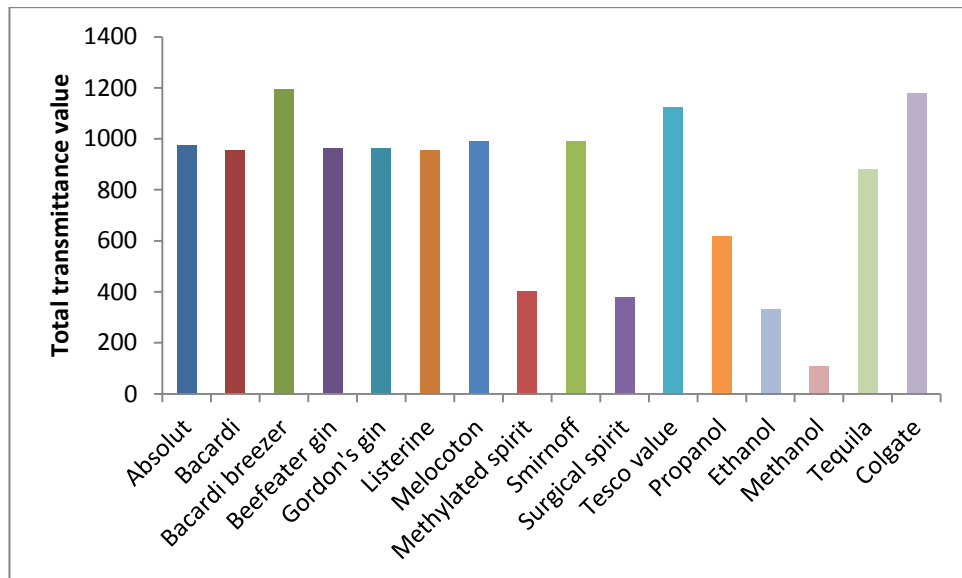


Figure 5.16 Profile of variables for the region 2915-2950 cm^{-1}

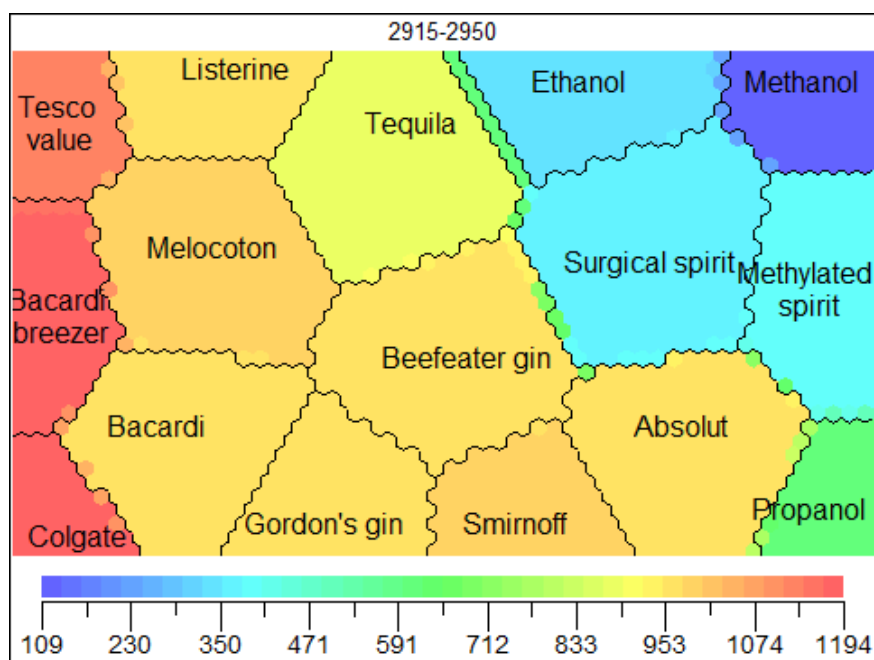


Figure 5.17 Component map for the region 2915-2950 cm^{-1}

The component maps also demonstrate the separation of the laboratory grade alcohols and those with more additives. Figure 5.18 shows the overlaid spectra for the region 1340-1360 cm^{-1} , figure 5.19 shows the profile of variables and figure 5.20 the corresponding component map. This region shows the majority of the alcohols shaded red and orange, with the exception of methanol, ethanol, propanol and methylated and surgical spirits, which can be considered virtually laboratory grade when compared to alcoholic drinks and mouthwashes. Once again methanol and propanol, in particular methanol, appear least similar to the other alcohols, further confirming the results of the HCA. The absorption in this area may be due to C-O-H in plane bending.

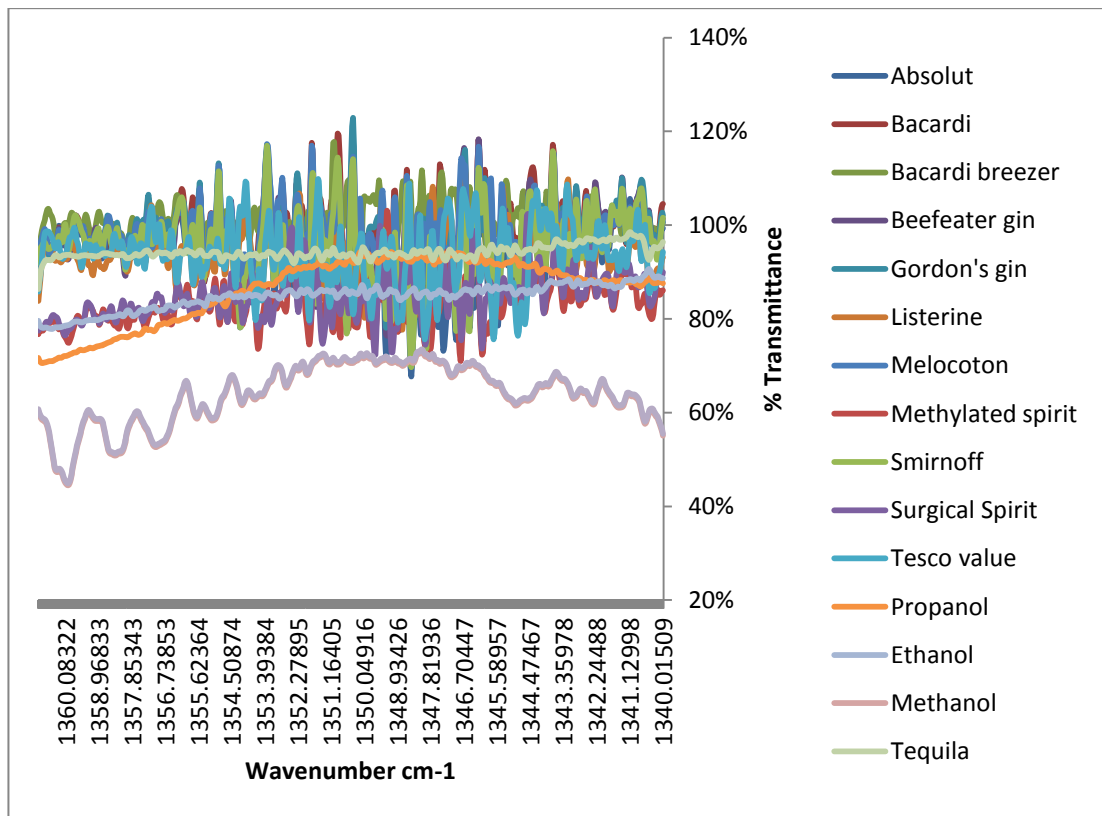


Figure 5.18 Overlaid spectra of the alcohols analysed in the region 1340-1360 cm^{-1} (plotted in Microsoft Excel)

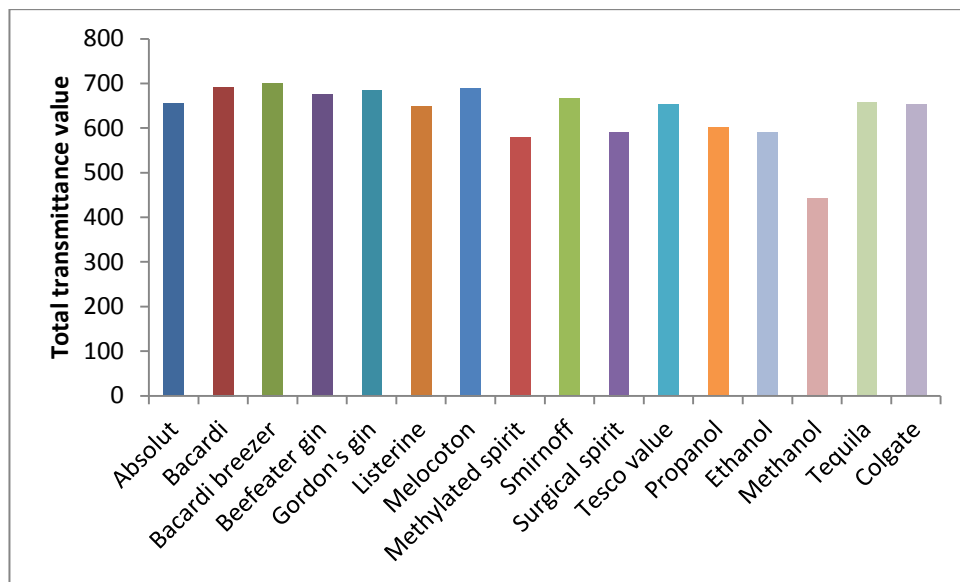


Figure 5.19 Profile of variables for the region 1340-1360 cm^{-1}

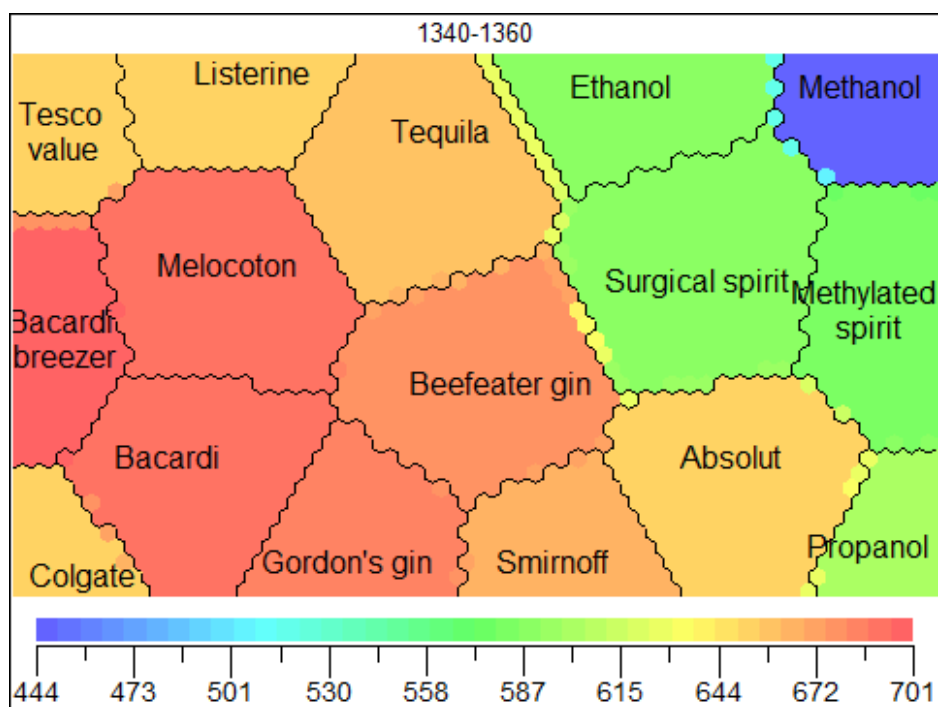


Figure 5.20 Component map for the region 1340-1360 cm^{-1}

5.5 Conclusions

The results demonstrate that high resolution Fourier Transform spectroscopy coupled with multivariate analysis is a suitable tool for the discrimination of different alcoholic materials. While the concentration of the alcohol will aid discrimination when there is a significant difference, the type of alcohol present will have a greater effect on discrimination by type but not necessarily by brand. This applies not only to different alcohols in the sense of ethanol, methanol or propanol but also in terms of different ethanol based spirits.

The results support the findings of the analysis of acetone and acetone based nail polish removers that this technique is suitable for discriminating a range of potential explosive precursors. Significantly the range of different samples used in this experiment was much larger than for the acetone experiment yet the ability to discriminate was still observed. This strengthens the observation that this technique is suitable for discriminating between brands, and potentially to tie precursors to final products.

The ability to discriminate between different alcoholic materials has implications for the detection of potential bomb makers, but also could have applications in several other areas. The most obvious would be in the detection of counterfeit, or tainted alcoholic spirits.

5.6 References

1. Wigmore, J.G. and Langille, R.M., *Six Generations of Breath Alcohol Testing Instruments: Changes in the Detection of Breath Alcohol Since 1930. An Historical Overview*. Canadian Society of Forensic Science Journal, 2009. **42**(4): p. 276-283.
2. Pontes, M.J.C., Santos, S.R.B., Araujo, M.C.U., Almeida, L.F., Lima, R.A.C., Gaiao, E.N. and Souto, U.T.C.P., *Classification of distilled alcoholic beverages and verification of adulteration by near infrared spectrometry*. Food Research International, 2006. **39**(2): p. 182-189.
3. Wang, M., Choong, Y., Su, N. and Lee, M., *A Rapid Method for Determination of Ethanol in Alcoholic Beverages Using Capillary Gas Chromatography*. Journal of Food and Drug Analysis, 2003. **11**(2): p. 133-140
4. Nieuwoudt, H.H., Prior, B.A., Pretorius, I.S., Manley, M. and Bauer, F.F., *Principal component analysis applied to Fourier transform infrared spectroscopy for the design of calibration sets for glycerol prediction models in wine and for the detection and classification of outlier samples*. Journal of Agricultural and Food Chemistry, 2004. **52**(12): p. 3726-3735.
5. Palma, M. and Barroso, C.G., *Application of FT-IR spectroscopy to the characterisation and classification of wines, brandies and other distilled drinks*. Talanta, 2002. **58**(2): p. 265-271.
6. Patz, C.D., Blieke, A., Ristow, R. and Dietrich, H., *Application of FT-MIR spectrometry in wine analysis*. Analytica Chimica Acta, 2004. **513**(1): p. 81-89.
7. Saiz-Abajo, M.J., Gonzalez-Saiz, J.M. and Pizarro, C., *Classification of wine and alcohol vinegar samples based on near-infrared spectroscopy. Feasibility study on the detection of adulterated vinegar samples*. Journal of Agricultural and Food Chemistry, 2004. **52**(25): p. 7711-7719.
8. Arzberger, U. and Lachenmeier, D.W., *Fourier Transform Infrared Spectroscopy with Multivariate Analysis as a Novel Method for Characterizing Alcoholic Strength, Density, and Total Dry Extract in Spirits and Liqueurs*. Food Analytical Methods, 2008. **1**(1): p. 18-22.
9. Lachenmeier, D.W., *Rapid quality control of spirit drinks and beer using multivariate data analysis of Fourier transform infrared spectra*. Food Chemistry, 2007. **101**(2): p. 825-832.
10. [cited 2014 23/06/14]; Available from: <http://www.foss.co.uk/industry-solution/products/winescan-so2>.
11. Nishiyama, T., Tsukamoto, I., Shirakawa, Y., Komatsu, H., Maekawa, N., Kinoshita, H., Ameno, K. and Ijiri, I., *Fourier transform infrared (FTIR) analysis*

- of volatile compounds in expired gas for the monitoring of poisonings 1. Ethanol. Pharmaceutical Research, 2001. 18(1): p. 125-128.*
12. Młyńczak, J., Kubicki, J. and Kopczyński, K., *Stand-off detection of alcohol in car cabins. Journal of Applied Remote Sensing, 2014. 8(1): p. 083627-083627.*
 13. Kubicki, J., Mlynczak, J. and Kopczynski, K., *Application of modified difference absorption method to stand-off detection of alcohol in simulated car cabins. Journal of Applied Remote Sensing, 2013. 7.*

Chapter 6. Brand Discrimination - Hydrogen Peroxide

6.1 Introduction

The role of hydrogen peroxide as an explosive precursor came to prominence following the terrorist attacks on the 7th July 2005 on the London transport system. The terrorists had used hexamethylene triperoxide diamine (HMTD) as an explosive in the attacks[1]. Triacetone triperoxide or TATP has also been used in terrorist attacks[2]. In addition to the explosive materials that it can produce, hydrogen peroxide in a sufficiently concentrated form is explosive in its own right[3] which makes it an important target for explosive detection.

As with the other precursors for 'homemade' explosive materials, hydrogen peroxide is readily available for legitimate purposes. However, efforts are made to prevent the use of hydrogen peroxide as an explosive precursor by limiting the availability of hydrogen peroxide in high concentrations. Despite this, it is possible to purchase large quantities of lower concentration peroxide, without having to declare the purpose of the purchase. In addition to this, as with the majority of the other 'homemade' explosives, it is possible to find detailed 'recipes' for peroxide based explosives online[4, 5]. This makes it relatively easy for individuals wishing to make peroxide based explosives to do so.

Legitimate uses for hydrogen peroxide include hair lightening and bleaching, peroxide mouthwash, cleaning wounds and even as a food supplement[6]. These legitimate uses result in additives being present in the hydrogen peroxide solution, and the concentration of the hydrogen peroxide varying depending upon the use. It is possible that the inclusion of such additives may be exploited to provide the opportunity for brand specificity of hydrogen peroxide samples using spectroscopic analysis. Identifying an unknown source as a particular brand could aid the intelligence gathering against a suspected bomb maker.

As the majority of the hydrogen peroxide available is in relatively low concentrations, solutions are often concentrated prior to their use in the production of, for example, TATP and HMTD or in attempts to reach a concentration where the hydrogen peroxide itself was explosive. As a consequence the detection of attempts to concentrate hydrogen peroxide is of a critical interest. Furthermore, having an ability to detect modified hydrogen peroxide solutions and potentially link these back to a particular brand of unmodified commercial products could have significant strategic and intelligence value. A key example of this is the investigation into the failed bombings on 21st July 2005, where the argument for the defence was that the hydrogen peroxide had not been concentrated enough to make a viable explosive mixture, and that this was intentional[7]. The results of the research in this chapter could have been used in such a context to determine whether hydrogen peroxide had been concentrated and provide an qualitative assessment of the level of the concentration.

The analysis and detection of hydrogen peroxide has been the subject of substantial research. The presence of hydrogen peroxide is significant in many biological areas[8], as well as its use in more commercial settings as a sterilising agent[9, 10], this has resulted in the development of sensors aimed at detection of hydrogen peroxide in these settings primarily using three techniques, electrochemical detection[8, 9, 11-18], chemiluminescent detection[19-22] and spectrophotometric detection[23, 24]. High performance liquid chromatography has also been used[25] but this is less commonplace as a major feature required by many of the sensors is portability.

Some research into the analysis of hydrogen peroxide using infrared spectroscopy has been carried out[26, 27], including some work into vapour phase analysis[10], however the resolution of the equipment used has been relatively low and the hydrogen peroxide analysed in the vapour phase was laboratory grade. The use of QCLs for the detection of hydrogen peroxide has been researched, with two

wavelength regions (1274 and 1285 cm^{-1}) identified as being suitable for detection[28].

The premise of this experiment was to utilise high resolution FTIR to determine whether discrimination between different brands of hydrogen peroxide based materials was possible when analysing samples in the vapour phase, and furthermore whether it was possible to identify if a sample had been adulterated through concentration.

6.2 Materials

Five hydrogen peroxide containing materials were selected for the initial analysis along with laboratory grade hydrogen peroxide. The concentrations and source of purchase for each of the materials is given in table 6.1. Further information on the additives for each of the materials can be found in appendix 3.

Table 6.1 Peroxide concentration and source information for the hydrogen peroxide containing materials

Name	Hydrogen peroxide concentration (v/v)	Source
Laboratory grade Hydrogen peroxide	50	Sigma Aldrich UK
Jerome Russell Cream Peroxide	9	Boots
Health Leads Food Grade Peroxide	35	Health Leads UK
Colgate Peroxyl Mouthwash	1.5	Boots
Sunin Lightening Spray	6	Boots
Botanics	Not stated	Boots

The samples were contained within the sample cell in aluminium dishes purchased from Sigma Aldrich UK.

Two of the brands, Health Leads food grade peroxide (from this point referred to as Health Leads) and Sunin lightening spray (from this point referred to as Sunin), were selected for concentration and further analysis.

6.3 Experimental protocol

6.3.1 Visual and statistical analysis of un-concentrated samples

The analysis of hydrogen peroxide as a compound of interest had demonstrated that the temperature for each analysis should be set at 75°C. Six 100 µL samples of each brand and the laboratory grade material were analysed at this temperature. The six repeats were used to create an average spectrum for a visual comparison with the six average spectra overlaid.

Following the visual comparison of the average spectra, regions of variation were identified. The data from these regions was separated out from the rest of each spectrum for both the average spectra and the individual repeats. The transmittance values for each region were then 'binned' to produce a total transmittance value for each analysis or average spectrum for each sample. The total transmittance values were plotted to produce a profile of variables and input into Minitab (version 16) and Viscovery SOMine (4.0.2) for statistical analysis.

6.3.2 Concentrated samples

6.3.2.1 Concentration of samples

The concentration of the two brands (Health Leads and Sunin) followed the stepwise process detailed in table 6.2. The temperature was closely monitored to ensure that the liquid did not boil at any point, and heating took place in a combustion-modified fumehood.

Table 6.2 Protocol for the concentration of hydrogen peroxide containing materials

Step	Action
1	From start volume of 900 mL 100mL removed for titration and 6 mL for FTS analysis (T=0)
2	Remaining peroxide heated for one hour at 50-60°C
3	100 mL removed for titration and 6 mL for FTS analysis (T=1)
4	Remaining peroxide heated for one hour (two hours total) at 50-60°C
5	100 mL removed for titration and 6 mL for FTS analysis (T=2)
6	Remaining peroxide heated for one hour (three hours total) at 50-60°C
7	100 mL removed for titration and 6 mL for FTS analysis (T=3)
8	Remaining peroxide heated for one hour (four hours total) at 50-60°C
9	100 mL removed for titration and 6 mL for FTS analysis (T=4)
10	Remaining peroxide heated for one hour (five hours total) at 50-60°C
11	100 mL removed for titration and 6 mL for FTS analysis (T=5)

The samples were kept refrigerated until the time of analysis to reduce any decomposition of the hydrogen peroxide.

6.3.2.2 Titration of samples

The samples were titrated to determine the concentration of hydrogen peroxide at each temperature interval. The titration used was adapted from Vogel's Textbook of Quantitative Chemical Analysis[29] and followed the stepwise process shown in table 6.3 for the Sunin samples and table 6.4 for the Health Leads samples, due to the higher concentration requiring an alteration to the method to reduce the volume of potassium permanganate needed for the analysis.

Table 6.3 Titration protocol for the Sunin samples

Step	Action
1	10 mL of sample made up to 500 mL with distilled water and mixed thoroughly
2	25 mL of solution pipetted to a conical flask and mixed with 200 mL distilled water
3	20 mL dilute sulfuric acid (1:5) added to the flask and mixed thoroughly
4	Solution titrated with 0.02M potassium permanganate to the first permanent faint pink colour
5	Repeated until two concordant results obtained

Table 6.4 Titration protocol for the Health Leads samples

Step	Action
1	5 mL of sample made up to 500 mL with distilled water and mixed thoroughly
2	10 mL of solution pipetted to a conical flask and mixed with 200 mL distilled water
3	20 mL dilute sulfuric acid (1:5) added to the flask and mixed thoroughly
4	Solution titrated with 0.02M potassium permanganate to the first permanent faint pink colour
5	Repeated until two concordant results obtained

The results of the titration were used to calculate the percentage hydrogen peroxide concentration of the two brands at each temperature interval. Full details of the calculation can be found in appendix 4.

6.3.2.3 FTS and statistical analysis

The concentrated samples were analysed following the same method as the un-concentrated samples, with 100 μ L analysed at 75°C repeated six times to produce an average. The data was also handled in the same manner with the transmittance data extracted for the regions of variation identified with the un-concentrated samples and the total transmittance values calculated from this data. The total transmittance values were then analysed using hierarchical cluster analysis and SOFM to determine the levels of similarity between the data sets.

6.4 Results and discussion

6.4.1 Un-concentrated hydrogen peroxide samples

6.4.1.1 Visual analysis

Figure 6.1 shows the spectra for the individual repeats of laboratory grade hydrogen peroxide, and table 6.5 shows the breakdown of the data for these six repeats including the mean, standard deviations and RSD values for the regions of interest identified when comparing the six hydrogen peroxide based samples.

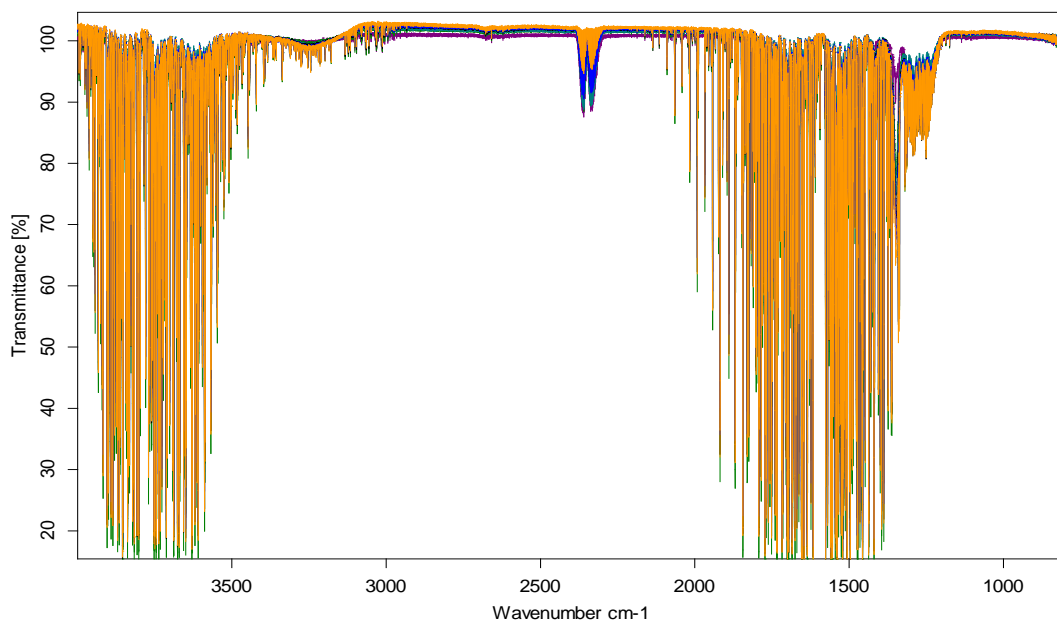


Figure 6.1 Six overlaid spectra of the six repeat analyses of hydrogen peroxide

The RSD values demonstrate that, while there is some variation between the different repeats, it is minimal with none of the RSD values above 5%. This indicates that the results are reproducible.

Table 6.5 Breakdown of the data from six repeats of laboratory grade hydrogen peroxide with total transmittance values, average, standard deviation and RSD

Region (cm ⁻¹)	H ₂ O ₂ 1	H ₂ O ₂ 2	H ₂ O ₂ 3	H ₂ O ₂ 4	H ₂ O ₂ 5	H ₂ O ₂ 6	Average	St dev	RSD
800-820	663.08	661.87	662.92	661.87	661.44	661.85	662.17	0.61	0.09
860-920	1999.44	2004.69	2003.61	2006.43	2005.72	2007.55	2004.57	2.61	0.13
930-1000	2336.83	2345.87	2344.67	2348.80	2348.69	2351.35	2346.04	4.65	0.20
1020-1100	2672.17	2686.35	2685.48	2690.54	2690.87	2694.05	2686.58	7.06	0.26
1106-1110	134.74	135.41	135.44	135.68	135.70	135.84	135.47	0.36	0.26
1220-1330	3419.10	3382.83	3439.98	3338.28	3371.78	3335.36	3381.22	38.57	1.14
1230-1255	771.79	764.37	778.81	753.21	762.75	753.77	764.12	9.15	1.20
1250-1265	464.23	459.64	468.34	453.24	458.85	453.57	459.64	5.40	1.18
1265-1275	309.95	306.67	312.74	302.74	306.35	302.89	306.89	3.59	1.17
1270-1290	457.83	451.92	461.93	444.36	450.69	444.50	451.87	6.44	1.43
1290-1320	927.29	915.39	932.99	902.99	912.14	901.36	915.36	11.64	1.27
1320-1325	162.84	161.06	161.74	159.62	159.59	158.61	160.58	1.44	0.90
1330-1370	1255.91	1154.44	1152.58	1120.93	1103.16	1081.06	1144.68	56.07	4.90
2655-2665	335.26	337.71	338.19	338.83	339.32	339.86	338.19	1.49	0.44
2665-2670	168.05	169.29	169.53	169.83	170.08	170.34	169.52	0.74	0.44
2675-2680	166.89	168.12	168.36	168.61	168.90	169.14	168.34	0.73	0.43
2850-3050	6701.03	6760.21	6770.79	6791.95	6800.15	6815.70	6773.30	37.12	0.55
3100-3450	11643.50	11651.09	11653.35	11647.41	11641.16	11637.77	11645.71	5.46	0.05
3710-3790	2366.28	2294.11	2425.11	2333.13	2363.57	2338.80	2353.50	39.90	1.70

The visual analysis revealed that there were some differences that could be seen between the average spectra for the six samples. Figure 6.2 shows the spectra overlaid, while figure 6.3 shows a close up of the region of absorption identified as containing two potential targets for hydrogen peroxide with QCLs (located at 1274 and 1285 cm⁻¹). In total 19 regions were identified as regions of variation and the wavelengths of these regions are presented in table 6.6.

Table 6.6 Regions of variation identified from visual examination of the average overlaid spectra of hydrogen peroxide containing materials

Region of variation		
800-820	1250-1265	2665-2670
860-920	1265-1275	2675-2680
930-1000	1275-1290	2850-3050
1020-1100	1290-1320	3100-3450
1106-1110	1320-1325	3710-3790
1220-1330	1330-1370	
1230-1255	2655-2665	

The Colgate peroxy mouthwash in particular showed several differences from the other spectra. This is due to the alcohol content of the mouthwash, with absorption bands present that were also present in the spectra of alcohols.

In general, across the brands, the visual comparison of the region of absorption containing the detection targets suggested that the concentration of the hydrogen peroxide had a substantial effect on the absorption bands, with some bands not visible for brands with very low concentrations. This could be a significant factor for the detection of hydrogen peroxide either as a precursor, explosive material or breakdown product of a peroxide based explosive.

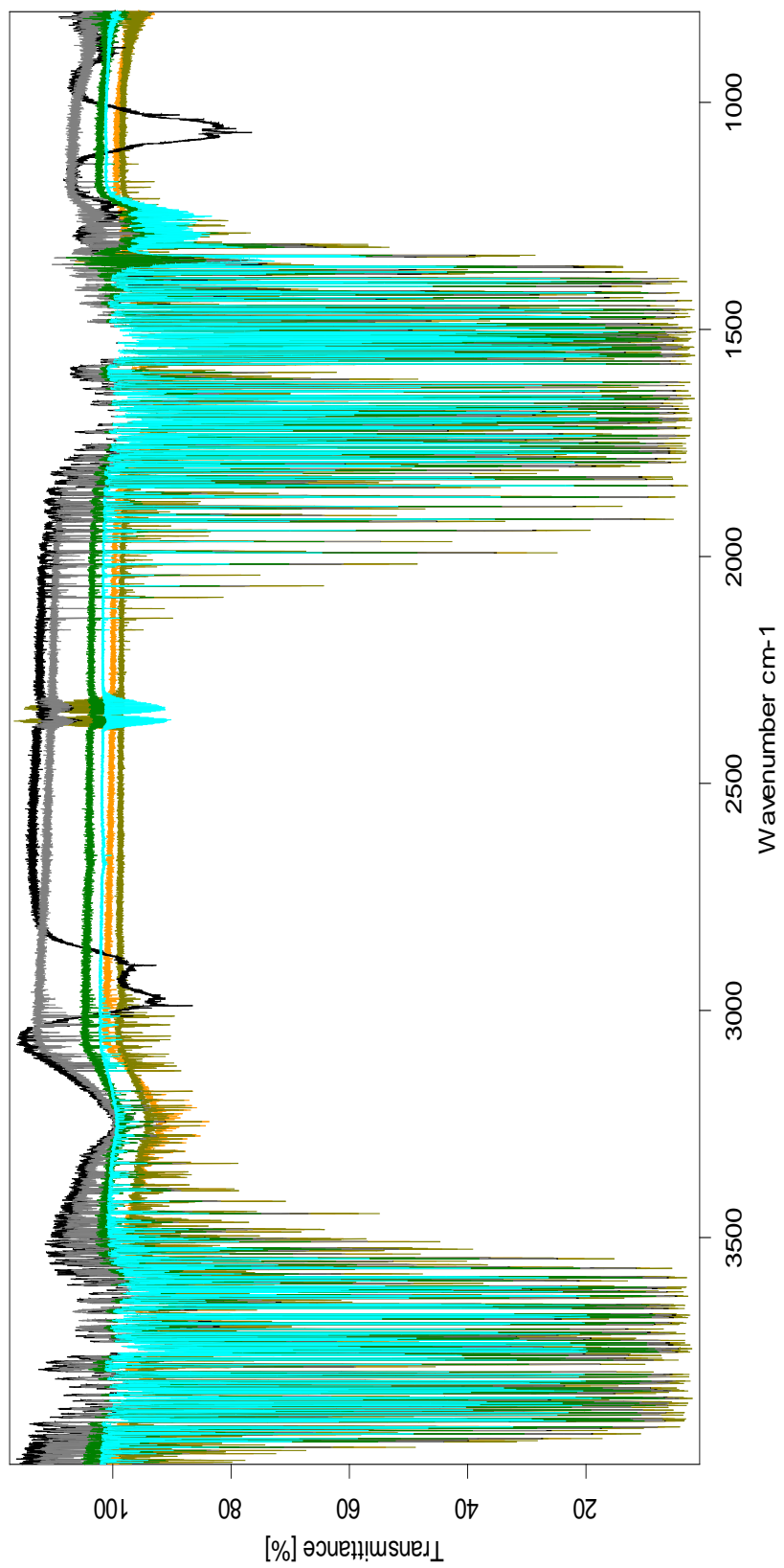


Figure 6.2 Comparison of average spectra for 100 μ L hydrogen peroxide (aqua), Health Leads (green), Jerome Russell (grey), Colgate mouthwash (black), Sunin (khaki) and Botanics (orange) at 75°C

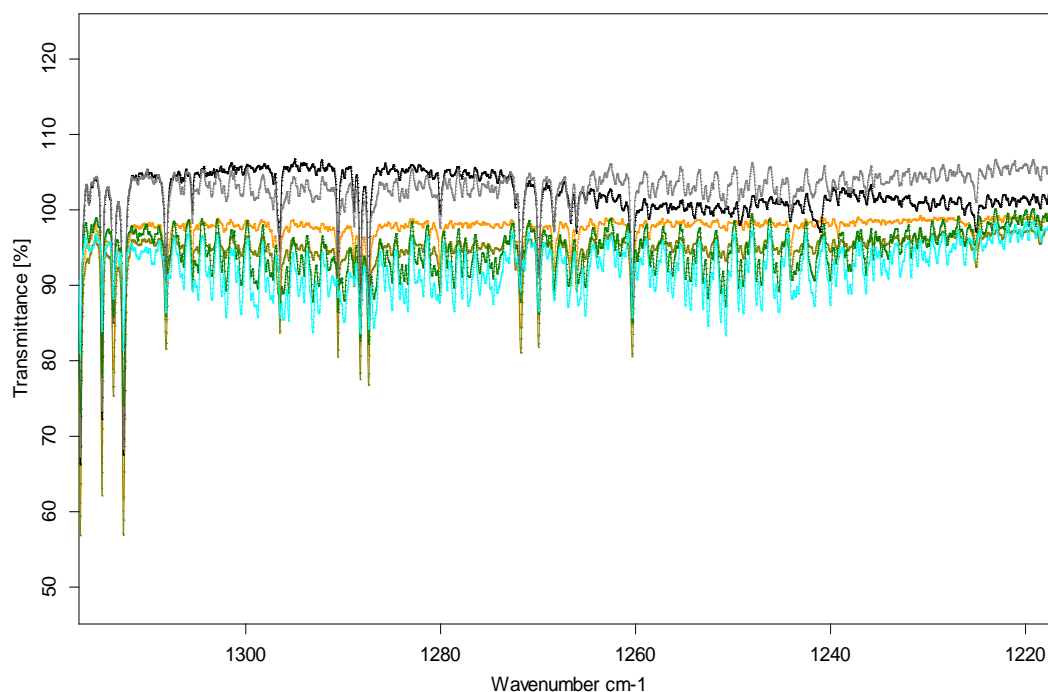


Figure 6.3 Close up of the spectral region covering the two existing hydrogen peroxide QCL detection targets (1274 and 1285 cm^{-1}) for hydrogen peroxide (aqua), Health Leads (green), Jerome Russell (grey), Colgate mouthwash (black), Sunin (khaki) and Botanics (orange)

6.4.1.2 Statistical analysis

The total transmittance values for each region were calculated and plotted to give a profile of variables, shown in figure 6.4. In addition to this the RSD values for the 19 regions of variation for each of the hydrogen peroxide based materials was calculated. The results are presented in table 6.7 and demonstrate that overall the variability of the data was very low with only three RSD values above 5% out of the 114 calculated (3%) and all three of these values were for the same region ($3710\text{--}3790\text{ cm}^{-1}$). The average RSD values for each brand were calculated ($n=19$) and none of these values were above 5%, this suggests that the data is reproducible.

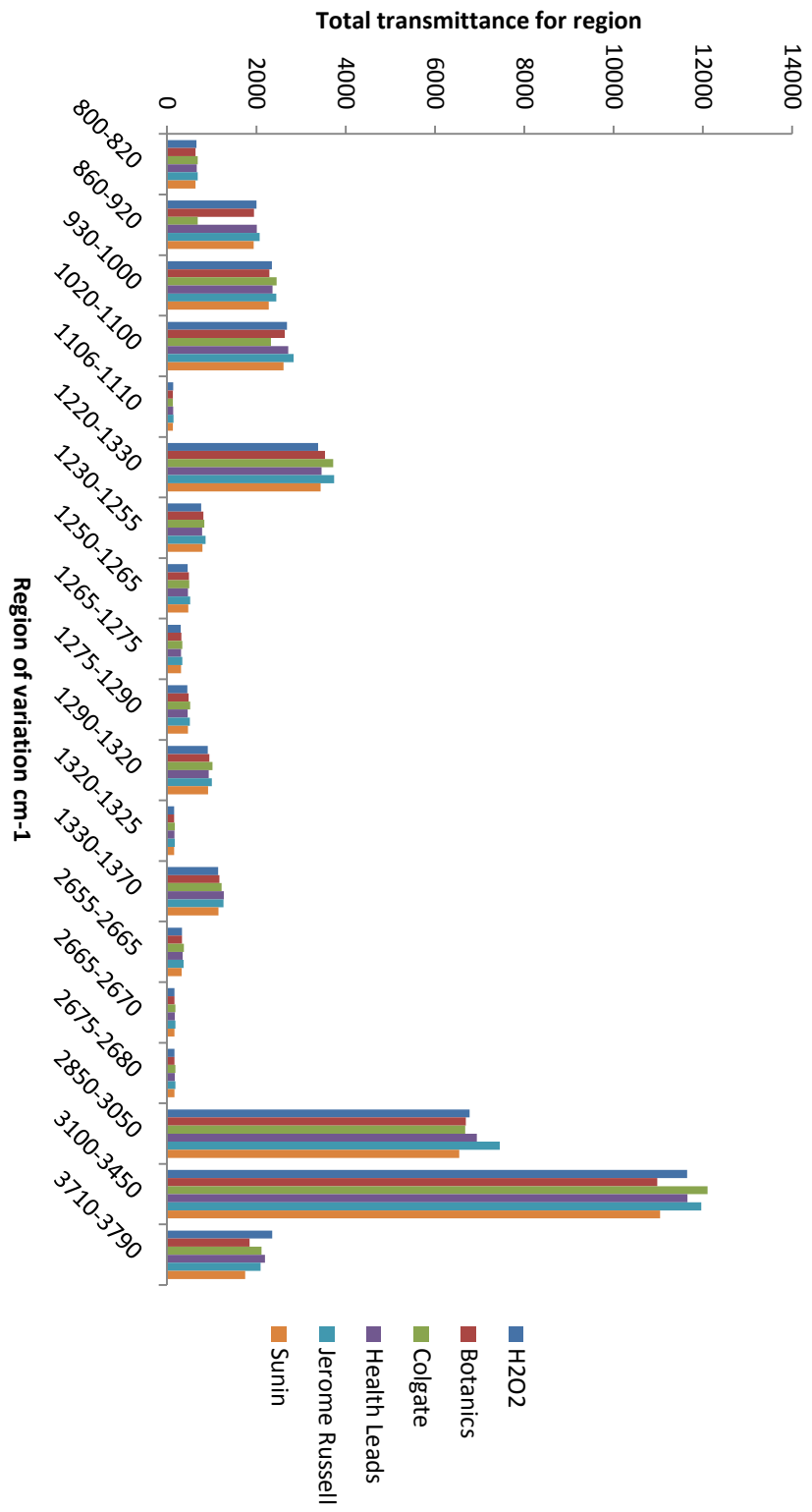


Figure 6.4 Profile of variables for the laboratory hydrogen peroxide and hydrogen peroxide containing materials

Table 6.7 RSD values for the six materials analysed with those RSD values above 5% shown in red

Region (cm ⁻¹)	Botanics	Colgate	Health Leads	Jerome Russell	Sunin	Laboratory H ₂ O ₂
800-820	0.06	0.26	0.34	0.32	0.43	0.09
860-920	0.03	0.34	0.50	0.34	0.23	0.13
930-1000	0.06	0.29	0.71	0.37	0.20	0.20
1020-1100	0.07	0.93	0.88	0.42	0.27	0.26
1106-1110	0.07	0.49	0.89	0.39	0.27	0.26
1220-1330	0.63	0.46	0.42	1.18	0.96	1.14
1230-1255	0.44	0.32	0.41	1.41	1.02	1.20
1250-1265	0.50	0.36	0.42	1.35	1.01	1.18
1265-1275	0.77	0.59	0.42	1.28	1.07	1.17
1270-1290	0.70	0.42	0.40	1.51	1.20	1.43
1290-1320	1.01	0.83	0.40	1.27	1.09	1.27
1320-1325	0.73	0.63	0.63	0.60	0.53	0.90
1330-1370	2.29	2.40	0.53	2.19	0.83	4.90
2655-2665	0.18	0.45	1.53	0.65	0.59	0.44
2665-2670	0.18	0.45	1.54	0.67	0.59	0.44
2675-2680	0.18	0.44	1.53	0.69	0.59	0.43
2850-3050	0.20	0.81	1.71	0.64	0.70	0.55
3100-3450	0.34	0.18	0.46	0.20	0.63	0.05
3710-3790	6.99	7.14	0.71	6.64	2.34	1.70
Average	0.81	0.94	0.76	1.16	0.76	0.93

6.4.1.2.1 Hierarchical cluster analysis

The data from the individual repeats of each material were input into Minitab and the dendrogram produced with this data is presented in figure 6.5. The individual repeat measurements of each brand and the laboratory grade material clustered together with only a small amount of overlap, however, taking several repeats to produce an average spectrum would be advised to reduce any within brand measurement variation.

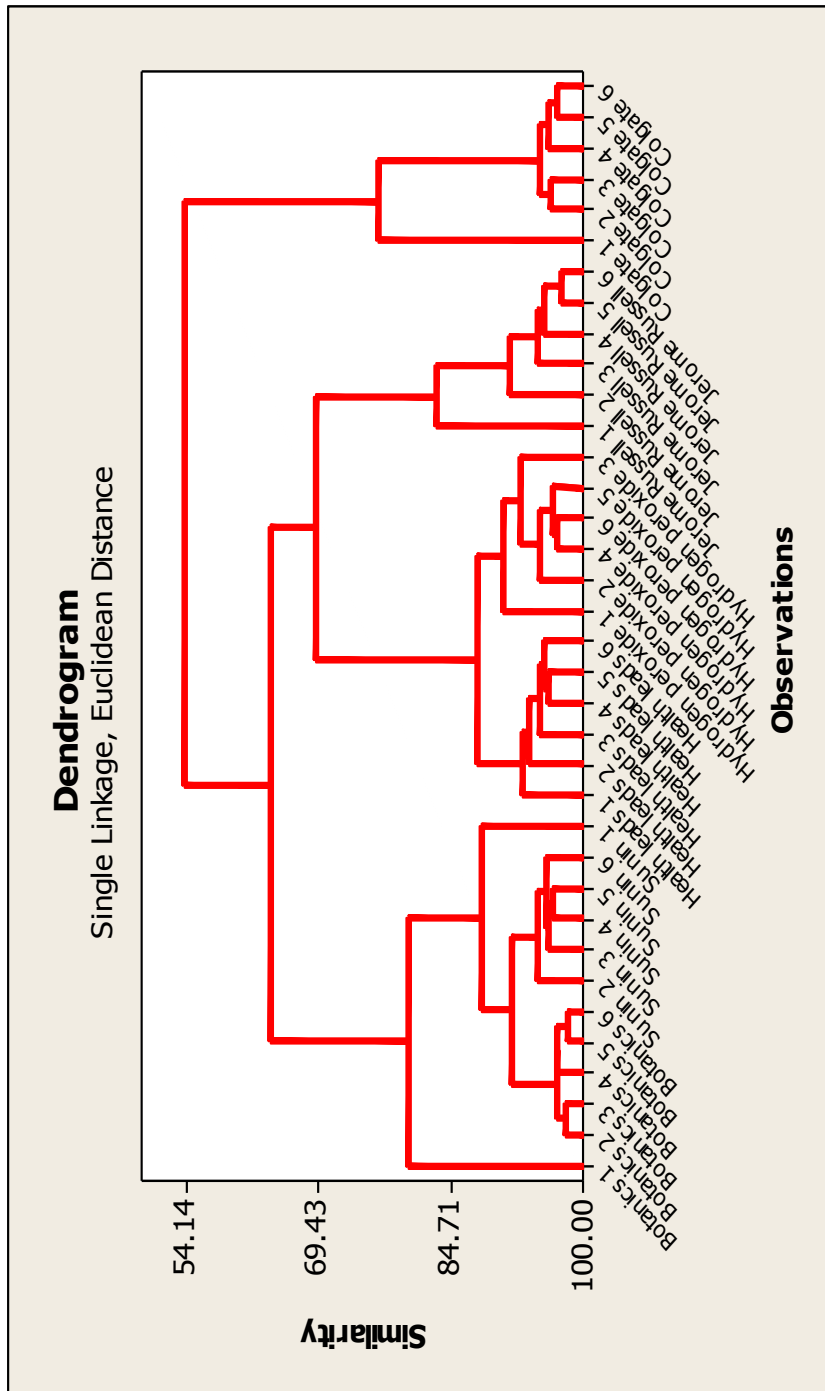


Figure 6.5 Dendrogram produced using the data from individual repeats of each material analysed

The data from the average values was also analysed and is shown in figure 6.6. The Health Leads hydrogen peroxide is shown to be the most similar to the laboratory grade peroxide. This is unsurprising as these materials are the closest in hydrogen peroxide concentration and the Health Leads solution contains very few other impurities that would be likely to have an effect on the infrared spectrum.

The Botanics and Sunin products also appear similar. This is perhaps more surprising as the Botanics is a cream while the Sunin is a liquid. However, as the hydrogen peroxide concentration of the Botanics is not known it is possible that the hydrogen peroxide concentrations of the two materials are very similar. Colgate peroxy mouthwash was shown to be the least similar to the other peroxide containing materials. This was expected as it had the most different spectrum.

Overall the results indicate that it is possible to discriminate between different brands of hydrogen peroxide containing products based on their infrared spectra.

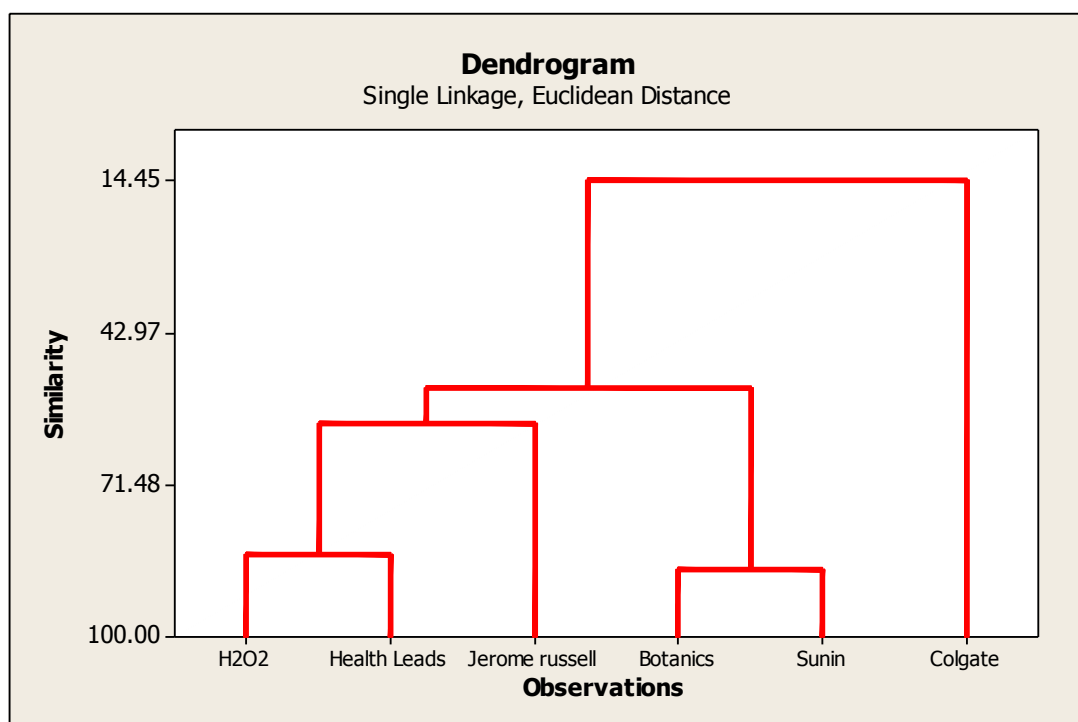


Figure 6.6 Dendrogram produced using the average values for the hydrogen peroxide containing materials

6.4.1.2.2 Self organising feature maps

The data was subsequently analysed using SOFM. Figure 6.7 presents the cluster map for the data from the individual repeats (n=6) for each material. This cluster map corresponds to the individual values dendrogram where the majority of the repeat analyses for each material have clustered together. The two exceptions to this clustering are a repeat of Sunin (Sunin 1) which has clustered with the Botanics repeats and a repeat of the laboratory hydrogen peroxide (Hydrogen peroxide 1) which has clustered with the Health Leads repeats. This correlates with the dendrogram where Sunin 1 showed similarities to both Botanics and Sunin clusters, and Hydrogen peroxide 1 was the least similar of the laboratory peroxide repeats. As a whole the laboratory peroxide repeats showed the greatest similarity to the Health Leads repeats compared to the other materials.

It is also worth noting the shading within some of the clusters. For example Botanics 1 is shaded darker than the rest of the Botanics cluster, this corresponds to the dendrogram where Botanics 1 is less similar than the other Botanics repeats. The Sunin repeat (Sunin 1) that is also found in this cluster also has darker shading, which corresponds to the fact that it is less similar to the other repeats present in this cluster, similarly the hydrogen peroxide repeat that has clustered with the Health Leads repeats (Hydrogen peroxide 1) has dark shading. Colgate 1 which demonstrated a lower level of similarity to the rest of the Colgate cluster in the dendrogram is also shaded darker than the rest of the Colgate cluster in the cluster map.

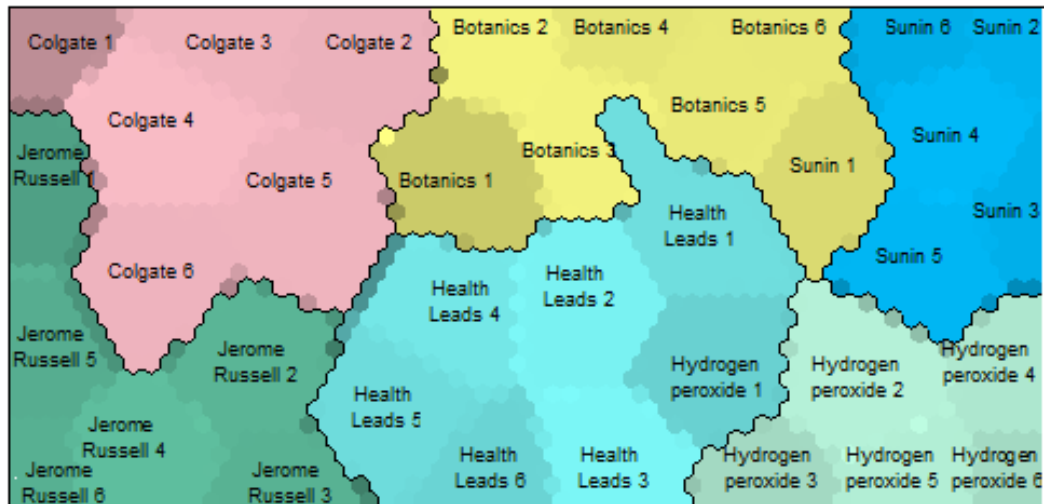


Figure 6.7 Cluster map for the individual repeats for each hydrogen peroxide containing material

Figure 6.8 reveals the cluster map for the average values (n=6) of the different materials where it can be seen that the six material have been separated completely. Figures 6.9 – 6.10 show the component maps for the average spectral data.

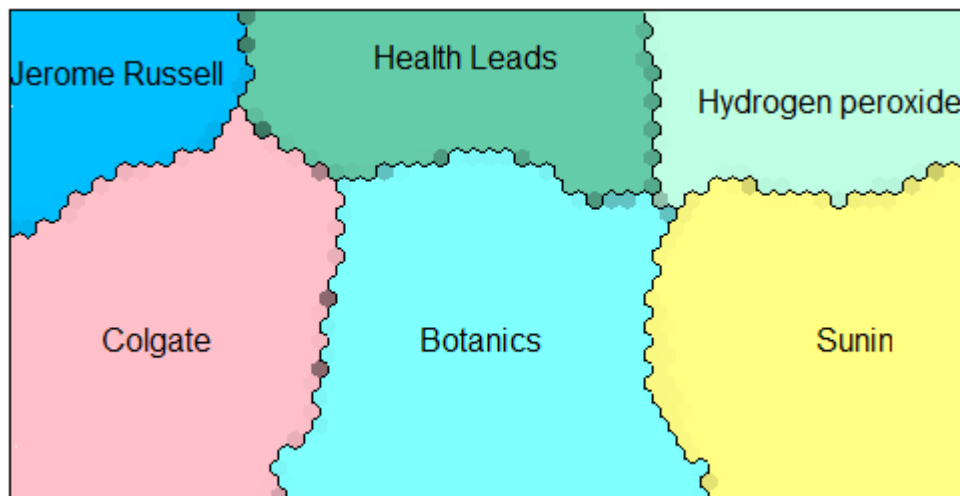


Figure 6.8 Cluster map for the average values for the six hydrogen peroxide based materials analysed

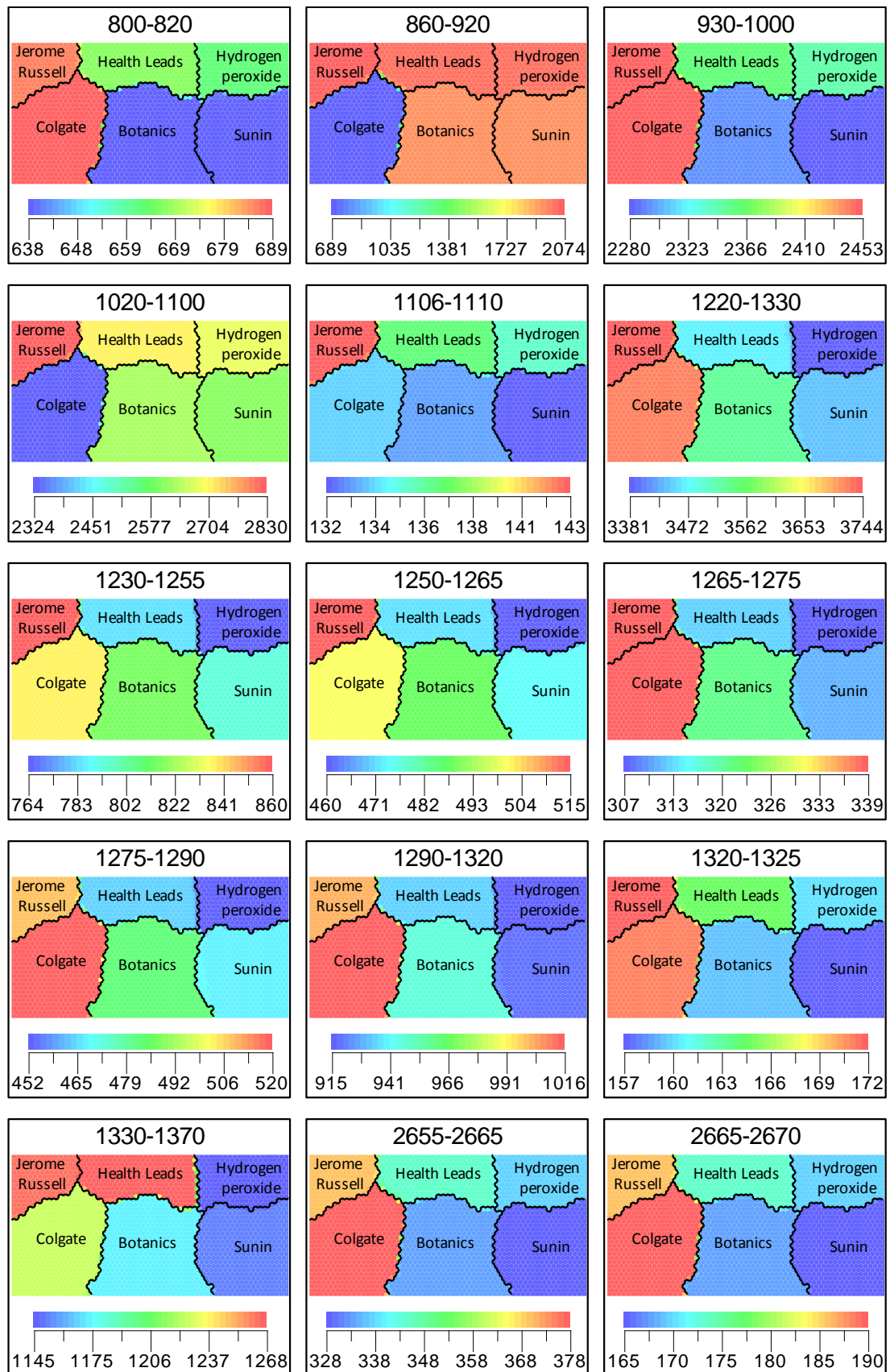


Figure 6.9 Component maps covering the regions of variation between 800-2670 cm⁻¹

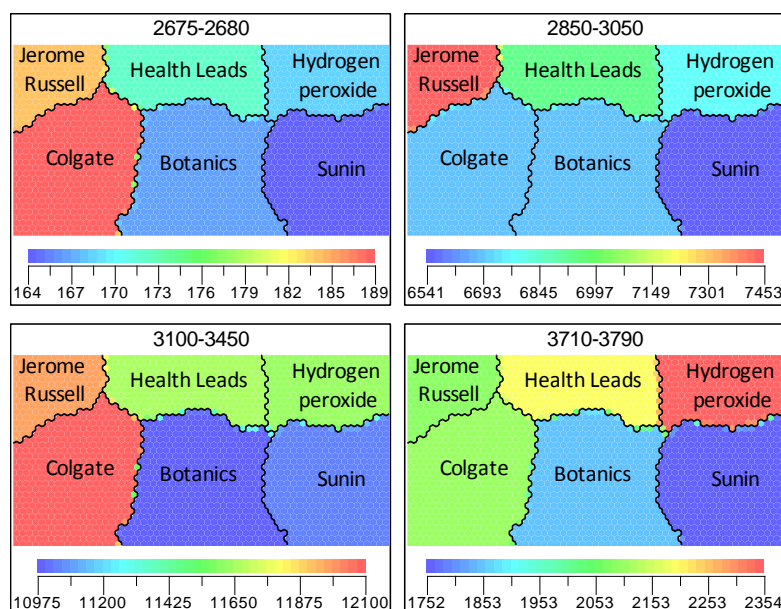


Figure 6.10 Component maps for the regions of variation between 2675 – 3790 cm^{-1}

The component maps reveal that virtually all of the features show variation between the different brands, without being strong discriminators for a single brand. This indicates that a combination of regions is required for discrimination and a reduction in the number of regions might not be successful in maintaining the discriminating power. The components maps also correspond to the information seen in the cluster maps and the HCA analysis, Sunin and Botanics show multiple similarities as do Health Leads and the laboratory hydrogen peroxide.

Figure 6.11 shows the overlaid spectra for the region 1250-1265 cm^{-1} , figure 6.12 shows the profile of variables for while figure 6.13 presents the corresponding component map. The component map demonstrates that this feature is not a strong discriminator for a single brand (which would appear as one red cluster and all others appearing blue) but shows separation across the brands with five out of the six materials shaded differently. In this way this component can be seen to have discrimination across the brands, but also emphasises the need to have multiple components in order to build up the ability to discriminate between very similar materials.

Figure 6.11 demonstrates that this region has several small differences in absorption features seen, with variance in the size of an oscillating pattern seen, as well as different amounts of absorption for the small peak observed. The absorption seen in this region is thought to be due to O-H asymmetric bending. Figure 6.13 demonstrates that with SOFM even small differences can result in discrimination, this is an advantage of SOFM that has previously been described when characterising ignitable liquids[30, 31].

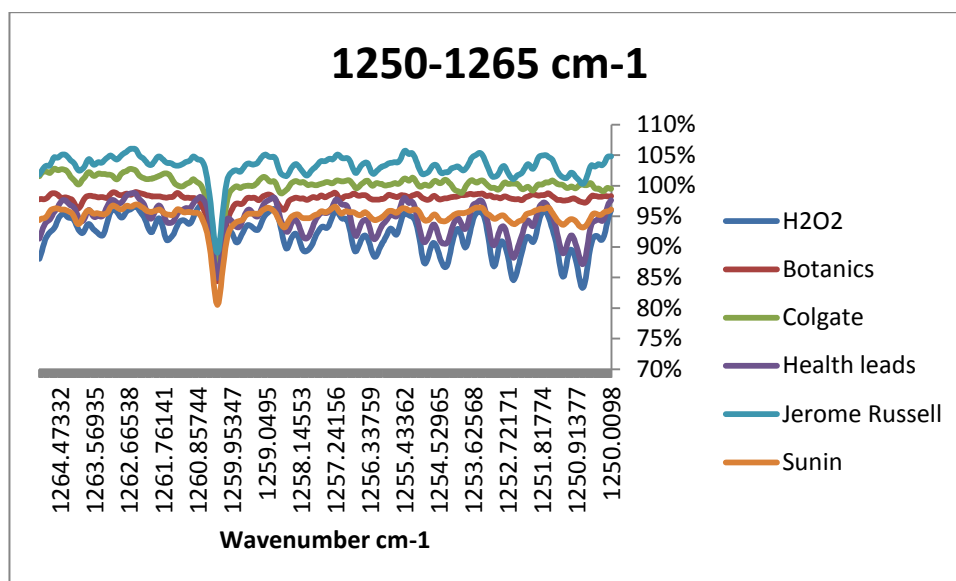


Figure 6.11 Overlaid spectra for the six hydrogen peroxide brands in the region 1250-1265 cm^{-1} (plotted in Microsoft Excel)

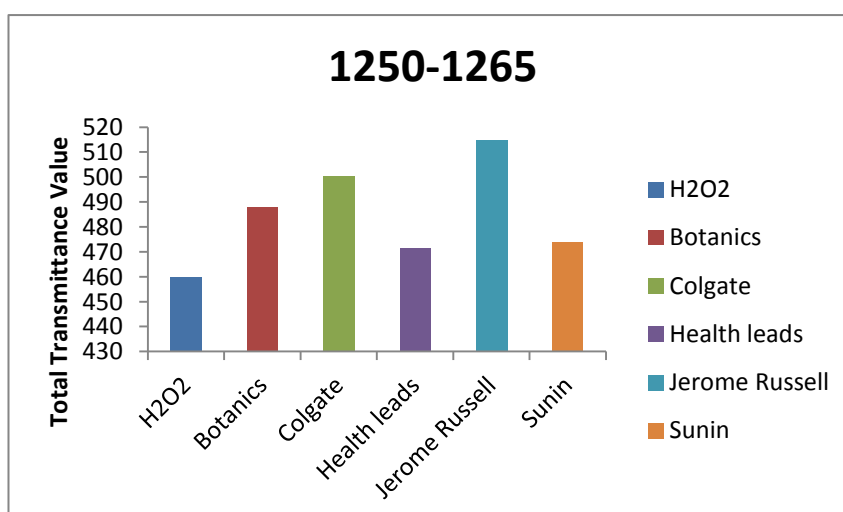


Figure 6.12 Profile of variables for the region 1250-1265 cm^{-1}

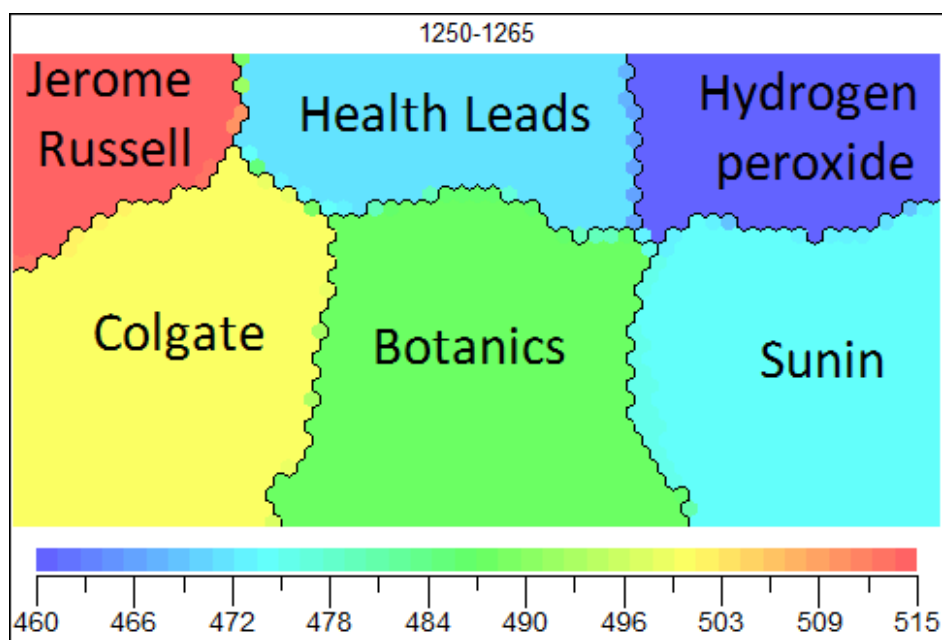


Figure 6.13 Component map for the region 1250-1265 cm⁻¹

6.4.2 Concentrated samples

6.4.2.1 Sunin

The increase in hydrogen peroxide concentration as the solution was heated over time for the Sunin sample is presented in figure 6.14. The starting concentration was approximately 7% hydrogen peroxide and the different concentrations are presented in table 6.8.

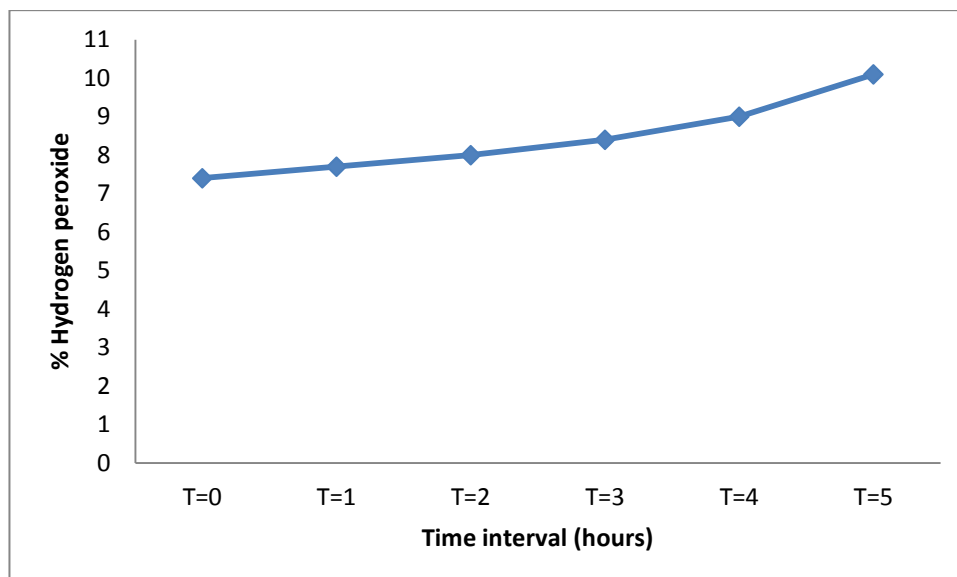


Figure 6.14 Graph showing the calculated concentration of hydrogen peroxide in Sunin at each time interval

Table 6.8 Summary of time intervals

Time interval (hours)	Description	Concentration (% Hydrogen peroxide)
T=0	Un-concentrated sample	7.4
T=1	Sample heated for 1 hour	7.7
T=2	Sample heated for 2 hours	8.0
T=3	Sample heated for 3 hours	8.4
T=4	Sample heated for 4 hours	9.0
T=5	Sample heated for 5 hours	10.1

Figure 6.15 shows the average spectra for each time interval, with figure 6.15 showing a close up of the spectral region containing two detection targets (1274 and 1285 cm^{-1}) for hydrogen peroxide. It can be observed that as the concentration of the Sunin increases (as the time interval increases) the size of the oscillating pattern in this region also increases.

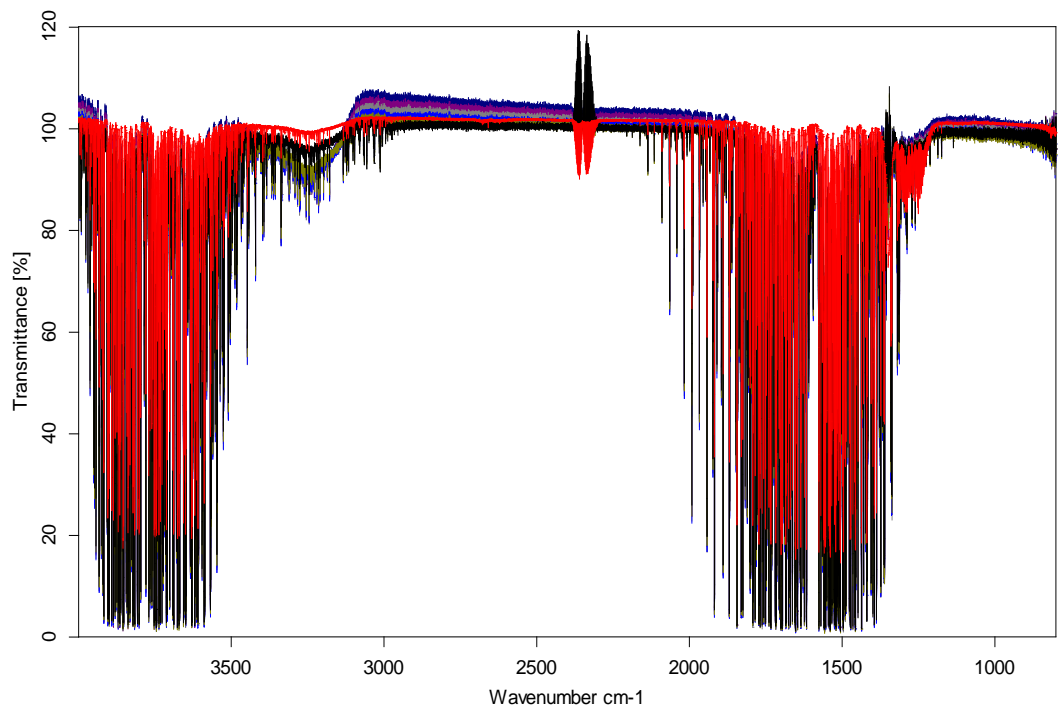


Figure 6.15 Overlaid average spectra for 50% laboratory grade with hydrogen peroxide (red) and Sunin T=0 (black), T=1 (khaki), T=2 (blue), T=3 (grey), T=4 (purple), T=5 (navy)

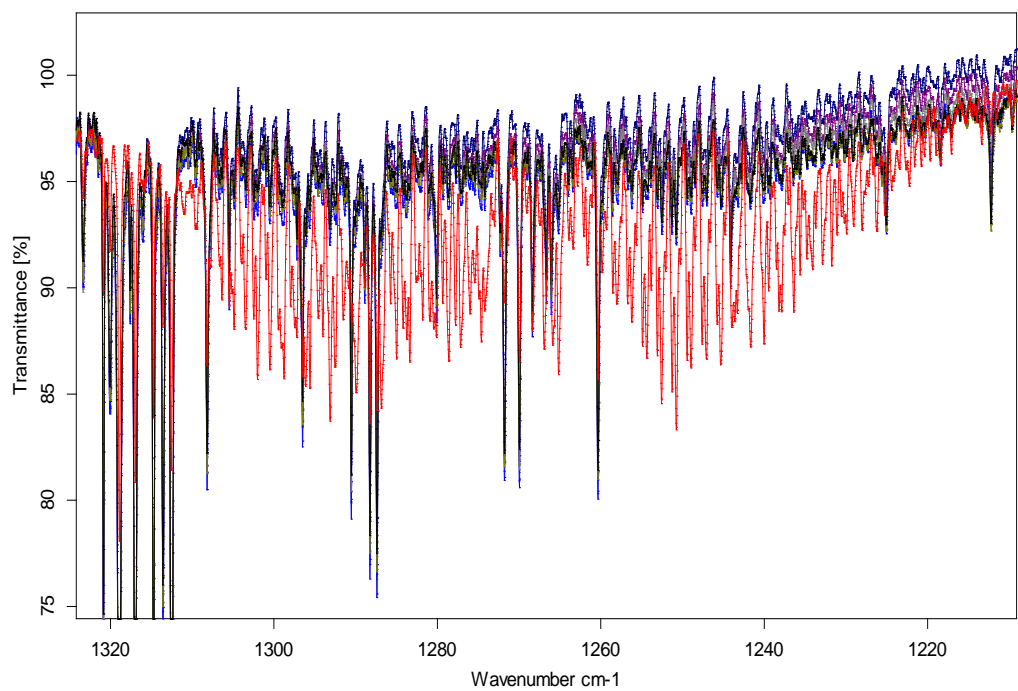


Figure 6.16 Close up of the spectral region containing two hydrogen peroxide QCL detection features with 50% laboratory grade hydrogen peroxide (red) and Sunin T=0 (black), T=1 (khaki), T=2 (blue), T=3 (grey), T=4 (purple), T=5 (navy) overlaid

6.4.2.1.1 Hierarchical cluster analysis

The same 19 regions of variation as the un-concentrated samples were used for data analysis. Figure 6.17 shows the dendrogram produced with the individual repeats for each time interval, while figure 6.18 shows the dendrogram produced with the average values.

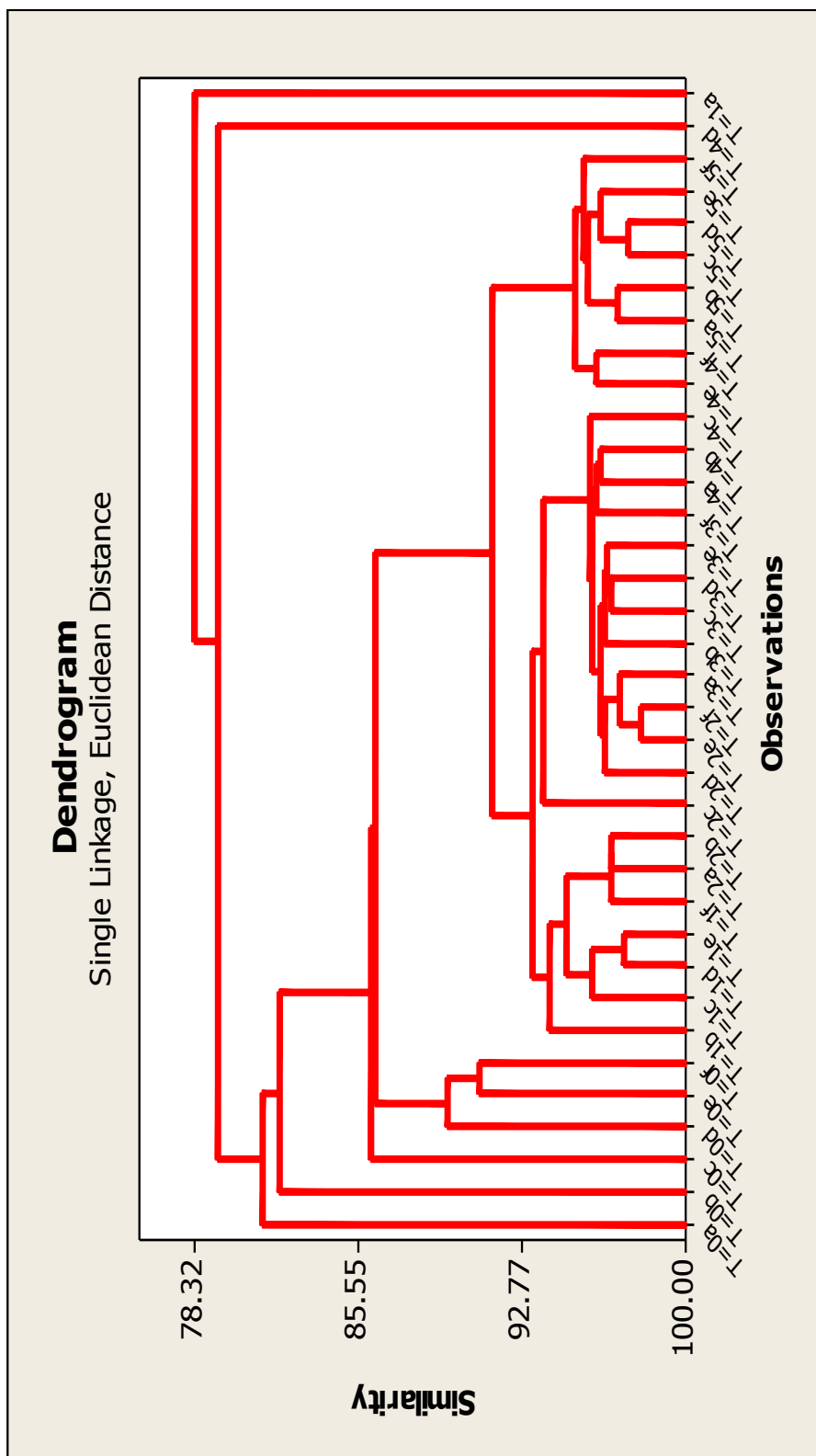


Figure 6.17 Dendrogram produced using the total transmittance data from the individual repeats of each concentration time interval for Sunin

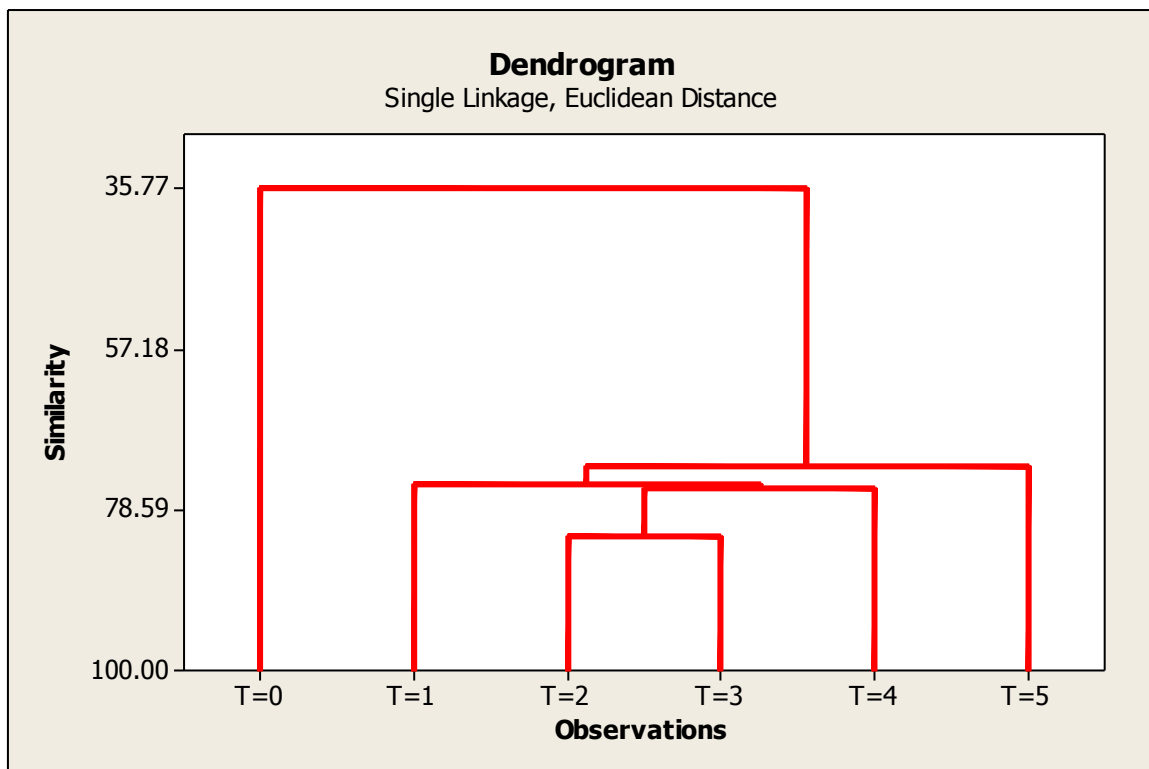


Figure 6.18 Dendrogram produced using the average total transmittance data from each of the concentration time intervals for Sunin

Figure 6.17 shows that while the individual repeats do cluster to a degree there is still overlap across the individual samples across the different time intervals. Figure 6.18 demonstrates that with average values this overlap was resolved. Therefore, it is best to produce an average spectrum for comparison. Figure 6.18 shows that T=0 showed the greatest level of variation to the others. However, a degree of discrimination could be seen for all of the time intervals. This suggests that it is possible to monitor the degree of concentration spectroscopically.

6.4.2.1.2 Self organising feature maps

The data was also analysed using SOFM and the cluster map for the individual repeats for each time interval for the Sunin samples is presented in figure 6.19. This correlates well with the results of the HCA which showed that there was overlap between the different time intervals. T=4 repeat d has formed a cluster on its own, corresponding to the dendrogram which also has this repeat on its own. The six T=5 repeats have clustered together but also with two of the T=4 repeats (e and f), which again replicates the findings of the HCA.

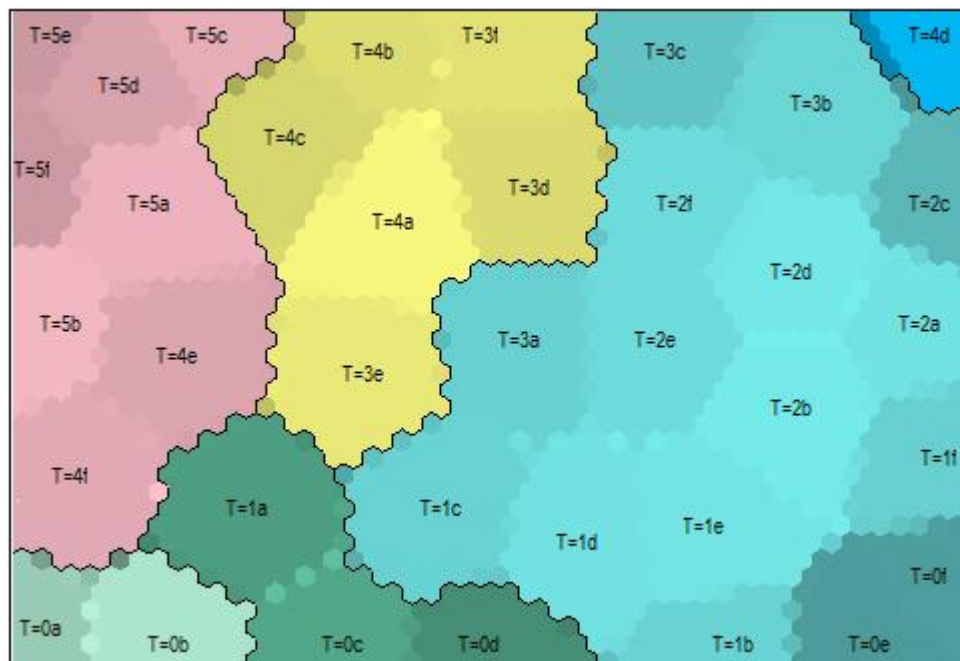


Figure 6.19 Cluster map for the individual repeats for each time interval (T=0 to T=5) for Sunin

A trend can be seen across the repeats with the lowest concentrations found towards the bottom of the map and then moving upwards and counter-clockwise to the top left hand corner as the concentration increases. The clustering of the samples also improves across this trend. This suggests that as the sample becomes more concentrated the likelihood for the sample to form a discrete cluster increases. This is significant as the concentrations of an adulterated sample would be expected to be high.

The results shown in figure 6.19 confirm the findings of the HCA analysis that an average value for each time interval would be required for the effective discrimination of the different time intervals. Figure 6.20 presents the cluster map for the average Sunin values for the six time intervals and corresponding concentrations. As with the individual values, a trend can be seen with the clusters moving counter-clockwise as the concentration increases.

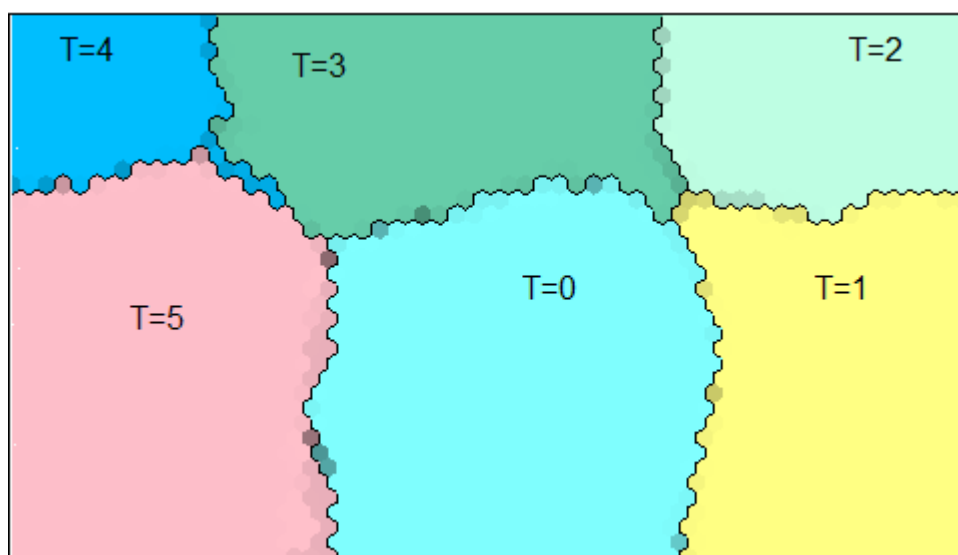


Figure 6.20 Cluster map for the average values of the six time intervals (T=0 to T=5) for Sunin

6.4.2.2 Health Leads

The starting concentration determined from the titration of the Health Leads sample was almost 10% higher than the concentration stated on the bottle. It was believed that the reason for this was the alterations to the titration method resulting in a greater relative volume of sulfuric acid to hydrogen peroxide. In order to confirm this, a known concentration of hydrogen peroxide (40%) was analysed using the same method and the calculated concentration was also seen to be higher than the known concentration by approximately 10%. As a consequence the concentration values were adjusted for this overestimation and are presented in figure 6.21. Table 6.9 presents a summary of the time intervals and adjusted concentrations.

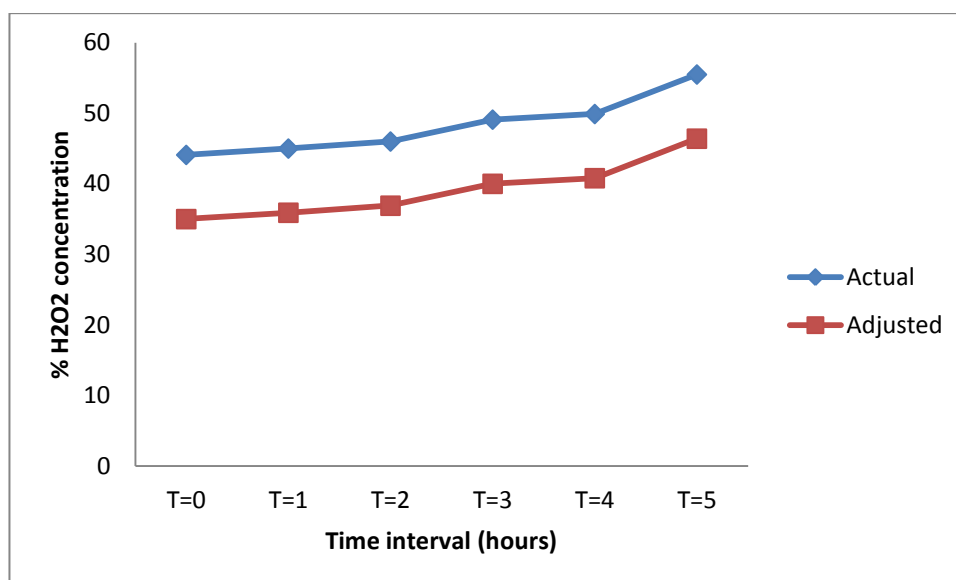


Figure 6.21 Graph showing the calculated concentrations of hydrogen peroxide in Health Leads at each time interval and the corresponding adjusted concentration values

Table 6.9 Summary of time intervals and adjusted concentrations

Time interval (hours)	Description	Adjusted Concentration (% Hydrogen peroxide)
T=0	Un-concentrated sample	35
T=1	Sample heated for 1 hour	35.9
T=2	Sample heated for 2 hours	36.9
T=3	Sample heated for 3 hours	40
T=4	Sample heated for 4 hours	40.8
T=5	Sample heated for 5 hours	46.4

The starting concentration for the Health Leads was considerably higher than the Sunin and the increase in hydrogen peroxide concentration achieved over time was also higher.

Figure 6.22 shows the six average spectra overlaid, while figure 6.23 shows a close up of the spectral region containing two targets for QCL detection (1274 and 1285 cm^{-1}). It can be seen that as the concentration increased the size of the absorption bands in this region also increased.

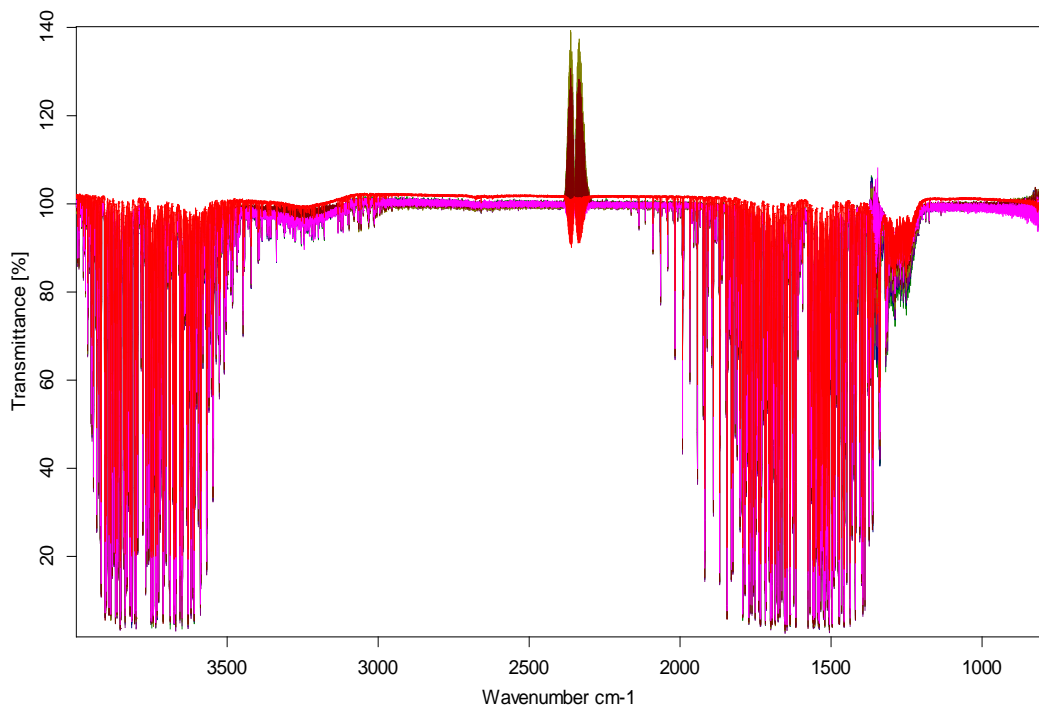


Figure 6.22 Overlaid average spectra of 50% laboratory grade hydrogen peroxide (red) and Health Leads T=0 (pink), T=1 (brown), T=2 (khaki), T=3 (purple), T=4 (navy), T=5 (green)

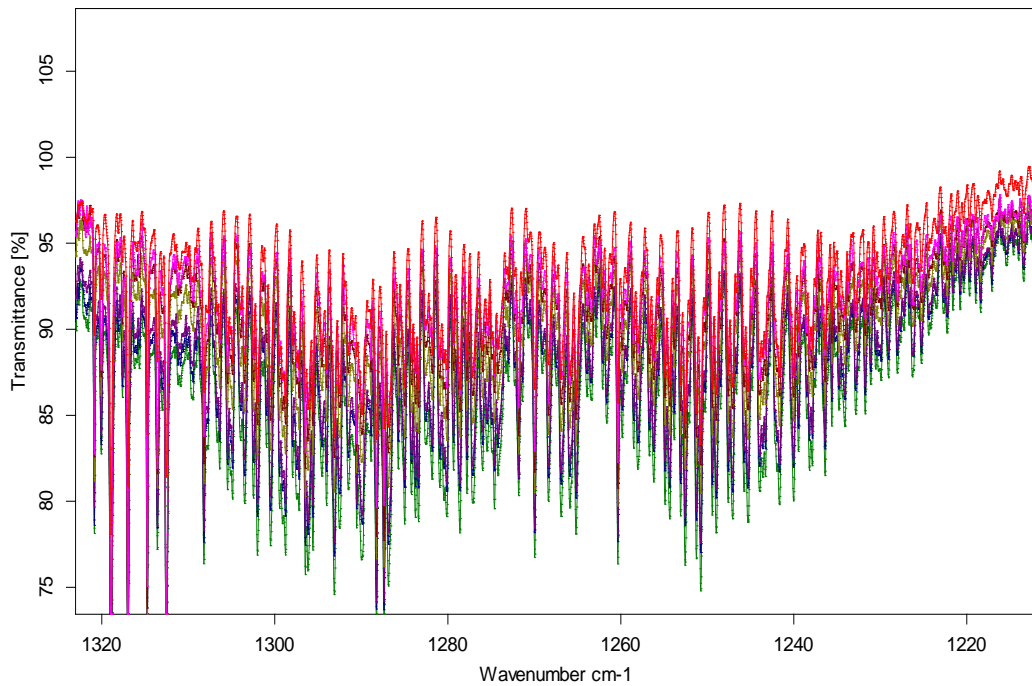


Figure 6.23 Close up of the spectral region containing the two detection targets for hydrogen peroxide with 50% laboratory grade hydrogen peroxide (red) and Health Leads T= 0 (pink), T=1 (brown), T=2 (khaki), T=3 (purple), T=4 (navy), T=5 (green) overlaid

6.4.2.2.1 Hierarchical cluster analysis

The dendrogram produced using the data from the individual repeats of each concentrated sample at each time interval is presented in figure 6.24. This shows that when examining the individual repeats there is some overlap between the time intervals. This is to be expected as it had been seen with the majority of other compounds analysed. Once again these results demonstrate that in order for discrimination to be possible several repeats should be taken and used to produce an average spectrum.

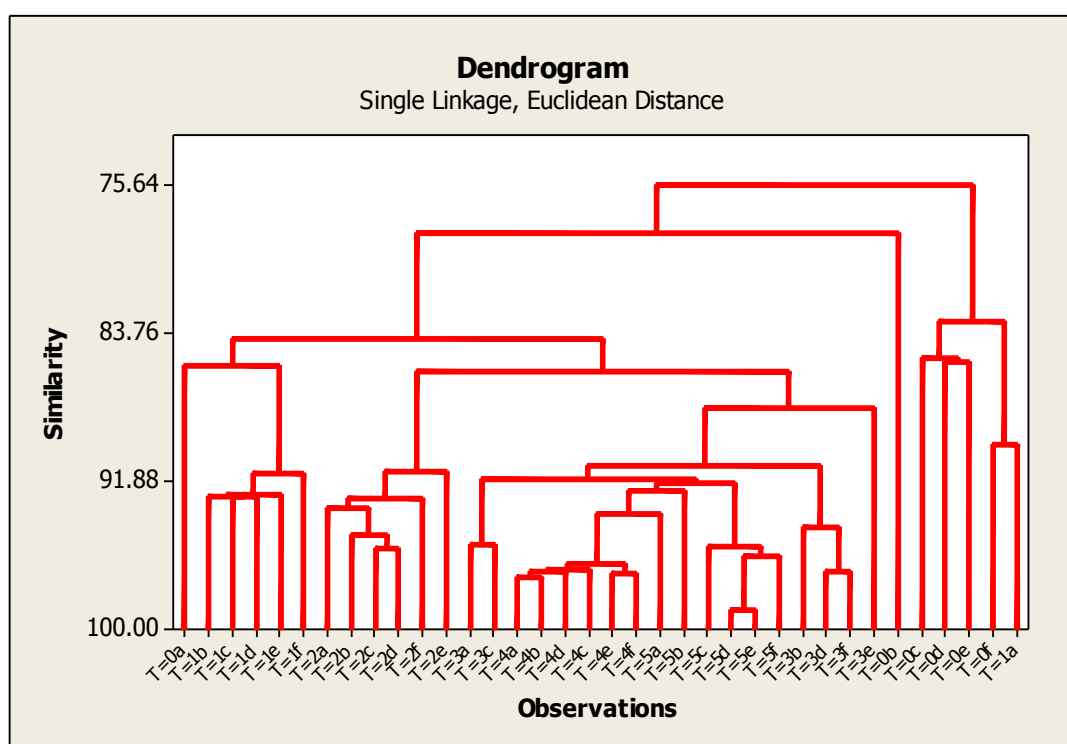


Figure 6.24 Dendrogram produced using the total transmittance data from the individual repeats from each concentration time interval

Figure 6.25 shows the dendrogram produced using the average values derived from the spectra produced for each time interval. As with the Sunin, T=0 is show to be the least similar to the other time intervals. The dendrogram shows that it is possible to discriminate between the six different time intervals. The discrimination

of the higher concentrated samples appears more pronounced than that observed within the Sunin samples with a threshold of approximately 40% hydrogen peroxide concentration (seen at T=3) resulting in greater discrimination.

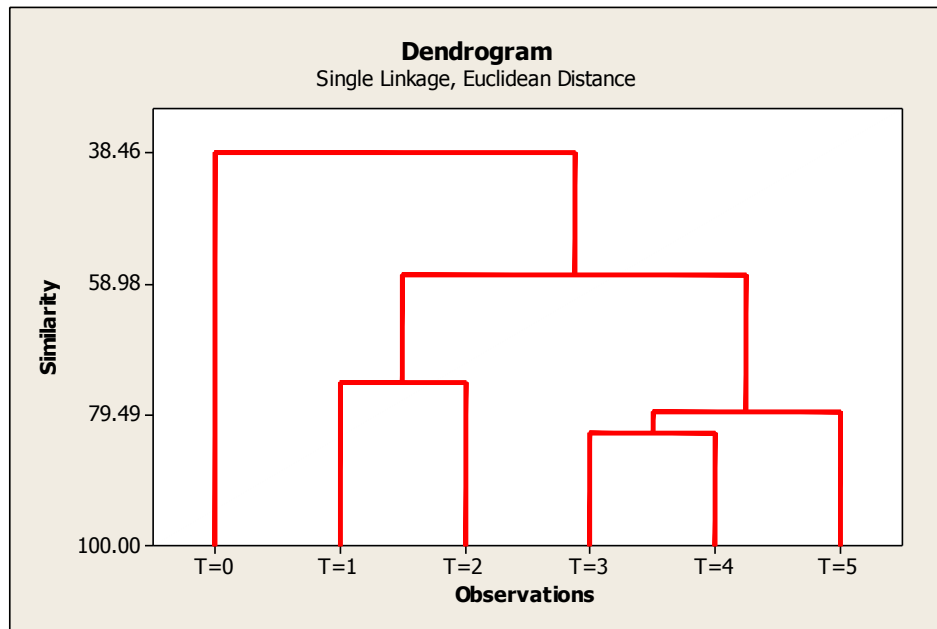


Figure 6.25 Dendrogram produced using the average total transmittance data for the Health Leads concentration time intervals

6.4.2.2.2 Self organising feature maps

The data was also analysed using SOFM. Figure 6.26 reveals the cluster map produced with the data from the individual repeats for each time interval.

The cluster map demonstrates that the individual repeats, in the same way as the Sunin individual repeats, show a degree of overlap which correspond to the results of the HCA analysis. The results also show a similar trend, in that the higher the concentration the more likely it is to form a discrete cluster. Once again there is also a trend in the location of the different clusters, this time a clockwise movement is observed with the lowest concentrations found in the bottom left hand corner and the highest concentrations found in the bottom right hand corner of the map.

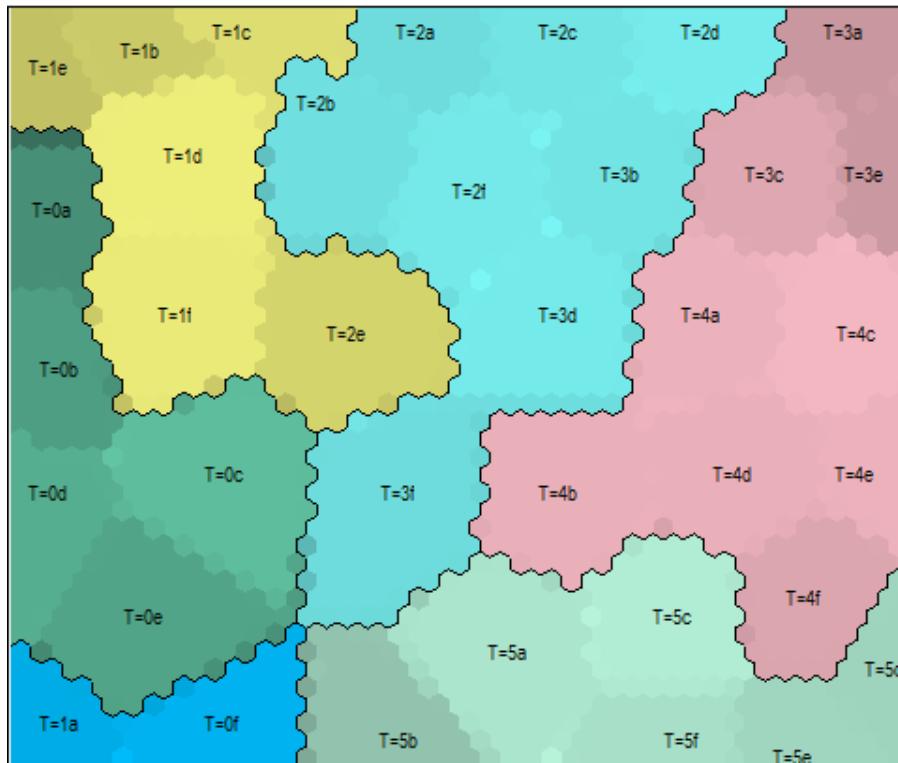


Figure 6.26 Cluster map for the individual repeats for the six time intervals (T=0 to T=6) for Health Leads

Figure 6.27 reveals the cluster map for the average values. This map demonstrates the same clockwise movement through the concentrations seen with the individual repeats.

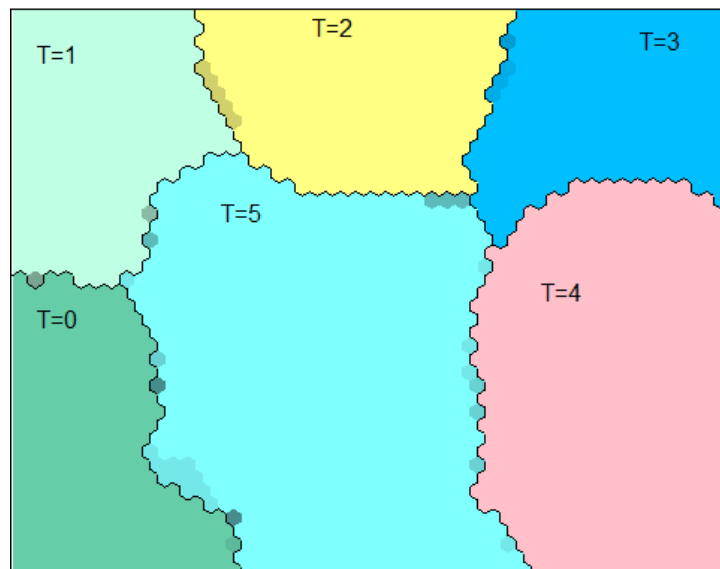


Figure 6.27 Cluster map for the average values for the six time intervals (T=0 to T=5) for Health Leads

6.4.2.3 Sunin and Health Leads comparison

Following the successful discrimination of the different concentrated samples for each hydrogen peroxide brand, the data from both the Sunin and Health Leads samples were combined to explore whether or not it was possible to link the concentrated samples to the appropriate un-concentrated brand from which they were derived. Based on the results of the analysis of the individual repeats for both Sunin and Health Leads where some overlap was seen between the concentrations it was decided to focus the comparison of the two data sets on the average values.

6.4.2.3.1 Hierarchical cluster analysis

The dendrogram produced with the average values for both Sunin and Health Leads samples is presented in figure 6.28. This convincingly illustrates the discrimination of the samples by brand, and furthermore that the more concentrated Health leads samples have also maintained their discrimination from the less concentrated samples within the grouping.

This is a highly significant result and suggests that spectroscopic analysis can identify when hydrogen peroxide samples have been modified as well as being able to distinguish which brand of material has been modified.

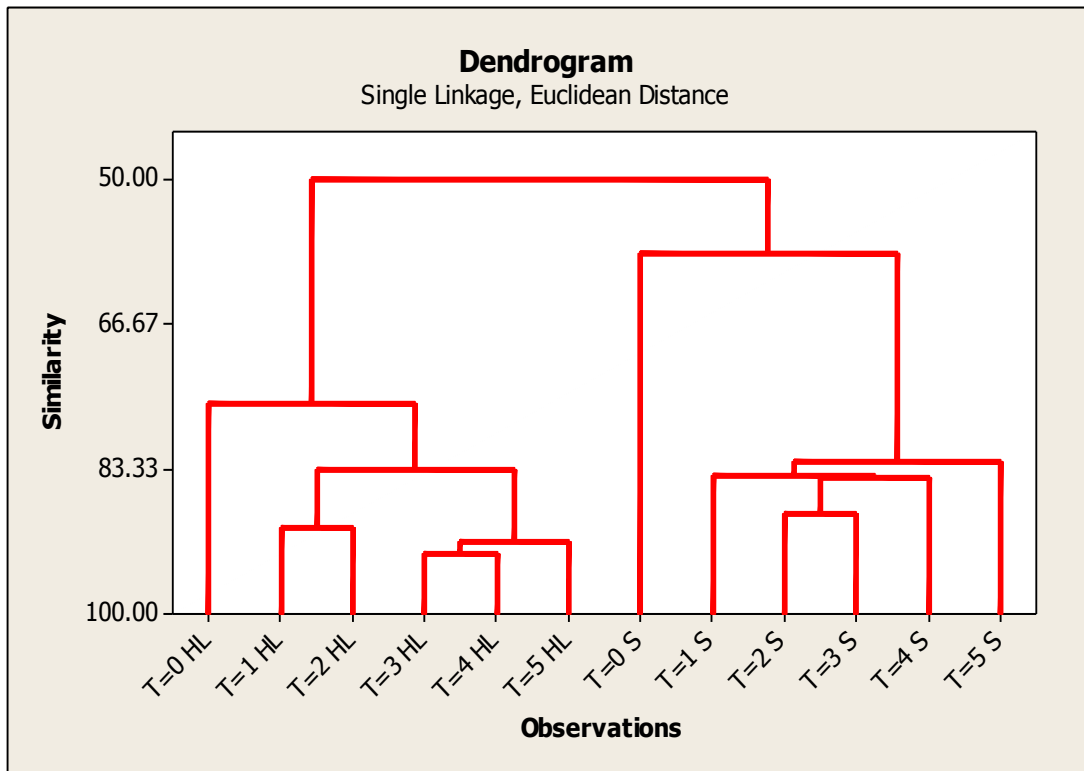


Figure 6.28 Dendrogram produced from a comparison of the total transmittance data for Health Leads (HL) and Sunin (S)

6.4.2.3.2 Self organising feature maps

The average data was also analysed using SOFM and figure 6.29 shows the cluster map for the average spectral data. The cluster map reveals that the two materials cluster separately with no overlap and that within the two main clusters the different time intervals also separate, although in the case of Sunin T=0 and T=4 this separation is not quite complete. This corroborates the HCA findings very well.

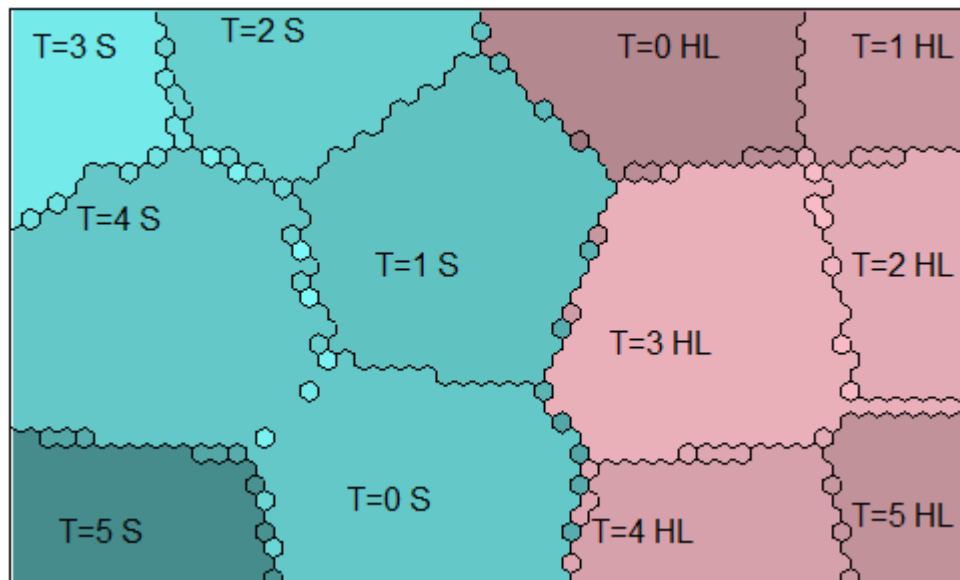


Figure 6.29 Cluster map comparing the average data for the six time intervals (T=0 to T=5) for Sunin (S) and Health Leads (HL) showing the two clusters, and contour lines separating the time intervals

Where SOFM comes into its own is in exposing the contribution that the identified regions of interest have to discrimination via component maps and these are presented in figures 6.29 - 6.31.

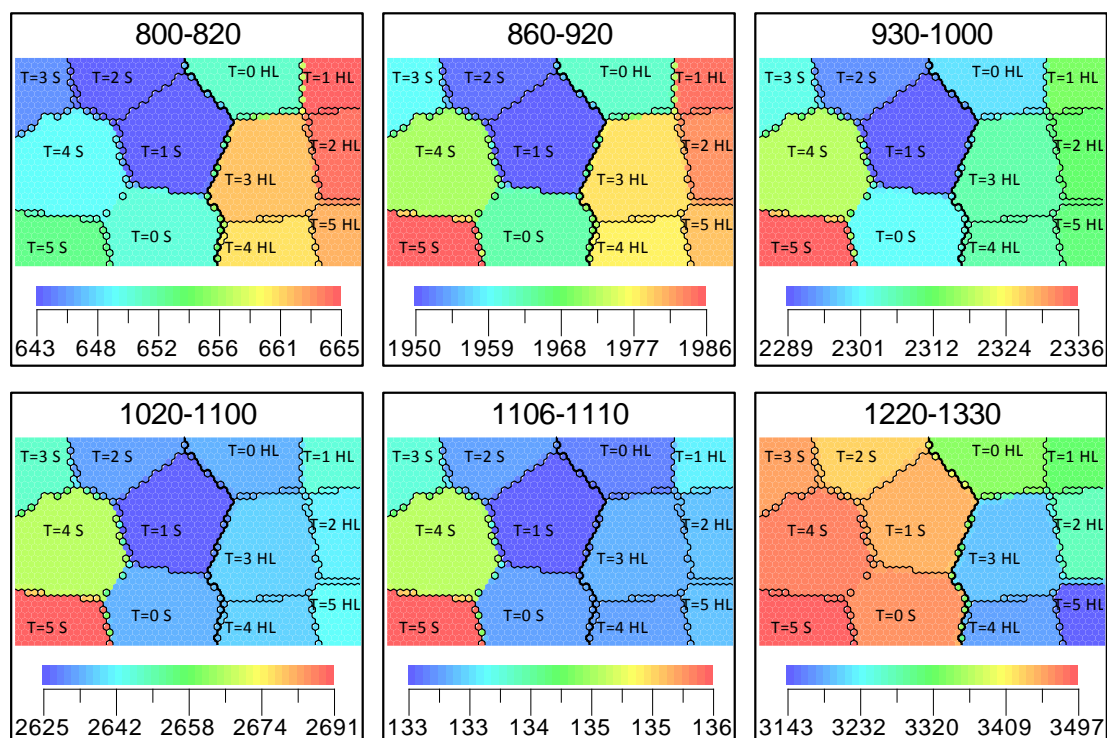


Figure 6.30 Component maps for regions of variation between 800-1330 cm^{-1}

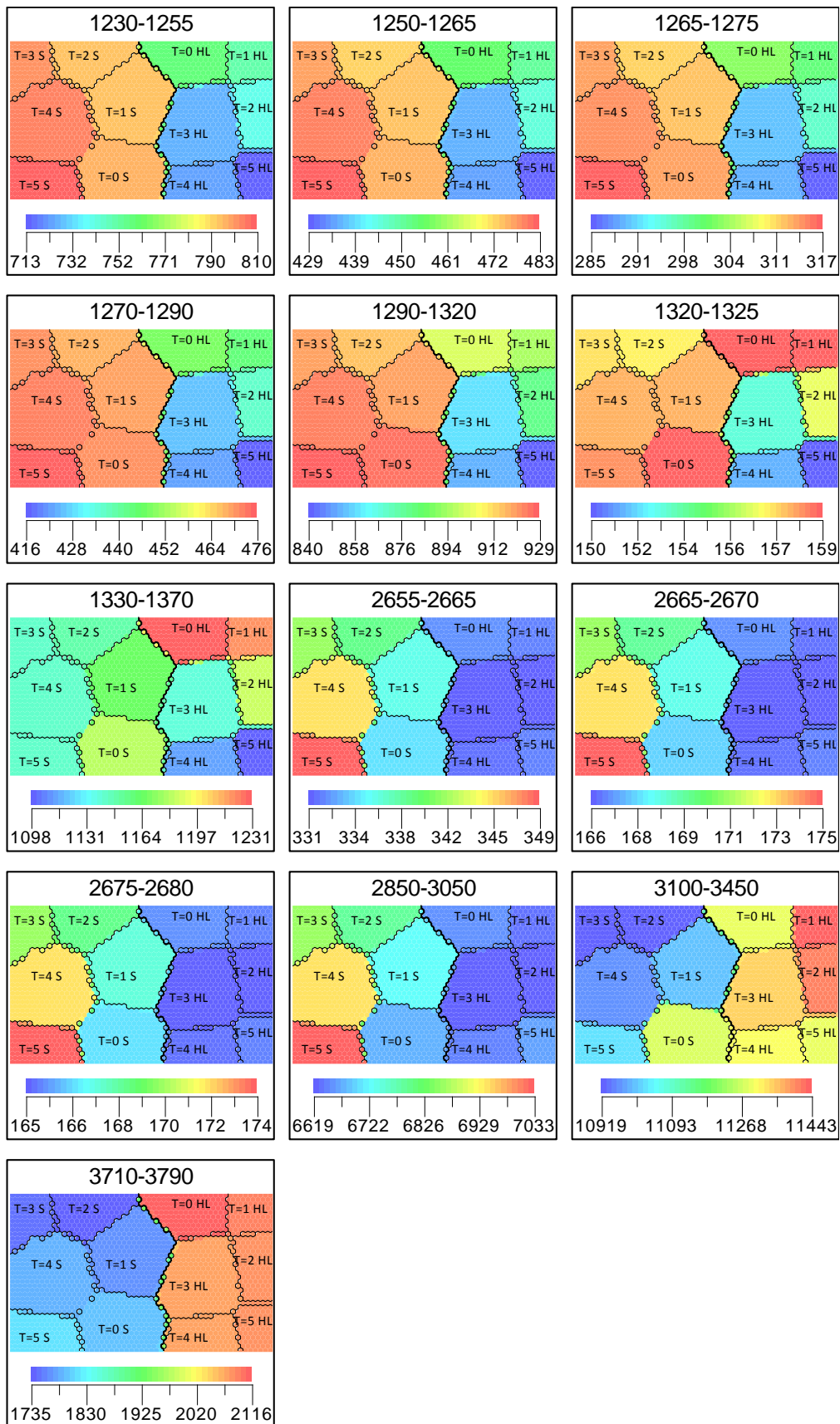


Figure 6.31 Component maps for regions of variation between 1230-3790 cm^{-1}

The component maps demonstrate that for some components there is overlap for the two materials, however in many cases the shading is quite different, showing the discrimination between the two materials. A particular example of this is the region 2665-2670 cm^{-1} where, while the Sunin time intervals display a range of shading toward the red end of the scale, the Health Leads samples are all shaded blue. The best separation of the two sets of samples is provided in the region 3710-3790 cm^{-1} . Viewing the component maps also confirms that while there isn't a full separation of T=4 and T=0 for Sunin on the cluster map, several of the components fully separate the two. For example region 3100-3450 cm^{-1} has T=0 S shaded yellow while T=4 S is shaded blue. This once again highlights the power of the component maps to break down the information and observe the underlying trends of the data. Being in a position to determine which wavenumbers provide the sample separation provides obvious opportunities for exploitation in relation to the development of specific single or multi-array stand-off detection systems.

6.5 Conclusions

The results of the hydrogen peroxide study demonstrate that high resolution Fourier Transform spectroscopy combined with multivariate analysis can be used to discriminate between different brands of hydrogen peroxide containing products and that such discrimination require the use of average recorded spectra. This could provide information to intelligence services when trying to identify such components and narrow down potential sources. The results also highlighted the differences that can be seen in the spectra depending upon the additives present and also the concentration of the hydrogen peroxide within the solution. This could have an effect of the spectra of any explosive materials such as TATP made from different brands of hydrogen peroxide product, or on hydrogen peroxide used as an explosive material in its own right. Any effects on the spectra could have implications on the detection of the explosive material and therefore this warrants further investigation.

The effects of concentrating different brands of hydrogen peroxide products was also investigated, and it was found that it was possible to discriminate between different concentrations of the same starting material using the regions of variation identified for the brand discrimination and multivariate analysis. The results showed that a material that had been concentrated could be discriminated from the original product, but also still identified as originating from the original product when compared with a different brand. This could provide significant information for intelligence services, through the identification of hydrogen peroxide materials and the determination that a product had been concentrated.

The results of this research indicate that with further work this technique could become a very powerful tool for the analysis of hydrogen peroxide as an explosive precursor. There is the potential to adapt the technique to allow for the linking of precursors to final explosive products.

6.6 References

1. Lubczyk, D., Siering, C., Lorgen, J., Shifrina, Z.B., Mullen, M. and Waldvogel, S.R., *Simple and sensitive online detection of triacetone triperoxide explosive*. Sensors and Actuators B-Chemical, 2010. **143**(2): p. 561-566.
2. Dubnikova, F., Kosloff, R. and Zeiri, Y., *Rational Detection Schemes for TATP NATO Advanced Research Workshop*, in *Detection and Disposal of Improvised Explosives*, H. Schubert and A. Kuznetsov, Editors. 2006, Springer.
3. Monger, J.M., Baumgartner, H.J., Hood, G.C. and Sanborn, C.E., *Explosive Limits of Hydrogen Peroxide Vapor*. Journal of Chemical & Engineering Data, 1964. **9**(1): p. 119-124.
4. Wilson, R. and Brittain, A., *Explosives Detection by Ion Mobility Spectrometry*, in *Explosives in the service of man: The Nobel Heritage*, J.E. Dolan and S.S. Langer, Editors. 1997, Royal Society of Chemistry.
5. Wilson, P.F., Prince, B.J. and McEwan, M.J., *Application of Selected-Ion Flow Tube Mass Spectrometry to the Real-Time Detection of Triacetone Triperoxide*. Analytical Chemistry, 2006. **78**(2): p. 575-579.
6. Yinon, J., *Forensic and Environmental Detection of Explosives*. 1999: Wiley.
7. [cited 2014 04/10/14]; Available from: <http://www.bbc.co.uk/news/uk-19652202>.
8. Li, X., Liu, X., Wang, W., Li, L. and Lu, X., *High loading Pt nanoparticles on functionalization of carbon nanotubes for fabricating nonenzyme hydrogen peroxide sensor*. Biosensors and Bioelectronics, 2014. **59**(0): p. 221-226.
9. Wang, C., Zou, X.C., Wang, Q., Shi, K.Y., Tan, J., Zhao, X., Chai, Y.Q. and Yuan, R., *A nitrite and hydrogen peroxide sensor based on Hb adsorbed on Au nanorods and graphene oxide coated by polydopamine*. Analytical Methods, 2014. **6**(3): p. 758-765.

10. McVey, I.F., *Non-dispersive mid-infrared sensor for vaporized hydrogen peroxide*. 2005, Google Patents.
11. Wang, J., Xu, M., Zhao, R. and Chen, G., *A highly sensitive H₂O₂ sensor based on zinc oxide nanorod arrays film sensing interface*. *Analyst*, 2010. **135**: p. 1992-1996.
12. Lin, C.Y., Lai, Y.H., Balamurugan, A., Vittal, R., Lin, C.W. and Ho, K.C., *Electrode modified with a composite film of ZnO nanorods and Ag nanoparticles as a sensor for hydrogen peroxide*. *Talanta*, 2010. **82**(1): p. 340-347.
13. Kong, Y.T., Boopathi, M. and Shim, Y.B., *Direct electrochemistry of horseradish peroxidase bonded on a conducting polymer modified glassy carbon electrode*. *Biosensors & Bioelectronics*, 2003. **19**(3): p. 227-232.
14. Bui, M.P.N., Pham, X.H., Nan, K.N., Li, C.A., Kim, Y.S. and Seong, G.H. *Electrocatalytic reduction of hydrogen peroxide by silver particles patterned on single-walled carbon nanotubes*. *Sensors and Actuators B-Chemical*, 2010. **150**(1): p. 436-441.
15. Xu, J., Liu, C.H. and Teng, Y.L., *Direct electrochemistry and electrocatalysis of hydrogen peroxide using hemoglobin immobilized in hollow zirconium dioxide spheres and sodium alginate films*. *Microchimica Acta*, 2010. **169**(1-2): p. 181-186.
16. Xu, J., Shang, F.J., Luong, J.H.T., Razeed, K.M. and Glennon, J.D., *Direct electrochemistry of horseradish peroxidase immobilized on a monolayer modified nanowire array electrode*. *Biosensors & Bioelectronics*, 2010. **25**(6): p. 1313-1318.
17. Bahshi, L., Frasconi, M., Tel-Vered, R., Yehezkeili, O. and Willner, I., *Following the Biocatalytic Activities of Glucose Oxidase by Electrochemically Cross-Linked Enzyme-Pt Nanoparticles Composite Electrodes*. *Analytical Chemistry*, 2008. **80**(21): p. 8253-8259.
18. Prabhu, P., Babu, R.S. and Narayanan, S.S., *Synergetic effect of Prussian blue film with gold nanoparticle graphite-wax composite electrode for the enzyme-free ultrasensitive hydrogen peroxide sensor*. *Journal of Solid State Electrochemistry*, 2014. **18**(4): p. 883-891.
19. Lagalante, A.F. and Greenbacker, P.W., *Flow injection analysis of imidacloprid in natural waters and agricultural matrixes by photochemical dissociation, chemical reduction, and nitric oxide chemiluminescence detection*. *Analytica Chimica Acta*, 2007. **590**(2): p. 151-158.
20. Lei, W., Durkop, A., Lin, Z.H., Wu, M. and Wolfbeis, O.S., *Detection of hydrogen peroxide in river water via a microplate luminescence assay with time-resolved ("gated") detection*. *Microchimica Acta*, 2003. **143**(4): p. 269-274.
21. Hanaoka, S., Lin, J.M. and Yamada, M., *Chemiluminescent flow sensor for H₂O₂ based on the decomposition of H₂O₂ catalyzed by cobalt(II)-ethanolamine complex immobilized on resin*. *Analytica Chimica Acta*, 2001. **426**(1): p. 57-64.
22. Sanchez, J.C. and Trogler, W.C., *Polymerization of a boronate-functionalized fluorophore by double transesterification: applications to fluorescence detection of hydrogen peroxide vapor*. *Journal of Materials Chemistry*, 2008. **18**(42): p. 5134-5141.
23. Guo, Z.X., Shen, H.X. and Li, L., *Spectrophotometric determination of hydrogen peroxide and glucose based on hemin peroxidase-like catalyzed oxidation of bromopyrogallol red*. *Mikrochimica Acta*, 1999. **131**(3-4): p. 171-176.
24. Matsubara, C., Kawamoto, N. and Takamura, K., *Oxo 5,10,15,20-tetra(4-pyridyl)porphyrinato titanium(IV) - An ultra-high sensitivity spectrophotometric reagent for hydrogen-peroxide*. *Analyst*, 1992. **117**(11): p. 1781-1784.
25. Pinkernell, U., Effkemann, S. and Karst, U., *Simultaneous HPLC determination of peroxyacetic acid and hydrogen peroxide*. *Analytical Chemistry*, 1997. **69**(17): p. 3623-3627.

26. Lobanov, A.V. and Komissarov, G.G., *Hydrogen Peroxide in Artificial Photosynthesizing Systems*. Biofizika, 2014. **59**(2): p. 215-230.
27. Merayo, N., Hermosilla, D., Negro, C. and Blanco, A., *On-line FTIR as a novel tool to monitor Fenton process behavior*. Chemical Engineering Journal, 2013. **232**: p. 519-526.
28. Normand, E., *Compounds of interest*. 2010.
29. Vogel, A.I. and Jeffery, G.H., *Vogel's textbook of quantitative chemical analysis*. 5th ed. 1989: Longman Scientific & Technical.
30. Desa, W.N.S.M., *The Discrimination of Ignitable Liquids and Ignitable Liquid Residues using Chemometric Analysis*, in *Pure and Applied Chemistry*. 2012, University of Strathclyde: Glasgow.
31. Mat-Desa, W.N.S., D. Ismail, and N. NicDaeid, *Classification and Source Determination of Medium Petroleum Distillates by Chemometric and Artificial Neural Networks: A Self Organizing Feature Approach*. Analytical Chemistry, 2011. **83**(20): p. 7745-7754.

Chapter 7. Conclusions and Future Work

7.1 Summary

The overall aim of this work was to explore the application of high resolution Fourier transform infrared spectroscopy on the qualitative characterisation of specific explosive precursors in the vapour phase. This involved the development of an experimental methodology for the analysis of laboratory grade explosive precursor chemicals as well as the application of these methods to the analysis of operationally relevant commercial precursor materials and their statistical discrimination.

This project has demonstrated that high resolution Fourier transform spectroscopy is a very powerful tool for the characterisation of explosive materials and their precursors. The spectra produced have allowed for the identification of absorption bands suitable for detection, for example, through the use of a QCL system.

The analysis of diesel determined that temperature had a more substantial effect upon the amount of absorption seen than the sample volume. Based upon these results a starting temperature of 27°C for the analysis of the various compounds of interest was selected with the option to increase the temperature to 75°C if required for less volatile materials.

The analysis of compounds of interest demonstrated that the protocol developed from the diesel analysis was fit for purpose. All of the compounds analysed had detectable absorption bands at 27°C or 75°C, and from the spectra produced it was possible to determine whether these absorption bands would be suitable for use in QCL based detection systems. Some suitable absorption bands were observed outside the regions previously identified as potential detection targets, thereby demonstrating the importance of analysing a wide spectrum (800-4000 cm⁻¹) rather

than focusing on smaller regions in order to prevent potential detection targets being overlooked.

Two of the compounds of interest, ammonia and hydrazine, were in solvent. These solvents had an effect on the spectra of the compounds themselves. Subtraction software was used to remove the spectrum of each solvent from the spectrum of the compound of interest and allowed for the identification of potential absorption targets. In the case of hydrazine, hydrazine hydrate was also analysed as an alternative to hydrazine without solvent. However, this highlighted the differences even a slight change in chemical structure can produce, with only some shared spectral features. Thus it when selecting absorption features for detection it must be noted that absorption features may be altered or shifted depending upon other materials present.

Two different types of absorption bands were seen within the target regions for the compounds of interest. While in the majority of regions the absorption bands were discrete peaks, an oscillating pattern could also be identified in some regions, notably in the spectra for hydrogen peroxide and nitric acid. It was found that there was some discrepancy between the predicted wavenumber for an absorption band and the actual wavenumber seen in the spectra, with a shift of 1 cm^{-1} frequently observed. This was thought to be primarily due to instrumentation differences, and differences between the spectra produced with vapour analysis compared to direct analysis of liquid materials. These differences highlight the importance of creating a database for a particular instrument rather than relying on published information. This requirement was also evident when analysing ethanol as there were absorption bands present in the spectra that initially could not be seen in available reference spectra. This was found to be due to the majority of reference spectra being from direct analysis of the liquid rather than an analysis of ethanol vapour. A reference spectrum of the vapour analysis of ethanol did have the absorption bands present, although as with the other compounds of interest there was a small shift in the wavenumbers, most likely due to differences in instrumentation.

The analysis of methanol and ethanol as compounds of interest highlighted the ability of the FTS instrument to differentiate between chemically similar compounds.

The spectral and statistical analysis of acetone and acetone based nail polish removers demonstrated that it was possible to differentiate both between different brands of nail polish removers and between these and laboratory grade acetone. Similarly, the spectral and statistical analysis of alcohol containing materials and laboratory grade ethanol, methanol and propanol demonstrated that it is possible to differentiate between them. Furthermore it was determined that when analysing drinkable spirits, such as vodka and gin, the type of spirit had more of an effect on the level of discrimination than the alcohol concentration.

Laboratory hydrogen peroxide and hydrogen peroxide containing materials were also analysed. Two hydrogen peroxide containing materials were also systematically concentrated and their resultant spectra analysed to assess whether firstly, the different concentrations could be discriminated and secondly, whether the concentrated samples could be linked to the brand from which they were derived. The results obtained demonstrated that it was possible to discriminate between different commercially available hydrogen peroxide and laboratory grade material. Furthermore it was possible to discriminate between different concentrations of the same material, whilst still identifying the originating brand. This is a highly significant result and potentially facilitates not only the identification of material containing hydrogen peroxide by brand but also a mechanism by which alterations of the material can be identified in the vapour phase.

The results of the brand discrimination studies demonstrated the value of HCA and SOFM as statistical techniques for the analysis of multivariate data. In particular the use of component maps with SOFM allowed for a greater understanding of the data.

The results of this research demonstrated the potential for high resolution FTIR with HCA and SOFM to become a powerful technique in the investigation of explosives

related crime. Firstly, providing the ability to characterise materials to allow for their detection. Secondly, the ability to identify an unknown precursor material, and then to determine whether that material has been concentrated from its original state. Finally, with some adaptation it is possible for this technique to contribute towards the linking of precursors to explosive materials.

7.2 Future work

The work completed thus far has confirmed the suitability of high resolution FTIR for the characterisation and discrimination of explosive precursor materials. There are a number of avenues of future work that can readily be identified as a consequence of this research.

7.2.1 Compounds of interest

The protocol developed in this project should be used to continue the analysis of liquid explosive materials and precursors. The database produced would allow for the identification of potential detection targets, and for the identification of unknown samples through comparison with the known samples. Such a database could have uses for both the detection and intelligence communities.

Further investigation could be carried out on those compounds, such as nitromethane, which had two peaks within a single 'spectral window'. This work would involve determining how best to exploit the presence of two absorption peaks to enable more accurate detection and identification of a material. Work could also be carried out to determine if a single laser can detect more than one material if the absorption bands are slightly apart or if one takes the form of a discrete peak and the other an oscillating pattern. In addition to this, work could be carried out to develop more accurate identification of a material using absorption information from multiple lasers. For example this could be utilised to aid the identification of hydrazine hydrate and the differentiation of it from ammonia and hydrazine by using a combination of the absorption features seen at two wavenumbers. If absorption was present at both wavenumbers then the material present would be hydrazine hydrate, if absorption was only present at one

wavenumber then the material would be either hydrazine or ammonia depending upon the location of the absorption.

Future work should also involve the continued identification of suitable regions of detection as different QCLs become available.

7.2.1.1 Solid samples

Another avenue of future work would be to develop a protocol for the analysis of solid explosive materials, and solid precursors. This is important as many potentially explosive materials are found in solid form. However, this may prove challenging as the results of this experiment demonstrated that a high temperature is likely to be necessary in order to evolve sufficient vapour for detection. High temperatures are likely to produce significant background interference and also may cause safety concerns as explosive materials can become unstable at high temperatures. One potential solution to this would be to increase the path length of the sample cell, thereby increasing the amount of interaction between any vapour produced and the infrared beam. This method is already employed within the detection portal (developed by Cascade Technologies), allowing for the detection of hydrogen peroxide vapour at room temperature, whereas the FTS required the hydrogen peroxide to be heated. The only disadvantage to increasing the path length, most likely through the use of a multipass cell, would be that it would require adaptation of the instrument in order to accommodate it.

7.2.2 Brand discrimination

Further work in this area could be to increase the data sets for hydrogen peroxide and acetone as only five brands of each material were tested. This would help to ensure that discrimination was still possible with more brands to compare, although this has already been demonstrated to a degree with the results of the analysis of different alcohols. In addition to increasing the data sets, this information could then be collated in the form of a database. This would allow for the comparison of unknown materials to identify the compound and also the brand. Any such

database could also contain information on the effects of altering the brands, for example, using the work from this project on the concentration of hydrogen peroxide containing products.

The analysis of further explosive precursor materials could also be carried out and added to the database. This information would be of use to those investigating suspected bomb factories, and would also provide information for those developing detection systems as to how different additives in brands might have an effect on detection targets for explosive materials.

The work could also be extended to examine the effect of different brands on the spectra produced from the explosive materials created from the precursors. This project postulated that some of the differences seen in the spectra of precursors could have an effect upon the spectra of any explosive materials produced from these precursors and these effects could, in turn, impact upon the detection of the explosive materials. This could be examined by producing homemade explosive materials in the laboratory using a range of brands under the same conditions and then analysing the products, applying the same visual and statistical techniques performed in this project. In addition to this, following on from the investigation of different concentrations of hydrogen peroxide, hydrogen peroxide containing products could be concentrated to different levels prior to production of the explosive material and the effect of the peroxide concentration on the spectrum of the explosive material could be investigated.

7.2.3 Mixtures

Thus far all samples have been analysed separately. Future work could include the analysis of mixtures, as this is the state in which many explosive materials and explosive precursor materials are likely to be encountered by security services. The challenge with this analysis would be to manage the safe handling of potentially unstable mixtures.

In addition to this, potential interfering compounds, such as perfumes, hair products and fizzy drinks could be analysed, both separately but also mixed with explosive materials. Spectral information on the different interfering compounds could be added to a database, but more importantly any interfering absorption within the target regions for explosives detection could be identified and any effects on the spectra produced of explosive materials mixed with any interferents such as the shifting or broadening of absorption bands could also be identified.

Further work could also be carried out to determine if there are any differences in spectra produced when the liquid samples are soaked into clothing material and other matrices instead of being placed neat into the instrument, as this is another potential form in which the material might be found in by security services.

7.2.4 Alcohols

The brand discrimination of different alcoholic drinks highlighted the potential uses of the FTS and statistical analysis developed in this project for work outwith the field of explosives detection. The detection of additives and significant variation in concentration in alcohols could allow for the detection of counterfeit materials through identifying variation in the spectra produced and using statistical analysis such as the multivariate analysis used in this project.

7.2.5 Statistical analysis

The use of SOFM for the discrimination of different brands of the same material type demonstrated the power of this technique for the interpretation of multivariate data. Therefore, there is scope for the refinement of the technique and its application to other types of multivariate data.

The SOFM component maps could be used to reduce the number of regions of variation required for discrimination of materials. A reduction in the number of regions of variation would result in a reduction in the number of lasers required to target these regions and an increase in the portability of any such detection system.

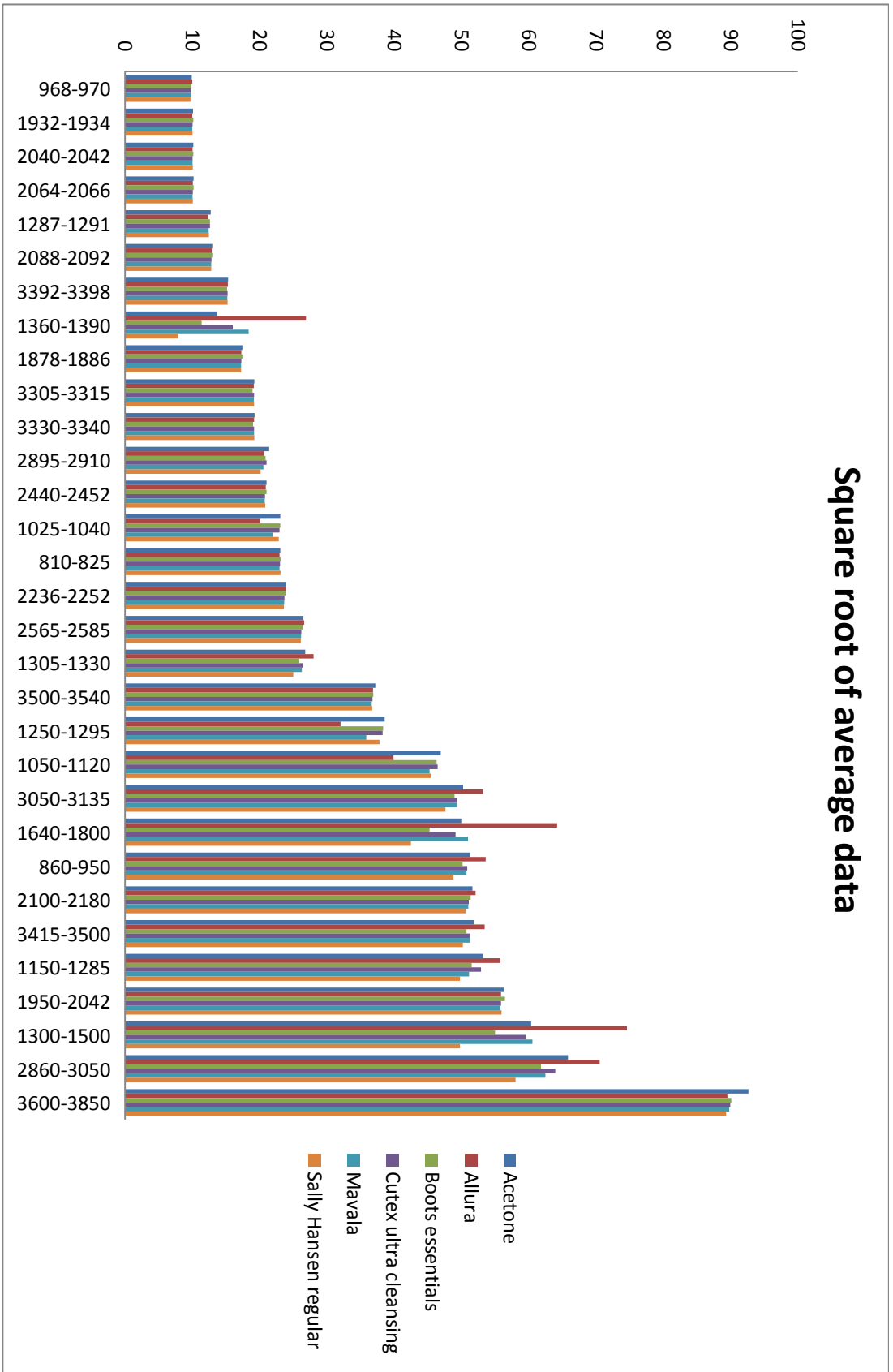
7.3 Conclusions

This project has demonstrated the suitability of high resolution Fourier transform spectroscopy for the vapour phase analysis of explosive precursor materials. Furthermore, it has revealed that when comparing different brands of a particular material it is possible to discriminate between them. This has implications for the detection of both these precursor materials and the explosive materials produced from them.

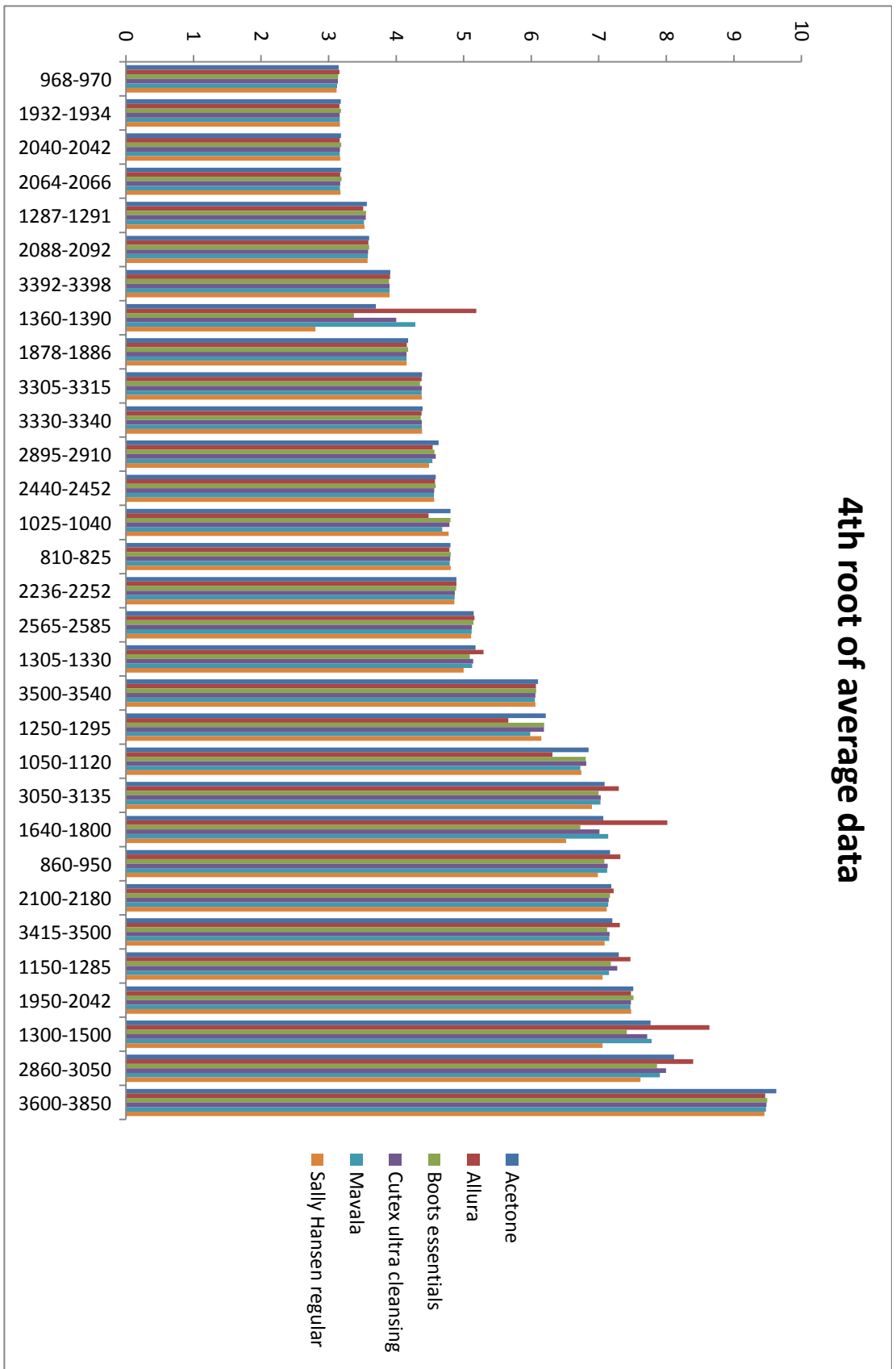
Appendix 1 – Pre-processed acetone data

The following pages show the pre-processed data for acetone with the square root, 4th root, 16th root and 265th root take of the 'binned' average data.

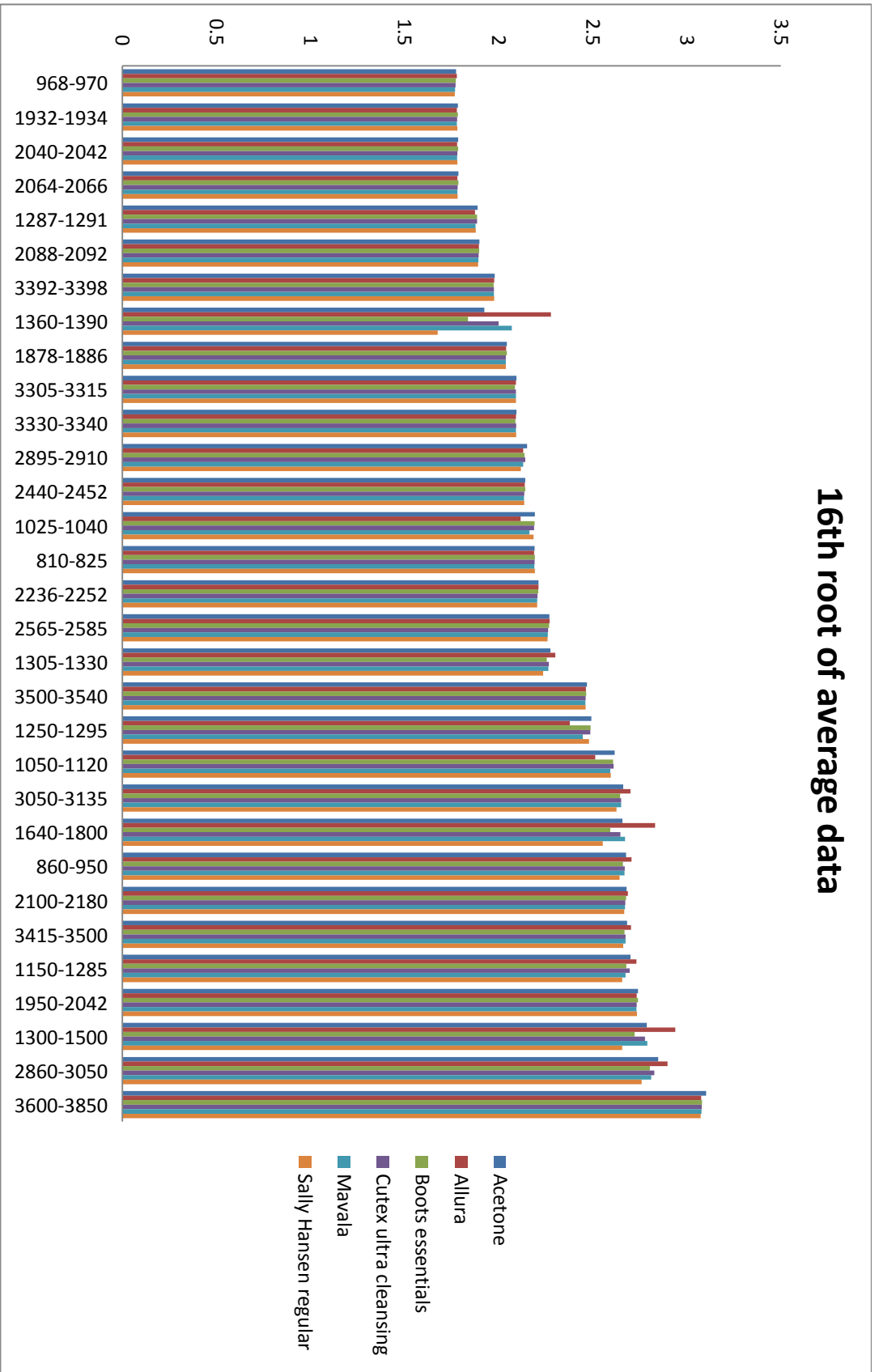
Square root of average data



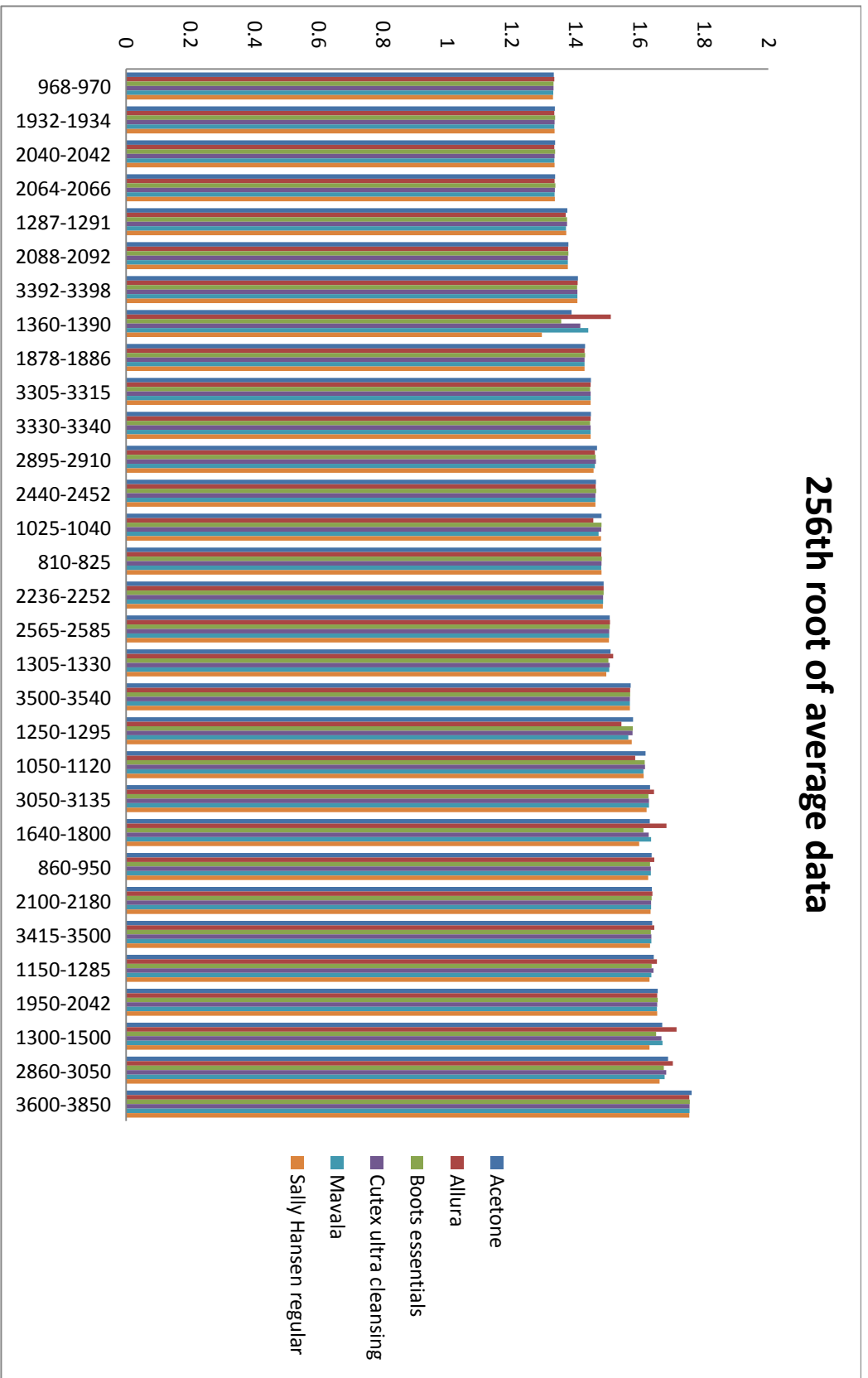
4th root of average data



16th root of average data



256th root of average data



Appendix 2 – Alcohol ingredients

Listed below are the ingredients, as much as was available, based upon the bottle labels of the shop bought alcohols.

1. Surgical spirit B.P - Boots
90% ethanol w/w, methanol 5% w/w, methyl salicylate, diethyl phthalate, castor oil
2. Methylated spirit - Barretine
Methylated spirit, methanol mineralised >50% voc content (MSDS states 60-100% ethanol, 1-5% methanol, <1% pyridine)
3. Listerine antibacterial mouthwash - Stay white arctic mint
Aqua, alcohol, sorbitol, poloxamer 407, benzoic acid, zinc chloride, eucalyptol, methyl salicylate, thymol, sodium benzoate, methanol, sucralose, aroma, sodium saccharin, CI 42090
4. Tesco everyday value mouthwash
Aqua, alcohol, glycerin, polysorbate 20, aroma, cetylpyridinium chloride, sodium fluoride, sodium saccharin, sodium benzoate, menthol, CI 42051, CI 19140
5. Colgate peroxy mouthwash
Hydrogen peroxide, sorbitol, ethanol (9.6% v/v), poloxamer 338, polysorbate 20, methyl salicylate, levo-menthol, sodium saccharin, brilliant blue FCF (E133) and purified water
6. Bacardi Breezer - 4% by volume
Carbonated water, fermented alcohol, Bacardi Rum, sugar, flavouring, citric acid, sodium citrate, E440, E445, E444, E202, E223, E950, E955, E104, E124

7. Smirnoff vodka 37.5% by volume
8. Absolut vodka 40% by volume
9. Beefeater gin 40% by volume
10. Gordon's gin 37.5% by volume
11. Bacardi rum 37.5% by volume
12. Melocoton 20% by volume
13. Jose Cuervo Tequila 38% volume

Appendix 3 – Hydrogen peroxide ingredients

The ingredients and concentrations of the five hydrogen peroxide containing materials analysed in Chapter 6 are listed below. These ingredients and concentrations are based upon the information provided on the packaging of each material.

1. Botanics

Conc. not stated

Developing lotion contains:

Aqua, cetearyl alcohol, hydrogen peroxide, cetareth-20, phosphoric acid, tetrasodium EDTA, sodium stannate

2. Colgate peroxy mouthwash

1.5% w/v

Hydrogen peroxide, sorbitol, ethanol (9.6% v/v), poloxamer 338, polysorbate 20, methyl salicylate, levo-menthol, sodium saccharin, brilliant blue FCF (E133) and purified water

3. Health Leads:

35% aqueous solution (Hydrogen peroxide food grade material)

4. Jerome Russell:

30 vol 9% (Cream peroxide)

Aqua, hydrogen peroxide, cetyl alcohol, cetearyl alcohol, polysorbate 60, sodium stannate, phosphoric acid, disodium EDTA, persea gratissima (avocado) oil, fucus vesiculosus (seaweed) extract

5. Sunin:

6%

Aqua, hydrogen peroxide, hydroxyethyl cetyldimonium phosphate, dimethicone PEG-7 phosphate, polysorbate 20, parfum, aloe barbadensis, calendula officinalis, chamomilla recutita, linum usitatissimum, panthenol, quaternium-80, silk amino acids, benzoic acid, disodium EDTA

Appendix 4 – Hydrogen peroxide concentration calculation

The following calculation was utilised to calculate the concentration of the samples of Sunin and Health Leads that were concentrated under lab conditions and titrated with potassium permanganate.

1. Moles of Manganese [Mn] = volume [in L] x concentration = volume [L] x 0.02
2. Moles of H_2O_2 = moles of Mn x 2.5
3. Mass of H_2O_2 = moles x Relative Molecular Mass = moles x 34.0147
4. mL of H_2O_2 = Mass of H_2O_2 [assuming 1mL = 1g]
5. % H_2O_2 = (mL H_2O_2 / total volume) x 100
6. H_2O_2 in the sample [25 mL or 10 mL] transferred to make the total volume =
 $V_1 \times C_1 = V_2 \times C_2$
 $C_1 = (V_2 \times C_2) / V_1$
7. H_2O_2 in the original sample [10 mL or 5 mL] =
 $V_1 \times C_1 = V_2 \times C_2$
 $C_1 = (V_2 \times C_2) / V_1$
8. % H_2O_2 = $C_1 \times 100$

Appendix 5 – Publication

The following pages consist of the conference proceedings paper entitled '*Exploiting High Resolution Fourier Transform spectroscopy to inform the development of a quantum cascade laser based explosives detection system*' that was produced using work presented in this thesis.

Exploiting High Resolution Fourier Transform spectroscopy to inform the development of a quantum cascade laser based explosives detection system

Felicity Carlysle^{a*}, Niamh Nic Daeid^a, Erwan Normand^b, Michael McCulloch^b

^aCentre for Forensic Science, University of Strathclyde, 204 George St, Glasgow, G1 1XW, UK

^bCascade Technologies, Glendevon House, Castle Business Park, Stirling, FK9 4TZ

*felicity.carlysle@strath.ac.uk

ABSTRACT

Fourier Transform infrared spectroscopy (FTIR) is regularly used in forensic analysis, however the application of high resolution Fourier Transform infrared spectroscopy for the detection of explosive materials and explosive precursors has not been fully explored. This project aimed to develop systematically a protocol for the analysis of explosives and precursors using Fourier Transform infrared spectroscopy and basic data analysis to enable the further development of a quantum cascade laser (QCL) based airport detection system. This paper details the development of the protocol and results of the initial analysis of compounds of interest.

Keywords: Infrared spectroscopy, quantum cascade laser, explosives detection, high resolution

1. INTRODUCTION

The ongoing threat of terrorism around the world has resulted in the rapid development of systems capable of detecting concealed explosive devices. As the terrorist threat evolves, so must the systems designed to detect devices and device components. A successful detection system needs to fulfil several criteria, some dependent upon the situation where the system will be used, but all systems must be accurate and sensitive¹.

In order for a system to detect explosive compounds and their precursors successfully, these compounds must first be characterised in order to determine which identifying features of the compound can be targeted by the system. Not all identifying features may be suitable for a particular detection system and therefore it is important to select a method of characterisation that is compatible. This work aimed to characterise compounds through analysis in the mid-infrared region of the electromagnetic spectrum, thereby making it suitable for detection systems which target mid-infrared wavelengths. This includes quantum cascade laser based systems such as the airport detection system currently under development at Cascade Technologies. The detection system from Cascade Technologies is designed to detect vapours from potential explosive devices present either on passengers themselves or within their hand luggage.

Fourier Transform spectroscopy is already used in many areas of forensic science². High resolution Fourier Transform spectroscopy is capable of producing information rich spectra^{3,4}, with the increased resolution available allowing for the visualisation of small spectral features. This makes it a potentially powerful tool for the determination of suitable regions of a spectrum, for detection with currently available quantum cascade lasers which have a limited 'spectral window' of approximately 6cm^{-1} .⁵

This project comprised of two stages, firstly the development of a protocol for the analysis of liquid compounds of interest, and secondly the initial analysis of two compounds of interest. Diesel was selected for the development of the protocol as it is moderately volatile but easy to work with safely. It would also be expected to produce several regions of absorption across the mid-infrared due to the large number of different components present in the liquid. The compounds of interest have been referred to as F1 and F2 for the purposes of this paper. They were selected for analysis both because of their potential use in explosive devices and because their predicted mid-infrared absorption features occurred within the 'spectral windows' of currently available QCLs. Therefore the analysis of F1 and F2 would serve to test the suitability of the newly developed protocol and determine whether absorption does occur within these 'spectral windows'.

2. METHODS AND MATERIALS

2.1 Materials

The analysis was carried out using a Bruker IFS/125/HR Fourier Transform spectrometer. The instrument settings were kept constant throughout the experiment with the exception of the aperture size and pre-amplification gain which were altered after the diesel analysis from 0.5 mm and gain setting B to 1.0 mm and gain setting A for the analysis of the compounds of interest. The resolution was set at 0.1 cm^{-1} and 100 scans were taken for each analysis with the spectrum saved from $4000\text{-}800\text{ cm}^{-1}$ ($2.5\text{-}12.5\text{ }\mu\text{m}$).

Diesel was supplied by the University of Strathclyde and compounds F1 and F2 were purchased from Sigma Aldrich UK.

2.2 Method

The experiment can be split into two distinct parts; the development of a protocol using diesel, and the initial analysis of the compounds of interest.

2.2.1 Protocol development

Two factors, sample volume and temperature, were identified as potentially having significant effects on the spectra produced. Three levels; low, medium and high, were selected for each factor and these are shown in Table 1.

Table 1. The factors involved in the experiment and the levels under investigation

	Volume (mL)	Temperature (°C)
Low level	0.5	27
Medium level	1	75
High level	3	150

Each combination of the two factors at the three levels was repeated twice resulting in a total of 36 analytical runs to examine the effects of the two factors on the diesel spectra produced.

2.2.1.1 Experimental procedure

The diesel analysis followed an eight step experimental procedure shown in Table 2. The order of the different combinations was determined by the fact that the sample cell could not actively cool itself, therefore it was necessary to start with the low temperature level first. The procedure was repeated twice to provide two repeats for each factor combination.

Table 2. Eight step experimental procedure used to analyse diesel samples with the different factor combinations

Step	Action
1	Background scan taken of empty sample cell at lowest temperature
2	Analysis of each sample volume level at lowest temperature
3	Sample cell heated to medium temperature
4	New background scan taken of empty sample cell at medium temperature
5	Analysis of each sample volume level at medium temperature
6	Sample cell heated to high temperature
7	New background scan taken of empty sample cell at high temperature
8	Analysis of each sample volume level at high temperature

2.2.1.2 Data analysis

The diesel spectra were examined visually using the OPUS software provided with the instrument, and this software was used to calculate average spectra and standard deviations. The data was then transferred to Microsoft Excel to enable further statistical analysis and closer examination of regions of absorption that had been identified using OPUS.

2.2.1 Analysis of compounds of interest

This work was carried out after the diesel analysis, the results of which directly influenced the experimental procedure for this section.

2.2.1.1 Experimental procedure

Each compound was analysed six times to produce an average spectrum and ensure that the results were reproducible. A nine step experimental procedure was followed and this is shown in Table 3.

Table 3. Nine step experimental procedure for analysis of compounds of interest

Step	Action
1	Background scan taken of empty sample cell at 27°C
2	100µl sample analysed at 27°C
3	Repeated Step 2 five times to provide a total of six spectra
4	An average spectrum created and examined for visible absorption features
5	If absorption features were not clear increase the temperature of the sample cell to 75°C otherwise proceeded to data analysis
6	Background scan taken of empty sample cell at 75°C
7	Six 100µl samples analysed at 75°C
8	Created an average spectrum of six repeats at 75°C
9	Data analysis of spectra at 75°C

2.2.1.2 Data analysis

As with the diesel analysis a visual analysis was first carried out of the average spectrum, and standard deviations calculated using OPUS. The data was then transferred to Microsoft Excel where specific regions of the spectrum were then further examined using relative standard deviations and graph plotting. These regions corresponded to specific 'spectral windows' of available QCLs.

3. RESULTS AND DISCUSSION

3.1 Diesel analysis

Visual examination of the diesel spectra indicated two regions of absorption at approximately 1400 cm⁻¹ (7.1 µm) and 2900 cm⁻¹ (3.4µm). These regions were visible at all three temperature levels with all three sample volumes. Also present in the spectra were absorptions for water and carbon dioxide. Figure 1 shows a comparison of the average spectra produced with 0.5 mL of diesel across the three temperature levels. It is clear from these spectra that as the temperature increases so does the amount of absorption. Figures 2 and 3 are close up views of the regions of absorption taken from the spectra shown in Figure 1.

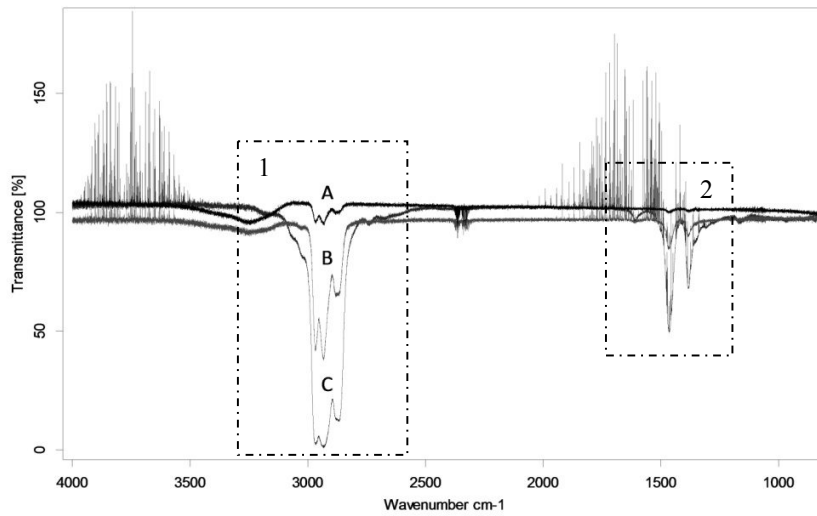


Figure 1. Diesel spectra produced with 0.5 mL diesel at A 27°C, B 75°C and C 150°C showing absorption within the highlighted regions at 1400 cm⁻¹ (2) and 2900 cm⁻¹ (1) and the variation in the absorption in these areas across the temperature levels

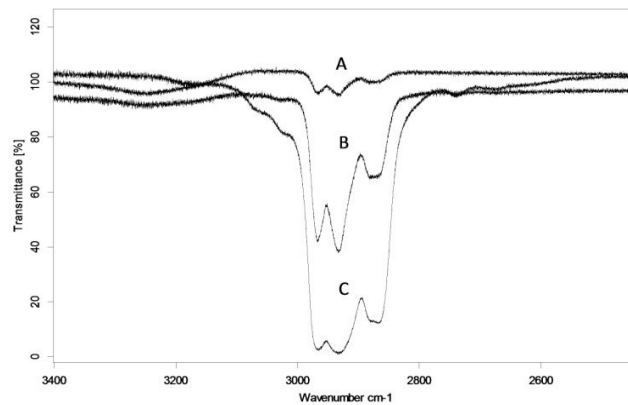


Figure 2. Close up of the absorption seen with 0.5 mL diesel at 2900 cm⁻¹ showing the difference across the temperature levels A 27°C, B 75°C and C 150°C

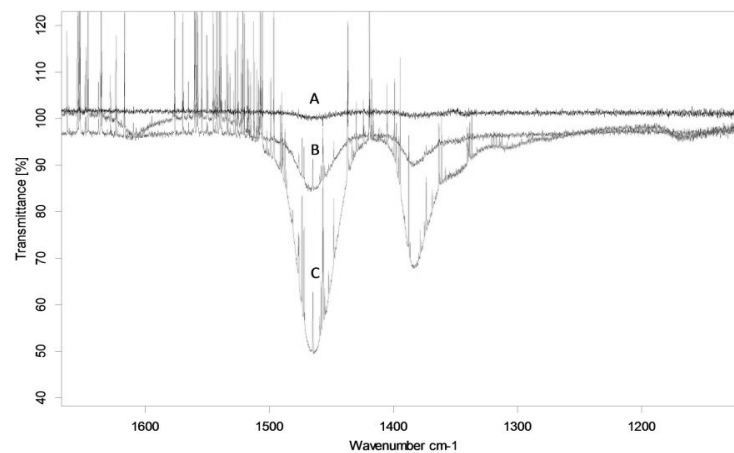


Figure 3. Close up of the absorption seen with 0.5 mL diesel at 1400 cm⁻¹ showing the difference across the temperature levels A 27°C, B 75°C and C 150°C

Calculation of the standard deviation and relative standard deviations across the average spectra at the three temperature levels showed that as the temperature increases so does the variability of the absorption seen. Therefore the optimum temperature for maximum absorption is unlikely to be the optimum for producing the most consistent results. In addition to this, at 150°C the absorption band at 2900 cm^{-1} is near saturation which suggests that this temperature is likely to be too high for many volatile compounds. While the absorption at 27°C is lower than at 75°C and 150°C it is sufficient to produce absorption, although in the 1400 cm^{-1} region this is very small. This suggests that 27°C would be a suitable initial temperature for analysis of compounds of interest, however less volatile compounds may require 75°C in order to produce clear absorption. This is not hugely surprising as the path length of the sample cell is only 100 mm which greatly limits the amount of interaction between the vapour and infrared beam, therefore less volatile compounds require an increased temperature to produce sufficient vapour for detection. While ideally all the analysis of compounds would be carried out as close to room temperature as this is the temperature at which the QCL system will be working, the QCL system has a significantly longer path length therefore reducing the temperature required for detection.

While the temperature appeared to have a substantial effect on the absorption seen the sample volume did not have such an effect with very little difference in the absorption seen across the three levels. Thus, the optimum volume for analysis of compounds of interest is more dependent on ease of handling rather than volume needed for producing sufficient vapour for detection. In this respect smaller volumes were easier to handle and given the nature of some potential compounds of interest smaller amounts would also be favourable from a safety perspective. Therefore 100 μL would be a suitable start volume for analysis of compounds of interest, with the potential to increase this volume to 1 mL if a temperature increase was not sufficient to produce detectable absorption.

3.2 Analysis of compounds of interest

3.2.1 Compound F1

The F1 spectrum as a whole shows several regions of absorption which might be suitable for QCL detection at a later stage, in particular broader features which might be detectable with a broadband or multi DFB laser system. This highlights the future use of these initial analyses as the foundation of a knowledge base for future work.

Compound F1 was predicted to have detectable absorption at around 920 cm^{-1} (10.9 μm) and as figure 4 shows this was found to be the case. Further plotting of the data demonstrated that the main peak was slightly offset from the predicted wavenumber, however this still falls within the QCL 'spectral window' and therefore would not be a significant issue for detection with a suitable QCL. The presence of a second smaller peak also within the 6 cm^{-1} 'window' enhances the suitability of this feature for detection of F1 as both peaks can be detected strengthening the identification.

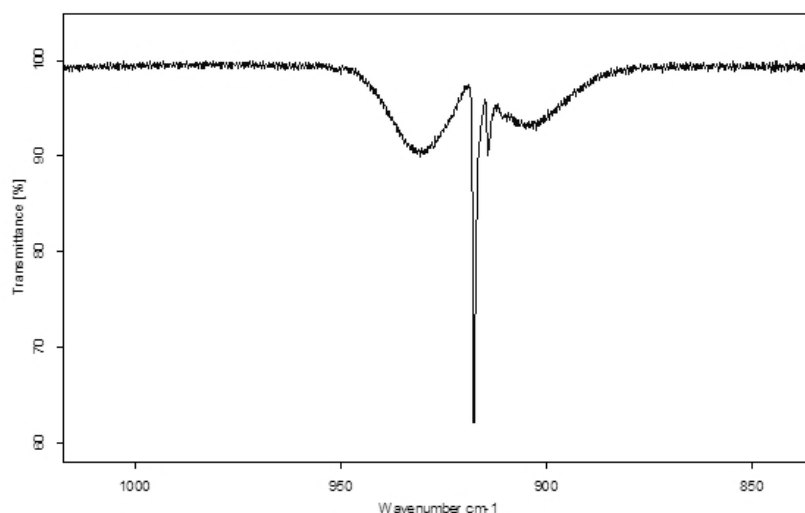


Figure 4. Close up of the average spectra produced from six repeats of compound F1 at 27°C showing the two peaks present in the 'spectral window' of a QCL around 920 cm^{-1}

The suitability of this feature is further enhanced by the results of calculating the relative standard deviations for the region across the six repeats. These show that within this region the variation is low, meaning that the feature is highly reproducible.

3.2.2 Compound F2

Compound F2 was less volatile than F1, and due to the structure of the compound produced a spectrum with multiple OH bond lines which caused a degree of masking of the feature that this investigation was targeting. It was therefore deemed necessary to increase the temperature to 75°C in order to increase the size of the absorption feature to allow for it to be identified, although care had to be taken as the increase in temperature also increased the size of the OH bond lines. Figure 5 shows a close up of the absorption feature of interest at 75°C. It can be seen that the feature in this region is not a discrete peak like those seen with F1. Instead, within the 'spectral windows' present between 1225 and 1325 cm⁻¹ (8.2-7.5 μm), an oscillating pattern can be seen. This pattern is suitable for detection with a QCL and appears in the regions that it was predicted to. While the temperature had to be increased in order to visualise properly the two 'spectral windows' using FTIR this will not prevent the detection of F2 at room temperature by the QCL system since, as figure 5 shows, when the region is viewed close up there is no significant interference from OH lines within the 'spectral windows' and, as mentioned previously, the path length of the QCL system is significantly longer allowing for greater absorption at a lower temperature.

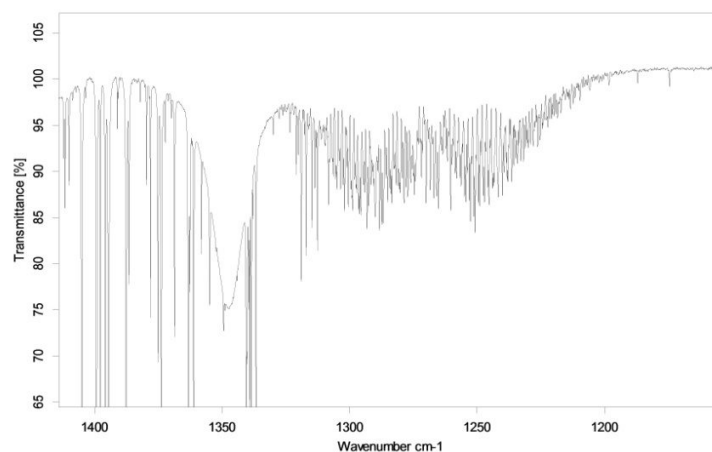


Figure 5. Close up of the average spectrum of F2 at 75°C showing the oscillating pattern seen in the 'spectral windows' between 1225 and 1325 cm⁻¹

4. CONCLUSIONS

The results of the diesel analysis suggested that high resolution Fourier Transform spectroscopy was suitable for the characterisation of explosive materials and their precursors. The analysis demonstrated that the conditions for analysis of compounds of interest would need to be a compromise between the level of absorption and the level of variability. From this analysis it was possible to develop a protocol for the analysis of compounds of interest with 100 μL sample size and 27°C acting as the start point for any investigation. The diesel analysis also demonstrated that OPUS and Microsoft Excel were sufficient for the data analysis required for a basic characterisation of a potential 'spectral window'.

The analysis of compounds F1 and F2 has confirmed that high resolution Fourier Transform spectroscopy is suitable for the characterisation of explosive materials and their precursors. The results demonstrate that the protocol developed via the analysis of diesel is appropriate for the analysis of liquid compounds of interest. The spectra produced for both compounds highlight the different forms of absorption features that are suitable for detection via a QCL. The spectra also reveal absorption features present that are currently not suitable for QCL detection, but with the development of broadband lasers could be used as detection targets in the future. The results obtained, in addition to future analysis utilising the protocol developed, are able to inform directly the development of a QCL based detection system, and also have the potential to contribute to the knowledge of the wider forensic science community.

Acknowledgements

The authors would like to thank Deepthi Chana for his assistance starting up this project and The University of Strathclyde and Cascade Technologies for providing funding and facilities for the project.

References

- [1] Yinon, J., [Counterterrorist Detection Techniques of Explosives], Elsevier (2007).
- [2] Ricci, C., Kazarian, S.G., "Enhancing forensic science with spectroscopic imaging," Proc SPIE 6402, 64020J (2006).
- [3] Smith, B.C., [Fundamentals of Fourier Transform Infrared Spectroscopy], CRC press (2011).
- [4] Larkin, P., [Infrared and Raman Spectroscopy: Principles and Spectral Interpretation], Elsevier (2011).
- [5] Normand, E., McCulloch, M., Duxbury, G., Langford, N., "Fast, real-time spectrometer based on a pulsed quantum-cascade laser," Optics Letters 28(1) , 16-18 (2003).